Multi-scale modelling of ions in solution : from atomistic descriptions to chemical engineering

John Jairo Molina

UPMC
SORBONNE UNIVERSITÉS

THÈSE DE DOCTORAT DE L'UNIVERSITÉ PIERRE ET MARIE CURIE

Spécialité

Chimie Physique et Chimie Analytique

Présentée par

John Jairo MOLINA

Pour obtenir le grade de

DOCTEUR de l'UNIVERSITÉ PIERRE ET MARIE CURIE

Sujet de la thèse:

Multi-scale modelling of ions in solution: from atomistic descriptions to chemical engineering

Soutenue le 29 septembre 2011

devant le jury composé de:

M.	Luc BELLONI	(Rapporteur)
M.	Thomas ZEMB	(Rapporteur)
M.	Jean AUPIAIS	(Examinateur)
M.	Jean-François DUFRÊCHE	(Examinateur)
M.	Pascal FRIES	(Examinateur)
M.	Jean-Pierre HANSEN	(Examinateur)
Mme.	Marie JARDAT	(Examinateur)
M.	Pierre TURQ	(Examinateur)

Thèse préparée au
Département de Chimie Physique et Chimie Analytique de Paris Centre
Laboratoire de Physicochimie des Electrolytes, Colloïdes et Sciences Analytiques (UMR 7195).
Université Paris VI Pierre et Marie Curie
75 005 Paris CEDEX

Abstract

Ions in solution play a fundamental role in many physical, chemical, and biological processes. For industrial applications these systems are usually described using simple analytical models which are fitted to reproduce the available experimental data. In this work, we propose a multi-scale coarse graining procedure to derive such models from atomistic descriptions. First, parameters for classical force-fields of ions in solution are extracted from *ab-initio* calculations. Effective (McMillan-Mayer) ion-ion potentials are then derived from radial distribution functions measured in classical molecular dynamics simulations, allowing us to define an implicit solvent model of electrolytes. Finally, perturbation calculations are performed to define the best possible representation for these systems, in terms of charged hard-sphere models. Our final model is analytical and contains no free "fitting" parameters. It shows good agreement with the exact results obtained from Monte-Carlo simulations for the thermodynamic and structural properties. Development of a similar model for the electrolyte viscosity, from information derived from atomistic descriptions, is also introduced.

Keywords : electrolytes, coarse-graining, effective potentials, perturbation theory, specific effects, primitive model.

Modélisation multi-échelle des ions en solution: des descriptions atomiques jusqu'au génie chimique

Résumé

Les ions en solutions ont un rôle fondamental dans de nombreux processus physiques, chimiques et biologiques. Dans le cadre des applications industrielles, l'ingénieur les décrits par des modèles analytiques simples, qui sont paramétrisés et ajustés afin de réproduire des données expérimentales. Dans ce travail, nous proposons une procédure multi-échelle à gros-grains pour obtenir ces modèles simples à partir de descriptions atomiques. D'abord, les paramètres de forces classiques pour des ions en solutions sont extraits de calculs *ab-initio*. Des potentiels effectifs (McMillan-Mayer) ion-ion sont ensuite obtenus à partir des fonctions de distribution de paire mesurées dans des simulations de dynamique moléculaire. Avec ces potentiels effectifs, nous pouvons établir une description à solvant continu des électrolytes. Finalement, nous mettons en oeuvre un calcul de perturbation, pour définir la meilleure représentation possible pour ces systèmes, en termes de sphères dures chargées (éventuellement associées). Le modèle final ainsi obtenu est analytique et il ne contient pas de paramètres ajustables. On montre qu'il est en bon accord avec les résultats exacts obtenus par des simulations Monte-Carlo pour la structure et la thermodynamique. La thèse se termine en proposant la mise au point d'une analyse similaire pour la viscosité des éléctrolytes, obtenue à partir d'une base moléculaire

Mots-clefs : électrolytes, gros-grains, potentiels effectifs, théorie des perturbations, effets spécifiques, modèle primitif.

Acknowledgements/Remerciements/Agradecimientos

This work has been performed primarily at the PECSA laboratory, formerly the LI2C, of the *Université Pierre et Marie Curie* (Paris 6) under the direction of Pierre Turq. I would like to thank him for his invaluable encouragement and guidance, as well as the trust he has shown me.

I must also thank the other members of my jury. Messrs Luc Belloni and Thomas Zemb, for having agreed to serve as *rapporteurs*, and Messrs Jean Aupiais, Jean-François Dufrêche, Pascal Fries, and Jean-Pierre Hansen and Madame Marie Jardat for showing interest in my work and agreeing to serve as judges on the commission.

I wish to express my appreciation to all those who have helped me in carrying out the work presented here. Above all, I would like to express my deepest gratitude to Jean-François Dufrêche, who has closely supervised the development of my work. Most, if not all, of what I know of electrolyte theory I owe to him. His enthusiasm and passion for science, and the patience he was shown me, have made working with him an immense pleasure. Without his assistance and support over the last three years, none of this would have been possible.

The part of the work concerning the force-field development has been carried out in collaboration with Mathieu Salanne and Benjamin Rotenberg. I am very grateful to them for allowing me to participate in the project, and for taking the time to show me how to work with the simulation codes. I also thank Mathieu for his constant attention and the help he has provided during the preparation of this manuscript.

The work on the primitive models was performed with the aid of Olivier Bernard. I appreciate his patience and willingness to explain the intricacies of the MSA and BIMSA theories. The investigation into the non-additive models has been done under the guidance of Jean-Pierre Hansen. I kindly thank him for his encouragement and support.

The work on the lanthanoids was possible thanks to Magali Duvail and Phillippe Guilbaud, who were kind enough to provide me with their simulation results.

I will fondly remember the time spent at PECSA for the opportunity of working amongst such a wonderful group of people and researchers. You have created an ideal working environment, making it a pleasure to go to lab every morning. I give warm thanks to Bernard Ancian, Pascal Bernard, Valérie Cabuil, Jean Chevalet, Didier Devilliers, Emmanuelle Dubois, Serge Durand-Vidal, Marie Jardat, Virginie Marie, Guillaume Mériguet, Christian Simone (who recruited me during a trip to Rome), and Jean-Pierre Simonin. I also wish to thank Brigitte Carrez, Isabelle Duc, and Lise Michelot for their assistance with all the administrative tasks.

I cannot forget the other PhD students with whom I have shared part or all of this journey: those who were there before, Vincent Dahirel, Ali Abou Hassan, and Gaëlle Roger, those who started alongside me, Alexandru Botan (with whom I suffered the burdens of French bureaucracy) and Debsindu Bowmik, and those who arrived after, Sami Tazi (without whom the fitting would not have been half as *fun*).

Over the last year and a half, I have spent a considerable amount of time at the ICSM at Marcoule. I would like to thank Thomas Zemb for receiving me at the institute, as well

as all the researchers and administrators for making my stay as comfortable as possible. In particular, I want to thank Dominique Alpe-Conchy, Hélène Martin, Vainina Russello, Bertrand Siboulet, and Alice Vidal. I must also thank Prof. Pavel Jungwirth for having invited me to visit his group in Prague.

Last, but certainly not least, I want to thank my family and friends for their unconditional support, both long-distance (Nancy and Vanessa) and local (Nicky, Sebastián, and the rest of my friends from school, who have been forced, at one time or another, to leave Colombia in search of *something* more...).

No sólo no hubiéramos sido nada sin ustedes, sino con toda la gente que estuvo a nuestro alrededor desde el comienzo; algunos, siguen hasta hoy.

¡Gracias... totales!

-Cerati

Contents

List of Figures

List of Tables

Chapter 1

Introduction et Résumé (version française)

Summary

1.1 Importance d'une description à plusieurs échelles

Les ions en solution jouent un rôle fondamental dans beaucoup de processus physiques, chimiques, biologiques et industriels. Par exemple, les ions aident la régulation des fonctions cellulaires de base [2] et ils participent aussi à la destruction de la couche d'ozone [3]. En outre, ils déterminent comment le retraitement et le stockage du combustible nucléaire usé peuvent être accomplis [4]. Si les simulations numériques nous ont aidé à développer une compréhension détaillée des propriétés microscopiques impliquées dans cette classe de phénomènes, le lien avec les propriétés thermodynamiques macroscopiques, que l'on obtient expérimentalement, n'est pas toujours facile à établir. De plus, de telles simulations nécessitent des ressources informatiques considérables, qui peuvent, dans certains cas, prendre plusieurs semaines ou plusieurs mois. Pour cette raison la plupart des modélisations en génie chimique adoptent les modèles les plus simples capables de décrire les données expérimentales disponibles, pour ensuite ajuster les paramètres à fin de les reproduire.

Le but de ce travail est de dépasser cette difficulté le mieux possible en développant une description à plusieurs échelles des ions en solution. Il s'agit de passer d'une description microscopique (déterminée par des simulations à échelle atomique) à un modèle mésoscopique approprié pour des applications en génie chimique. Ce travail est ainsi motivé par deux raisons principales. Premièrement, un tel processus nous permet de donner une interprétation physique, voir une explication aux modèles simples utilisés pour étudier les systèmes complexes qui se présentent typiquement dans le cadre industriel. Il ne suffit pas de dire qu'un modèle donné "fonctionne" (i.e. qu'il est capable

de reproduire des données expérimentales), nous devons aussi être capables d'expliquer pourquoi il "fonctionne". Deuxièmement, si cette procédure est réalisée correctement, elle n'aura pas besoin des données expérimentales externes. Ceci est particulièrement important pour des applications nucléaires, où les expériences sont bien connues pour être difficiles à réaliser. Pour donner une idée de ce dont nous aurons besoin pour une description des ions en solution à plusieurs échelles réussie, nous allons brièvement analyser le procédé PUREX (Plutonium–Uranium Refining by Extraction en anglais) utilisé dans le traitement du combustible nucléaire usé [4], parce qu'il illustre convenablement les bénéfices et le besoin d'une approche à plusieurs échelles.

Contexte: Le procédé PUREX

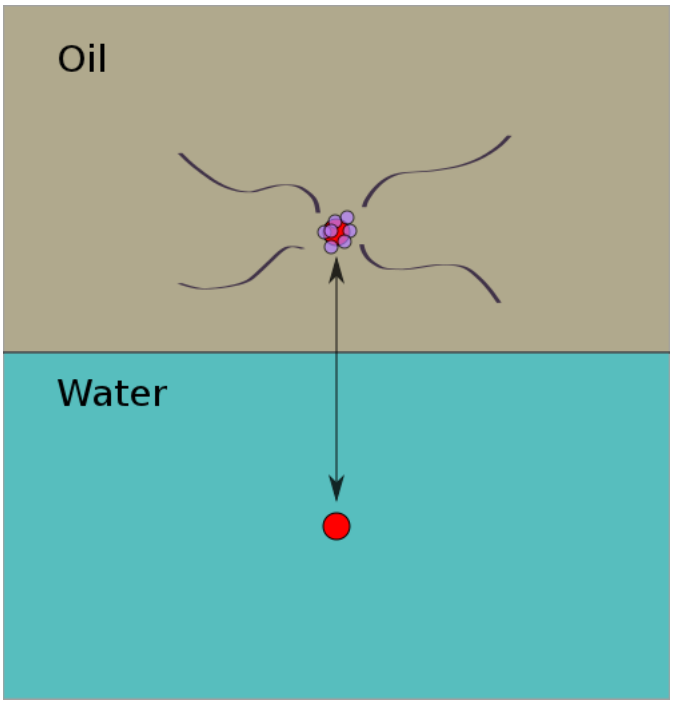

Figure 1.1: Un schéma représentant le procédé d'extraction liquide–liquide (PUREX) utilisé dans le traitement du combustible nucléaire usé.

Développé pendant les années 1940 comme une des parties du projet Manhattan, le procédé PUREX fut ensuite développé pour un usage non lié à l'industrie militaire et il est devenu depuis le procédé de–facto du recyclage des combustibles nucléaires usés des réacteurs à eau. A la fin du cycle nucléaire, quand le combustible est enlevé du réacteur, celui–ci contient des produits de transmutation et de fission (lanthanindes, actinides « mineurs » hautement radioactifs : Np, Am et Cm), parmi lesquels une quantité considérable de matériel encore fissile (plutonium et uranium), qui pourrait être réutilisé. Le procédé PUREX a été conçu précisément pour récupérer ce plutonium et cet uranium. Outre cette possibilité de réutilisation de combustible nucléaire, ce traitement réduit aussi fortement le volume des déchets et leur radioactivité, ce qui permet de les stocker plus facilement. Ainsi, sans traitement les déchets ont une durée de vie (estimée comme le temps que met le déchet pour retrouver une radioactivité semblable à celle du minerai d'uranium naturel) de l'ordre de plusieurs centaines de milliers d'années, mais elle tombe à environ 10000 ans après cette séparation. Une telle

politique à long terme n'a bien sûr un sens que si l'on construit les futures centrales utilisant le plutonium et l'uranium (centrale de génération IV).

Le procédé PUREX est une procédure d'extraction liquide–liquide qu'utilise la haute sélectivité d'une molécule organique particulière, le TBP (Tributyle Phosphate), pour extraire les actinides majeurs (U et Pu) du combustible nucléaire usé. Une représentation schématique du processus est présentée dans la Figure1.1. Les déchets nucléaires sont dissous dans une solution d'acide nitrique aqueuse et mélangés avec une solution organique et du TBP. Cela donnera une extraction de l'uranium et du plutonium de la phase liquide à la phase organique. Cette extraction est réalisée à travers une réaction de complexation entre le soluté (dans la phase aqueuse) et le TBP (dans la phase organique), qui a lieu à l'interphase. Un exemple de ceci peut être l'extraction de l'uranium[1], pour lequel la réaction d'équilibre avec les solutés dans la phase organique peut être représentée par [4]:

$$n\mathrm{H_2O} + \mathrm{UO_{2\,aq}^{2+}} + 2\mathrm{NO_{3\,aq}^{-}} + 2\mathrm{TBP} \rightarrow (\mathrm{UO_2(NO_3)_2}, 2\mathrm{TBP(H_2O)}_n)_{\mathrm{org}} \tag{1.1}$$

pour lequel la loi d'action de masse donne

$$K_{\mathrm{U(VI)}} = \frac{[\mathrm{UO_2(NO_3)_2}, 2\mathrm{TBP}]_{\mathrm{org}}}{\left[\mathrm{UO_2^{2+}}\right]_{\mathrm{org}} \left[\mathrm{NO_3^{-}}\right]_{\mathrm{aq}}^2 [\mathrm{TBP}]_{\mathrm{org}}^2} \cdot \frac{\gamma_{\mathrm{U(VI)_{org}}}}{\gamma_{\mathrm{U(VI)_{aq}}} \gamma_{\mathrm{NO_{3aq}}}^2 \gamma_{\mathrm{TBP_{org}}}^2} \tag{1.2}$$

pour la constante d'équilibre d'extraction. Dans cette équation $[X]$ et γ_X représentent la concentration et le coefficient d'activité de l'espèce X dans la phase donnée (aqueuse ou organique). Afin de déterminer les conditions de travail optimales pour ce processus, nous devons pouvoir calculer les coefficients d'activité ; en particulier ceux de la phase aqueuse. Normalement, ces coefficients sont calculés en adoptant des simples représentations semi–empiriques de solution ionique, comme celles fournies par le modèle de Pitzer ou le modèle de Zdanovskii–Mikulin, avec des paramètres ajustés pour reproduire les données expérimentales disponibles. Alors que des systèmes aussi complexes doivent forcement être décrits en utilisant des modèles simples, nous proposons qu'au lieu d'ajuster les paramètres de ce type de modèles, nous tentions de les déduire des descriptions atomiques plus précises. Nous cherchons ainsi à mettre en place une stratégie de « coarse–graining » qui pourra nous permettre d'aller d'une description à échelle atomique (où le soluté et le solvant sont traités de la même manière) à un modèle analytiquement soluble dans lequel nous prendrons en considération uniquement les degrés de liberté du soluté.

1.2 Plan de Travail

L'exemple donné ci–dessus montre la nécessité de développer une description à plusieurs échelles des ions en solution. En tout, nous considérerons trois niveaux distincts de description : (1) une description *ab–initio* atomique dans laquelle on tient compte des degrés de liberté électroniques, (2) un modèle atomique classique où les interactions entre les atomes et les molécules sont menés par des champs de force classiques et (3) une description à solvant continu. Une représentation schématique de ces différentes

[1] Dans un état d'oxydation (VI):

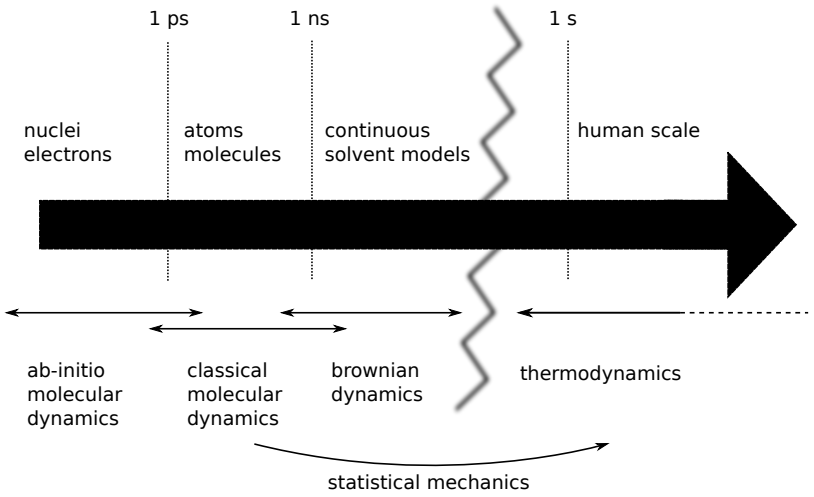

Figure 1.2: Un schéma représentant les différents échelles (et modèles) qui peuvent êtres utilisées pour décrire les solutions d'électrolytes.

échelles, avec ses modèles et méthodes de simulation correspondants, est donnée dans la Figure1.2. Dans le chapitre suivant, nous donnerons les concepts théoriques de base nécessaires pour comprendre et interpréter le travail qu'on a réalisé. Ensuite, nous rentrerons dans le travail proprement de la thèse. Tout d'abord, nous montrerons comment faire le lien entre le niveau 1 et 2 en déduisant les champs de force classiques pour des ions en solution à partir de calculs *ab–initio*. Après cela, nous montrerons comment établir un lien similaire entre les niveaux 2 et 3, nous permettant de définir des potentiels effectifs ion–ion pour un modèle à solvant continu. Même si cette approche réduit énormément la complexité du système, elle nécessite toute de même des coûteuses simulations numériques, mais elle reste pratiquement la seule réalisable pour le calcul des activités en solution. La partie suivante montre comment déduire des modèles analytiques simples (en fonction des sphères dures chargées, éventuellement associées) à partir des potentiels effectifs ion–ion. On constatera que l'additivité des tailles, utilisée dans les solutions MSA et BIMSA mises en oeuvre pour décrire ces systèmes de sphères dures est incompatible avec la structure microscopique des électrolytes, aussi, le chapitre suivant se centre sur le développement de modèles non additifs pour les électrolytes. La thèse se termine en proposant la mise au point d'une analyse similaire pour la viscosité des électrolytes, obtenu à partir d'une base moléculaire par une théorie de couplage de mode.

1.3 Résumé

Ici nous proposons un résumé détaillé de notre travail et les résultats principaux que nous avons obtenus.

Effets spécifiques à partir d'une description *ab–initio*

Nous commençons notre travail en déduisant des champs de force classiques à partir d'une description *ab–initio* basée sur la théorie de la fonctionnelle de la densité (DFT). En adoptant l'approximation de Born–Oppenheimer, les noyaux peuvent être traités comme des particules classiques qui évoluent sur la surface d'énergie potentielle créée

par les électrons. Grâce au théorème de Hohenberg et Kohn, la force subie par les noyaux, peut être déterminée à partir de la densité électronique, en nous épargnant le calcul de la solution de l'équation de Schrödinger pour un système d'électrons qui interagissent entre eux. En utilisant la méthode de Kohn et Sham, cette densité électronique est facilement évaluée en fonction de propriétés à un seul électron. Cette formulation de type « Density Functional Theory » (DFT) est en principe exacte, mais plusieurs approximations doivent être introduites pour que la solution du problème soit obtenues dans un laps de temps raisonnable. Les approximations principales sont les suivantes : (1) l'utilisation d'un pseudo potentiel pour remplacer les électrons fortement liés au noyau, (2) l'utilisation d'une base finie d'ondes planes pour représenter les orbitales et (3) l'utilisation des fonctionnelles locales simples pour approximer l'énergie d'échange et corrélation.

Les deux problèmes principaux de la DFT sont: (1) le fait qu'elle fournit une densité électronique qui est délocalisée dans l'espace, ce qui est difficile à interpréter en fonction des propriétés locales et, (2) l'impossibilité de la plupart de fonctionnelles d'échange et corrélation de décrire adéquatement les interactions de dispersion. Heureusement, ces deux problèmes peuvent être résolus en utilisant les fonctions de Wannier de localisation maximale. Celles–ci sont obtenues à partir d'une transformation unitaire des orbitales canoniques de Kohn et Sham. Cette transformation est choisie pour que les orbitales aient l'extension la plus réduite possible, ce qui permet de les attribuer à des atomes ou à des molécules individuelles. Une fois que ces orbitales sont connues, les interactions de dispersion (au deuxième ordre) sont facilement calculées en utilisant une méthode développé par Silvestrelli et généralisée par Aguado et al [5].

Nous avons réalisé des simulations de dynamique moléculaire (MD) pour une série d'ions monovalents dans l'eau afin de générer une trajectoire suffisamment longue et adéquate pour nos calculs DFT. Ensuite, nous avons utilisé l'information fournie par les fonctions de Wannier pour étudier la réponse de la densité électronique locale à un champ électrique extérieure. A partir de cela, nous pouvons calculer les polarisabilités des ions en solution. Ceci est important parce qu'il n'existe pas des données expérimentales pour les polarisabilités en phase condensée. Nos résultats, donnés dans le Tableau 1, montrent une décroissance dans les polarisabilités des anions en solution par rapport à leurs valeurs en phase gazeuse tandis que les valeurs des cations ne changent pratiquement pas.

Finalement, en utilisant un simple schéma de « force–matching », nous paramétrons les champs de force classiques pour reproduire les forces données par les calculs *ab–initio* (avec la correction de dispersion). Les champs de force pour une série de cations monovalents ont été utilisés dans des simulations de dynamique moléculaire (MD) pour comparer les prédictions données par nos potentiels aux données expérimentales connues. Nous avons reproduit une large gamme de propriétés d'équilibre et dynamique, telles que les distances de contact moyen ion–eau, les nombres de coordination, les énergies libres d'hydratation et les coefficients d'auto–diffusion. Dans tous les cas, on obtient un très bon accord avec les expériences.

Descriptions moléculaires à solvant continu

Nous savons qu'il est possible d'obtenir des champs de force « précis » directement des calculs *ab–initio*, mais la quantité de propriétés thermodynamiques qui peuvent être mesurées avec des simulations de MD est assez réduite. Les propriétés ion–eau sont facilement obtenues mais les propriétés ion–ion (tels que les coefficients d'activité) sont

presque impossibles à calculer directement. Même si la théorie de Kirkwood–Buff , qui est exacte, peut être utilisée dans ce but, les temps de simulation requis sont trop longs. Une autre approche est fournie par la théorie des électrolytes en solution de McMillan–Mayer. Cette théorie, qui est aussi exacte, nous permet de réaliser le calcul des propriétés thermodynamiques des ions en trois étapes : premièrement, on fait la moyenne sur les degrés de liberté du solvant et on mesure les corrélations ion–ion. Deuxièmement, on utilise cette information pour définir des potentiels effectifs ion–ion pour un modèle solvant continu, où il n'y a que des ions. Dernièrement, les propriétés thermodynamiques structurales sont mesurées en faisant des simulations Monte–Carlo (MC) pour ce système simplifié. Le fait d'avoir enlevé les molécules d'eau réduit énormément le nombre de de degrés de liberté, ce qui rend la simulation beaucoup plus rapide.

Malgré le fait que la théorie de McMillan–Mayer est rigoureusement exacte, elle dépend des potentiels de force moyenne (PMF) à n–corps qu'on ne peut pas calculer. Ainsi, l'approximation usuellement utilisée est de considérer que les potentiels sont additifs par paire. Pour éviter des calculs complexes nécessaires pour calculer le PMF à deux corps, nous avons utilisé une équation intégrale pour déduire le potentiel effectif des corrélations ion–ion obtenues par des simulations de MD (solvant explicite). Grâce à sa simplicité et à la précision avec laquelle elle décrit les systèmes ioniques, nous avons choisi d'utiliser l'équation intégrale HNC («hyper–netted chain») donnée dans l'équation (5.1). Cette équation donne un lien direct entre les fonctions de distribution radiale ion–ion et les potentiels d'interaction correspondants. Malheureusement, elle nécessite que les fonctions de distribution soient connues pour toutes les distances ou, au moins jusqu'au point où les fonctions ont convergé à leur valeur asymptotique. Puisque ceci n'est pas possible pour les simulations qu'on utilise, il est nécessaire de corriger ce comportement à longue distance. Nous utilisons une méthode d'inversion qui utilise deux relations exactes pour les systèmes ioniques (les lois d'addition de Stillinger–Lovett) pour ajuster le comportement à longue distance (à petit vecteur d'onde) des fonctions de distribution radiale. Ceci nous permet de fixer sans ambiguïtés le niveau de référence de nos potentiels interactions et de retrouver leur valeur asymptotique espérée. Ces potentiels effectifs sont naturellement décomposés en une interaction à courte portée (moyennée sur le solvant) et une interaction de Coulomb à longue portée. La première de ces deux contributions est celle qui contient les effets spécifiques des ions.

Nous avons étudié deux types de systèmes : (1) les sels simples halogenures alcalino–terreux et (2) les sels de chlorure de lanthanides. Pour le premier système, nous prenons des combinaisons des cations Li^+, Na^+ et K^+ avec des anions Cl^-, Br^- et I^-, et pour le deuxième système, nous prenons les cation La^{3+}, Nd^{3+}, Eu^{3+}, Dy^{3+} et Lu^{3+} comme représentant la série de lanthanides. Les fonctions de distribution radiale obtenue des simulations à concentration finie ($c \simeq 0,5\,\mathrm{mol.L^{-1}}$) sont ensuite utilisées dans notre procédure d'inversion HNC pour déduire des potentiels effectifs ion–ion. Les résultats que nous avons obtenus pour les alcalins sont donnés dans les figures (5.3) et (5.4). Les résultats pour les lanthanides sont donnés dans la figure (5.11). Dans les deux cas, les potentiels cation–cation et anion–anion sont assez bien représentés par des potentiels de sphères dures chargées : les potentiels à courte portée sont très répulsifs à courte distance et ils présentent des faibles oscillations à longue distance (les oscillations sont toujours en dessous de l'énergie thermique de fluctuation). Par contre, les potentiels cation–anion présentent une structure assez particulière qui ne peut pas être représentée en termes de sphères dures. Ces potentiels ont deux minima locaux séparés par une barrière

d'énergie potentielle importante ($> k_{\mathrm{B}}T$). Le premier minimum correspond à la paire au contact (CIP) tandis que le deuxième minimum correspond à la paire séparée par une molécule d'eau (SSIP). La stabilité relative de ces deux configurations est déterminée par l'énergie libre de solvatation. De plus, en utilisant le modèle d'association généralisant celui de Bjerrum, les potentiels cation–anion peuvent être utilisés pour déterminer les constants d'association d'équilibre K_0. La valeur de K_0 pour les alcalins est présentée dans le tableau 5.2. Ces valeurs permettent de quantifier la stabilité de la CIP à partir desquelles nous pouvons constater que les sels Li^+ sont les moins associés et les K^+ sont les plus associés et les sels Na^+ ont un comportement intermédiaire. Les valeurs de K_0 pour les lanthanides sont données dans le tableau 5.4. Nous récupérons l'ordre espéré dans la série de lanthanides et nos résultats sont en très bon accord avec les résultats obtenus par Ruas et al. [6] qui les ont ajustés au modèle BIMSA pour récupérer les coefficients osmotiques expérimentaux.

Nous utilisons ces potentiels pour réaliser les simulations MC sur plusieurs concentrations. Pour rester simples, nous avons supposé que la dépendance à n corps des potentiels peut être négligée, ce qui devrait être une approximation valide jusqu'aux concentrations molaires. Le bon accord entre les fonctions de distribution radiale obtenues à partir des deux niveaux de description (solvant explicite et solvant continu) montrent la validité du processus d'inversion. Les coefficients osmotiques des solutions sont facilement mesurables dans les simulations MC étant donné qu'ils correspondent à la pression du gaz de solutés. Les comparaisons avec les coefficients osmotiques expérimentaux (avec la conversion au système de référence de McMillan–Mayer) montrent un accord acceptable. Ces résultats sont présentés dans les figures 5.7 et 5.13. Globalement, l'ordre dans les coefficients osmotiques, en fonction de l'anion, est reproduit. Cependant, cette comparaison est d'autant plus intéressante que les champs de force atomiques que nous avons utilisés dans les simulations MD n'ont pas du tout été ajustés pour redonner les bonnes valeurs des activités ioniques. Un test important serait de calculer les coefficients osmotiques directement à partir des simulations MD, en utilisant la théorie de KB, mais c'est précisément pour éviter ces calculs beaucoup trop longs pour en déduire les activités avec une précision suffisante que nous avons développé notre méthode de «coarse–graining».

D'une description moléculaire aux modèles primitifs

Même si les potentiels effectifs fournissent une description adéquate pour des solutions d'électrolytes, qui ne fait référence qu'aux degrés de liberté des solutés, la description a toujours besoin d'une simulation numérique relativement coûteuse. Pour des applications industrielles, où des solutions analytiques explicites sont nécessaires, il est clair qu'on doit simplifier encore plus nos modèles. Pour accomplir cela, nous utilisons la théorie des perturbations des fluides. L'idée est simple, nous voulons établir un lien entre les propriétés du système modèle (qui n'a pas de solution analytique) et celles d'un système de référence connu. Il est possible de déduire un développement en série de l'énergie libre du système modèle autour de l'énergie libre de référence (Eq. (6.1)), dans laquelle les coefficients dans le développement sont obtenus comme des moyennes prises dans l'ensemble du système de référence. Au premier ordre, nous avons besoin juste de l'énergie libre et les fonctions de distribution radiale du système de référence au même temps que l'énergie de perturbation (Eq. (6.2)). En outre, ce développement au premier ordre est aussi une borne supérieure rigoureuse. Cela signifie que pour n'importe quelle référence que nous choisissons, l'énergie donnée par ce développement

sera toujours au–dessus de l'énergie libre du système modèle. Grâce à cette inégalité de Gibbs–Bogoluibov, la procédure pour déduire le meilleur modèle simple est directe : une fois le système de référence est choisi et adéquatement paramétré, le développement de l'énergie libre (au premier ordre) est minimisée. Tout ce qui reste à faire est de choisir le meilleur système de référence possible. Évidemment, lorsque la référence s'approche le plus du système modèle que nous voulons étudier, les résultats seront meilleurs.

Pour les solutions d'électrolytes, le premier choix est celui d'un système de sphères dures chargées pour lequel la solution MSA fournit des expressions analytiques pour les propriétés thermodynamiques et structurales (l'énergie libre et les fonctions de distribution radiale). Malheureusement, lorsque nous utilisons des potentiels de référence avec des singularités, une partie de l'espace de configuration du système modèle sera systématiquement négligée. Cela nous amène à une erreur intrinsèque dans les calculs de perturbation qui doit absolument être prise en compte. Cela signifie que nous ne pouvons pas fournir une description adéquate en utilisant un modèle à deux composants. Ceci est dû au fait que les potentiels effectifs d'interaction cation–anion présentent deux minima qui sont impossibles à représenter en utilisant juste une distance de moindre approche. La solution que nous proposons est de traiter le CIP et le SSIP indépendamment. Du coup, nous allons considérer un système associé à trois composants comme la référence dans nos calculs de perturbation.

Pour les systèmes de référence à trois composants nous avons utilisé deux représentations pour la paire : (1) comme une sphère neutre et (2) comme un «dumbbell» dipolaire. Dans le premier cas, l'énergie libre et les fonctions de distribution radiale sont facilement obtenues à partir de la solution MSA. Dans le deuxième cas, nous utilisons la solution BIMSA pour la thermodynamique et la solution MSA pour les fonctions de distribution radiale (en considérant un système de sphères dures équivalent). Afin de corriger les régions négatives (non–physiques) qui peuvent apparaître dans les fonctions de distribution radiale données par MSA, nous utilisons une approximation exponentielle. Avant de réaliser les calculs de perturbation, il est nécessaire d'établir une relation entre les propriétés de ce système à trois composants et celles du système originale à deux composants. Pour les calculs de perturbation nous avons besoin d'une relation entre les énergies libres et les potentiels effectifs de ces deux systèmes ; pour comparer les résultats prédits par notre modèle primitif avec ceux du modèle moléculaire (MC ou MD) nous avons aussi besoin d'une relation entre les fonctions de distribution radiale des systèmes à deux et à trois composants.

En utilisant un formalisme de fonction caractéristique, nous avons établi une relation entre les énergies libres des deux systèmes qui est exacte à dilution infinie. La différence entre les énergies libres correspond au potentiel chimique de la paire. En prenant les interactions moyennées sur les rotations entre un ion libre et une paire (dipôle), et entre deux dipôles, nous avons aussi obtenu des relations approximatives pour les potentiels d'interaction de la paire (en fonction des potentiels entre les ions dans le système à deux composants). Les équations qui définissent les potentiels paire–ion et paire–paire sont données dans l'équation (6.52). Un calcul similaire de champ moyen et de dilution infinie permet d'établir un lien entre les fonctions de distribution radiale du système à trois composants avec celle dus système à deux composants. Cette relation est donnée dans l'équation (6.67).

Les potentiels effectifs pour les neuf sels alcalins que nous avions obtenu ont été

utilisés dans des calculs PFT pour déduire le meilleur modèle analytique (au premier ordre) pour ces systèmes. Lorsque nous comparons les énergies libres des différents modèles que nous avons utilisé (pour les différents systèmes de référence et les différents paramétrisations de la paire) avec les valeurs exactes calculées par MC, nous avons observé ceci : (1) Le modèle non–associé à deux composants est trop répulsif (pas assez attractif). Ceci est dû au fait qu'un tel modèle néglige complètement la paire au contact. (2) La paramétrisation précise de la paire n'est pas importante. Nous avons utilisé quatre paramétrisations et elles donnent toutes, essentiellement, les mêmes résultats jusqu'aux concentrations molaires. (3) L'inégalité de Gibbs–Bogoluigov est toujours satisfaite. Même si c'est une relation exacte, qui devrait toujours être vrai, le fait d'avoir utilisé des solutions approximatives (MSA et BIMSA) pour calculer les énergies libres et les fonctions de distribution radiale de référence permettrait une possible exception à cette règle. Le fait qu'il n'y ait pas d'exception est une façon de valider a posteriori les différentes approximations que nous avons utilisées. (4) Nous avons obtenu des très bons accords avec les résultats exacts. L'erreur relatif entre les prédictions de notre modèle finale et les calculs exacts est de l'ordre de $10 \sim 20\%$ jusqu'aux concentrations molaires. (5) Les diamètres optimaux, déduits par la minimisation, sont essentiellement indépendants de la concentration. (6) Les fonctions de distribution radiale cation–anion, obtenus en utilisant une représentation à trois composants, peuvent prendre en compte la CIP et la SSIP (ce qui n'est pas possible avec une représentation à deux composants). Les paramètres finaux de notre modèle sont donnés dans le tableau (6.3). Une comparaison entre les résultats exacts et les valeurs prédites par notre modèle pour les énergies libres et les coefficients osmotiques est donné dans les figures (6.9) et (6.10).

Perspectives

Nous concluons cette thèse en proposant deux perspectives possibles pour continuer avec le développement d'une description multi-échelle des ions en solution. D'abord, étant donné que la non-additivité des potentiels effectifs a été le principal problème auquel nous nous sommes confrontés pour établir un modèle primitif des électrolytes (en termes de sphères dures chargées), nous envisageons qu'une théorie de perturbation spécialement conçue pour traiter des potentiels de perturbations infinis peut être utilisée pour déterminer les propriétés thermodynamiques et structurales d'un système de sphères dures non-additives. Ceci est important car tous les modèles de sphères dures (comme Percus-Yevick ou MSA) supposent que les diamètres sont additifs. Il n'existe pas une solution analytique pour ce genre de modèles si les diamètres ne sont pas additifs. La théorie que nous proposons est une extension de celle développée par Sillren et Hansen [7, 8], qui ont montré qu'au lieu d'utiliser un développement en série du potentiel $v(r)$, il est plus pratique de le faire avec le facteur de Boltzmann ($\exp(-\beta v(r))$). En effet, même si le potentiel tend vers l'infini, cette quantité restera dans tous les cas finie. Nous montrons comment un tel développement doit être évalué, pour un système à plusieurs composants, au premier ordre pour la structure et à deuxième ordre pour l'énergie libre. Nous finissons en donnant un exemple pour le cas d'un système simple de sphères dures, à deux composantes A et B, avec une non-additivité dans l'interaction A–B.

Finalement, nous essayons de mettre au point une procédure similaire pour étudier les propriétés de transport des ions en solution (jusqu'ici nous avons seulement considéré les propriétés thermodynamiques d'équilibre). Nous nous sommes particulièrement intéressé à la viscosité des électrolytes. À la différence des autres coefficients de transport,

comme les coefficients d'autodiffusion, de diffusion mutuelle ou la conductivité, aucun réel progrès n'a été possible pour la viscosité depuis les travaux originaux d'Onsager, Fuoss et Falkenhagen dans les années 1930 [9]. Leur théorie, qui est basée sur le modèle de charges ponctuelles de Debye et Hückel, est seulement valide à très basse concentration et elle est incapable de décrire les effets spécifiques (elle donne uniquement la contribution ionique d'excès). Expérimentalement, il est observé que la contribution dominante à la viscosité est linéaire en concentration c (au moins jusqu'aux concentrations molaires) et est caractéristique de chaque ion. C'est ce terme linéaire (qui donne le coefficient de Jones-Dole) qu'il n'a pas été jusqu'à présent possible d'expliquer à partir d'une base moléculaire, car il peut être positif pour certains ions et négatif pour d'autres. Ce phénomène est parfois considéré comme étant une conséquence de la nature faiseur ou briseur de structure du solvant («structure-maker» ou «structure- breaker») de chaque ion, mais il n'existe aucune théorie microscopique capable d'expliquer ce phénomène. Un premier pas vers une telle théorie de la viscosité a été récemment donne par Chandra et Bagchi [10], qui ont utilisé une théorie de couplage de modes pour trouver une expression analytique pour la viscosité d'excès ionique qui dépend uniquement des facteurs de structure ion–ion. En utilisant cette théorie ils ont été capables d'en déduire exactement la loi limite de Debye-Falkenhagen pour la viscosité. Nous avons essayé de généraliser leur théorie pour qu'elle prenne en compte l'effet du solvant. Au premier ordre en c, nous devons seulement considérer le terme ion-ion et solvant-solvant. Pour le premier, nous utilisons la solution donnée par MSA pour les facteurs de structure, tandis que pour le deuxième nous utilisons des résultats obtenus par des simulations de dynamique moléculaire. En tout, il y a trois contributions à la viscosité: (1) un terme de collision à temps court, (2) un terme ion-ion à temps long et (3) un terme solvant-solvant à temps long. La contribution à temps court est calculée en utilisant la théorie d'Enskog (pour un système effectif de sphères-dures), et les contributions à temps long sont calculées en utilisant la théorie de couplage de mode. De ces trois termes, tous sont positifs, sauf la contribution solvant-solvant calculée par le couplage de mode, qui est toujours négative. C'est la compétition entre ces trois termes qui va déterminer si le coefficient de Jones-Dole est négatif ou positif (Figure 8.7). Nous avons ainsi réussi pour la première fois à expliquer pourquoi certains ions peuvent diminuer la viscosité du solvant. Cette première approche pourra être améliorée en particulier en précisant différemment la séparation entre les contributions aux temps court et long, qui est nécessaire pour calculer le terme de couplage de mode, ou en tenant compte de la rotation des molécules de solvant.

Chapter 2

Introduction

Summary

2.1 The Importance of a Multi-Scale Description

Ions in solution play a fundamental role in many physical, chemical, biological, and industrial processes. They not only help to regulate basic cellular functions [2], but they also participate in the destruction of the ozone layer [3] and dictate how the reprocessing and storage of spent nuclear fuel can be performed [4]. Although computer simulations have helped us develop a detailed understanding of the microscopic properties involved in these types of phenomena, the link with macroscopic thermodynamics, which we probe experimentally, is not always easy to establish. Furthermore such simulations require considerable computational resources, taking in some cases several weeks or months to finish. For these reasons, most engineering solutions adopt the simplest possible models able to reproduce the available experimental data, and then adjust the parameters to do exactly that.

The goal of this work is to develop a multi-scale description of ions in solution, allowing us to go from a fully microscopic description (determined by atomic-scale simulations), to a mesoscopic model suitable for engineering applications. The reasons for doing this are twofold. First, such a process allows us to give a physical interpretation (explanation) of the simple models *required* to study the complex systems typically encountered within industrial settings. It is not enough to say that a given model works (i.e. reproduces the experimental data), we should also be able to explain *why* it works. Second, if done correctly, this procedure requires no external experimental data. This is particularly important for nuclear applications, where experiments are notoriously difficult to perform. To give an idea of what we expect from a successful multi-scale description of ions in solution, we will briefly review the PUREX process (which is an acronym for **P**lutonium-**U**ranium **R**efining by **Ex**traction) used in the treatment of spent nuclear fuel [4], as it illustrates nicely the benefits and the need of a multi-scale approach.

Context: The PUREX process

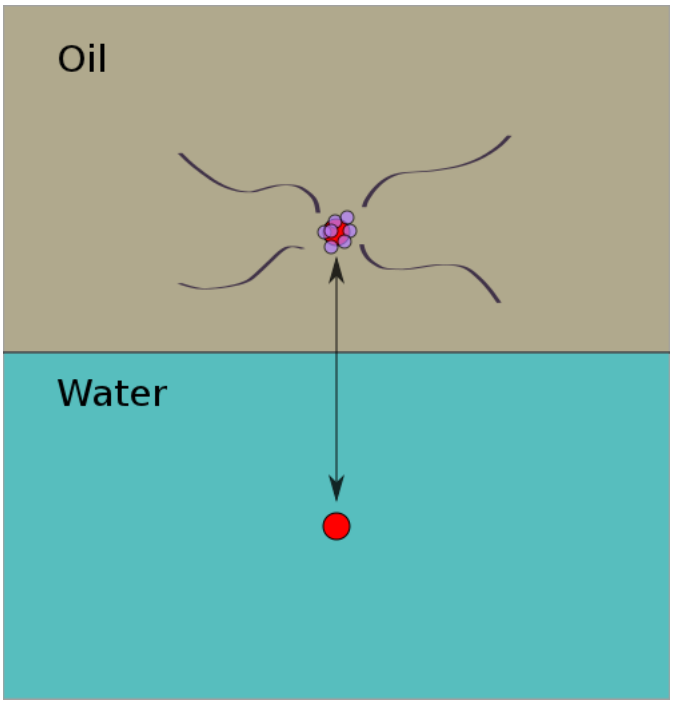

Figure 2.1: A schematic representation of the PUREX (liquid-liquid extraction) process used in the recycling of spent nuclear fuel.

Developed in the 1940s as part of the Manhattan project, the PUREX process [4] was later extended for non-military industrial use, and has since become the *de-facto* standard for the recycling of spent nuclear fuel from water reactors. At the end of the nuclear cycle, when the fuel is removed from the reactor, it not only contains the transmutation and fission products (the most important of which are the highly radiotoxic "minor" actinoids: Np, Am, and Cm), but also a considerable amount of fissile material (Plutonium and Uranium), which could be reused. The PUREX process was designed precisely to recover this Plutonium and Uranium. Besides providing fresh nuclear fuel, it reduces the volume of the waste and its radioactivity, making it much easier to store.

The PUREX process is a liquid-liquid extraction procedure which uses the high selectivity of a particular organic molecule, TBP (Tributyle Phosphate), to extract the major actinoids (U and Pu) from the spent nuclear fuel. A (very) schematic representation of the process is given in Figure 2.1. The nuclear waste is dissolved in a solution of aqueous nitric acid and mixed with an organic solution of TBP. This results in an extraction of the Uranium and the Plutonium from the liquid to the organic phase. This extraction is performed through a complexation reaction between the solutes (in the aqueous phase) and the TBP (in the organic phase), which occurs at the interface of the two phases. As an example, we can consider the extraction of Uranium[1], whose

[1]Besides having to consider all the different elements present in the solution, one must also take into account the different oxydation states in which they can be present. The example presented here corresponds to the extraction of Uranium (VI).

equilibrium reaction with the aggregates in the organic phase can be represented by [4]

$$n\mathrm{H_2O} + \mathrm{UO}^{2+}_{2\,\mathrm{aq}} + 2\mathrm{NO}^{-}_{3\,\mathrm{aq}} + 2\mathrm{TBP} \rightarrow (\mathrm{UO_2(NO_3)_2}, 2\mathrm{TBP(H_2O)}_n)_{\mathrm{org}} \tag{2.1}$$

for which case the mass-action law gives

$$K_{\mathrm{U(VI)}} = \frac{[\mathrm{UO_2(NO_3)_2}, 2\mathrm{TBP}]_{\mathrm{org}}}{\left[\mathrm{UO}^{2+}_2\right]_{\mathrm{org}} \left[\mathrm{NO}^{-}_3\right]^2_{\mathrm{aq}} [\mathrm{TBP}]^2_{\mathrm{org}}} \cdot \frac{\gamma_{\mathrm{U(VI)_{org}}}}{\gamma_{\mathrm{U(VI)_{aq}}} \gamma^2_{\mathrm{NO_{3aq}}} \gamma^2_{\mathrm{TBP_{org}}}} \tag{2.2}$$

for the equilibrium extraction constant. In this equation $[X]$ and γ_X represent the concentration and the activity coefficient of species X in the given phase (aqueous or organic). To determine the optimal working conditions for this process, we must be able to calculate the activity coefficients. In particular, for the the aqueous phase. Normally, this has been done by adopting simple semi-empirical representations of ionic solution, such as those provided by the Pitzer or the Zdanovskii-Mikulin model, and fitting the parameters to reproduce the available experimental data. While such complicated systems must necessarily be described using these types of simple models, we propose that instead of fitting their parameters, they should be derived from more *exact* atomistic descriptions. We thus seek to put in place a coarse-graining strategy that will allow us to go from an atomic scale description (where the solute and solvent are treated equally) to an analytically solvable model in which only the solute degrees of freedom are considered.

2.2 Plan of our Work

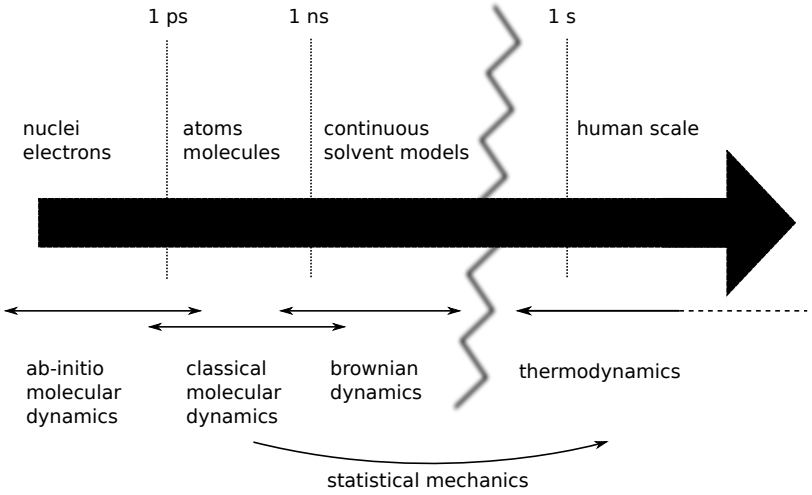

Figure 2.2: Schematic representation of the different scales, and models, that can be used to describe electrolyte solutions. Note that Monte-Carlo (MC) simulations can be performed at any level of description; we will employ them only for the continuous solvent models.

The example given above has shown the necessity of developing a multi-scale description of ions in solution. In total, we will consider three distinct levels of description: (1) an *ab-initio* atomistic description, in which the electronic degrees of freedom are

taken into account, (2) a classical atomic scale model, where the interactions between atoms and molecules are given by classical force-fields, and (3) and implicit solvent description. A schematic representation of the different scales, with their corresponding models and simulation methods, are given in Fig. 2.2. In the next chapter, we briefly cover the basic theoretical concepts needed to understand and interpret the work we have carried out. In the following chapter, we show how to provide a link between levels (1) and (2), i.e. how to obtain a classical potentials for ions in solution from *ab-initio* (density functional theory) calculations. We then show how the same link can be established between levels (2) and (3), allowing us to define effective ion-ion potentials for an implicit solvent model. While this greatly reduces the complexity, it still requires costly numerical simulations. The following part shows how simple analytical models, in terms of charged hard-spheres, can be derived from the effective ion-ion potentials. As the additivity of the MSA and BIMSA theories we use to describe these hard-sphere systems is shown to be incompatible with the microscopic structure of *real* electrolytes, the following part of our work is focused on the development of non-additive models. Finally, we try to develop a similar (simple) description for the viscosity of electrolytes, by using the information derived from atomistic simulations within a Mode-Coupling Theory to study the solute-solvent effects.

Chapter 3

Basic Concepts in the Theory of Electrolytes

Summary

We begin with a brief overview of the standard theoretical framework used to describe ionic solutions. First, we summarize the basic principles of Classical Statistical Thermodynamics, the branch of Physics which provides *the* link between a microscopic description and a macroscopic one, between mechanics (equations of motion) and thermodynamics (state variables). It is not surprising then, that it provides the framework needed to derive realistic models of electrolyte solutions. From a simulation point of view, the toolbox of Statistical Mechanics not only determines what can be measured, but also how it should be measured. We proceed by summarizing the two exact theories used to study electrolytes: the Kirkwood-Buff (explicit solvent) and the McMillan-Mayer (implicit-solvent) theories. No attempt is made at providing a complete description of the different theoretical concepts introduced in this chapter, nor do

we pretend to give rigorous derivations for the different formulae presented; instead, we have tried to provide a brief, self-contained, summary of the theory used throughout this work. The interested reader should turn to the standard textbooks in statistical mechanics [11, 12, 13, 14, 15, 16] and the theory of liquids [17, 18].

3.1 Statistical Thermodynamics of Simple Liquids

3.1.1 Statistical Averages and Distributions

Consider a macroscopic system of volume V with N identical (point) particles. The state of such a system, at any given time, is completely specified by the N generalized coordinates $\{\boldsymbol{q}_i\}$ and momenta $\{\boldsymbol{p}_i\}$, where the bold-symbols are used to represent vector quantities. These variables define a point $\Gamma = (\boldsymbol{q}_1, \ldots, \boldsymbol{q}_N, \boldsymbol{p}_1, \ldots, \boldsymbol{p}_N)$ in the $6N$-dimensional *phase space*. As the system evolves in time, this point will describe a trajectory within the phase space that is entirely determined by Hamilton's equations of motion [11, 14]

$$\dot{\boldsymbol{q}}_i = \frac{\partial \mathcal{H}}{\partial \boldsymbol{p}_i} \qquad \dot{\boldsymbol{p}}_i = -\frac{\partial \mathcal{H}}{\partial \boldsymbol{q}_i} \tag{3.1}$$

where the Hamiltonian $\mathcal{H}$ is defined as

$$\mathcal{H} = K_N + V_N + \Phi \tag{3.2}$$

with K_N and V_N, the kinetic and (internal) potential energies, respectively, and Φ the energy due to any possible external potentials. For a macroscopic system, the value of a given property $\mathcal{A}(\Gamma)$, a function of the position and momenta of the particles at a particular moment in time, is of no practical interest. Its average, on the other hand, is an intrinsic property of the system. There are two ways of measuring these averages: (1) as a time average $\overline{\mathcal{A}}$ over the trajectory (Boltzmann method) or (2) as an ensemble average $\langle \mathcal{A} \rangle$ (Gibbs method). If the system is ergodic, these two averages are equivalent [15]

$$\overline{\mathcal{A}} = \langle \mathcal{A} \rangle \tag{3.3}$$

The time average $\overline{\mathcal{A}}$ is formally defined as

$$\overline{\mathcal{A}} = \lim_{\tau \to \infty} \frac{1}{\tau} \int_0^\tau \mathrm{d}t \mathcal{A}(\Gamma(t)) \tag{3.4}$$

where $\Gamma(t)$ is the phase-space trajectory described by a point initially at $\Gamma(0)$ at $t = 0$. Notice that $\mathcal{A}$ depends on time implicitly, through its dependence on Γ, its time evolution is therefore governed by the Liouville operator $\mathcal{L}$ [17]

$$\frac{\mathrm{d}\mathcal{A}(\Gamma(t))}{\mathrm{d}t} = i\mathcal{L}\mathcal{A}(\Gamma(t)) \tag{3.5}$$

$$\mathcal{L} \equiv i\{\mathcal{H}, \} \tag{3.6}$$

where $\{\,,\,\}$ is the Poisson bracket

$$\{\mathcal{A},\mathcal{B}\} = \sum_i^N \left(\frac{\partial \mathcal{A}}{\partial \boldsymbol{r}_i} \cdot \frac{\partial \mathcal{B}}{\partial \boldsymbol{p}_i} - \frac{\partial \mathcal{A}}{\partial \boldsymbol{p}_i} \cdot \frac{\partial \mathcal{B}}{\partial \boldsymbol{r}_i} \right) \tag{3.7}$$

such that

$$A(\Gamma(t)) = e^{i\mathcal{L}t} A(\Gamma(0)) \tag{3.8}$$

This is the type of average one measures during a Molecular Dynamics simulation, where the positions and velocities of the particles are propagated in time $\Gamma(t)$ by solving Newton's equation of motion (which yield the same dynamics as $\mathcal{L}$).

The ensemble average of Gibbs [19] $\langle \mathcal{A} \rangle$ is defined through the use of statistical distributions $f(\Gamma)$ in phase space. The idea is as follows. We imagine a very large number $\mathcal{N}$ of identical copies of the system, each in the same macrostate (i.e. same energy), but in possibly different microstates Γ (i.e. different positions and velocities) compatible with the macrostate. We wish to compute the probability of observing a given state Γ. This is done by counting the total number $D(\Gamma)$ of systems, among all the $\mathcal{N}$ mental copies, which are within a region $\mathrm{d}\Gamma$ of Γ. The ratio between these two numbers defines the phase-space probability density $f(\Gamma) = \mathcal{D}(\Gamma)/\mathcal{N}$, such that the integral of $f(\Gamma)$ over a given region in phase-space will give the ratio between the number of systems in that region and the total number of systems. The genius of Gibbs' work was to realize that this ratio could be used to specify the probability that a given system, among the *ensemble* of mental copies, lies within the same region. The average of a given property $\mathcal{A}$ can then be computed as

$$\mathcal{A} = \int \mathrm{d}\Gamma A(\Gamma) f(\Gamma) \tag{3.9}$$

although it is usually expressed in terms of the relative (not normalized) probability distributions f'

$$\mathcal{A} = \frac{\int \mathrm{d}\Gamma A(\Gamma) f'(\Gamma)}{\int \mathrm{d}\Gamma f'(\Gamma)} \tag{3.10}$$

The quantity appearing in the denominator is the so-called partition function, which essentially gives the volume (number of states) of the phase-space. This is the main object of study within (equilibrium) Statistical Mechanics (if we know this, we know everything). These are the types of averages one measures during a Monte-Carlo simulation. In what follows, we give a brief account of the basic ensembles used to perform these measurements; where the difference among them is due to the different ways in which the macrostate of the system can be specified, each leading to a distinct form of $f(\Gamma)$. For simplicity we have only considered point particles in three-dimensional space, but the generalization to more complicated systems is straightforward [14].

Before proceeding, it is important to note that not all averages are created equal. Within a simulation, the time and ensemble averages defined by Equations (3.4) and (3.9), respectively, will only allow us to measure a particular kind of property. Namely, those which do not depend on the absolute value of the phase-space

volume. As such, we are unable to directly measure the partition functions $\int \mathrm{d}\Gamma f(\Gamma)$, or any of the thermodynamic potentials (the S, F, Ω, and G introduced below). However, we can measure the ratio of two such volumes, which means that the derivatives of these thermodynamic potentials can be directly obtained. Once we know the derivatives, the *difference* between the thermodynamic potentials at two distinct states can be obtained by a simple integration procedure.

Micro-Canonical Ensemble (NVE)

Consider an ensemble of closed and isolated systems. The macrostate of all these systems is specified by the number of particles N, the volume V, and the total energy E. As there is no macroscopic difference among them, the only difference being the position and momenta of their particles, it does not make sense to favor one configuration over another. The probability is then defined as being the same for all the microstates

$$f(\Gamma) = \begin{cases} \text{constant} & \text{if } H(\Gamma) = E \\ 0 & \text{otherwise} \end{cases} \tag{3.11}$$

and the micro-canonical partition function, which counts the number of valid microstates, is then given by

$$W = \frac{1}{N! h^{3N}} \int \mathrm{d}\Gamma \delta(\mathcal{H}(\Gamma) - E) \tag{3.12}$$

where h^{3N} is a measure of the "volume" of a particular state and the $N!$ term is needed to (approximately) correct for the over counting of states (as the particles are indistinguishable) [11, 14]. The contact with thermodynamics is given by the celebrated Boltzmann relation, which gives the entropy of the system as a function of the partition function [11]

$$S = k_\mathrm{B} \ln W \tag{3.13}$$

where k_B is the Boltzmann constant. From this, all other thermodynamic quantities are easily obtained. In particular the temperature T, pressure P, and chemical potential μ are given by

$$\begin{aligned} \mathrm{d}S &= \frac{1}{T}\mathrm{d}E + \frac{P}{T}\mathrm{d}V - \frac{\mu}{T}\mathrm{d}N \\ \frac{1}{T} &= k_\mathrm{B}\left(\frac{\partial \ln W}{\partial E}\right)_{N,V}, \; \frac{P}{T} = k_\mathrm{B}\left(\frac{\partial \ln W}{\partial V}\right)_{E,N}, \; \frac{\mu}{T} = k_\mathrm{B}\left(\frac{\partial \ln W}{\partial N}\right)_{E,V} \end{aligned} \tag{3.14}$$

Canonical Ensemble (NVT)

We again consider an ensemble of systems, with the same number of particles N and the same volume V, but now we allow for them to exchange energy with each other. Although the energy of any given system will fluctuate, the total energy (for the whole ensemble) remains constant, and at equilibrium the temperature will be the same for all of them. In this sense, every system is considered to be in contact with a heat bath

or thermostat (temperature T) formed by all the other systems. The probability distribution for this *canonical* ensemble can then be obtained by considering the number of ways in which the total energy can be partitioned among the different systems, and finding the most probable distribution [14]. This is naturally expressed as a constrained minimization problem, which is solved using Lagrange's method of undetermined multipliers. In this case, the Lagrange multiplier (which guarantees the conservation of energy : system + heat bath) is the inverse temperature $\beta^{-1} = k_{\mathrm{B}}T$. The other ensembles are derived in exactly the same manner: we open the systems, allowing for the exchange of some conserved quantity among themselves, and look for the best (most likely) way of performing this distribution.

The probability distribution $f(\Gamma)$ for this ensemble is given by the Boltzmann distribution [14]

$$f(\Gamma) \sim e^{-\beta H(\Gamma)} \tag{3.15}$$

The canonical partition function Q is then given by

$$Q = \frac{1}{N!h^{3N}} \int \mathrm{d}\Gamma e^{-\beta H(\Gamma)} \tag{3.16}$$

Since the momentum integrals can be performed analytically, each yielding a factor of $\sqrt{2\pi m k_{\mathrm{B}}T}$, we can simplify this equation to obtain

$$Q = \frac{1}{N!} \frac{Z}{\Lambda^{3N}} \tag{3.17}$$

where $\Lambda = \sqrt{h^2/2\pi m k_{\mathrm{B}}T}$ is the de Broglie wavelength for a particle of mass m, and Z is the configuration integral

$$Z = \int \mathrm{d}\boldsymbol{q}^N e^{-\beta V_N} \tag{3.18}$$

The associated potential, providing the link with thermodynamics, is the Helmholtz free energy F [14]

$$F = -k_{\mathrm{B}}T \ln Q \tag{3.19}$$

from which we may directly obtain the entropy S, pressure P, and chemical potential μ

$$\mathrm{d}F = -S\mathrm{d}T - P\mathrm{d}V + \mu \mathrm{d}N \tag{3.20}$$

$$S = k_{\mathrm{B}} \ln Q + k_{\mathrm{B}}T \left(\frac{\partial \ln Q}{\partial T}\right)_{N,V}, \; P = k_{\mathrm{B}}T \left(\frac{\partial \ln Q}{\partial V}\right)_{N,T}, \; \mu = k_{\mathrm{B}}T \left(\frac{\partial \ln Q}{\partial N}\right)_{V,T}$$

as well as the internal energy $U \equiv F + TS$

$$U = -\left(\frac{\partial \ln Q}{\partial \beta}\right)_{N,V}$$

Grand-Canonical Ensemble (μVT)

If we take the canonical ensemble NVT, and now allow for the systems to exchange particles among themselves, we obtain the grand-canonical ensemble. An additional Lagrange multiplier γ is introduced in order to fix the total number of particles in the ensemble. This new parameter $\gamma = -\beta\mu$ is directly related to the chemical potential of the reservoir μ, which (at equilibrium) should be the same for all the systems. The probability distribution for this ensemble is of the same Boltzmann form as before [14], and is given by

$$f(\Gamma, N) \sim e^{-\beta(\mathcal{H}(\Gamma)-\mu N)} \tag{3.21}$$

with the grand-canonical partition function Ξ defined as

$$\Xi = \sum_N \frac{1}{N!} \frac{e^{N\beta\mu}}{h^{3N}} \int \mathrm{d}\Gamma e^{-\beta H(\Gamma)} \tag{3.22}$$

By performing the integration over momenta, this equation can be written in terms of the N particle configuration integrals Z_N as

$$\Xi = \sum_N \frac{z^N}{N!} Z_N \tag{3.23}$$

where $z = \frac{e^{\beta\mu}}{\Lambda^3}$ is the activity. The link with thermodynamics is now given by the Grand-Potential Ω [14]

$$\Omega = -k_\mathrm{B} T \ln \Xi \tag{3.24}$$

from which the entropy S, pressure P, and number of particles follow directly

$$\mathrm{d}\Omega = -S\mathrm{d}T - N\mathrm{d}\mu - P\mathrm{d}V \tag{3.25}$$

$$S = k_\mathrm{B} \ln \Xi + k_\mathrm{B} T \left(\frac{\partial \ln \Xi}{\partial T}\right)_{V,\mu},\ N = k_\mathrm{B} T \left(\frac{\partial \ln \Xi}{\partial \mu}\right)_{V,T},\ P = k_\mathrm{B} T \left(\frac{\partial \ln \Xi}{\partial V}\right)_{V,T}$$

as well as the Helmholtz free energy

$$F = \Omega + N\mu \tag{3.26}$$

The fact that the Grand-Potential Ω is a function of only one extensive parameter (V) provides an additional relationship, since application of Euler's Theorem[1] gives $\Omega = -PV$.

Isobaric-Isothermal Ensemble (NPT)

Again, we start from the canonical ensemble, but now we open the systems to changes in volume. As the total volume of the ensemble must remain constant, we obtain an

[1]Let $f(x_1, \ldots, x_N; X_1, \ldots, X_M)$ be a homogeneous thermodynamic function of order n, which depends on x_i extensive variables and X_i intensive variables, Euler's theorem states that $nf = \sum_{i=1}^{N} x_i \frac{\partial f}{\partial x_i}$. By definition, all extensive thermodynamic variables are homogeneous of order 1 and all intensive variables homogeneous of order 0.

additional Lagrange multiplier of the form $\gamma = \beta PV$, where P is the pressure of the reservoir or barostat [14, 20]

$$f(\Gamma, V) \sim e^{-\beta(\mathcal{H}(\Gamma)+PV)} \tag{3.27}$$

The partition function for this ensemble is

$$\Delta = \frac{\beta P}{N! h^{3N}} \int \mathrm{d}V e^{-\beta PV} \int \mathrm{d}\Gamma e^{-\beta H(\Gamma)} \tag{3.28}$$

and the connection with thermodynamics is given by the Gibbs free energy G

$$G = -k_\mathrm{B} T \ln \Delta \tag{3.29}$$

from which we directly derive the entropy S, average volume V, and chemical potential μ

$$\mathrm{d}G = -S\mathrm{d}T + V\mathrm{d}P + \mu \mathrm{d}N \tag{3.30}$$

$$S = k_\mathrm{B} \ln \Delta + k_\mathrm{B} T \left(\frac{\partial \ln \Delta}{\partial T}\right)_{N,P}, \; V = -k_\mathrm{B} T \left(\frac{\partial \ln \Delta}{\partial P}\right)_{N,T}, \; \mu = -k_\mathrm{B} T \left(\frac{\partial \ln \Delta}{\partial N}\right)_{T,P}$$

Which Ensemble to Choose?

In principal, it makes no difference which ensemble we choose, as they are all equivalent in the thermodynamic limit, when the size of the system (in both volume and number of particles) approaches infinity at constant density. This is due to the fact that, at equilibrium, the probability of observing a given value for $\mathcal{A}$, which is far from its average value $\langle \mathcal{A} \rangle$, becomes infinitely small as the size of the system increases. Usually, the relative fluctuations for a given microscopic quantity will scale as $\mathcal{O}(N^{-1/2})$ [14], and they can be safely ignored. The choice of ensemble will thus depend on the quantity we wish to measure, and on how easy this calculation can be performed.

From a theoretical perspective, where we can always go to the thermodynamic limit, the choice of ensemble is purely one of convenience[2]: in which ensemble is it easiest to carry out the calculations? The micro-canonical ensemble, although simple in appearance is actually the most difficult to work with, which is why it is relegated to being a stepping-stone towards the more friendly canonical and grand-canonical ensembles. From a simulation point of view, no ensemble is more difficult than the others[3], but since we are restricted to working with a finite number of particles, we cannot ignore the fluctuations in our system. Given that experiments are usually performed at constant temperature T and pressure P, special care should be taken when comparing our results to experimental values, to make sure that the fluctuations (if important) are properly taken into account. Hopefully, the reader will have an idea of just how tedious this process can be, particularly when dealing with multi-component systems, after reading Chapter 7.

[2] Although some results, which depend directly on the fluctuations, can only be derived in a given ensemble.

[3] This is true once the programming has been performed, since the computer will do all the work, but this is different matter.

3.1.2 Distribution Functions

N-particle Densities and Distributions

In the study of dense media, the particle distribution functions, which measure the spatial density correlations in the fluid, play a fundamental role in most of the theories of liquids that have been developed. Furthermore, they provide a direct link to experimental observations, since scattering experiments measure these type of correlations. Consider a system described by one of the ensembles mentioned above. The probability $\rho^{(n)}(\boldsymbol{r}_1, \ldots, \boldsymbol{r}_n)$ of finding n particles at positions $\boldsymbol{r}_1, \ldots, \boldsymbol{r}_n$, irrespective of the positions of all the other particles or their momenta, is obtained by integrating (tracing out) the phase-space probability distribution $f(\Gamma)$ over these irrelevant degrees of freedom. This n-particle density is then defined as

$$\rho^{(n)}(\boldsymbol{r}_1, \ldots, \boldsymbol{r}_n) = \mathrm{Tr}^{'} f \tag{3.31}$$

where the prime indicates that the trace (for the given ensemble) is constrained to those states which contain n atoms at positions $\boldsymbol{r}_1, \ldots, \boldsymbol{r}_n$. The n-particle distribution function $g^{(n)}(\boldsymbol{r}_1, \ldots, \boldsymbol{r}_n)$ is then defined by

$$g^{(n)}(\boldsymbol{r}_1, \ldots, \boldsymbol{r}_n) = \frac{\rho^{(n)}(\boldsymbol{r}_1, \ldots, \boldsymbol{r}_n)}{\prod_{i=1}^{n} \rho^{(1)}(\boldsymbol{r}_i)} \tag{3.32}$$

These functions provide a measure of the structure in the fluid with respect to a completely random system (in which there are no spatial correlations among particles). For what follows, it is convenient to consider the precise definition of these distribution functions in the canonical and grand-canonical ensembles [17]

$$\rho^{(n)}_{NVT}(\boldsymbol{r}_1, \boldsymbol{r}_2, \ldots, \boldsymbol{r}_n) = \frac{N!}{(N-n)!} \frac{1}{Z} \int \mathrm{d}\boldsymbol{r}'^{(N-n)} e^{-\beta V_N} \tag{3.33}$$

$$\rho^{(n)}_{NPT}(\boldsymbol{r}_1, \boldsymbol{r}_2, \ldots, \boldsymbol{r}_n) = \frac{1}{\Xi} \sum_{N=n}^{\infty} \frac{z^N}{(N-n)!} \int \mathrm{d}\boldsymbol{r}'^{(N-n)} e^{-\beta V_N} \tag{3.34}$$

The Radial Distribution Function and the Structure Factor

The most useful of these functions are the single and two-body densities, which can be expressed as averages of the corresponding microscopic densities by

$$\rho^{(1)}(\boldsymbol{r}_1) = \left\langle \hat{\rho}^{(1)}(\boldsymbol{r}_1) \right\rangle = \left\langle \sum_{i=1}^{N} \delta(\boldsymbol{r}_1 - \boldsymbol{r}'_i) \right\rangle \tag{3.35a}$$

$$\rho^{(2)}(\boldsymbol{r}_1, \boldsymbol{r}_2) = \left\langle \hat{\rho}^{(2)}(\boldsymbol{r}_1, \boldsymbol{r}_2) \right\rangle = \left\langle \sum_{i=1}^{N} \sum_{j \neq i}^{N} \delta(\boldsymbol{r}_1 - \boldsymbol{r}'_i) \delta(\boldsymbol{r}_2 - \boldsymbol{r}'_j) \right\rangle \tag{3.35b}$$

where $\delta(r)$ is the Dirac distribution. If the fluid is homogeneous and isotropic, the corresponding two-particle density $g^{(2)}(\boldsymbol{r}, \boldsymbol{r}')$ is a scalar function of only one variable $r_{12} = |\boldsymbol{r}_1 - \boldsymbol{r}_2|$, and is then called the radial distribution function $g(r)$. This function, which essentially gives the conditional probability for observing a particle at $\boldsymbol{r}_2$ given

that there is already a particle at $\boldsymbol{r}_1$, plays a fundamental role in the theory of liquids for two reasons: (1) If the potential energy of the system is pair-wise additive, the thermodynamic properties can be obtained as integrals over the $g(r)$, and (2) the $g(r)$ are directly related, through a Fourier transform, to the structure factors $S(k)$ obtained from scattering experiments [17]

$$S(\boldsymbol{k}) = 1 + \rho\widetilde{h}(\boldsymbol{k}) \tag{3.36}$$

where $h(\boldsymbol{r})$ is the pair correlation function

$$h(\boldsymbol{r}) = g(\boldsymbol{r}) - 1 \tag{3.37}$$

and the tilde denotes a three-dimensional Fourier transform, such that

$$\widetilde{f}(\boldsymbol{k}) = \int \mathrm{d}\boldsymbol{r}\, e^{-i\boldsymbol{k}.\boldsymbol{r}} f(\boldsymbol{r}) \tag{3.38a}$$

$$f(\boldsymbol{r}) = \frac{1}{(2\pi)^3} \int \mathrm{d}\boldsymbol{k}\, e^{i\boldsymbol{k}.\boldsymbol{r}} f(\boldsymbol{k}) \tag{3.38b}$$

For homogeneous isotropic systems, this transform pair can be simplified to

$$\widetilde{f}(k) = \int_0^\infty \mathrm{d}r\, 4\pi r^2 \frac{\sin(kr)}{kr} f(r)$$

$$f(r) = \frac{1}{(2\pi)^3} \int_0^\infty \mathrm{d}k\, 4\pi k^2 \frac{\sin(kr)}{kr} f(k)$$

Besides being an experimentally measurable quantity, the structure factor is useful because it provides a direct link with the thermodynamics of the system. This is achieved through the compressibility equation

$$S(k=0) \equiv \rho k_\mathrm{B} T \chi_T \tag{3.39}$$

where $\rho = N/V$ is the number density and χ_T is the isothermal compressibility [17].

The potential of mean force

Additionally, the radial distribution function can be used to obtain information on the interactions between particles. It can be shown [17] that at infinite dilution, the $g(r)$ are given directly by the pair interaction potential $v(r)$ between particles

$$g(r) \underset{\rho\to 0}{=} e^{-\beta v(r)} \tag{3.40}$$

This relation can be extended to finite concentration systems to yield the Potential of Mean Force (PMF) [14] $w(r)$

$$g(r) = e^{-\beta w(r)} \tag{3.41}$$

which, as its name suggests, gives the average force $\langle F \rangle = -\nabla w(r)$ felt by two particles, at a fixed distance r from each other.

The ensemble dependence

Although the definition given in Eq. (3.35) is valid for any ensemble, there is a subtle difference between the radial distribution functions obtained in the canonical and

grand-canonical ensembles, $g_{NVT}(r)$ and $g_{NPT}(r)$, which merits special attention. The difference is in the asymptotic form of $g(r)$ as $r \longrightarrow \infty$. If two particles are infinitely far from one another, we expect them to be uncorrelated, and the probability of observing two particles at $\boldsymbol{r}_1$ and $\boldsymbol{r}_2$ should be equal to the product of the probabilities of observing each one separately $\rho^{(2)}(\boldsymbol{r}_1, \boldsymbol{r}_2) \simeq \rho^{(1)}(\boldsymbol{r}_1)\rho^{(2)}(\boldsymbol{r}_2)$. This would imply that $g(r) \longrightarrow 1$ for $r \longrightarrow \infty$. However, this is only true for a system in which the number of particles is allowed to fluctuate; if the number of particles remains fixed, a term proportional to N^{-1} appears [17]

$$g_{NVT}(r) \underset{r\to\infty}{\longrightarrow} 1 - \mathcal{O}\left(\frac{1}{N}\right) \tag{3.42}$$

$$g_{NPT}(r) \underset{r\to\infty}{\longrightarrow} 1 \tag{3.43}$$

Although this difference seems unimportant, and it often is, if we integrate the $g(r)$ over all of space, this $1/N$ term can give a finite contribution. Equations which involve these types of integrals (such as the Ornstein-Zernicke or Kirkwood-Buff equations) are usually derived in a grand-canonical ensemble (where no finite size correction is present) and should not be used with radial distribution functions obtained from constant particle ensembles, unless the appropriate corrections are made.

The Direct Correlation Function

Finally, it is necessary that we mention one more distribution function, the direct correlation function $c(r)$. We have seen that $h(r)$ gives a measure of the total correlation between two particles, averaged over all the other particles in the system. It is thus natural to seek a separation of the direct and indirect contributions to these correlations. The direct correlation function $c(r)$ was introduced by Ornstein and Zernicke precisely for this reason, by means of the following equation

$$h(r) = c(r) + \rho \int \mathrm{d}\boldsymbol{r}' c(|\boldsymbol{r} - \boldsymbol{r}'|)h(r') \tag{3.44}$$

where the distribution functions are those of the grand-canonical ensemble [21]. Furthermore, it can be shown that the asymptotic form of the direct correlation function is given by the pair potential $v(r)$ as [17]

$$c(r) \underset{r\to\infty}{=} -\beta v(r) \tag{3.45}$$

In the case of a mixture, the Ornstein-Zernicke equation can be easily generalized to give [17]

$$h_{ij}(r) = c_{ij}(r) + \sum_k \int \mathrm{d}\boldsymbol{r}' c_{ik}(|\boldsymbol{r} - \boldsymbol{r}'|)\rho_k h_{kj}(r') \tag{3.46}$$

where h_{ij} and $c_{ij}(r)$ are the pair and direct correlation functions for particles of type i and j, respectively, ρ_i is the (number) density of species i, and the sum runs over all the species in the system. As before, the asymptotic behaviour of the direct correlation functions is determined by the pair potentials through

$$c_{ij}(r) \underset{r\to\infty}{=} -\beta v_{ij}(r) \tag{3.47}$$

3.1.3 Integral Equations

A considerable effort has been made during the last half century to develop theories which are able to predict the radial distribution functions $g(r)$ of a given system, since the thermodynamic properties can then be easily obtained. The challenge is to find a link between the interaction potential $v(r)$ and the radial distribution function $g(r)$. We have already seen one such relation, Eq. 3.40, but it is only valid at infinite dilution. The different integral equations that have been developed attempt to provide a *general*, though approximate, theory of liquids, from which the structural and thermodynamic properties at any density or temperature (within the fluid phase) can be obtained. Using a diagrammatic expansion [17, 22], it is possible to derive the following exact relation between the various distribution functions and the interaction potential

$$\ln\left[h(r)+1\right] = -\beta v(r) + d(r) + h(r) - c(r) \tag{3.48}$$

but this is of limited practical use, since yet another unknown function $d(r)$, the so-called bridge function, has been introduced. Given that the Ornstein-Zernicke equation (Eq. (3.44)) provides an additional relationship between $h(r)$ and $c(r)$, we are left with two equations for three unknown functions: $h(r)$, $c(r)$, and $d(r)$. We thus require one additional relation among them, in order to solve this set of equations. We proceed by briefly discussing the three most popular approximations, or closure relations, that have been proposed, two of which (MSA and HNC) will be extensively used in our work.

Percus-Yevick (PY) Equation

For systems with strongly repulsive, short-ranged potentials, the PY solution provides an accurate description for their structural and thermodynamic properties [23, 14]. In terms of the bridge function, the PY equation can be expressed as [17]

$$d(r) = \ln\left[h(r) - c(r) + 1\right] - h(r) + c(r) \tag{3.49}$$

For hard-sphere systems, where the PY equation (and its improvements) admits an analytical solution [24, 25, 26], it provides an almost exact theory up to the crystallization point (at a packing fraction of $\eta = 0.49$). This remains valid in the case of mixtures, as long as the size asymmetry between the different components is small. Unfortunately, for charged systems the PY approximation is of absolutely no use.

Mean-Spherical Approximation (MSA)

The MSA [27, 28, 29] was proposed in an attempt to study systems which present a short-range repulsion and a long-range tail in the potential, with the repulsion modelled as a hard-sphere interaction, such that

$$v(r) = \begin{cases} \infty & r < \sigma \\ v_{\text{tail}}(r) & r > \sigma \end{cases} \tag{3.50}$$

where σ is the hard-sphere diameter. The MSA closure is given by

$$g(r) = 0, \qquad r \leq d \tag{3.51}$$

$$c(r) = -\beta v(r), \qquad r > d \tag{3.52}$$

where the first expression is exact, while the second assumes that the asymptotic form of the direct correlation function (Eq. (3.45)) is valid for all distances (beyond contact). These two relations, together with Equations (3.48) and (3.44), provide a closed set of equations for the $g(r)$. The main advantage of MSA is the fact that it allows for an analytical solution for many different potentials $v_{\text{tail}}(r)$. In particular, for Coulomb interactions, an analytic solution to the primitive model of electrolytes (i.e. charged hard spheres) can be obtained [27].

Hypernetted Chain (HNC) Equation

The HNC closure [30] can obtained by completely ignoring the bridge terms

$$d(r) = 0 \tag{3.53}$$

and although this might seem like a poor approximation, the HNC equation is particularly well suited for the description of electrolyte systems, and systems with long-range potentials in general [17, 14]. Unfortunately, no analytical solution exists in this case. The $g(r)$ must then be obtained numerically, using an iterative procedure to solve Equations (3.48) and (3.44). In the case of electrolyte solutions, which is what interests us, the HNC equation yields radial distribution functions which are in very good agreement with simulation results [31]. While convergence problems arise near the phase separation boundary [32], we do not consider such systems in this work.

3.1.4 Thermodynamic Integration and Perturbation Theory

Introduction

As mentioned before, the thermodynamic potentials cannot be directly obtained during a simulation (Molecular Dynamics or Monte Carlo), whereas their derivatives are easily measured. It is then natural to think of measuring the differences between the potentials by integrating their derivatives. For simplicity, we will focus on the canonical (NVT) ensemble, and thus on the Helmholtz free energy $F(N, V, T)$. The generalization to other ensembles is straightforward.

Consider the two thermodynamic relations given in Eq. (3.20), which relate the derivatives of the free energy F with respect to volume V and temperature T, to the pressure P and the internal energy U, both of which can be directly measured during a simulation (See Equation (4.35)). The simplest procedure to obtain the free energy of a given (fluid) system, is to start at infinite dilution $\rho_A = 0$, and to integrate P with respect to ρ, until the desired density ρ_B is reached. As the free energy of the ideal gas is known, we would thus obtain the absolute free energy, and not just a free energy difference. In general, this is only valid for low densities ρ_B, such that the thermodynamic trajectory does not cross a phase boundary. To overcome such a problem, a two-step thermodynamic integration can be performed, which avoids the coexistence region by starting at an artificial temperature T_A above the critical temperature T_c. The system can then be compressed along the T_A isotherm to the desired density ρ_B, before being cooled to the target temperature T_B. A schematic representation of this procedure is

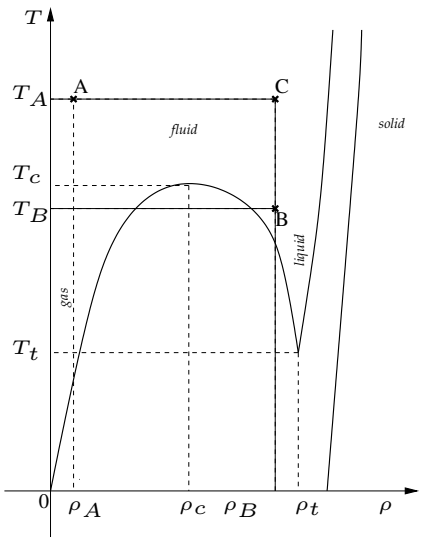

Figure 3.1: Typical phase diagram of a monatomic system, the c and t subscripts refer to the critical and triple point, respectively.

given in Figure 3.1. Formally, the procedure is expressed as follows: we integrate the derivative of F with respect to ρ (V), from ρ_A to ρ_B, to obtain

$$\frac{\beta_A F(\rho_B, T_A)}{N} = \frac{\beta_A F(\rho_A, T_A)}{N} + \int_{\rho_A}^{\rho_B} \mathrm{d}\rho' \frac{\beta_A P(\rho', T_A)}{\rho'^2} \tag{3.54}$$

We then perform an analogous integration, this time over the derivative of F with respect to temperature, to obtain the following expression for the free energy of the system at ρ_B and T_B

$$\frac{\beta_B F(\rho_B, T_B)}{N} = \frac{\beta_A F(\rho_A, T_A)}{N} + \int_{\rho_A}^{\rho_B} \mathrm{d}\rho' \frac{\beta_A P(\rho', T_A)}{\rho'^2} + \int_{\beta_A}^{\beta_B} \mathrm{d}\beta' \frac{U(\rho_B, \beta')}{N} \tag{3.55}$$

For the electrolyte solutions studied here, Equation 3.54 will always be valid, as the systems are always *supracritical* [4] [33, 34].

The λ Coupling Parameter

Fortunately, we are not just limited to actual thermodynamic variables, such as V, T, or N, when performing the thermodynamic integration. Since the free energy F is a thermodynamic state variable, all paths through the thermodynamic state space, whose endpoints coincide, will give the same result[5]. In particular, we can choose to use unphysical degrees of freedom, thereby augmenting the dimension of the configuration space, and allowing us to relate arbitrarily distinct systems with each other. Suppose we wish to measure the change in free energy between a system in a state A and one in state B, which are characterized by two distinct potentials V_A and V_B, with all other state variables (density and temperature) being equal. We need to construct a path through the configuration space that takes us from state A to state B, and integrate the

[4] The critical temperature T_c being well below the ambient temperature of $T = 298.15$ K.

[5] Again, this is true as long as no phase transition boundaries are crossed

change in free energy along this trajectory. This (reversible) work, required to change the Hamiltonian from H_A to H_B will give us the free energy difference between the two states. The most common way of doing this is to use Kirkwood's method [35], which introduces an additional (coupling) parameter λ into the Hamiltonian of the system, in such a way that $F(\lambda = 0) = F_A$ and $F(\lambda = 1) = F_B$. By definition (Eq. (3.19)), we have

$$\left(\frac{\partial F(\lambda)}{\partial \lambda}\right)_{N,V,T} = -\frac{1}{\beta}\frac{\partial}{\partial \lambda} \ln Q(N, V, T, \lambda) \tag{3.56}$$

$$= \left\langle \frac{\partial H(\lambda)}{\partial \lambda} \right\rangle_{\lambda} \tag{3.57}$$

where the ensemble averages $\langle \cdots \rangle$ are taken with respect to the system with Hamiltonian $H(\lambda)$. We thus obtain the free energy difference ΔF as

$$\Delta F = F_B - F_A = \int_{\lambda=0}^{\lambda=1} \left\langle \frac{\partial H(\lambda)}{\partial \lambda} \right\rangle_{\lambda} \tag{3.58}$$

This approach to the calculation of free energies is very common when performing simulations. The integration is discretized over a set of points λ_i, and a separate simulation (with a Hamiltonian $H(\lambda_i)$) is performed for each λ-point in order to measure the ensemble average appearing in the integrand. Finally, the integral is approximated using a suitable quadrature scheme (see Appendix C).

Perturbation Theory

Although the λ-coupling parameter approach provides a powerful method for measuring the thermodynamic properties of a system, it requires (several) costly numerical simulations, and it is thus unsuitable for applications which require explicit expressions for the thermodynamic or structural properties. A solution to this problem is provided by the standard perturbative fluid theory (PFT) [17, 14, 36], which allows us to relate the properties of the system of interest, to those of a simpler well known system, for which accurate analytical solutions exist. Let $\mathcal{V}$ be the total potential energy of our (model) system, $\mathcal{V}^{(0)}$ the potential energy of an arbitrary reference system, and $\delta\mathcal{V} = \mathcal{V} - \mathcal{V}^{(0)}$ the perturbation energy between the two. From the Kirkwood coupling parameter approach, using a simple linear interpolation between the two states ($\mathcal{V}^{(0)}$ and $\mathcal{V}^{(0)} + \delta\mathcal{V}$), we have

$$V(\lambda) = V^{(0)} + \lambda \delta V \tag{3.59}$$

the free energy of the model system is given by

$$\beta F = \beta F^{(0)} + \beta \int_0^1 \mathrm{d}\lambda \langle \delta\mathcal{V} \rangle_{\lambda} \tag{3.60}$$

If we perform a series expansion of the ensemble average around its value for $\lambda = 0$, we obtain [17]

$$\beta F = \beta F^{(0)} + \beta \langle \delta\mathcal{V} \rangle_0 - \frac{1}{2}\beta^2 \left(\left\langle (\delta\mathcal{V})^2 \right\rangle_0 - \langle \delta\mathcal{V} \rangle_0^2 \right) + \mathcal{O}(\beta^3) \tag{3.61}$$

where the ensemble averages $\langle \cdots \rangle_0$ are taken in the reference system ensemble (characterized by $\mathcal{V}^{(0)}$). This cumulant expansion was first obtained by Zwanzig [37] from an expansion of the free energy as a power series in β. The advantage of this approach is the fact that all the coefficients in the expansion are given by averages in the reference system ensemble: no properties of the model system need to be known beforehand. Furthermore, assuming pair-wise additivity in the potentials (including the perturbation),

$$\mathcal{V}^{(0)} = \sum_{i<j} v_{ij}(r_{ij}), \quad \delta\mathcal{V} = \sum_{i<j} \delta v_{ij}(r_{ij}) \tag{3.62}$$

these averages can all be expressed in terms of the n-body distribution functions [36]. Unfortunately, we usually only have access to the two-body distribution functions $g(r)$, and are thus forced to stop at first order

$$\beta F \lessapprox \beta F^{(0)} + \beta \langle \delta\mathcal{V} \rangle_0 \tag{3.63}$$

$$\lessapprox \beta F^{(0)} + \frac{\beta N \rho}{2} \int \mathrm{d}\boldsymbol{r} g^{(0)}(r) \delta v(r) \tag{3.64}$$

In Chapter 7 we show how the second order corrections to the free energy could be obtained, but they require an approximate solution to the three- and four-body distribution functions, and are considerably more complicated to evaluate.

Besides being the simplest approximation to the free energy, the first-order expansion also provides a strict upper bound. This is referred to as the Gibbs-Bogoluibov inequality [17], and is a consequence of the convexity of the exponential function appearing in the Boltzmann distribution. Once a reference system has been chosen, and suitably parametrized, Eq. (3.63) is minimized to determine the best, first order approximation to the free energy of the model system. It is clear that the closer the reference and model potentials are to each other, the more accurate this approximation will become. In fact, to first-order, the corrections to the free energy are computed under the assumption that the structure of the model and reference fluids is the same [17].

This procedure is useful if, and only if, the properties of the reference system are well known, or at least easier to calculate than those of the model system. Although the minimization must be done numerically, no simulations are required[6]. It is not surprising then, that PFT is commonly used with hard-and soft-core reference potentials, which have been extensively studied [38, 39]. This has proven to be very successful in the case of dense fluids, since it is well known that at high densities, their structure is essentially determined by the short-range repulsive interactions [17], for which hard-cores are a very good approximation. In particular, the use of hard-sphere reference systems is convenient, since the exact solution to the Percus-Yevick integral equation and its improvements, provides very accurate estimates for their structural and thermodynamic properties. For charged particles in solution, the simplest implicit solvent model representation is that of charged hard-spheres, which is usually described within the MSA approximation. This is the approach we shall adopt when trying to derive implicit solvent models of electrolytes in solution.

[6] If simulations are needed to compute the properties of the reference system, we might as well use the exact expression (3.60), and not just the first-order correction

3.1.5 Time Correlation Functions: The Green-Kubo Formalism

Up to this point, we have only discussed equilibrium properties, and no mention has been made of the dynamic properties, or how these can be obtained, as they fall into the domain of non-equilibrium statistical mechanics. If the central role in equilibrium statistical mechanics is played by the partition function, the corresponding role in the study of non-equilibrium phenomena is played by the time correlation function $C_{AB}(t)$, defined as an ensemble average by

$$C_{AB}(t) = \langle A(t)B(t=0)\rangle = \int \mathrm{d}\Gamma A(\Gamma(t))B(\Gamma(0))f(\Gamma(0)) \tag{3.65}$$

or as a time average by

$$C_{AB}(t) = \overline{A(t)B(t=0)} = \lim_{\tau\to\infty}\frac{1}{\tau}\int_0^\tau \mathrm{d}t' A(\Gamma(t'+t))B(\Gamma(t')) \tag{3.66}$$

Kubo showed that, within a linear-response regime, all of the phenomenological transport coefficients γ can be expressed as integrals over a specific time auto-correlation function $C_{AA}(t)$[7]. The procedure for deriving these equations is relatively straightforward: the solutions, in reciprocal k-space, to the macroscopic and microscopic transport equations are compared to each other, in order to establish a microscopic expression for the macroscopic transport coefficient γ. Such expressions are of the form [14]

$$\gamma = \left\langle (A(t) - A(0))^2 \right\rangle \tag{3.67}$$

where $A = A(\Gamma(t))$ is some microscopic property of the system. Finally, by expressing $A(t)$ as the integral of its time derivative $\dot{A}$, this equation can then be written as

$$\begin{aligned}\gamma &= \int_0^\infty \mathrm{d}t \left\langle \dot{A}(t)\dot{A}(0)\right\rangle \\ &= \int_0^\infty \mathrm{d}t C_{\dot{A}\dot{A}}(t)\end{aligned} \tag{3.68}$$

The expressions for the self-diffusion coefficient D, shear viscosity η, and thermal conductivity λ, in terms of the mean-squared fluctuations of a microscopic property (3.67), are given by [14, 40, 41]

$$D = \lim_{t\to\infty}\frac{1}{6t}\left\langle [\boldsymbol{r}(t) - \boldsymbol{r}(0)]^2\right\rangle \tag{3.69}$$

$$\eta = \lim_{t\to\infty}\frac{1}{2Vk_\mathrm{B}Tt}\left\langle \left[\sum_i^N r_{i,z}(t)p_{i,x}(t) - r_{i,z}(0)p_{i,x}(0)\right]^2\right\rangle \tag{3.70}$$

$$\lambda = \lim_{t\to\infty}\frac{1}{2Vk_\mathrm{B}T^2t}\left\langle \left[\sum_i^N r_{i,x}(t)\Delta E_i(t) - r_{x,i}(0)\Delta E_i(0)\right]^2\right\rangle \tag{3.71}$$

[7]Unlike with equilibrium thermodynamics, where a unique partition function determines all the equilibrium properties, each transport coefficient is obtained from a distinct auto-correlation function.

with $\Delta E_i = E_i - \langle E_i \rangle$. The corresponding Green-Kubo relations, expressing the transport coefficients as the time-integral of an auto-correlation function, are

$$D = \frac{1}{3}\int_0^\infty \mathrm{d}t \langle \boldsymbol{v}(t).\boldsymbol{v}(0)\rangle \tag{3.72}$$

$$\eta = \frac{1}{Vk_\mathrm{B}T}\int_0^\infty \mathrm{d}t \langle \sigma^{xz}(t)\sigma^{xz}(0)\rangle \tag{3.73}$$

$$\lambda_T = \frac{1}{3Vk_\mathrm{B}T^2}\int_0^\infty \mathrm{d}t \langle \boldsymbol{S}(t)\boldsymbol{S}(0)\rangle \tag{3.74}$$

where σ^{xz} are the off-diagonal components of the shear-stress tensor and $\boldsymbol{S}$ is a vectorial flux defined as

$$\sigma^{xz} = \sum_i^N \left(\frac{p_{i,x}p_{i,z}}{m} + r_{i,z}F_{i,x}\right) \tag{3.75}$$

$$\boldsymbol{S} = \frac{\partial}{\partial t}\sum_i^N \boldsymbol{r}_i \Delta E_i \tag{3.76}$$

Finally, we note that Eqs.(3.69-3.71) are only strictly valid for non-periodic systems [40, 41].

3.2 Experimental Properties of Electrolytes Solutions

Before continuing with the theoretical description of electrolyte solutions, it is important to discuss how such systems are characterized in the laboratory. As most experiments are performed at constant temperature T and pressure P, the natural thermodynamic potential is the Gibbs potential (Eq. (3.30)). For an electrolyte solution, the differential form of this potential is given by

$$\mathrm{d}G = V\mathrm{d}P - S\mathrm{d}T + \mu_w \mathrm{d}N_w + \sum_i \mu_i \mathrm{d}N_i \tag{3.77}$$

where w and i refer to the water (solvent) and ion (solute) particles. Among the various thermodynamic properties of the system, the chemical potentials of the individual components μ_w and μ_i are probably the most important, since the Gibbs potential can be directly obtained from them. Experimentally, however, such properties are usually measured with respect to some standard state[8], which we denote with a superscript (0).

For the ions, the chemical potential difference $\Delta\mu_i = \mu_i - \mu_i^{(0)}$, is given directly by the ratio of the activities of the two states $a_i = z_i/z_i^{(0)}$, since

$$k_\mathrm{B}T \ln a_i = \mu_i - \mu_i^{(0)} \tag{3.78}$$

If we let $a_i = c_i\gamma_i$, with c_i and γ_i the ion concentration and activity coefficient for species i, we obtain

$$\mu_i = \mu_i^{(0)} + k_\mathrm{B}T \ln c_i + k_\mathrm{B}T \ln \gamma_i \tag{3.79}$$

[8]Not necessarily the ideal gas preferred by physicists

where the standard term $\mu_i^{(0)}$, which represents the solvent-ion interactions, is chosen in such a way that $\gamma_i = 1$ as $c_i \to 0$. For the water, the formula for the chemical potential reads

$$\mu_w = \mu_w^{(0)} + k_{\mathrm{B}} T \ln a_w \tag{3.80}$$

where the standard term $\mu_w^{(0)}$ represents the chemical potential of the pure solvent. In this manner, $a_w = 1$ at infinite salt dilution.

The water activity a_w is an experimentally measurable quantity, which is used to define the osmotic coefficient ϕ, by [42]

$$\ln a_w = \frac{\sum_i c_i}{c_w} \phi \tag{3.81}$$

Furthermore, thanks to the Gibbs-Duhem relation [43], there is a link between the chemical potentials (activities) of the ions and the water; and thus, between the osmotic coefficient ϕ of the solution and the activity coefficients γ_i of the ions. Since experimentally we cannot consider the ions individually, but instead have to work with the salt as a whole, it is normal to define an activity coefficient for the salt γ_{salt}. For a simple binary electrolyte, $\mathrm{S} \longrightarrow \nu_1 \mathrm{C}^+ + \nu_2 \mathrm{A}^-$, where C^+ and A^- refer to the cations and the anions, respectively, and the ν_i to the corresponding stoichiometric coefficients, we have

$$\gamma_{\mathrm{salt}} = (\gamma_1^{\nu_1} \gamma_2^{\nu_2})^{\frac{1}{\nu_1 + \nu_2}} \tag{3.82}$$

and the Gibbs-Duhem relation reads

$$\ln \gamma_{\mathrm{salt}} = \phi(m) - 1 + \int_0^m \mathrm{d}m \, \frac{\phi - 1}{m} \tag{3.83}$$

where m is the salt concentration (in the molality scale). Thus, a calculation of the osmotic coefficient ϕ is equivalent to a calculation of the activities of the solute particles γ_i. For our simulations, we have only considered ϕ, since the other properties can easily be obtained from it.

The Solute Gas Model

Finally, we note that many models of electrolyte solutions consider the system as a solute gas, in which the solvent is treated as a dielectric continuum. The link between the solute gas and the experimental thermodynamic properties was obtained by McMillan-Mayer, as will be discussed in Section 3.4.3. In such cases, care should be taken when comparing the thermodynamic properties predicted by the solute gas (implicit solvent) models with their experimental counterparts. The former are said to have been performed in the McMillan-Mayer (MM) reference frame and the latter in the Lewis-Randall (LR) reference frame. Generally speaking, the difference between the two arises from the fact that derivatives taken in the LR reference frame are performed at constant solute concentration; whereas derivatives taken in the MM reference frame are performed at constant solvent chemical potential. It is thus necessary to establish conversion laws to pass between the two reference frames.

For the solute gas model, the Gibbs free energy is now given by

$$\mathrm{d}G = V \mathrm{d}\Pi - S \mathrm{d}T + \sum_i \mu_i \mathrm{d}N_i \tag{3.84}$$

where Π is the pressure of the solute gas and the sum is over all solute particles (no explicit reference is made to the solvent). This *fictitious* pressure Π, which is referred to as the osmotic pressure, can be shown to depend on the activity of the solvent a_w [42]. Thus, it provides an alternative definition of the osmotic coefficient (Eq.(3.81)), in terms of the pressure of the solute gas Π

$$\phi^{\mathrm{MM}} = \frac{\beta\Pi}{\sum_i c_i} \tag{3.85}$$

where we have been careful to note that this quantity has been derived in the MM reference frame. The link with the LR osmotic coefficient is provided by the following simplified formula [44]

$$\phi^{\mathrm{LR}} = (1 - \sum_i c_i \overline{V}_i)\phi^{\mathrm{MM}} \tag{3.86}$$

where $\overline{V}_i$ is the partial volume of solute i.

3.3 The Implicit Solvent Model

Within an implicit solvent description of electrolyte solutions, the solvent is considered as a dielectric continuum, and the system is defined by the interaction potential between the solute particles. The simplest choice, referred to as the Primitive Model (PM), is to describe the solutes as charged hard spheres. Let us consider an m-component system of volume V, with ρ_i, σ_i, and $q_i = z_i e$ the number densities, hard-sphere diameters, and charges of species i (e is the elementary charge). The pair potential of such a system is given by

$$\beta v_{ij}(r) = \beta v_{ij}^{\mathrm{HS}}(r) + \frac{L_{\mathrm{B}} z_i z_j}{r} \tag{3.87}$$

where L_{B} is the Bjerrum length[9] (ϵ_0 is the vacuum permittivity and ϵ_r is the dielectric constant of the solvent)

$$L_{\mathrm{B}} = \frac{\beta e^2}{4\pi\epsilon_0\epsilon_r} \tag{3.88}$$

and $v_{ij}^{\mathrm{HS}}(r)$ is the hard-sphere potential

$$v_{ij}^{\mathrm{HS}}(r) = \begin{cases} +\infty & \text{if } r \leq \sigma_{ij} \\ 0 & \text{if } r > \sigma_{ij} \end{cases} \tag{3.89}$$

with $\sigma_{ij} = (\sigma_i + \sigma_j)/2$ the contact distance between particles of species i and j. For the special case of a two-component system with equal diameters and valence charges, the resulting model is commonly referred to as the *restricted* primitive model.

Unfortunately, even such a simple model as this one doesn't admit an *exact* analytical solution. However, several approximations exist which yield satisfactory results,

[9] This characteristic length gives the distance at which the interaction between two elementary charges is equal to the thermal energy $k_{\mathrm{B}}T$. For liquid water at standard temperature, $L_{\mathrm{B}} = 7.14$ Å.

particularly for $1-1$ electrolytes. In the infinite dilution limit, where the short range interactions between the particles can be neglected, the Debye-Hückel theory [14] provides exact limiting laws for the thermodynamics of electrolyte solutions. At higher concentrations, the repulsive short-range interactions cannot be neglected, and a different approach is required. Such a solution was provided by Blum [27, 28], who solved the MSA closure (3.51), giving explicit (approximate) expressions for the thermodynamic and structural properties of electrolyte solutions. This theory was generalized to include ion association, by allowing for the formation of bonds between the charged hard-spheres, and is known as the binding MSA (BIMSA) [45, 46]. In what follows, we give a brief description of these three theories, as they will be extensively referenced throughout our work; in particular, the MSA and BIMSA theories, which we use within a first-order perturbation theory to derive the best primitive model representation of electrolytes.

3.3.1 The Limiting Laws

The Debye-Hückel (DH) theory, first published in 1923, holds a special position within the theory of electrolytes, as it was the first theory capable of predicting the activity coefficients of ions in solution, correctly describing their deviation from ideal behaviour up to millimolar concentrations. This mean-field theory predicts the following for the thermodynamic properties of a solution [14]

$$\frac{\beta U^{\text{ex}}}{N} = -\frac{\kappa_D^3}{8\pi\rho_N} \tag{3.90a}$$

$$\frac{\beta F^{\text{ex}}}{N} = -\frac{\kappa_D^3}{12\pi\rho_N} \tag{3.90b}$$

$$\phi \equiv \frac{\beta P}{\rho_N} = 1 - \frac{\kappa_D^3}{24\pi\rho_N} \tag{3.90c}$$

$$\ln\gamma_i = -\frac{\kappa_D L_{\text{B}} z_i^2}{2} \tag{3.90d}$$

where U^{ex} and F^{ex} are the excess internal and Helmholtz free energies, respectively, ϕ is the (MM) osmotic coefficient, γ_i is the activity coefficient of species i, and $\rho_N = \sum_i \rho_i$ is the total number density. All quantities are seen to depend on the Debye length Λ_D, defined as

$$\Lambda_D^{-1} \equiv \kappa_D = \sqrt{4\pi L_{\text{B}} \sum_i \rho_i z_i^2} \tag{3.91}$$

which gives a measure of the size of the electrostatic screening cloud surrounding each ion. Most importantly, all quantities are seen to vary linearly with the square root of the salt concentration. It turns out that this is a general property of electrolyte solutions: At sufficiently low concentrations, any thermodynamic or physical property f can be expressed as

$$f - f^{(0)} = A\sqrt{c} + \dots \tag{3.92}$$

where $f^{(0)}$ gives the value corresponding to the pure solvent, and A is a constant which depends only on the charged nature of the system, making the DH expressions exact limiting laws.

3.3.2 The MSA Solution

The problem with the DH theory is the fact that it does not consider the short-range interactions between particles, which become important as the concentration is increased. The MSA solution (Eq. (3.51)) attempts to address these problems by taking into account the finite size of the particles, as well as the long-range electrostatic interactions. It has been widely adopted in the study of electrolytes, since explicit algebraic equations can be obtained for the excess (electrostatic) thermodynamic properties and the radial distribution functions. In order to obtain a complete description of electrolytes, within the primitive model, the results provided by the MSA theory must be complimented with the remaining (non-electrostatic) terms. We proceed to give a detailed description of the different contributions to the thermodynamics and the radial distribution functions of a primitive model, within the MSA description.

Thermodynamics

The free energy density $f = F/V$ of a mixture of charged hard-spheres is naturally decomposed in the following manner

$$\beta f = \beta f^{\mathrm{id}} + \beta f^{\mathrm{ev}} + \beta f^{\mathrm{el}} \tag{3.93}$$

where f^{id} is the ideal contribution to the free energy, f^{ev} is the excluded-volume term (i.e. the hard-sphere term), and f^{el} is the electrostatic term.

Ideal Contribution:
The ideal contribution is given by the free energy of an ideal gas of the same composition [17]

$$\beta f^{\mathrm{id}} = \sum_i \rho_i \left(\beta \mu_i^{\mathrm{id}} - 1\right) \tag{3.94}$$

where $\beta \mu_i^{\mathrm{id}} = \ln\left[\Lambda_i^3 \rho_i\right]$. Notice that this term depends only on the density and mass of the distinct species.

Excluded Volume Contribution:
To compute the excluded volume term, we use the semi-empirical equation of state of Boublik, Mansoori, Carnahan, Starling, and Leland (BMCSL) [47, 48, 49], since it is known to provide an accurate description of hard-sphere mixtures over a wide range of concentrations and size ratios. The (hard-sphere) excess free energy density is given by

$$\beta f^{\mathrm{ev}} = \frac{6}{\pi}\left(\frac{\zeta_2^3}{\zeta_3^2} - \zeta_0\right)\ln\Delta + \frac{3\zeta_1\zeta_2}{\Delta} + \frac{\zeta_2^3}{\zeta_3\Delta^2} \tag{3.95}$$

where ζ_j and Δ are defined as[10]

$$\zeta_j = \frac{\pi}{6}\sum_i \rho_i (\sigma_i)^j \tag{3.96}$$

$$\Delta = 1 - \zeta_3 \tag{3.97}$$

[10]Notice that Blum and Høye [28] do not include the $\pi/6$ factor in their definition.

Electrostatic Contribution:
The excess free energy density, as given by the MSA solution, is

$$\beta f^{\mathrm{el}} = \beta \Delta E + \frac{\Gamma^3}{3\pi} \tag{3.98}$$

where the excess internal energy ΔE is defined as

$$\beta \Delta E = -L_{\mathrm{B}} \left\{ \Gamma \left[\sum_i \frac{\rho_i z_i^2}{1+\Gamma\sigma_i} \right] + \frac{\pi}{2\Delta} \Omega P_n^2 \right\} \tag{3.99}$$

and Γ, which can be considered as a generalized screening parameter (akin to κ_D), is obtained by solving the following algebraic equation

$$2\Gamma = \alpha \left\{ \sum_i \rho_i \left[\frac{z_i - \frac{\pi}{2\Delta}\sigma_i^2 P_n}{1+\Gamma\sigma_i} \right]^2 \right\}^{\frac{1}{2}} \tag{3.100}$$

with

$$\alpha^2 = 4\pi L_{\mathrm{B}} \tag{3.101a}$$

$$P_n = \frac{1}{\Omega} \sum_i \frac{\rho_i \sigma_i z_i}{1+\Gamma\sigma_i} \tag{3.101b}$$

$$\Omega = 1 + \frac{\pi}{2\Delta} \sum_i \frac{\rho_i \sigma_i^3}{1+\Gamma\sigma_i} \tag{3.101c}$$

In practice, the solution for Γ is easily found using an iterative scheme. A good starting value is the Debye screening length: $2\Gamma^{(0)} = \kappa_D$.

Structure

Finally, Blum and Høye [28] have also provided explicit expression for the radial distribution functions of the primitive model, which we will use extensively in our perturbation calculations. However, they do not give a closed algebraic formula for the $g_{ij}(r)$, but instead for the Laplace transform of $rg_{ij}(r)$

$$\widehat{G}_{ij}(s) \equiv \int_0^\infty \mathrm{d}r\, e^{-sr} r g_{ij}(r) \tag{3.102}$$

Fortunately, these equations can be easily transformed numerically, since they are proportional to the Fourier transform of $g_{ij}(r)$ for a wave vector $k = is$ (See Appendix D and Eq. (3.38)).

The solution for $\widehat{G}_{ij}(s)$ is found to be

$$\widehat{G}_{ij}(s) = \frac{D_0 D_\pm}{D_T} \widehat{G}^0_{ij}(s) - \frac{D_0 \Gamma^2}{s\alpha^2 \pi D_T} e^{-s\sigma_{ij}} a_i a_j + \Delta \widehat{G}_{ij}(s) \tag{3.103}$$

where the first term on the right hand side corresponds to the Percus-Yevick (hard-spheres) radial distribution function, the second term gives the pure electrostatic contributions (charges), and the third term provides the contribution arising from the cross

interactions (hard-spheres + charges). The different terms appearing in Eq. (3.103) are defined as

$$D_T = D_0 D_\pm + \Delta D_T \tag{3.104a}$$

$$D_0 = 1 - \frac{2\pi}{\Delta}\sum_i \rho_i \varphi_2(\sigma_i)\left(1 + \frac{3\zeta_3}{\Delta}\right) \tag{3.104b}$$

$$- \frac{2\pi}{\Delta}\left\{\sum_i \rho_i \varphi_1(\sigma_i)\left[\sigma_i\left(1 + \frac{3\zeta_2\sigma_i}{2\Delta}\right) + \frac{\pi}{4\Delta}\sum_j \rho_j \varphi_1(\sigma_j)\left(\sigma_j - \sigma_i\right)^2\right]\right\}$$

$$D_\pm = 1 + \frac{2\Gamma}{s}\left[1 + \frac{\Gamma}{\alpha^2}\sum_i \rho_i a_i^2 \varphi_0(\sigma_i)\right] - \frac{\pi}{s\Delta} P_m P_{\varphi_1} \tag{3.104c}$$

$$\Delta D_T = \frac{\pi}{s\Delta}\left\{P_m P_{\varphi_1}\left[\delta_1^2 - \frac{2\pi}{\Delta}\delta_2 \sum_i \rho_i \varphi_2(\sigma_i)\right]\right. \tag{3.104d}$$

$$\left. + 4\frac{\Gamma^2}{\alpha^2}\left[P_{\varphi_1}(\delta_2 P_{\varphi_1} + \delta_1 P_{\varphi_0}) + \frac{\pi}{2\Delta} P_{\varphi_0}^2 \sum_i \rho_i \varphi_2(\sigma_i)\right]\right\} \tag{3.104e}$$

with

$$P_{\varphi_0} = \sum_i \rho_i \sigma_i a_i \varphi_0(\sigma_i) \tag{3.105a}$$

$$P_{\varphi_1} = \sum_i \rho_i a_i \varphi_1(\sigma_i) \tag{3.105b}$$

$$P_m = \frac{2\Gamma}{\alpha^2}\sum_i \rho_i \sigma_i a_i \tag{3.105c}$$

and

$$\delta_1 = 1 - \frac{\pi}{\Delta}\sum_i \rho_i \sigma_i \varphi_1(\sigma_i) \tag{3.106a}$$

$$\delta_2 = 1 + \frac{\pi}{2\Delta}\sum_i \rho_i \sigma_i^2 \varphi_0(\sigma_i) \tag{3.106b}$$

$$\delta_3 = \frac{\pi}{\Delta}\sum_i \rho_i \varphi_2(\sigma_i) \tag{3.106c}$$

where

$$a_i = \frac{\alpha^2}{2\Gamma\left(1 + \Gamma\sigma_i\right)}\left(z_i - P_n \sigma_i^2 \frac{\pi}{2\Delta}\right) \tag{3.107}$$

and the φ_i functions are defined as

$$\varphi_0(\sigma) = s^{-1}\left(1 - e^{-s\sigma}\right) \tag{3.108a}$$

$$\varphi_1(\sigma) = s^{-2}\left(1 - e^{-s\sigma} - s\sigma\right) \tag{3.108b}$$

$$\varphi_2(\sigma) = s^{-3}\left(1 - e^{-s\sigma} - s\sigma + \frac{1}{2}s^2\sigma^2\right) \tag{3.108c}$$

The hard-sphere term is given by

$$\widehat{G}^0_{ij}(s) = \frac{e^{-s\sigma_{ij}}}{s^2\Delta D_0}\Bigg\{ s\left[\sigma_{ij} + \sigma_i\sigma_j\frac{3\zeta_2}{2\Delta}\right] + 1 + \frac{3\zeta_3}{\Delta} + \frac{\pi s}{2\Delta}\sum_k \rho_k\varphi_1(\sigma_k)\left(\sigma_k-\sigma_i\right)\left(\sigma_k-\sigma_j\right)\Bigg\} \tag{3.109}$$

and the cross-contribution by

$$\begin{aligned}\Delta\widehat{G}_{ij}(s) = \frac{e^{-s\sigma_{ij}}}{2\Delta s^2 D_T}\Bigg\{ &\frac{\pi}{s\Delta}\left(2\delta_2 P_m P_{\varphi_1} - \frac{2\Gamma^2}{\alpha^2}P^2_{\varphi_0}\right) \\ &+ \frac{2\pi}{\Delta}\sigma_{ij}P_{\varphi_1}\left(\frac{2\Gamma^2}{\alpha^2}P_{\varphi_0} + \delta_1 P_m\right) - \frac{s\pi}{\Delta}P_{\varphi_1}\sigma_i\sigma_j\left(\frac{2\Gamma^2}{\alpha^2}P_{\varphi_1} - P_m\delta_3\right) \\ &- \frac{2\Gamma^2}{\alpha^2}\left[\left(a_i+a_j\right)\left(\delta_1 P_{\varphi_0} + 2\delta_2 P_{\varphi_1}\right) + s\left(a_i\sigma_j + a_j\sigma_i\right)\left(\delta_1 P_{\varphi_1} + \delta_3 P_{\varphi_0}\right)\right]\Bigg\}\end{aligned} \tag{3.110}$$

3.3.3 The BIMSA Solution

For highly-charged systems, or systems with a low solvent dielectric constant, the strong electrostatic attraction will favor the association of the free ions into ion pairs. However, the MSA solution is known to provide a very poor description of such systems. Fortunately, a generalization of the MSA theory, which allows for the formation of bonds between ions (through a sticky-point potential), has been developed by Blum and Bernard [45, 46, 50]. For what follows, we assume that we are working with a binary electrolyte, in which the cations and anions are allowed to form pairs with each other. We thus have a three component system, composed of free cations (1) and anions (2), along with the pairs (3). We consider the general case, where the diameters of the cations and anions within the pair, σ_C and σ_A, respectively, are allowed to differ from those of the free cations and anions, σ_1 and σ_2. Our system is thus characterized by four diameters $\{\sigma_1, \sigma_2, \sigma_C, \sigma_A\}$ but only three densities $\{\rho_1, \rho_2, \rho_3\}$. For this model, the free energy can now be decomposed as

$$\beta f = \beta f^{\text{id}} + \beta f^{\text{ev}} + \beta f^{\text{el}} + \beta f^{\text{as}} \tag{3.111}$$

where we have added an extra term to Eq. (3.93) to take into account the contributions arising from the association of ion pairs. The ideal and excluded volume terms are computed exactly as before, using the ideal gas (Eq. (3.94)) and BMCSL expressions (Eq. (3.95)), only now we have an effective four component system (free and paired cations and anions). The expressions for the electrostatic and association contributions that we use are those obtained by Vilariño and coworkers [50], although we have adopted a slightly different definition for the reference free energy of the pair[11].

Electrostatic Contribution:
The excess electrostatic free energy density of the BIMSA model takes the same form

[11]This is detailed in Section 6.4, where we establish a link between the free energy of a binary electrolyte in a two- and three-component (paired) representation

as its MSA counterpart (Eq. (3.98)), namely

$$\beta f^{\mathrm{el}} = \beta \Delta E + \frac{\Gamma^3}{3\pi} \tag{3.112}$$

$$\tag{3.113}$$

but the excess internal energy is now given by

$$\Delta E = -L_{\mathrm{B}} \left\{ \left[\sum_i \rho_i z_i \frac{\Gamma z_i + \eta \sigma_i}{1 + \Gamma \sigma_i} \right] - \rho_3 \frac{\eta}{\sigma_A + \sigma_C} \left[\frac{\sigma_C^2}{1 + \Gamma \sigma_C} Y_A + \frac{\sigma_A^2}{1 + \Gamma \sigma_A} Y_C \right] \right\} \tag{3.114}$$

with

$$\eta = \frac{\pi}{2\Delta} \left\{ \left[\sum_i \rho_i \sigma_i Y_i \right] + \frac{\rho_3}{\sigma_A + \sigma_C} \left[\frac{\sigma_A^2}{1 + \Gamma \sigma_A} Y_C + \frac{\sigma_C^2}{1 + \Gamma \sigma_C} Y_A \right] \right\} \tag{3.115a}$$

$$Y_i = \frac{z_i - \eta \sigma_i^2}{1 + \Gamma \sigma_i} \tag{3.115b}$$

and the screening parameter Γ must now be obtained by solving the following equation

$$(2\Gamma)^2 = \alpha \left\{ \left[\sum_i \rho_i Y_i^2 \right] + \frac{2\rho_3}{\sigma_C + \sigma_A} \left(\frac{\sigma_A}{1 + \Gamma \sigma_A} + \frac{\sigma_C}{1 + \Gamma \sigma_C} \right) Y_A Y_C \right\} \tag{3.116}$$

Association Contribution:
Finally, the excess free energy due to the pairing of the ions (using a simple sticky point model) is given by

$$\beta f^{\mathrm{as}} = -\rho_3 \ln \frac{g_{CA}(\sigma_{CA})}{g_{CA}^{\infty}} \tag{3.117a}$$

$$\ln \frac{g_{CA}(\sigma_{CA})}{g_{CA}^{\infty}} = \ln g_{CA}(\sigma_{CA}) - \frac{2L_{\mathrm{B}}}{\sigma_C + \sigma_A} \left(Y_C Y_A - z_C z_A \right) \tag{3.117b}$$

where the contact value of the radial distribution function for the paired ions $g_{CA}(\sigma_{CA})$ is obtained from

$$g_{CA}(\sigma_{CA}) = \frac{1}{\Delta} + \frac{3\zeta_2}{\Delta^2} \frac{\sigma_C \sigma_A}{\sigma_C + \sigma_A} + \frac{2\zeta_2^2}{\Delta^3} \left(\frac{\sigma_C \sigma_A}{\sigma_C + \sigma_A} \right)^2 \tag{3.117c}$$

3.4 Exact theories of Electrolyte Solutions

3.4.1 Introduction

The pioneering works of Debye, Hückel, and Onsager in the 1920s and 30s provided a theoretically sound description of the thermodynamic and dynamical properties of electrolyte solutions, able to explain the experimental observations. However, these so-called Limiting Laws, though exact, are only valid at very low concentrations. Furthermore, they were derived using extremely simple models (i.e. point charges in a

dielectric continuum), for which no rigorous justification existed, and which could not provide a detailed description of the solvation effects (only excess ion properties could be measured). Fortunately, we would not have to wait too long for an exact, statistical-mechanical description of ions in solution to appear. Such a theory was provided by McMillan and Mayer (MM) in 1945 [51], with their seminal article on the "Statistical Thermodynamics of Multicomponent Systems". Their theory, which is exact, provided a theoretical support for the earlier models of Debye, Hückel, and Onsager, by showing that one can always define an implicit solvent model which exactly describes the microscopic (explicit solvent) system. Less than a decade later, an alternative theory (which is also exact and thus equivalent to the MM description) was proposed by Kirkwood and Buff (KB) [52]. Their theory relies on the microscopic distribution functions (for the solvent and the ions) to provide a complete thermodynamic description of the solutions. Although there is a lively debate within the community as to which of the two is best, or preferable, the MM theory provides the natural framework for working with implicit solvent solutions. Since our stated goal is to go from a fully atomistic microscopic description of ions in solutions, to an analytically solvable implicit solvent model, we shall focus mainly the MM theory. Nevertheless, it is important to understand the KB description, and how it is applied; as this will allow us compare our methods and results to those of other groups working in the field. As such, we proceed by presenting a brief description of these two theories. For the KB theory, we follow the presentation of the original article [52]; but for the MM theory we favor a simplified version, due to Friedman [13], as the original formulation of McMillan and Mayer is somewhat mathematically involved.

3.4.2 Kirkwood-Buff Theory of Electrolyte Solutions

Consider a multi-component system within the grand-canonical ensemble, the partition function, Eq. (3.22) is now given by

$$\Xi = \sum_{\boldsymbol{N}} \left(\prod_i \frac{z_i^{N_i}}{N_i!} \right) Z_{\boldsymbol{N}} \tag{3.118}$$

where the z_i and N_i denote the activities and number of particles of species i, and $\boldsymbol{N} = (N_1, \ldots, N_i, \ldots)$ and $\boldsymbol{\mu} = (\mu_1, \ldots, \mu_i, \ldots)$ will be used as a short-hand notation for the particle numbers and chemical potentials of all the species. The single- and two particle densities, obtained from a straight-forward generalization of Eq. (3.35)

$$\rho_i(\boldsymbol{r}_1) = \langle \hat{\rho}_i(\boldsymbol{r}_1) \rangle \tag{3.119a}$$

$$\rho_{ij}(\boldsymbol{r}_1, \boldsymbol{r}_2) = \langle \hat{\rho}_{ij}(\boldsymbol{r}_1, \boldsymbol{r}_2) \rangle \tag{3.119b}$$

They are normalized, by definition, as follows

$$\int \mathrm{d}\boldsymbol{r}_1 \rho_i(\boldsymbol{r}_1) = \langle N_i \rangle \tag{3.120a}$$

$$\int \mathrm{d}\boldsymbol{r}_1 \mathrm{d}\boldsymbol{r}_2 \rho_{ij}(\boldsymbol{r}_1, \boldsymbol{r}_2) = \langle N_i N_j \rangle - \delta_{ij} \langle N_i \rangle \tag{3.120b}$$

After a simple algebraic manipulation, we can express the relative fluctuations in the number of particles, in terms of the integrals over the distribution functions, as

$$\iint \mathrm{d}\boldsymbol{r}_1\mathrm{d}\boldsymbol{r}_2 \left[\rho_{ij}(\boldsymbol{r}_1,\boldsymbol{r}_2) - \rho_i(\boldsymbol{r}_1)\rho_j(\boldsymbol{r}_j)\right] = \langle N_i N_j\rangle - \langle N_i\rangle\langle N_j\rangle - \delta_{ij}\langle N_i\rangle \tag{3.121}$$

For a homogeneous, isotropic system this equation can be simplified to read

$$V^{-1}G_{ij} = \frac{\langle N_i N_j\rangle - \langle N_i\rangle\langle N_j\rangle}{\langle N_i\rangle\langle N_j\rangle} - \frac{\delta_{ij}}{\langle N_i\rangle} \tag{3.122}$$

where we have introduced the KB integrals G_{ij}

$$G_{ij} \equiv \int \mathrm{d}\boldsymbol{r}\,(g_{ij}(r) - 1) \tag{3.123}$$

All that remains is to relate the fluctuations in the number of particles to some thermodynamic quantity. Such a relationship is trivial to find, as the following two equations follow directly from the definition of the grand-canonical partition function (Eq. (3.22))

$$z_i\frac{\partial \ln \Xi}{\partial z_i} \equiv \beta^{-1}\frac{\partial \ln \Xi}{\partial \mu_i} = \langle N_i\rangle \tag{3.124a}$$

$$z_i z_j \frac{\partial^2 \ln \Xi}{\partial z_i\,\partial z_j} \equiv \beta^{-2}\frac{\partial^2 \ln \Xi}{\partial \mu_i\,\partial \mu_j} - \delta_{ij}\beta^{-1}\frac{\partial \ln \Xi}{\partial \mu_i} = V\rho_i\rho_j G_{ij} \tag{3.124b}$$

We have here a relationship between the distribution functions and the derivatives of the grand-potential, from which a complete thermodynamic description can (in principle) be derived. However, as these equations have been derived in the grand-canonical ensemble (μVT), they do not correspond to the standard experimental conditions of constant temperature and pressure. The main work of Kirkwood and Buff [52] was to show how these results could be carried over into the experimental (NPT) ensemble. This is done by using the standard theory of partial derivatives, to transform between derivatives taken in the different ensembles (i.e. with different fixed variables).

Theoretical and Experimental Setups

The first step is to express the chemical potential derivatives as derivatives over the number of particles, essentially going from a μVT to an NVT description. The standard chain-rule for differentiation gives

$$\left.\frac{\partial}{\partial \mu_i}\right|_{\boldsymbol{\mu}/\mu_i,V} = \sum_k \left.\frac{\partial N_k}{\partial \mu_i}\right|_{\boldsymbol{\mu}/\mu_i,V} \left.\frac{\partial}{\partial N_k}\right|_{\boldsymbol{N}/N_k,V} \tag{3.125}$$

where $\left.\frac{\partial}{\partial X_i}\right|_{\boldsymbol{X}/X_i}$ refers to a partial derivative taken with respect to X_i, with all other $X_{j\neq i}$ held constant. By inserting μ_j on both sides, we obtain[12]

$$\delta_{ij} = \sum_k A_{ik}B_{kj} \tag{3.126}$$

[12]In their original paper [52], Kirkwood and Buff take an alternative route, proving instead that $A = ABA$ and not $A = B^{-1}$ directly.

where the auxiliary A and B matrices are defined as

$$B_{ij} = \frac{1}{\beta V}\frac{\partial N_i}{\partial \mu_j}\bigg|_{\boldsymbol{\mu}/\mu_j,V} \equiv \rho_i\rho_j G_{ij} + \delta_{ij}\rho_i \tag{3.127a}$$

$$A_{ij} = \beta V \frac{\partial \mu_i}{\partial N_j}\bigg|_{\boldsymbol{N}/N_j,V} \tag{3.127b}$$

The second step is to express the derivatives with respect to particle numbers at constant V and T, which appear in the A factors, as derivatives at constant P and T instead. Using the following two properties of partial derivatives

$$\frac{\partial}{\partial N_i}\bigg|_{\boldsymbol{N}/N_i,V} = \frac{\partial}{\partial N_i}\bigg|_{\boldsymbol{N}/N_i,P} + \frac{\partial P}{\partial N_i}\bigg|_{\boldsymbol{N}/N_i,V}\frac{\partial}{\partial P}\bigg|_{\boldsymbol{N}} \tag{3.128}$$

$$-1 = \left(\frac{\partial P}{\partial N_i}\right)_{\boldsymbol{N}/N_i,V}\left(\frac{\partial N_i}{\partial V}\right)_{\boldsymbol{N}/N_i,P}\left(\frac{\partial V}{\partial P}\right)_{\boldsymbol{N}} \tag{3.129}$$

the coefficients of the A matrix can be redefined as

$$(\beta V)^{-1}A_{ij} = \left(\frac{\partial \mu_i}{\partial N_j}\right)_{\boldsymbol{N}/N_j,P} + \frac{\overline{V}_i\overline{V}_j}{V\kappa_T} \tag{3.130}$$

where we have used the definition of the partial volumes $\overline{V}_i$ and the isothermal compressibility κ_T

$$\overline{V}_i = \left(\frac{\partial V}{\partial N_i}\right)_{\boldsymbol{N}/N_i,P} = \left(\frac{\partial \mu_i}{\partial P}\right)_{\boldsymbol{N}} \tag{3.131}$$

$$\kappa_T = -\frac{1}{V}\left(\frac{\partial V}{\partial P}\right)_{\boldsymbol{N},T} \tag{3.132}$$

Furthermore, use of Euler's theorem[13] provides two additional equations for the partial volumes and the chemical potential derivatives.

$$V = \sum_j N_j\overline{V}_j \tag{3.133}$$

$$0 = \sum_j N_j\left(\frac{\partial \mu_i}{\partial N_j}\right)_{\boldsymbol{N}/N_j,P,T} \tag{3.134}$$

From these equations, the following three expressions, relating a macroscopic thermodynamic quantity (in the NPT ensemble) to the fluctuations in the number of particles (in the μVT ensemble), are easily derived [18, 52]

$$(k_{\mathrm{B}}T\kappa_T)^{-1} = |B|^{-1}\sum_{ij}\rho_i\rho_j B^{\dagger}_{ji} \tag{3.135a}$$

$$\overline{V}_i = k_{\mathrm{B}}T\kappa_T|B|^{-1}\sum_j \rho_j B^{\dagger}_{ji} \tag{3.135b}$$

$$\left(\frac{\partial \mu_i}{\partial N_j}\right)_{N'_j,P} = \frac{k_{\mathrm{B}}T}{V}|B|^{-1}\left[\frac{\sum_{kl}\rho_k\rho_l\left(B^{\dagger}_{ji}B^{\dagger}_{kl} - B^{\dagger}_{li}B^{\dagger}_{kj}\right)}{\sum_{kl}\rho_k\rho_l B^{\dagger}_{lk}}\right] \tag{3.135c}$$

[13] $V(N,P,T)$ is a homogeneous function order 1 and $\mu(N,P,T)$ is an intensive property (homogeneous of order 0).

where $B^\dagger$ denotes the cofactor matrix of B, and $|B|$ its determinant. Inspection of Eq. (3.135a) shows that we have arrived at an expression for the compressibility χ_T in terms of the radial distribution functions (Eq.(3.127)), which generalizes the compressibility equation (Eq.(3.39)) to the case of multi-component systems. An expression for the osmotic pressure Π (the pressure due to the solute particles) can also be obtained

$$\beta \left(\frac{\Pi}{\rho_i} \right)_{T,\mu_1,\rho_k} = \sum_{j \geq 2} \rho_j |B|^{-1} B^\dagger_{ji} \tag{3.136}$$

where the solvent is labelled 1 and the solutes $j = 2, 3, \ldots$. The derivative on the left-hand side of this equation is taken at constant solvent chemical potential and solute densities ($k \neq i$).

We end by noting that the Kirkwood-Buff theory, although providing an exact description of solutions, has been derived in a grand-canonical ensemble. As such, the particle numbers, for all the components in the system, will fluctuate independently of each other. This is incompatible with the electro-neutrality usually imposed when dealing with electrolyte solutions, and charged systems in general. Furthermore, Eq. (3.135) *only* provides expressions for single-ion quantities, which cannot be determined experimentally. A solution to these problems was proposed by Kusalik and Patey [53], who developed a k-dependant generalization of the KB equations, before taking the $k \longrightarrow 0$ limit under the appropriate constraints (i.e. electro-neutrality). Finally, the G_{ij} integrals are very sensitive to the long-range value of the radial distribution functions, which means that the $\mathcal{N}^{-1}$ tail that appears in the canonical $g_{ij}(r)$ must absolutely be corrected for. The reader will probably guess as to why we have not adopted the KB theory in our description of electrolyte solutions: (1) its application is not entirely straightforward, (2) it makes explicit reference to the solvent (we wish to derive an implicit solvent model), and (3) it is computationally very demanding (the $g_{ij}(r)$ need to be computed with a very high degree of accuracy to obtain converged results for the G_{ij}), making it practically impossible to use for aqueous electrolyte solutions.

3.4.3 McMillan-Mayer Theory of Electrolyte Solutions

The Implicit-Solvent Model

In general, the statistical mechanical theory of multi-component systems developed by McMillan and Mayer can be considered to be a generalization of the theory of imperfect gases. It provides expressions for the thermodynamic properties and the distribution functions of a multi-component system, at a given activity(chemical potential), in terms of the distribution functions at an arbitrary reference activity; provided the two sets do not bridge a phase transition [51]. These expressions are given as a power series in the activity change between the two states. An exact implicit solvent theory of electrolyte solutions is obtained when the reference activity of the solvent is taken to be that of the pure solvent (at some standard state), while the reference for the solutes is chosen to be zero. With this choice, the expansion coefficients contain no explicit reference to the solute-solvent or solvent-solvent potentials, they depend only on the n-body solute-solute potentials of mean force.

In practice, this McMillan-Mayer theory of electrolyte solutions is obtained by tracing out the unwanted (solvent) degrees of freedom from the full grand-canonical partition

function. This procedure, or mathematical trick, allows us to define an equivalent system, which is described by an effective Hamiltonian that makes no reference to the solvent. For simplicity, consider a solution with only two species, the solvent and one solute. The positions of the former are represented by $\boldsymbol{R}_i$, those of the latter by $\boldsymbol{r}_i$. In this case, the grand-canonical partition function takes the form

$$\begin{aligned}\Xi(z,y,V,T) &= \sum_N \sum_M \frac{z^N}{N!}\frac{y^M}{M!}\int \mathrm{d}\boldsymbol{r}^N \int \mathrm{d}\boldsymbol{R}^M e^{-\beta\mathcal{V}_{N+M}(\{\boldsymbol{r}^N;\boldsymbol{R}^M\})} \\ &= \sum_N \frac{z^N}{N!}\int \mathrm{d}\boldsymbol{r}^N \left[\sum_M \frac{y^M}{M!}\int \mathrm{d}\boldsymbol{R}^M e^{-\beta\mathcal{V}_{N+M}(\{\boldsymbol{r}^N,\boldsymbol{R}^M\})}\right]\end{aligned} \tag{3.137}$$

where $\mathcal{V}_{N+M}$ is the total interaction potential for a system with N solute particles and M solvent particles, and z and y are the activities of the solute and solvent, respectively. The quantity inside square brackets is then related to the potentials of mean-force. For this two-component system, the n-body (solute-solute) particle distribution function (Eq. (3.33)) takes the form

$$\begin{aligned}g^{(n)}(\boldsymbol{r}_1,\ldots,\boldsymbol{r}_n) = \frac{1}{\rho^n \Xi(z,y,V,T)} \sum_{N\geq n} \frac{z^N}{N!}\int \mathrm{d}\boldsymbol{r}^{(N-n)} \\ \times \left[\sum_M \frac{y^M}{M!}\int \mathrm{d}\boldsymbol{R}^M e^{-\beta V_{N+M}(\{\boldsymbol{r}^N;\boldsymbol{R}^M\})}\right]\end{aligned} \tag{3.138}$$

where ρ is the solute density. By changing the variable in the summation, this expression can be brought to a form which resembles that of Eq. (3.137)

$$\begin{aligned}g^{(n)}(\boldsymbol{r}_1,\ldots,\boldsymbol{r}_n) = \left(\frac{z}{\rho}\right)^n \frac{1}{\Xi(z,y,V,T)} \sum_{N\geq 0} \frac{z^N}{N!}\int \mathrm{d}\boldsymbol{r}^N \\ \left[\sum_M \frac{y^M}{M!}\int \mathrm{d}\boldsymbol{R}^M e^{-\beta V_{N+M+n}(\{\boldsymbol{r}^{N+n};\boldsymbol{R}^M\})}\right]\end{aligned} \tag{3.139}$$

(3.140)

Taking the limit of this last expression as $z \longrightarrow 0$ (as the chemical potential of the solute tends to minus infinity), we obtain

$$g^{(n)}(\boldsymbol{r}_1,\ldots,\boldsymbol{r}_n) \underset{z\to 0}{=} \frac{\gamma^n}{\Xi(z=0,y,V,T)} \left[\sum_M \frac{y^M}{M!}\int \mathrm{d}\boldsymbol{R}^M e^{-\beta V_{M+n}(\{\boldsymbol{r}^n;\boldsymbol{R}^M\})}\right] \tag{3.141}$$

with $\gamma = z/\rho$. For a one component system, it is well known that $z \to \rho$ at infinite dilution [17], and thus γ should tend to 1, but this is no longer true in the multi-component case, since $\gamma \neq 0$ [13]. Using Eq. (3.141), we can rewrite the term in brackets in Eq. (3.138) in terms of the n-body (solute-solute) particle distribution function, thus eliminating all explicit references to the solvent degrees of freedom

$$\Xi(z,y,V,T) = \Xi(z=0,y,V,T) \sum_N \frac{a^N}{N!}\int \mathrm{d}\boldsymbol{r}^N \; g^{(N)}(\boldsymbol{r}_1,\ldots,\boldsymbol{r}_n)\big|_{z=0} \tag{3.142}$$

where we have redefined the solute activity as[14]

$$a = z/\gamma \equiv z \lim_{z\to 0} \frac{\rho}{z} \tag{3.143}$$

Finally, using the definition of the PMF (3.41) we obtain

$$\Xi(x, y, V, T) = \Xi(z = 0, y, V, T) \sum_N \frac{a^N}{N!} \int \mathrm{d}\boldsymbol{r}^N e^{-\beta w^{(N)}(\{\boldsymbol{r}^N\})} \tag{3.144}$$

where the $w^{(N)}(\{\boldsymbol{r}^N\})$ are the N-body potentials of mean force at infinite dilution (i.e. for a solution with exactly N solute particles). Note that the sum appearing on the right-hand side of this equation takes the exact form of a grand-canonical partition function (Eq. (3.22)). We can thus express the full partition function as a product of the partition functions of the pure solvent (at the same activity and temperature as the solution) $\Xi(0, y, V, T)$ and the partition function of an effective solute gas $\Xi(a, V, T)$.

$$\Xi(x, y, V, T) = \Xi(z = 0, y, V, T) \times \Xi_{MM}(a, V, T) \tag{3.145}$$

From the definition of the grand-potential $\Omega = \ln \Xi$ (3.24), we see that the pressure of the solution is naturally separated into a pure solvent P_{sol} and pure solute term P_{MM}. The latter is, by definition, equivalent to the osmotic pressure of the solution ($\Pi = P_{\mathrm{osm}}$)

$$P = P_{\mathrm{sol}} + P_{\mathrm{osm}} \tag{3.146}$$

Although we have only considered the case of a two component system of point particles, the generalization to many solutes and molecular systems is straightforward. When compared to the KB description presented in the previous section, we see that the MM theory provides a much more comfortable representation for electrolytes in solution. This is obtained at the "cost" of hiding all the effects of the solvent within the PMF.

Theoretical and Experimental Reference Frames

As mentioned above, the thermodynamics of the solute gas within the MM framework are computed with respect to a pure solvent at constant chemical potential. The measured values will not correspond to those observed experimentally, at constant temperature and pressure [54]. A schematic representation of the these two setups, the experimental or Lewis-Randall (LR) and McMillan-Mayer (MM) is given in Figure 3.2. The approximate relation used to perform the conversion between the osmotic coefficients obtained at these two levels of description, which is exact if the solution is incompressible, has been given in Eq. (3.86).

All the values for ϕ presented in this work are given in the MM (implicit solvent) reference system. For the alkali halide salts we use the experimental values provided by Robinson and Stokes [42], and for the lanthanoid chloride salts we use the values given by Spedding and coworkers [55]. The conversion between the LR and MM reference systems requires knowledge of the mass density of the solution, as well as the concentration derivative of the density (needed to compute the partial volume $\overline{V}$), for which we use the data given by Novotný [56] and Spedding [57].

[14] This transformation amounts to a constant shift in the solute chemical potential.

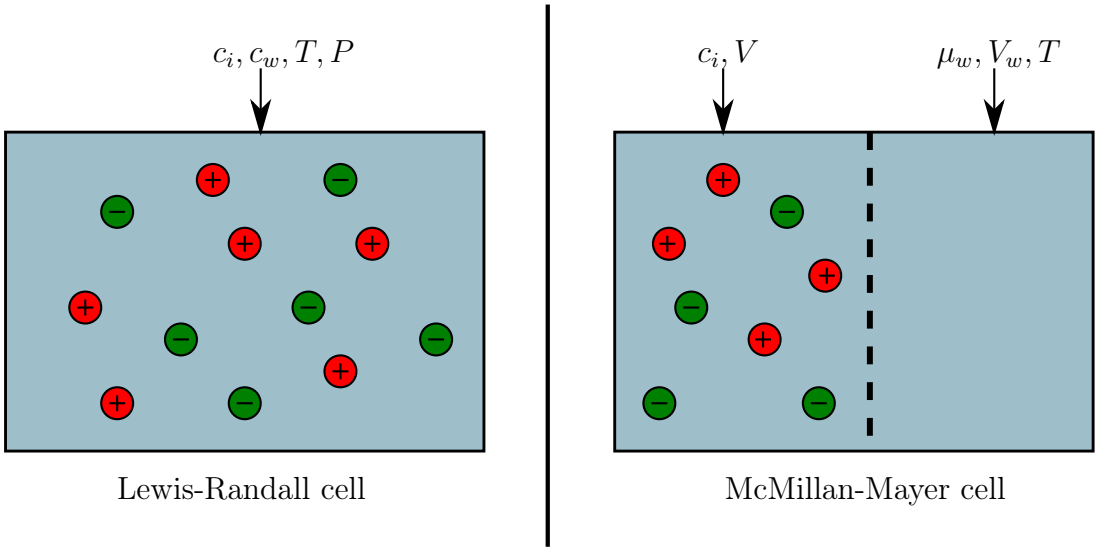

Figure 3.2: Schematic representation of the difference between the Lewis-Randall (experimental) and McMillan-Mayer reference frames.

Chapter 4

Ion-Specific Effects from *Ab-Initio* Descriptions

Summary

4.1 Introduction

Inorganic ions are known to be of fundamental importance in many fields of chemistry. In particular, their role within biological processes has recently attracted widespread attention, as they are known to influence the solvation of proteins [58], as well as their diffusion along DNA [2]. A proper description of the thermodynamic and dynamic properties of ions in solution (and at interfaces) also presents important industrial applications. Within the nuclear industry, for example, basic properties such as the ion

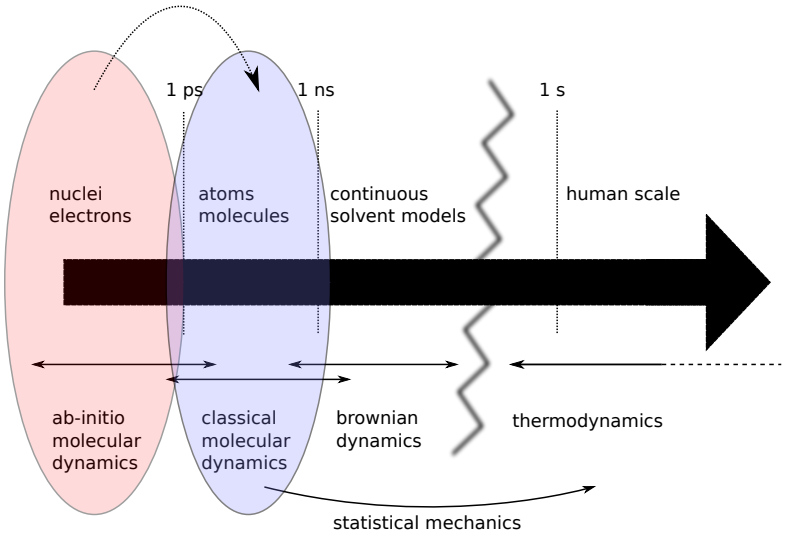

Figure 4.1: The first step in the multi-scale description of electrolyte solutions: Deriving classical potentials from *ab-initio* calculations.

activities and the hydration free energies are of fundamental importance for the reprocessing of spent nuclear fuel and its subsequent storage [4, 59].

Within the engineering community, such systems have traditionally been treated using simple, almost phenomenological implicit solvent descriptions, which are fitted to reproduce the experimental data. While this has the advantage of providing (in a best case scenario) perfect agreement with experiments, it is not evident how such models can be interpreted in terms of the physically relevant microscopic parameters. This is important in order to quantify the environmental effects which strongly influence the ion-specific behaviour. Furthermore, the predictability provided by these simple models is somewhat of a mystery. What happens if the parameters of the model are varied? What happens if I try to apply the model to a different system from that to which it was parametrized? Finally, and this is probably the biggest question mark hanging over such an approach, what can we do if little or no experimental data is available?

To sidestep these difficulties, the obvious solution is to start at the bottom and slowly build up the more approximate (less computationally demanding) models. The advantage of such a bottom-up approach is that, at each step, we know exactly what it is we are taking out, and what we are replacing it with. In this chapter we will deal with the first step in our multi-scale description of ionic solutions: that of deriving classical force-fields for the ions, from *ab-initio* calculations. We begin with a brief overview of the *ab-initio* density functional theory used to treat the electronic degrees of freedom, before introducing the basic concepts of classical molecular dynamics. We then proceed to show how the use of *ab-initio* calculations, in particular those for the (localized) electronic density, can be used to unambiguously define the classical interaction potentials between polarizable ions in solution. Finally, we test our potentials against a wide variety of experimental data to see how they behave.

4.2 Principles of *Ab-Initio* Simulations

It is well known that trying to solve the Schrödinger equation for any but the simplest of systems, such as a particle in a potential well, a harmonic oscillator, or the hydrogen atom, is a formidable task, which can only be done approximately. Unfortunately, the situation quickly becomes insurmountable, as the number of degrees of freedom $\mathcal{N}$ increases, since the complexity of the available methods typically scales as $\mathcal{O}(\mathcal{N}^{4\sim7})$ [60]. Attempting a fully quantum description of the structural or dynamic properties of ionic solutions, for which the characteristic length and time scales are of the order of nanoseconds and nanometers, respectively, is clearly out of the question. It is not surprising then, to see that most high-level quantum chemistry calculations, which give approximate solutions to Schrödinger's equation, are restricted to electronic structure calculations of isolated molecules in vacuum or within small water clusters (i.e. to optimize the geometry or compute the electronic spectra) [61]. This approach is clearly ill suited for the study of condensed phases.

The first approximation that is usually made in order to reduce the complexity inherent to a fully quantum description, is to assume that the electrons evolve over a time scale that is much shorter (faster) than that which governs the motion of the nuclei[1]. The electrons remain in their ground state as they adiabatically follow the nuclei motion. This is the Born-Oppenheimer approximation [62, 63, 64], which allows us to replace the total wavefunction of the system with a separable wavefunction

$$\Psi_{\mathrm{S}}(\{\boldsymbol{R}_I\},\{\boldsymbol{r}_i\}) = \Psi\left(\{\boldsymbol{R}_I\}\right)\Psi_0\left(\{\boldsymbol{r}_i\}|\{\boldsymbol{R}_I\}\right) \tag{4.1}$$

where $\Psi_0(\{\boldsymbol{r}_i\}|\{\boldsymbol{R}_I\})$ is the ground state wavefunction[2] of the electronic Hamiltonian ($\widehat{H}_e$) for a fixed ionic (nuclei) configuration $\{\boldsymbol{R}_I\}$, and $\Psi(\{\boldsymbol{R}_I\})$ is the nuclear part of the total wavefunction. Under this adiabatic approximation, the Hamiltonian determining the time evolution of the ionic wavefunction is given by

$$\widehat{H}_N = \widehat{T}_N + \widehat{V}_{NN} + E_0(\{\widehat{\boldsymbol{R}}_I\}) \tag{4.2}$$

where $\widehat{T}_N$ is the nuclear kinetic energy operator, $\widehat{V}_{NN}$ the nuclei-nuclei potential energy operator, and E_0 is the ground-state electronic energy for the particular nuclear configuration $\{\boldsymbol{R}_I\}$

$$E_0 = \min_{\Psi(\{\boldsymbol{r}_i\})} \langle\Psi|\widehat{H}_e|\Psi\rangle \tag{4.3}$$

By definition, this minimum is obtained for $\Psi = \Psi_0$. The electronic Hamiltonian is given by the sum of the electron kinetic energy $\widehat{T}_e$, the electron-electron potential energy $\widehat{V}_{ee}$, and the electron-nuclei (external) potential energy $\widehat{V}_{Ne} = \widehat{V}_{\mathrm{ext}}$ operators

$$\widehat{H}_e = \widehat{T}_e + \widehat{V}_{ee} + \widehat{V}_{\mathrm{ext}} \tag{4.4}$$

Taking into account the large mass of the nuclei, the second approximation that is made is to consider the classical limit for the nuclei dynamics. In this case, the potential

[1] This is due to the large mass ratio between the nuclei and the electrons. For a hydrogen atom this ratio of proton to electron mass is $m_p/m_e \simeq 2\times10^3$

[2] We consider only non-degenerate ground states.

energy surface describing the nuclei dynamics is, from Eq. (4.2), $v_{NN}(\{\boldsymbol{R}\}_I)+E_0(\{\boldsymbol{R}_I\})$, which is a function only of the nuclei coordinates. To compute the forces on the nuclei, it is then necessary to compute the gradient (with respect to the nuclei coordinates) of this function. The first term (v_{NN}) is trivially obtained, leaving just the gradient of the electronic energy (E_0), which can be evaluated with the help of the Hellmann-Feynman theorem [62], which states that

$$\frac{\partial E_0}{\partial R_I} = \int \mathrm{d}\boldsymbol{r} \frac{\partial v_{Ne}(\boldsymbol{r}, \{\boldsymbol{R}_J\})}{\partial R_I} \rho^0(\boldsymbol{r}) \tag{4.5}$$

where $\rho^0(\boldsymbol{r})$ is the equilibrium electronic density

$$\rho^0(\boldsymbol{r}) = N \int \mathrm{d}\boldsymbol{r}_2 \ldots \mathrm{d}\boldsymbol{r}_N |\Psi_0(\boldsymbol{r}, \ldots, \boldsymbol{r}_N)|^2 \tag{4.6}$$

with N the number of electrons. This theorem proves that the force exerted by the electron cloud on the nuclei, within a Born-Oppenheimer approximation, can be computed within a completely classical framework, i.e. by computing the classical electrostatic interaction between a set of point charges $\{\boldsymbol{R}_i\}$ (the nuclei) immersed in an electronic charge distribution $\rho^0(\boldsymbol{r})$. We can thus replace the problem of determining the $3(N+M)$-dimensional wavefunction $\Psi(\{\boldsymbol{R}_I\}, \{\boldsymbol{r}_i\})$ (N electrons and M nuclei), with that of determining the much "simpler" 3-dimensional electron density function $\rho(\boldsymbol{r})$.

4.2.1 Solving the N-body Problem: A Variational Approach

The Hohenberg - Kohn Theorem

The fact that we can consider the electronic density $\rho(r)$ as the fundamental function, from which we can derive all the ground state properties of the system, in lieu of the more complicated electronic wavefunction Ψ, is due to the well-known Hohenberg-Kohn theorem [62]. This theorem states that there exists a one to one map between the external potential $v_{\text{ext}}(\boldsymbol{r})$ and the electron density $\rho(\boldsymbol{r})$[3], both of which determine all the ground state properties of the system (Ψ_0)

$$\begin{array}{ccc} \rho^0(\boldsymbol{r}) & \longleftrightarrow & v_{\text{ext}}(\boldsymbol{r}) \\ & \searrow \quad \swarrow & \\ & \Psi_0 & \end{array} \tag{4.7}$$

The electron density $\rho(r)$ is considered simpler than the full wavefunction Ψ, since the function space that needs to be searched has been reduced to the more reasonable case of scalar three-dimensional real functions. However, all that has been done is to write one unknown quantity Ψ in terms of another $\rho(r)$, without specifying how either is to be calculated. Since $\rho(\boldsymbol{r})$ determines all ground state properties of the system, the total energy is a functional of ρ, and can be written as

$$E[\rho] = \int \mathrm{d}\boldsymbol{r} \rho(\boldsymbol{r}) v_{ext}(\boldsymbol{r}) + F_{\text{HK}}[\rho] \tag{4.8}$$

[3]This is only true if the density is v-representable, which is not easy to prove; however, the formulation of density functional theory only requires the density be N-representable, which is a weaker condition, that should be satisfied by most non-pathological density functions [62].

where $F_{\mathrm{HK}}[\rho]$ is the so-called Hohenberg-Kohn functional, which is independent of the external potential

$$F_{\mathrm{HK}}[\rho] = T[\rho] + V_{ee}[\rho] \tag{4.9}$$

Fortunately, it can be shown that the minimization of the functional $E[\psi]$ (Eq. (4.3)), can be expressed, due to the Hohenberg-Kohn theorem, as a minimization of the functional $E[\rho]$ [62]

$$E_0 = \min_{\rho(r)} E[\rho] \tag{4.10}$$

or equivalently as

$$E_0 \leq E[\rho] \tag{4.11}$$

with the ground state energy E_0 being obtained for the ground state density $\rho_0(\boldsymbol{r})$ (which is assumed to be non-degenerate). Any trial density $\rho'(\boldsymbol{r}) \neq \rho(\boldsymbol{r})$ will result in an energy value $E[\rho'] > E_0$.

The Kohn - Sham Method

The problem of determining the ground state properties of the system is then reduced to the variational problem of finding the minimum of Eq. (4.8). However, the (universal) HK functional $F_{\mathrm{HK}}[\rho] = T[\rho] + V_{ee}[\rho]$ is still undefined. The idea behind the Kohn-Sham method [65] is to introduce an auxiliary (fictitious) system of non-interacting electrons in order to evaluate the kinetic energy term $T[\rho]$ exactly; the remaining term $V_{ee}[\rho]$ is computed within a mean-field approximation, and the small correction (the difference with respect to the exact calculation) is treated separately. For this auxiliary system, the wave function is given by a single Slater determinant of $N/2$ one-electron orbitals ϕ_i [66], which correspond to the lowest $N/2$ eigenvectors (each state holds two electrons) of the single electron Hamiltonian

$$\widehat{H}_s = -\frac{1}{2}\nabla^2 + v_s(\boldsymbol{r}) \tag{4.12}$$

where $v_s(\boldsymbol{r})$ is determined uniquely by $\rho(\boldsymbol{r})$ thanks to the Hohenberg-Kohn theorem. The kinetic energy functional is then replaced by the corresponding quantity in the non-interacting case $T[\rho] \to T_s[\rho]$

$$T_s[\rho] = \sum_{i=1}^{N} \langle \phi_i[\rho]| - \frac{1}{2}\nabla^2 |\phi_i[\rho]\rangle \tag{4.13}$$

and the electron-electron potential energy is evaluated within a classical mean-field approximation $V_{ee}[\rho] \to J[\rho]$

$$J[\rho] = \frac{1}{2}\iint \mathrm{d}\boldsymbol{r}\mathrm{d}\boldsymbol{r}' \frac{\rho(\boldsymbol{r})\rho(\boldsymbol{r}')}{|\boldsymbol{r} - \boldsymbol{r}'|} \tag{4.14}$$

With these substitutions in mind, the energy functional is written as

$$E[n] = \int \mathrm{d}\boldsymbol{r} n(\boldsymbol{r}) v_{ext}(\boldsymbol{r}) + T_s[n] + J[n] + E_{xc}[n] \tag{4.15}$$

which is still exact, since all that has been done is to group the unknown quantities into the *exchange-correlation* term

$$E_{xc}[n] = (T[n] - T_s[n]) + (V_{ee}[n] - J[n]) \tag{4.16}$$

Practical Considerations: Approximative Functionals, Plane Waves, and PseudoPotentials

We have seen that the whole problem of DFT is reduced to finding an appropriate exchange-correlation functional E_{xc}. The first such functional to be proposed was the Local Density Approximation (LDA) [64], which assumes that the exchange-correlation energy is the same as that of a uniform electron gas at the corresponding density. This energy is known thanks to the work of Ceperley and Alder [67], who have tabulated it for several densities. The next generation of functionals, the generalized gradient approximations (GGA), attempted to improve on the simple LDA functional by not just using the local electron density, but also its gradient. When higher order terms (derivatives) in the expansion are included, we obtain the meta-GGA functionals [64]. The Becke-Lee-Yang-Parr (BLYP) [68, 69] and Perdew-Burke-Ernzerhorf (PBE) [70] functionals used in this work are of the GGA variety. Attempts to improve on these functionals, in order to include non-local effects, by using exact results for the exchange energy have led to the so-called hybrid functionals.

When solving the Kohn-Sham equations, it is convenient to search for a set of orbitals which diagonalize the Kohn-Sham Hamiltonian, as this greatly simplifies the calculations [63]. To take advantage of the underlying periodicity of the system (assuming periodic boundary conditions are used), the orbitals or wavefunctions ϕ_i are expanded in a plane wave basis set, which simplifies the calculations even further. However, this has the disadvantage that a great many number of plane-waves are required in order to properly describe the wavefunction close to the nuclei. As the wavefunctions must be orthogonal to each other $\langle\phi_i|\phi_j\rangle = \delta_{ij}$, the valence electron wavefunction is expected to undergo rapid oscillations in the vicinity of the nuclei [63, 64]. It is this fast localized variation in the wavefunctions which makes it computationally impossible to use a basis set of plane waves for all the orbitals. However, since it is the valence electrons which dictate the "chemistry" of the system, the core electrons being tightly bound and hardly participating in any type of bonding, we need only attempt a quantum description for the former, the effects of the latter can be approximated by using a pseudo-potential. There exist an ample number of pseudo-potentials, obtained by using different parametrizations and boundary conditions, which we will not attempt to cover. Unfortunately, the "science" behind pseudo-potential development is somewhat technical, not very interesting, and very hard to implement[4]. We will therefore ignore all further discussion on the subject, except to say that the pseudo-potentials are derived for use with a specific exchange-correlation functional and should obviously not be mixed. The Troullier-Martins (TM) [71] and Goedecker-Tetter-Hutter (GTH) [72, 73, 74] pseu-

[4]This is a matter of personal taste, but in the end, the whole business of pseudopotentials (which is better, which is worse) made me recall Olivier Heavyside's response to those who would criticize the rigour of his work: *"I do not refuse my dinner simply because I do not understand the process of digestion"*. Likewise, I dot not refuse a good (enough) pseudo-potential simply because I have not understood how it was obtained.

dopotentials we have used are standard for the condensed matter systems we consider, and are known to yield reasonably good results.

4.2.2 The Use of Maximally Localized Wannier Functions

Introduction

The problem with the canonical Kohn-Sham orbitals, and this is independent of the basis set that is used, is the fact that they are delocalized in space. This leads to an electronic density that is also delocalized over the entire simulation cell. It is thus not easy to directly obtain localized properties of individual atoms or molecules, such as information on the formation of bonds or the response of the molecular orbitals to an externally applied electric field. It is clear, however, that any unitary transformation of the Kohn-Sham orbitals, which leaves the density and energy unchanged, is a valid solution to the Kohn-Sham equations obtained from eqs. (4.10), (4.12) and (4.15). We must thus look for an equivalent set of orbitals which are localized around the individual ions ($\boldsymbol{R}_I$). This transformation, from the canonical delocalized Kohn-Sham orbitals to a set of localized orbitals, is achieved through the use of the maximally localized Wannier function (MLWF) formalism [75, 76, 77].

The Wannier functions are defined through a unitary transformation of the KS eigenvectors

$$|\phi_i^w\rangle = \sum_{j=1}^{N/2} U_{ij}|\phi_j\rangle \tag{4.17}$$

where the unitary matrix U is determined by an iterative minimization of the Wannier function spread Ω, defined as

$$\Omega = \sum_{i=1}^{N/2} S_i \tag{4.18}$$

where the S_i are the spreads of the individual Wannier orbitals ϕ_i^w

$$S_i = \sum_{\alpha} \frac{-1}{(2\pi)^3} \log |s_{i,\alpha}|^2 \tag{4.19}$$

$$s_{i,\alpha} = \langle \phi_i^w | e^{i(2\pi/L)r_{i,\alpha}} | \phi_i^w \rangle \tag{4.20}$$

with $\alpha = x, y, z$. Aside from their spread S_i (which gives the size of the localized electron cloud), the Wannier orbitals are defined in terms of their centers $\boldsymbol{r}_i^w$

$$r_{i,\alpha}^w = -\frac{L}{2\pi} \Im(\ln s_{i,\alpha}) \tag{4.21}$$

We have implicitly assumed that the calculations are performed on a cubic simulation box with periodic boundary conditions, since this is the only case that will interest us in this work.

Computing Ionic (Molecular) Polarizabilities

The MLWF provide a picture of the electron density around individual atoms which is easily interpreted from a chemical point of view. It is thus natural to consider the possibility of computing the molecular polarizabilities by studying the response of the MLWF to an applied external field. Since the dipole moments of single ions or molecules can be computed from the distribution of the charge centers of the MLWF localized in their vicinity. This approach has been recently validated [78, 79, 80] and used to develop a complete theory of electric polarization in crystalline dielectrics [81, 82, 83]. The partial dipole moment of a given ion or molecule I is defined, in atomic units, as

$$\boldsymbol{\mu}_I = \sum_J \Theta_I(J) \left(Z_J \boldsymbol{R}_J - 2 \sum_i \vartheta_J(i) \boldsymbol{r}_i^w \right) \tag{4.22}$$

where Z_I and $\boldsymbol{R}_I$ are the nuclear charges and positions. For notational simplicity, throughout this section we use capital indices $\{I, J, K, \ldots\}$ to refer to individual ions, or groups of ions (molecules), and lowercase indices refer to the Wannier orbitals (electronic degrees of freedom). The sum over J runs over the ions; with $\Theta_I(J)$ choosing those belonging to molecule I only

$$\Theta_I(J) = \begin{cases} 1, & \text{ion } J \text{ belongs to molecule } I = \{I_1, \ldots, I_n\} \\ 0, & \text{otherwise} \end{cases}$$

and the sum over i runs over the Wannier orbitals, with $\vartheta_J(i)$ choosing only those which are localized in the vicinity of ion J (itself belonging to molecule I)[5]

$$\vartheta_J(i) = \begin{cases} 1, & |\boldsymbol{r}_i^w - \boldsymbol{R}_J| < r_c \\ 0, & \text{otherwise} \end{cases} \tag{4.23}$$

For the condensed, non-metallic, systems we consider in this work, all Wannier orbitals are localized in the vicinity of one, and only one atom, such that if $\vartheta_I(k)\vartheta_J(k) = 1$ then ion I and ion J are necessarily the same. In practice, the cutoff radius used to determine the localization of the Wannier orbitals was chosen to be $r_c = 1.5a_0$ ($a_0 = 0.529$ Å is the Bohr radius).

If a small electric field $\boldsymbol{\mathcal{E}}$ is applied to the system, the linear response can be characterized by an additional field-induced dipole moment $\boldsymbol{\delta\mu}_I$ on each individual molecule. This externally applied field can be considered as an optical field, to differentiate it from the static electric field created by the charge distribution of the ions (molecules). The net induced dipole $\boldsymbol{\delta\mu}_I$ of molecule I can then be written in terms of the total (optical) electric field which acts on it

$$\boldsymbol{\delta\mu}_I(\{\boldsymbol{R}_K\}) = \boldsymbol{\alpha}_I(\{\boldsymbol{R}_K\}) \cdot \left[\boldsymbol{\mathcal{E}} + \sum_{J \neq I} \mathbb{T}_{IJ}^{\text{dip-dip}} \cdot \boldsymbol{\delta\mu}_J(\{\boldsymbol{R}_K\}) \right] \tag{4.24}$$

where the sum runs over all polarizable entities (ions or molecules) $J \neq I$. In this last equation, we have introduced the dipole polarizability tensor $\boldsymbol{\alpha}_I$ of molecule I,

[5] For systems for which this is no longer valid, i.e. when a Wannier center can be attributed to two distinct atoms, a different localization rule must be used.

as well as the dipole-dipole interaction tensor $\mathbb{T}_{IJ}^{\text{dip-dip}}$. As is usual, when dealing with periodic systems, this last term is evaluated using the Ewald summation technique (see Section 4.3.3) [84, 85]. The first term on the right-hand side of (4.24) gives the direct contribution of the external field $\boldsymbol{\mathcal{E}}$ to the induced dipole, while the second term gives the contribution due to the electric fields that are reradiated from the induced dipoles of all the other molecules ($I \neq J$) in the system. In principle, higher-order induced multiples will also contribute to this expansion, but we will ignore them in what follows. This approximation is justified, on the grounds that, for a uniform electric field $\boldsymbol{\mathcal{E}}$, the directly induced higher-order multiples of spherical atoms (ions) vanish; and even in the case of molecules, their effect is expected to be negligible compared to that of the dipoles.

Within DFT calculations on periodic systems, the coupling between the electronic density and the external electric field is expressed through the macroscopic polarization of the periodically replicated cell [86, 87]. This is accomplished using Resta's Berry phase approach [88], which proposes a novel definition for the position expectation values for use with periodic systems, where the conventional position operator becomes meaningless. The new partial dipole moment of each species, in the presence of the external field, is then calculated via another localization procedure (through Eq. (4.22)). In practice, this is performed for an externally applied field $\boldsymbol{\mathcal{E}}^{(\alpha)}$ in each of the three Cartesian directions $\alpha = x, y, z$, in order to compute the corresponding dipoles $\boldsymbol{\mu}_I(\boldsymbol{\mathcal{E}}^{(\alpha)})$. The field induced dipoles are then calculated from the difference between the total molecular dipoles in the presence and absence of the field $\boldsymbol{\delta\mu}_I^{(\alpha)} = \boldsymbol{\mu}_I(\boldsymbol{\mathcal{E}}^{(\alpha)}) - \boldsymbol{\mu}_I(\boldsymbol{\mathcal{E}} = 0)$[6]. In each case, the total (optical) electric field $\boldsymbol{f}_I^{(\alpha)}$ at the position $\boldsymbol{R}_I$ of each ion is obtained from

$$\boldsymbol{f}_I^{(\alpha)} = \boldsymbol{\mathcal{E}}^{(\alpha)} + \sum_{I \neq J} \mathbb{T}_{IJ}^{\text{dip-dip}} \cdot \boldsymbol{\delta\mu}_J^{(\alpha)} \tag{4.25}$$

which is conveniently evaluated using a dipolar Ewald sum. Finally, Equation (4.24) can be inverted to yield the individual electronic polarizabilities for the particular condensed phase configuration $\{\boldsymbol{R}_I\}$

$$\boldsymbol{\alpha}_I(\{\boldsymbol{R_J}\}) = (\mathbb{F}_I)^{-1} \cdot \boldsymbol{\Pi}_I \tag{4.26}$$

where $\mathbb{F}_I$ and $\boldsymbol{\Pi}_I$ are second-rank three-dimensional tensors defined as

$$\mathbb{F}_I^{\alpha\beta} = \boldsymbol{f}_I^{(\beta)} \cdot \hat{\boldsymbol{e}}_\alpha \tag{4.27}$$

$$\boldsymbol{\Pi}_I^{\alpha\beta} = \boldsymbol{\delta\mu}_I^{(\beta)} . \hat{\boldsymbol{e}}_\alpha \tag{4.28}$$

where $\hat{\boldsymbol{e}}_\alpha$ ($\alpha = x, y, z$) represents the canonical Cartesian unit vectors $\hat{\boldsymbol{x}}$, $\hat{\boldsymbol{y}}$, and $\hat{\boldsymbol{z}}$.

Computing Dispersion Interactions

It is a well known fact that DFT calculations are unsuited for the task of describing dispersion interactions, which arise from long-range density fluctuations, since most

[6] Within the linear response regime we consider, the induced dipoles from an arbitrary, externally applied field $\mathcal{E}$, can be computed by considering the response to the individual components of the electric field $\mathcal{E}^\alpha$ separately.

exchange-correlation functionals $E_{XC}[\rho]$ do not take into account these non-local effects. The most blatant example of this is the instability (or metastability) of liquid water at standard temperature and pressure: the overly structured water presents a density that can underestimate the experimental value by $10 \sim 25\%$ [89][7]. However, Silvestrelli has noticed that this dispersion interaction can be approximately introduced *a posteriori* within a DFT approach, by introducing an interaction of the form $-\widetilde{C}_6^{ij}/r_{ij}^6$ between Wannier centers [90], where the $\widetilde{C}_6^{ij}$ terms depend only on the spread S_i of the orbitals. Assuming an isotropic distribution of Wannier centers around the nuclei, Rotenberg et al. [91] hove shown that the dispersion interaction, to second leading order, is given by

$$E_{\text{dispersion}} = -\sum_{n=6,8} \frac{C_n^{IJ}}{R_{IJ}^n} \tag{4.29}$$

with

$$C_6^{IJ} = \sum_i \sum_j \vartheta_I(i)\vartheta_J(j)\widetilde{C}_6^{ij} \tag{4.30}$$

$$C_8^{IJ} = \sum_i \sum_j \vartheta_I(i)\vartheta_J(j)(d_I(i)^2 + d_J(j)^2)\widetilde{C}_6^{ij} \tag{4.31}$$

where d_I corresponds to the (fixed) distance between Wannier orbitals and the ion to which they belong. Note that this distance is determined by the localization procedure (as an average over the corresponding distance of all the relevant Wannier centers), it is not a free parameter.

The $-\widetilde{C}_6^{ij}/r_{ij}^6$ interaction between Wannier centers is computed using Silvestrelli's procedure [90], which is itself based on the expression proposed by Andersson to describe the long-range interaction between two separated fragments of matter [92]. For two Wannier centers i and j, belonging to two distinct molecules I and J, respectively, this interaction is given by

$$\widetilde{C}_6^{ij} = \frac{3}{32\pi^{3/2}} \iint\limits_{\substack{r \leq r_c \\ r' \leq r'_c}} \mathrm{d}\boldsymbol{r}\mathrm{d}\boldsymbol{r'} \frac{\sqrt{\rho_i^w(r)\rho_j^w(r')}}{\sqrt{\rho_i^w(r)} + \sqrt{\rho_j^w(r')}} \tag{4.32}$$

where $\rho_i^w(r)$ is the density of the i-th fragment, and $r_c = (1.475 - 0.866 \ln S_i)S_i$ is the corresponding cutoff radius used to perform the integration. Following Silvestrelli, this electron density is assumed to present a hydrogen-like (exponential) localization around the Wannier center $\boldsymbol{r}_i^w$, such that

$$\rho_i^w(\boldsymbol{r}) = n_i \frac{\kappa_i^3}{8\pi} e^{-\kappa_i |\boldsymbol{r} - \boldsymbol{r}_i^w|} \tag{4.33}$$

where $n_i = 2$ is the number of electrons per orbital and $\kappa_i = 2\sqrt{3}/S_i$.

[7] *Ab-Initio* MD simulations at ambient conditions were observed to describe the experimental properties of water at a temperature 20% lower ($T \simeq -30°$)!

4.3 Molecular Dynamics Simulations

4.3.1 Introduction to MD

Consider that we want to study a closed (isolated) system of N point particles in a volume V. The Molecular Dynamics (MD) approach to this problem is to solve Newton's equations of motion,

$$m_i \ddot{q}_i = -\nabla_i V_N(\{\boldsymbol{q}_j\}) \tag{4.34}$$

in order to follow the trajectory of the system through phase space $\{\boldsymbol{q}_i, \boldsymbol{p}_i\}$, where $\boldsymbol{q}_i$, $\boldsymbol{p}_i$, and m_i refer to the position, momentum, and mass of the i-th particle, ∇_i gives the gradient with respect to $\boldsymbol{q}_i$, and V_N is the total potential energy of the system (which is assumed to depend only on the positions of the particles). Although there is little interest in solving Eq. (4.34) just to obtain the positions and velocities as a function of time, which in themselves provide almost no useful information, knowledge of these quantities allows us to measure many relevant microscopic properties $\mathcal{A}(\boldsymbol{q}, \boldsymbol{p})$. By relevant, we mean that these quantities can be related to the dynamic, structural, and thermodynamic properties (usually measured experimentally) which characterize the system, by averaging them over a sufficiently long period of time τ. The simplest examples are the internal energy U, the temperature T, and the pressure P [20]

$$U = \overline{\mathcal{H}} = \lim_{\tau\to\infty} \frac{1}{\tau} \int \mathrm{d}t \left[\sum_i \frac{\boldsymbol{p}_i^2(t)}{2m_i} + V_N(\{\boldsymbol{q}_j(t)\}) \right] \tag{4.35a}$$

$$T = \overline{\mathcal{T}} = \lim_{\tau\to\infty} \frac{1}{\tau} \int \mathrm{d}t \left[\frac{1}{N} \sum_i \frac{\boldsymbol{p}_i(t)^2}{3k_\mathrm{B} m_i} \right] \tag{4.35b}$$

$$P = \overline{\mathcal{P}} = k_\mathrm{B} T \rho + \lim_{\tau\to\infty} \frac{1}{\tau} \int \mathrm{d}t \left[\frac{1}{6V} \sum_{i\neq j} \boldsymbol{f}(\boldsymbol{r}_{ij}(t)) \cdot \boldsymbol{r}_{ij}(t) \right] \tag{4.35c}$$

which are obtained from a time average of the corresponding (instantaneous) microscopic quantities $\mathcal{H}$, $\mathcal{T}$, and $\mathcal{P}$. As mentioned before, if the system is ergodic (which we will always assume), these time averages $\overline{\mathcal{A}}$ will correspond to the ensemble averages of Gibbs $\langle \mathcal{A} \rangle$, which form the basis of Statistical Mechanics.

Of the three state variables given in Eq. (4.35), the internal energy U is probably the most important, since it is a conserved quantity. Our simulations should, at the very least, respect this condition. However, since the propagator (integrator) used to solve the equations of motion is necessarily discretized (using a finite time step Δt) and approximate, it is not evident *a priori* that the energy will be conserved. Small fluctuations in the energy are inevitable, but the propagator should be such that there is no appreciable long-term energy drift. A considerable amount of study has been devoted to finding new and improved integrator schemes (generally by using the Liouville formulation of Classical Mechanics), and yet the most common one continues to be the *Verlet* algorithm, introduced by Loup Verlet at the dawn of the computer simulation era (1967). Among the many variants that have been proposed, the *velocity Verlet* algorithm is probably the best known. It gives a second (first) order expansion for the positions (velocities) at a time $t + \Delta t$, in terms of the positions and velocities (momenta) at time

t, and the forces at both t and $t + \Delta t$ [20]

$$\boldsymbol{q}_i(t + \Delta t) = \boldsymbol{q}(t) + \frac{\boldsymbol{p}_i}{m_i}\Delta t - \frac{\nabla_i V_N(\{\boldsymbol{q}_j(t)\})}{2m_i}(\Delta t)^2 \tag{4.36a}$$

$$\boldsymbol{p}_i(t + \Delta t) = \boldsymbol{p}_i(t) - \frac{\Delta t}{2}\nabla_i \left[V_N(\{\boldsymbol{q}_j(t + \Delta t)\}) - V_N(\{\boldsymbol{q}_j(t)\})\right] \tag{4.36b}$$

This algorithm has various properties one looks for in a "good" propagator: it is time reversible (like Newton's equations of motion), it preserves the volumes in phase-space, and it gives sufficiently small energy fluctuations [20].

So far, we have made no mention as to the form of the potential V_N of this N-body system of classical particles. If the N particles correspond to the nuclei, as discussed in the previous section, and the potential energy is computed from a quantum-mechanical description of the electrons (under the Born-Oppenheimer approximation), we obtain what is known as Born-Oppenheimer Dynamics. Notice that in this scenario, the potential energy V_N, and thus the electronic wavefunction or density (if using a DFT approach), must be solved for at each step. To avoid repeating this extremely expensive calculation, Car and Parrinello [93] devised a scheme in which this is done only once (at the beginning), and the wavefunction is then propagated alongside the nuclei. This is accomplished by using an extended Lagrangian formulation, essentially treating the Kohn-Sham wavefunctions as additional degrees of freedom, with an associated mass and momenta. This is what is known as Car-Parrinello molecular dynamics.

In this work we will only be interested with Classical Molecular Dynamics. So far we have considered only point particles, but the treatment of molecules is easily introduced. For the trivial case of non-rigid molecules, a model potential (typically of the harmonic form) is used to describe the intramolecular interactions and the equations of motion are propagated in the usual way. Instead of specifying the intramolecular interactions, a constraint on the geometry of the molecules can also be used. These constraints are typically specified as fixed distances (bonds) between atoms. In this case we are dealing with rigid-bodies, and an extra step must be introduced when propagating the positions to ensure that the constraints are always satisfied. This is generally done using the SHAKE algorithm [94, 95] (or one of its variants), which corrects for the change in bond lengths, appearing after a conventional propagation, by computing the constraint forces necessary to keep the bond at the desired length and correcting the positions accordingly.

4.3.2 Ensembles: Thermostats and Barostats

As mentioned in the discussion on statistical ensembles (Section 3.1.1) a micro-canonical (NVE) description, which represents closed isolated systems (constant number of particles N, volume V, and energy E) is not the most convenient. From a Statistical-Mechanical point of view, the micro-canonical ensemble is disfavored since it restricts the systems to the surface of constant energy E. The canonical (NVT) and grand-canonical (μVT) ensembles are much more comfortable to work with, since the integrations can be taken over the whole phase-space, with each configuration (point) weighted by the appropriate Boltzmann factor. With simulations the situation is slightly different, in that the NVE ensemble is by far the easiest to work with (and code), but

since the goal is usually to compare with experiments, the NVT or NPT ensembles are preferred. In theory, this is not a problem, since the ensembles are all equivalent in the thermodynamic limit $\frac{N}{V} \underset{N,V\to\infty}{=} \rho\,(\text{constant})$, but we can only simulate finite size systems.

Performing simulations under constant temperature or pressure requires special attention. Experimentally, the temperature or pressure of a given system is fixed by placing it in contact with an appropriate heat or pressure reservoir. As such, the interactions between the reservoir and the system give rise to mainly local surface effects. However, the treatment of such surface effects within simulations is best avoided, which means that we must find another way of simulating (approximating) the coupling between our system and the reservoir(s). The preferred method for doing this is to use Andersen's extended Lagrangian approach, which has the following two advantages: (1) it provides a method for performing deterministic molecular dynamics simulations and (2) the system possesses an effective Hamiltonian (conserved quantity)[8]. The application of this formalism to constant temperature simulations was given by Hoover [96], generalizing previous work done by Nosé [97, 98], and is known as a Nosé-Hoover thermostat. Their idea was to introduce an additional degree of freedom ζ, with an associated mass Q and momentum p_ζ, which acts as a thermodynamic friction coefficient. This fictitious variable acts as a thermostat, allowing us, in most cases, to generate the desired canonical (NVT) distribution.

The problem with the simple Nosé-Hoover thermostat is the fact that its efficacy depends strongly on the number of conserved constants of motion [99, 20]; furthermore, it is non-ergodic for low-dimensional systems, such as the harmonic oscillator [20]. To overcome these limitations, Martyna et al. [99] have proposed that a chain of Nosé-Hoover thermostats ζ_j could be used instead: the thermostat ζ_1 coupled to the system is itself coupled to another thermostat ζ_2, which in turn can be coupled to yet another thermostat ζ_3, and so on. The authors have also provided an analogous scheme to treat systems at constant pressure and temperature (NPT). In the end, the number of Nosé-Hoover thermostats which should be used will depend on the number of conserved quantities in the system. For our simulations, we have used a Nosé-Hoover chain of length three. The effective Hamiltonians for these two cases (NPT and NVT) are given by [99, 20]

$$H_{NPT} = \mathcal{H}(\{\boldsymbol{q}_i;\boldsymbol{p}_i\}) + \frac{p_\epsilon^2}{W} + \sum_{j=1}^{M}\frac{p_{\zeta_j}^2}{Q_j} + (N_f+1)k_{\mathrm{B}}T\zeta_1 \tag{4.37a}$$

$$H_{NVT} = \mathcal{H}(\{\boldsymbol{q}_i;\boldsymbol{p}_i\}) + \sum_{j=1}^{M}\frac{p_{\zeta_k}^2}{2Q_k} + N_f k_{\mathrm{B}}T\zeta_1 + \sum_{j=2}^{M} k_{\mathrm{B}}T\zeta_j \tag{4.37b}$$

where N_f denotes the number of degrees of freedom, and ϵ is the extra variable used to barostat the system (with associated mass W an conjugate momentum p_ϵ). The equations of motion (system + reservoir) for the general case of a system at constant temperature and pressure (NPT) are summarized in Eq. (4.38), along with the transformations required to obtain the corresponding equations for a system at constant volume

[8] Strictly speaking it is not a real Hamiltonian, as the equations of motion cannot be derived from it.

and temperature (NVT).

$$\dot{\boldsymbol{q}}_i = \frac{\boldsymbol{p}_i}{m_i} + \frac{p_\epsilon}{W}\boldsymbol{r}_i \qquad \longleftrightarrow \dot{\boldsymbol{q}}_1 = \frac{\boldsymbol{p}_i}{m_i} \tag{4.38a}$$

$$\dot{\boldsymbol{p}}_i = -\nabla_i V_N - \frac{p_{\zeta_1}}{Q_1}\boldsymbol{p}_i - \left(1 + \frac{3}{N_f}\right)\frac{p_\epsilon}{W}\boldsymbol{p}_i \qquad \longleftrightarrow \dot{\boldsymbol{p}}_i = -\nabla_i V_N - \frac{p_{\zeta_1}}{Q_1}\boldsymbol{p}_i \tag{4.38b}$$

$$\dot{\zeta}_j = \frac{p_{\zeta_j}}{Q_j} \qquad = \dot{\zeta}_j \tag{4.38c}$$

$$\dot{p}_{\zeta_1} = \left[\sum_i^N \frac{\boldsymbol{p}_i^2}{m_i} - N_f k_\mathrm{B} T\right] - p_{\zeta_1}\frac{p_{\zeta_2}}{Q_2} \qquad = \dot{p}_{\zeta_1} \tag{4.38d}$$

$$\dot{p}_{\zeta_j} = \left[\frac{p_{\zeta_{j-1}}^2}{Q_{j-1}} - k_\mathrm{B} T\right] - p_{\zeta_j}\frac{p_{\zeta_{j+1}}}{Q_{j+1}} \qquad = \dot{p}_{\zeta_j} \tag{4.38e}$$

$$\dot{p}_{\zeta_M} = \left[\frac{p_{\zeta_{M-1}}^2}{Q_{M-1}} - k_\mathrm{B} T\right] \qquad = \dot{p}_{\zeta_M} \tag{4.38f}$$

$$\dot{V} = \frac{3V p_\epsilon}{W} \qquad \not\longleftrightarrow \tag{4.38g}$$

$$\dot{p}_\epsilon = 3V(P_\mathrm{int} - P_\mathrm{ext}) + \frac{3}{N_f}\sum_i^N \frac{\boldsymbol{p}_i^2}{m_i} - \frac{p_{\zeta_1}}{Q_1}p_\epsilon \qquad \not\longleftrightarrow \tag{4.38h}$$

$$\underbrace{\qquad\qquad\qquad\qquad}_{\text{Constant Pressure and Temperature } (NPT)} \qquad\qquad \underbrace{\qquad\qquad\qquad\qquad}_{\text{Constant Temperature } (NVT)} \tag{4.38i}$$

Where we have assumed that the barostat is coupled to the same thermostat as the system, although a separate Nosé-Hoover chain could also be used [99].

This extended Lagrangian formalism is not the only method available for performing simulations within the NVT or NPT ensembles, and it is certainly not the easiest to implement. Among the most popular alternatives, we find the Andersen and Berendsen thermostats, as well as the Berendsen barostat. The Andersen method [100] is to randomly reassign the velocities of the particles, to velocities chosen from a Maxwell-Boltzmann distribution at the desired temperature; essentially simulating random stochastic collisions between the particles and an imaginary heat bath. The Berendsen method [101] is to periodically rescale the velocities (thermostat) and/or the volume of the simulation cell (barostat). Unfortunately, the Berendsen thermostat (barostat) is unable to reproduce the correct distribution (although the deviation is expected to be small); and while this is not a problem for the Andersen thermostat (which yields the correct canonical distribution), it has the disadvantage of not providing deterministic dynamics for the system (due to the stochastic collisions) [20]. It is for these reasons that the Nosé-Hoover chains are usually preferred.

4.3.3 Practical Considerations

Periodic Boundary Conditions

Although the goal of numerical simulation techniques is to study the properties of bulk systems, it is clear that a brute force approach is unfeasible, since we cannot expect to

store $N \sim 10^{23}$ positions and velocities on any computer in the foreseeable future. In practice, we do not necessarily need to simulate such large systems, the size just needs to be large enough so that surface (boundary) effects are negligible, but this is still prohibitively expensive. The solution to this problem was recognized early on, it consists in periodically replicating the simulation cell in all directions. When a particle leaves the simulation box through one side, it is immediately reinserted through the opposite side. This simple procedure allows us to effectively mimic bulk systems and remove the surface altogether, all the while using only a relatively small number of particles[9]. Furthermore, if the interaction potentials between the particles are sufficiently short-ranged, we need not consider the interactions between all the particles in the system. Usually, the cutoff r_c is chosen such that $r_c \leq L/2$. If this is the case, a given particle will only interact with the particles in its own cell and (at most) with the image particles in one of its neighbouring cells. This approximation dramatically reduces the simulation time. A schematic representation of the use of periodic boundary conditions, with a spherical cutoff to truncate the interactions, is given for the case of a two-dimensional system in Figure 4.2. This cutoff procedure is valid only if the interaction potentials are short ranged, for long-range electrostatic interactions we must therefore use a different procedure.

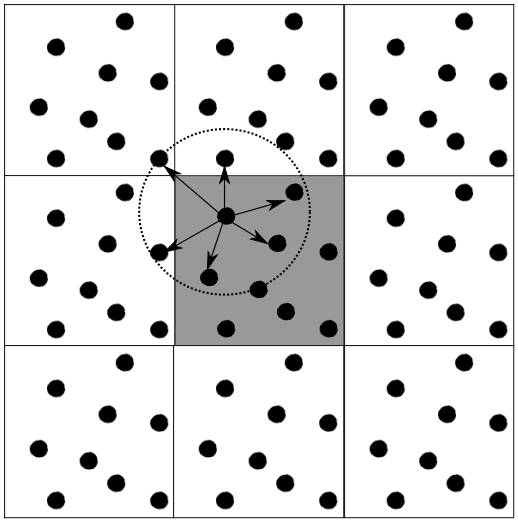

Figure 4.2: Schematic representation of a two-dimensional system under periodic boundary conditions, with a cutoff radius used to truncate the interaction potentials. The center (shaded) cell corresponds to the simulation cell, which is periodically replicated in all directions.

Treatment of Electrostatic Forces

The standard method for treating long-range interactions in periodic systems is the Ewald summation technique [20]. This formalism avoids a direct summation of the long-range interactions, which is only conditionally convergent, by separating the interactions in two terms: (1) a short-range part which can be summed directly, and (2) a

[9]The number of particles that should be used obviously depends on the system and the phenomena being studied, but for our purposes a few hundred to a few thousand is generally enough.

long-range part which is conveniently expressed as a Fourier series, and thus summed in reciprocal k-space. For a system of z_i point charges, the way of obtaining this separation is to introduce a diffuse screening charge distribution, of total charge $-z_i$, around each point charge z_i. The electrostatic potential of this new charge distribution (point particle + screening charge) is short ranged, decaying rapidly to zero, so that the interaction between the system of screened charges can be computed using the usual methods (a direct sum in real-space). It is then necessary to correct for the addition of the screening charge distributions. These interactions among screening charges can be easily computed in reciprocal space; however, in order to do this, the "self" interaction between the point charge and its corresponding screening charge must be included, and this needs be corrected for in the final result. We have mentioned only point charges, but the method can be easily extended to treat higher-order multipoles. A schematic representation of the Ewald procedure is given in Figure 4.3.

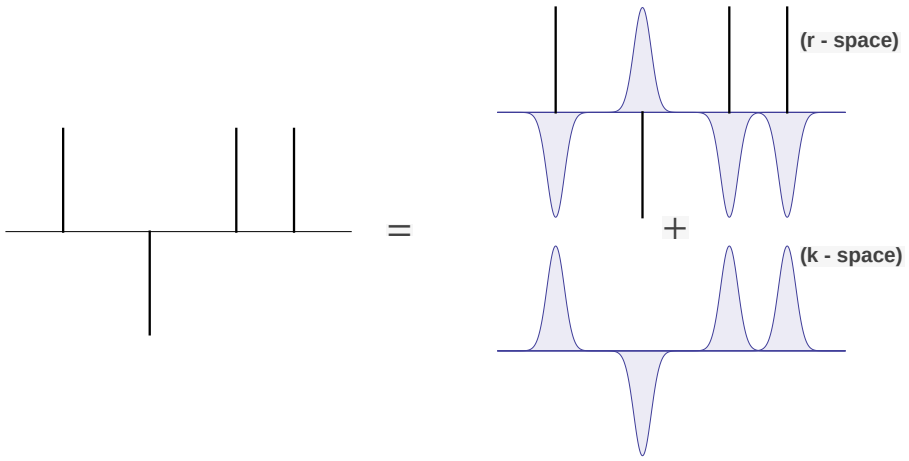

Figure 4.3: Schematic representation of the separation of charge interactions into real- and reciprocal-space sums. Note that the coupling between the two systems is assumed to be negligible.

Consider a finite system of charged, polarizable, particles. Let $\boldsymbol{r}_i$, z_i, and $\boldsymbol{\mu}_i$ denote their positions, charges, and (permanent) dipoles. The total potential energy for this system can be conveniently written in tensor notation as [84]

$$U = \sum_{i<j} \left[z_i \mathbb{T}_{ij}^{\text{chg-chg}} z_j - z_i \mathbb{T}_{ij}^{\text{chg-dip}} \cdot \boldsymbol{\mu}_j + z_j \mathbb{T}_{ij}^{\text{chg-dip}} \cdot \boldsymbol{\mu}_i - \boldsymbol{\mu}_i \cdot \mathbb{T}_{ij}^{\text{dip-dip}} \cdot \boldsymbol{\mu}_j \right] \tag{4.39}$$

where the various $\mathbb{T}_{ij}$ denote the multipole - multipole interaction tensors. For a system of charges and dipoles, we must consider three terms, the charge-charge, charge-dipole, and dipole-dipole interactions

$$\mathbb{T}_{ij}^{\text{chg-chg}} = \frac{1}{r_{ij}} \tag{4.40a}$$

$$(\mathbb{T}_{ij}^{\text{chg-dip}})^{\alpha} = \nabla_{\alpha} \mathbb{T}_{ij}^{\text{chg-chg}} = -\frac{\boldsymbol{r}_{ij}.\hat{\boldsymbol{e}}_{\alpha}}{r_{ij}^2} \tag{4.40b}$$

$$(\mathbb{T}_{ij}^{\text{dip-dip}})^{\alpha\beta} = \nabla_{\alpha}\nabla_{\beta} \mathbb{T}_{ij}^{\text{chg-chg}} = \frac{1}{r_{ij}^5} \left(3(\boldsymbol{r}_{ij}.\hat{\boldsymbol{e}}_{\alpha})(\boldsymbol{r}_{ij}.\hat{\boldsymbol{e}}_{\beta}) - r_{ij}^2 \delta_{\alpha\beta} \right) \tag{4.40c}$$

with $r_{ij} = |\boldsymbol{r}_i - \boldsymbol{r}_j|$ the distance between particles i and j. As mentioned above, this expression cannot be used to compute the energy for a system under periodic boundary conditions. To obtain the corresponding real-space Ewald contribution for such a system, one can replace the interaction tensors with their screened counterparts. This is accomplished by performing the following substitution [84, 102]

$$\frac{1}{r_{ij}^n} \longrightarrow \widehat{\frac{1}{r_{ij}^n}}$$

with

$$\widehat{\frac{1}{r_{ij}}} = \frac{\operatorname{erfc}(\alpha r_{ij})}{r_{ij}} \tag{4.41a}$$

$$\widehat{\frac{1}{r_{ij}^{2n+1}}} = \frac{1}{r_{ij}^2}\left(\widehat{\frac{1}{r_{ij}^{2n-1}}} + \frac{(2\alpha^2)^n}{\sqrt{\pi}\alpha\,(2n-1)!!} e^{-\alpha^2 r_{ij}^2}\right) \tag{4.41b}$$

where $\operatorname{erfc}(x) = \frac{2}{\sqrt{\pi}}\int_x^\infty \exp(-t^2)\mathrm{d}t$ is the complementary error function, α is the Ewald screening parameter, which determines the spread of the screening charge, and (!!) denotes a double factorial. The reciprocal space sum for the three contributions is given by [84]

$$U_{\text{recip}}^{\text{chg-chg}} = \frac{4\pi}{V}\sum_{|\boldsymbol{k}|>0}^{\infty} \frac{e^{-k^2/4\alpha^2}}{k^2}\left(\left[\sum_i z_i \cos(\boldsymbol{k}.\boldsymbol{r}_i)\right]^2 + \left[\sum_i z_i \sin(\boldsymbol{k}.\boldsymbol{r}_i)\right]\right) \tag{4.42a}$$

$$U_{\text{recip}}^{\text{chg-dip}} = \frac{8\pi}{V}\sum_{|\boldsymbol{k}|>0}^{\infty}\left(\sum_i z_i \sin(\boldsymbol{k}.\boldsymbol{r}_i) \times \sum_j (\boldsymbol{k}.\boldsymbol{\mu}_j)\cos(\boldsymbol{k}.\boldsymbol{r}_j)\right. \tag{4.42b}$$

$$\left. - \sum_i z_i \cos(\boldsymbol{k}.\boldsymbol{r}_i) \times \sum_j (\boldsymbol{k}.\boldsymbol{\mu}_j)\sin(\boldsymbol{k}.\boldsymbol{r}_j)\right)$$

$$U_{\text{recip}}^{\text{dip-dip}} = \frac{4\pi}{V}\sum_{|\boldsymbol{k}|>0}^{\infty}\left(\left[\sum_i (\boldsymbol{k}.\boldsymbol{\mu}_i)\cos(\boldsymbol{k}.\boldsymbol{r}_i)\right]^2 + \left[\sum_i (\boldsymbol{k}.\boldsymbol{\mu}_i)\sin(\boldsymbol{k}.\boldsymbol{r}_i)\right]^2\right) \tag{4.42c}$$

where V is the volume of simulation cell and the wave-vectors $\boldsymbol{k}$ are defined as $\boldsymbol{k} = 2\pi(n_x/L_x, n_y/L_y, n_z/L_z)$, with L_x, L_y, and L_z the side lengths of the cell. The self-energy corrections are

$$U_{\text{self}}^{\text{chg-chg}} = \frac{\alpha}{\sqrt{\pi}}\sum_i z_i^2 \tag{4.43a}$$

$$U_{\text{self}}^{\text{chg-dip}} = \frac{2\alpha^3}{3\sqrt{\pi}}\sum_i \mu_i^2 \tag{4.43b}$$

where the sums over i, j are understood to run over the particles in the primary (simulation) cell. Finally, we notice that the sums in Eq. (4.42) do not include the $\boldsymbol{k} = 0$ term. This contribution will depend on the boundary conditions at infinity, but can be safely ignored if the system is assumed to be surrounded by a conducting (metallic) material [20]. The use of these tin-foil boundary conditions is the norm when studying ionic systems. An approximation that is commonly used to reduce the computational

complexity of the reciprocal-space sum, is to solve Poisson's Equation on a grid (requiring the interpolation of the charges to the grid points), by using the very efficient Fast Fourier Transform routines (FFT) [103]. This is the Particle Mesh Ewald (PME) method [20].

4.4 Application to a Bottom-Up Approach for Deriving Classical Potentials

4.4.1 Introduction

We have seen that within a Born-Oppenheimer description, the nuclei can be considered as classical particles which evolve on a potential energy surface due to the presence of the electrons. There are two possible approaches to the problem of determining this potential energy contribution: (1) we either attempt to compute it directly, from knowledge of the electron density; or (2) we ignore the electron degrees of freedom altogether, and assume some ad-hoc form for the ion-ion potentials. The former is usually addressed by adopting the DFT approach introduced above, and leads to Born-Oppenheimer or Car-Parrinello Molecular Dynamics; while the latter is the basis of the molecular descriptions used in classical Molecular Dynamics or Monte-Carlo simulations.

These classical interaction potentials are usually parametrized to reproduce some combination of experimental results, such as enthalpic or structural properties of hydration. However, this approach has several disadvantages. First, it is not always possible to obtain reliable experimental data over the range of densities, temperatures, and pressures one wishes to study. This is true for the calculation of condensed phase polarizabilities, for which no experimental data is available, and for the thermodynamics of actinoid salt solutions, for which experiments are very difficult to perform. Second, the experimental data used for the fitting procedure very rarely gives direct information on the microscopic properties of the system. This means that different parametrizations can show the same level of experimental agreement with a given property, while at the same time giving rise to vastly different microscopic behaviour. Additionally, any agreement with respect to the other macroscopic properties (different from the ones used in the fit) is completely fortuitous. Finally, the choice of what property is used in the fitting is totally arbitrary; and the importance of said property to the physical and chemical processes relevant to the system is usually secondary to the ease with which it can be measured.

We use an alternative parametrization scheme which relies on the information obtained from DFT calculations (in particular the MLWF) to compute, either directly or by means of a fitting procedure, the main electronic contributions to the interaction potentials for ions in water. This method, developed by Aguado et al. [5], has been shown to give excellent results when applied to both molten salts and liquid water [91]. While this approach does not completely solve the difficulties enumerated above, and actually introduces some new ones, it presents two important advantages. First, it requires no experimental (fitting) data, all the required information is computed by a DFT calculation beforehand. Second, it uses a microscopic approach that can be consistently applied to most systems. Additionally, this method easily allows for further refinement,

whether it be to include a more exact DFT calculation (to incorporate a more robust exchange-correlation functional), or a more sophisticated classical potential (i.e. one with quadrupolar interactions), and has relatively few "free" parameters.

We proceed by presenting a general framework that can be used to derive classical potentials from it ab-initio simulations. Although the long term goal of this project is to obtain polarizable potentials that can accurately describe the structural, thermodynamic, and dynamic properties of divalent and trivalent radionuclides at the water/clay interface, in this work we will focus mainly on the halide cations in bulk water. We have decided not to attempt a new parametrization for water, as this would be beyond the scope of our work, and have instead chosen to use the polarizable Dang-Chang water model (DCW) [104]. This model has been developed to accurately describe the liquid/vapour interface, and manages to reproduce the strong water polarization induced by divalent cations. Although, as a first approximation, we are forced to consider the cations as non-polarizable (which is reasonable given their small polarizabilities), it is important to use a polarizable water model, in order to provide an accurate description of liquid water at interfaces.

4.4.2 Describing Atomic Interactions Within a Classical Framework

Classical potentials are usually divided into two classes, Bonded and Non-Bonded. The former determine the interactions between intramolecular atoms, which include the angle-bending, bond-stretching, and torsion potentials; the latter determine the intermolecular interactions, namely the charge-charge (Coulomb), Van der Waals, repulsion, and polarization (induction) interactions. Since we consider only ions in aqueous solution, and we use a rigid-model for the water molecules, there will be no further mention of bonded-potentials; any reference to a potential is understood to refer to the (non-bonded) water-water, water-ion, or ion-ion interactions.

A general interaction potential between two arbitrary atoms can be written as

$$V_{\text{total}} = V_{\text{charge}} + V_{\text{repulsion}} + V_{\text{dispersion}} + V_{\text{polarization}} \tag{4.44}$$

where the first three components appearing on the right hand side of this equation are pair-interaction potentials. The last component $V_{\text{polarization}}$ takes into account the many-body effects through the inclusion of the polarization energy. We follow by giving a brief description of each of the terms appearing in (4.44), we also specify the exact functional form that we will be using for each of them.

- Charge-Charge

$$V_{\text{charge}} = \sum_{i<j} \frac{z_i z_j}{r_{ij}} \tag{4.45}$$

  The charge-charge interaction between particles is given by the usual Coulomb potential between two point charges. Since the ion charges, which are the only parameters, are fixed beforehand, this contribution to the potential is trivially determined.

- Repulsion

$$V_{\text{repulsion}} = \sum_{i<j} B^{ij} e^{-A^{ij} r_{ij}} \tag{4.46}$$

The repulsion interaction is a short-range potential due to the electrostatic repulsion and the Pauli-exclusion principle of two electron clouds on neighbouring atoms.

- Dispersion

$$V_{\text{dispersion}} = -\sum_{i<j} \left[f_6^{ij}(r_{ij}) \frac{C_6^{ij}}{(r_{ij})^6} + f_8^{ij}(r_{ij}) \frac{C_8^{ij}}{(r_{ij})^8} \right] \tag{4.47}$$

The dispersion interaction arises from the (correlated) instantaneous density fluctuations between two separated fragments of matter (the electron density cloud), which give rise to an induced multipole - induced multipole attraction. As mentioned above, this contribution is not easily included within traditional DFT calculations due to their non-local origin.

The so-called damping functions $f_6^{ij}(r)$ and $f_8^{ij}(r)$ are introduced in order to correct the spurious short-range divergence of the dispersion potentials $\simeq 1/r^6, 1/r^8$. The functional form of these functions is that proposed by Tang-Toennies

$$f_n^{ij}(r_{ij}) = 1 - e^{b_D^{ij} r_{ij}} \sum_{k=0}^{n} \frac{(b_D^{ij} r_{ij})^k}{k!}, \qquad n = 6, 8 \tag{4.48}$$

The parameter b_D^{ij} determines the distance over which the dispersion interaction will be damped, with the dispersion potential assuming its asymptotic value for $r > 1/b_D^{ij}$.

- Polarization

$$V_{\text{polarization}} = \sum_{i<j} \left[g_I^{ij}(r_{ij}) \mathbb{T}_{ij}^{\text{chg-dip}} \cdot (z_i \boldsymbol{\mu}_j - z_j \boldsymbol{\mu}_i) - \boldsymbol{\mu}_i \cdot \mathbb{T}_{ij}^{\text{dip-dip}} \cdot \boldsymbol{\mu}_j \right] + \sum_i \frac{1}{2\alpha_i} \boldsymbol{\mu}_j^2 \tag{4.49}$$

The polarization (induction) potential is used to describe the distortions, caused by the electric fields, on the electronic density distribution around a given atom. These changes will induce multipole moments that will interact with the charges and multipoles of the remaining ions. Here we consider only the charge - dipole and dipole - dipole interactions. The addition of the last term, with respect to the potential energy given in Eq. (4.39), is due to the presence of the induced dipoles and represents the cost of deforming the electron shell (before we considered only permanent dipoles). The damping functions for these multipole interactions $g_I^{ij}(r_{ij})$ take the form

$$g_I^{ij}(r_{ij}) = 1 - c_I^{ij} e^{-b_I^{ij} r_{ij}} \sum_{k=0}^{4} \frac{(b_I^{ij} r_{ij})^k}{k!} \tag{4.50}$$

Our potential differs from the so-called Lennard-Jones or $12-6$ potential which are commonly used

$$V_{ij}^{\mathrm{LJ}}(r) = 4\epsilon \left[\left(\frac{\sigma_{ij}}{r_{ij}} \right)^{12} - \left(\frac{\sigma_{ij}{}^{6}}{r} \right) \right] \simeq V_{\mathrm{repulsion}} + V_{\mathrm{dispersion}} \tag{4.51}$$

since we allow for higher order dispersion interactions and we explicitly take into account the many-body polarization effects. The average effect of these missing terms can be included (implicitly) within the LJ potentials by artificially increasing the (C_6) dispersion interaction, or by modifying the charge distribution (in the case of molecules) to take into account the induced dipoles. As they are, by far, the most popular potentials, we give a brief description of their relevant parameters. The distance parameter σ_{ij} specifies the separation at which the potential is zero, and thus gives a measure of the size of the Lennard-Jones particles. The energy parameter ϵ gives the depth of the well at the minimum, which appears at a distance of $r_m = 2^{1/6}\sigma$. Although this potential includes the correct asymptotic form for the $1/r^6$ dispersion interaction, there is no physical justification for the $1/r^{12}$ form given to the repulsion[10]. By adopting a physically relevant functional form (4.44) for the various potential energy contributions, we can be certain that (in principle) they can be rigorously derived from *ab-initio* calculations.

4.4.3 The Procedure

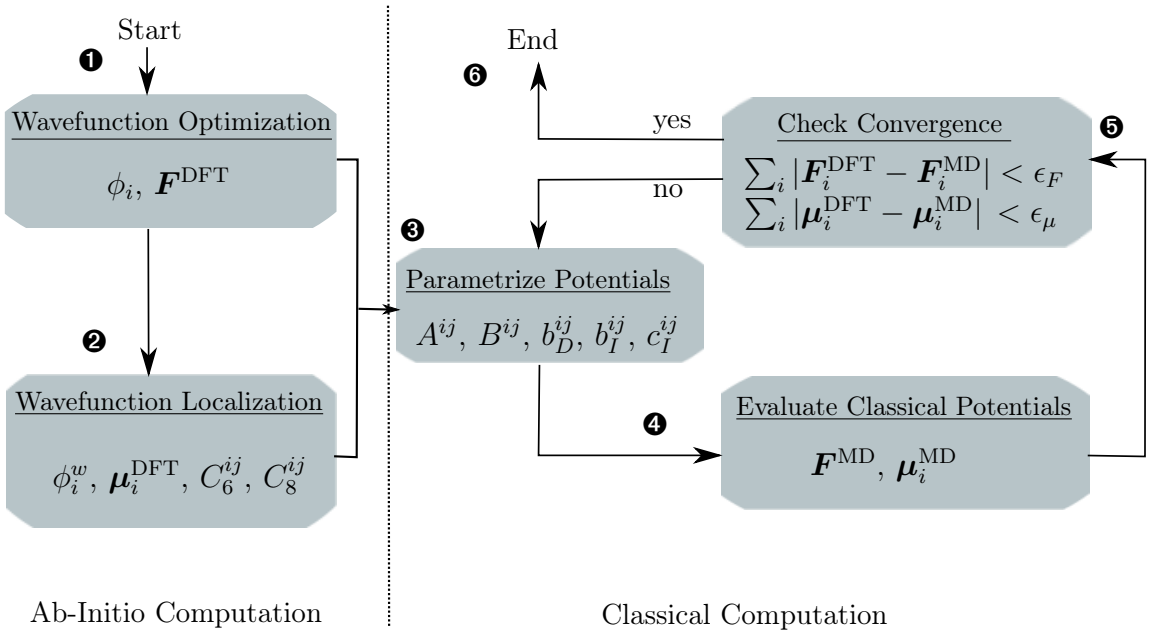

Figure 4.4: Schematic representation of the method used to derive the ion-water interaction parameters. The actual force-fitting scheme corresponds to the right-hand side of the diagram, the left-hand side being the necessary preliminary calculations.

[10]The historical reason for why this choice was so widely adopted is quite simple: Not so long ago, when the first computer simulations were being performed, processing resources were very expensive, and it was much more efficient to compute a power of $12 = 6 \times 2$, than to consider any other power, much less a more realistic exponential form for the repulsion

Water-Ion Interactions

The "input" required for our force-fitting procedure is a previously generated MD trajectory of a single in solution, basically a series of snapshots for the positions of the ion and water molecules. This trajectory can be generated using *ab-initio* MD or classical MD (with an already existing force-field), what matters is that the configurations provide an adequate sampling of the water structure around the ion. The first step is to compute the *ab-initio* forces $\boldsymbol{F}^{\mathrm{DFT}}$ on all the atoms (molecules), for the entire trajectory, through a DFT wavefunction optimization. The second step, which also involves a DFT calculation, is to compute the corresponding Wannier Orbitals. This allows us to obtain the ion-water dispersion parameters C_6^{ij} and C_8^{ij}, as well as the molecular dipoles $\boldsymbol{\mu}_I$ and the α_I polarizabilities (see previous section) for all the species in our system. Once this is done, we have all the *ab-initio* data required for the force-matching scheme[11]. The remaining potential parameters, for the repulsion and induction terms, are considered as free (adjustable) and used to minimize the error functions χ^2 for the forces and the dipoles. These functions take the form

$$\chi_F^2 = \frac{1}{N_{\mathrm{frames}} N_{\mathrm{molecules}}} \sum_{i=1}^{N_{\mathrm{frames}}} \sum_{j=1}^{N_{\mathrm{molecules}}} \sum_{\alpha=x,y,z} \frac{(F_{j,\alpha}^{\mathrm{DFT}}(i\Delta t) - F_{j,\alpha}^{\mathrm{MD}}(i\Delta t))^2}{\left|\boldsymbol{F}_j^{\mathrm{DFT}}(i\Delta t)\right|^2} \tag{4.52}$$

where F can just as well represent the forces or the dipoles. The total error function to be minimized is then taken to be

$$\chi^2_{\mathrm{total}} = \gamma_{\text{ion-frc}}\chi^2_{\text{ion-frc}} + \gamma_{\text{ion-dip}}\chi^2_{\text{ion-dip}} + \gamma_{\text{wat-dip}}\chi^2_{\text{wat-dip}} \tag{4.53}$$

where the weights for each of the terms are chosen such that $\sum_X \gamma_X = 1$. The three terms in the error function correspond to the three distinct families of fitting parameters available: the water – ion repulsion (a^{ij} and B^{ij}), and the ion (dipole) – water (charge) and water (dipole) – ion (charge) induction (c_D^{ij} and b_D^{ij}). This minimization procedure is represented on the right half Figure 4.4. An initial parametrization of the potentials is performed (step 3), and the classical forces and dipoles are then computed for the whole trajectory (step 4). Finally, we compare the "proposed" MD values with the reference DFT calculations (step 5). If the difference between the two is small enough (if the error function has been minimized) we stop the procedure (step 6); otherwise, we start over again, by reparametrizing the potentials (step 3).

Ion-Ion Interactions

The ion-ion interaction parameters are derived in the same manner as above, only now we consider a crystalline salt system (cation + anion), instead of an ion in solution. However, the fitted potentials must not only provide accurate (classical) approximations to the *ab-initio* forces and dipoles, but they must also give the correct crystalline structure and density. The work presented in this chapter was carried out in collaboration with Sami Tazi, who focused mainly on the divalent cations and who performed all the ion-ion parametrizations. We kindly thank him for allowing us to include unpublished results in this work.

[11] We note that this separation is purely conceptual, steps 1 and 2 can be carried out almost simultaneously, since most codes DFT codes perform the calculation of the forces and the Wannier orbitals directly

4.5 Results

4.5.1 Polarizabilities of Ions in Solution

The polarizabilities for a series of monatomic cations (Li^+, Na^+, K^+, Rb^+, and Cs^+) and anions (F^-, Cl^-, Br^-, and I^-) were computed using the CPMD package [105], as described above (Section 4.2). The intensity of the applied external field was set to a value of 0.001 a.u. The gradient-corrected BLYP functional [68, 69] was used for all the ions except Rb^+, for which a PBE functional [70] was used instead. The pseudopotentials were those of Troullier-Martins (Cl^-, Br^-, K^+, and Cs^+) and Goedecker-Teter-Hutter (I^-, Na^+, and Rb^+). A plane-wave basis set with an energy cutoff of at least 70 Ryd was used in all cases. A recent study [106] comparing the dipole polarizabilities of small water clusters ($n = 2-12$) obtained from DFT calculations, using various density functionals, has shown that hybrid functionals provide more accurate results (when compared to coupled-cluster calculations). However, the use of such functionals for the condensed-phase systems we consider here is prohibitively costly. We must thus expect (and accept) errors of a few percent in our calculated values.

The configurations have been extracted from classical molecular dynamics simulations performed in the NVT ensemble, with a time step of 1 fs., at a temperature of $T = 300K$, using a Berendsen thermostat with a coupling constant of $\tau = 0.1$ ps. The simulations were performed using the `Tinker` code [107]. The volume was determined by a previous simulation, of the same system, in the NPT ensemble. In all cases, a periodically replicated cubic simulation box, with one ion, and at least 31 water molecules, was used. The ions were described using the nonpolarizable LJ potentials of Dang and coworkers [108, 109, 110], while the water molecules where represented by the rigid nonpolarizable SPC/E model [111]. Simulations of 1 ns were performed, with the first 0.5 ns being discarded for equilibration purposes. Configurations (snapshots) were then saved every 1000 steps (1 ps) to generate the actual trajectory (500 total frames) used to compute the polarizabilities.

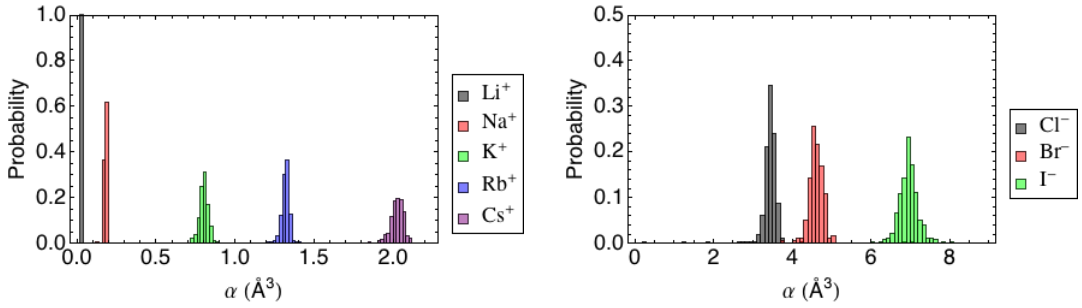

(a) Alkaline ions. (b) Halide ions.

Figure 4.5: Distribution of the isotropic polarizabilities $\overline{\alpha} = \frac{1}{3}\mathrm{Tr}(\boldsymbol{\alpha})$ of monovalent ions in water.

The polarizability tensor α for all the ions was observed to be isotropic, containing off diagonal elements equal to 0. The distributions for $\overline{\alpha} = \frac{1}{3}\mathrm{Tr}\alpha$ are given in Figure 4.5. The average isotropic polarizability for each species has been computed using these distributions; the results are summarized in Table 4.1, where the values for commonly used force fields, obtained empirically [112] or by fitting to *ab-initio* data [113, 114, 115,

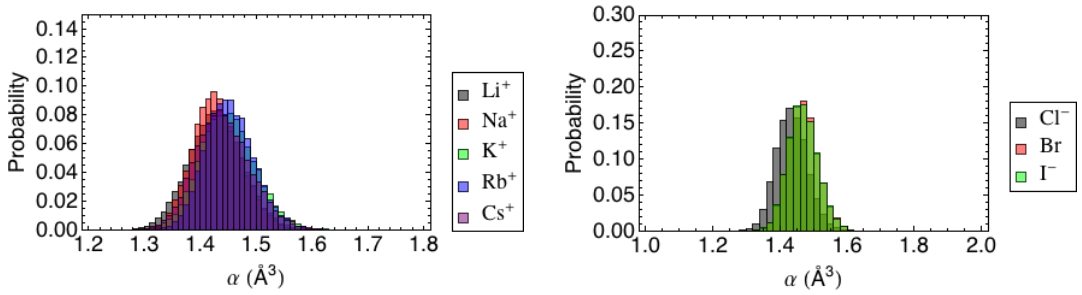

(a) Alkaline ions. (b) Halide ions.

Figure 4.6: Distribution of the isotropic molecular polarizability $\overline{\alpha} = \frac{1}{3}\mathrm{Tr}(\boldsymbol{\alpha})$ of water in the presence of monovalent ions.

116], are reproduced. Our theoretical predictions are in remarkably good agreement with the fitted values used in these force-fields. This is especially true for the cations, while some small discrepancies are observed in the case of the anion polarizabilities, especially for F^- and Br^-. The results obtained for the molecular polarizability of water are shown in Figure 4.6. The experimental value of $\alpha = 1.45$ Å^3 is recovered, and the effects of the ion are seen to be negligible (this is to be expected since the salt concentration is so low).

As far as we know, the only previous attempts of calculating the polarizabilities of ions in solution have focused solely on the nitrate [117], sulfate [118], and chloride ions [119]. Therefore, we can only compare our results with the latter. In this study [119], a point charge representation of the static charge distribution of solvating water molecules was used to calculate the electrostatic contribution to the confining potential felt by the ions. In a first attempt, using an SPC/E water model, the authors obtained a polarizability of around 4.2 Å^3. To improve these results, Jungwirth and Tobias proceeded to refine the water charge distribution, by performing a Wannier localization procedure. This led them to use net charges of $+6$, $+1$, and -2 on the positions of the oxygen atoms, hydrogen atoms, and Wannier centers [78, 120], respectively. This second attempt lead to a polarizability of 3.9 Å^3, which is still higher than our proposed value of 3.4 Å^3 for several reasons. First, and perhaps most importantly, is the lack of statistics, since they have used only five snapshots. Second, their partial charge model, derived from the Wannier localization procedure, may be too simple; in which case, higher order multipoles should be used to obtain a better representation of the electrostatic potential [121]. Finally, these calculations have not taken into account the multipole-induced dipole (polarization) contributions.

The importance of environmental effects on the polarizabilities of ions in solution can be easily quantified by comparing our results, for the condensed phase, with the gas phase isotropic polarizabilites [122, 123], (also reported in Table 4.1). These effects, which are known to play an important role for anions in ionic crystals and liquids [129, 130], are due to the existence of a confining potential. This potential arises from the Coulombic repulsion and exclusion between the electron density of the ion and those of the first neighbour solvation shell [131]. This effect is observed to be most important in the case of anions: the polarizability of the fluoride anion in solution is reduced by as much as 47% with respect to its gas value. Although this difference becomes less pronounced for the "bigger" ions, the value for the iodide anion is still reduced by 27%.

Ion	This work$^{(*)}$	SWM4-NDP$^{(a)}$	Amoeba$^{(b)}$	DC97$^{(c)}$	Gas phase
Cl^-	3.5	3.969	4.000	3.690	5.482
Br^-	4.6	5.262	5.650	4.770	7.268
I^-	7.0	7.439	7.250	6.920	10.275
Li^+	0.029	0.032	0.028	0.029	0.032
Na^+	0.18	0.157	0.120	0.240	0.157
K^+	0.81	0.830	0.780	0.830	0.830
Rb^+	1.32	1.370	1.350	–	1.370
Cs^+	2.02	2.360	2.260	2.440	2.360

Table 4.1: Average values of the isotropic polarizability $< \bar{\alpha} >$ of monatomic ions. All values are in Å^3. Also reported are the values employed in common force fields and the gas-phase polarizabilities [122, 123]. ($^{(a)}$: Reference [124], $^{(b)}$: provided in the TINKER molecular modeling simulation package [107] for Amoeba [113, 114, 115], $^{(c)}$: From DC97 [125, 104, 126, 127] force fields). $^{(*)}$ We note that Ref. [128] contains a typo which erroneously assigns a polarizability of 7.5 Å^3 to Li^+.

In the case of cations, no discernible effect is observed, except for Cs^+, which is by far the most polarizable one.

The variation of the polarizabilities of F^-, Cl^-, and Br^- ions in water clusters, with respect to their gas phase values, has been the object of a recent study by Bauer et al. [132] Their method is based on a Hirshfeld partitioning of the electron density [133], which is obtained by *ab-initio* calculations at the B3LYP level of theory. However, the strong basis set dependence, as well as the small system size, and the fact that the induced dipole-induced dipole contributions are not explicitly taken into account, makes it difficult to establish a clear comparison with the values we have obtained for bulk systems. This notwithstanding, their results are in good agreement with ours, as they have also shown a significant reduction of the polarizability of halide ions upon solvation by water molecules.

4.5.2 A New Force-Field for Ions in Solution

Ab -Initio Derived Potential Parameters

Ion-Water

We have parametrized the ion-water force fields for a series of alkali cations (Li^+, Na^+, K^+, Rb^+, and Cs^+) in solution. As mentioned above, since one of the interests of this work is to develop potentials that will eventually be used to study the specific effects of ions at interfaces, we are forced to use a polarizable water model, for which we have chosen the one provided by Dang and Chang (DCW) [104]. This is a four site polarizable water model, which assigns fixed charges to the Hydrogen atoms (HW) and to a fictitious polarizable point (MW) located on the bisector of the H-O-H angle, at a distance of 0.215 Å from the Oxygen atom (OW). Lennard-Jones parameters are only assigned to the oxygen atoms. Since we adopt a different water model, we do not use the trajectories previously employed to derive the ion polarizabilities. An alternative set

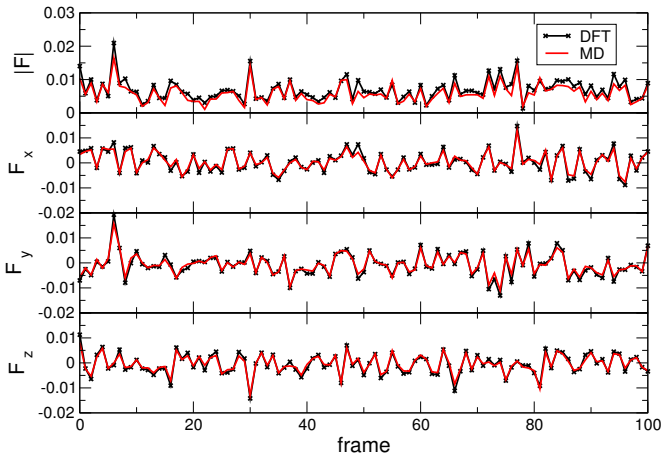

Figure 4.7: Comparison between the *ab-initio* (DFT) and the fitted (MD) forces felt by a single RB^+ ion in water, over a sample trajectory of 100 configurations (frames). The forces are given in atomic units E_h/a_0, where E_h is the Hartree energy.

of trajectories is generated using exactly the same procedure as before, only now we use polarizable potentials for both the ions and the water molecules. The Na^+ parameters were taken from Ref. [134], those for K^+ and Cs^+ from Ref. [135], and those for Li^+ and Rb^+ from Ref. [108] and [124], respectively.

Ion	distance (a_0)	spread (a_0)
Li^+	0.0012	0.682
Na^+	0.416	0.857
K^+	0.680	1.333
Rb^+	0.799	1.566
Cs^+	0.971	1.854

Table 4.2: Average distance and spreads of the (ionic) Wannier Orbitals.

The DFT calculations are exactly the same as those used above to derive the polarizabilites, although in this case no external field calculations are required. In this way we are able to obtain the forces and the Wannier orbitals for the entire trajectory. The average spread and distance of the Wannier orbitals (from their parent atom) are given in Table 4.2. From the localization procedure we can immediately derive the ion-water dispersion interaction parameters C_6^{ij} and C_8^{ij}, as detailed above, for which we have used a program written by Benjamin Rotenberg, which he was kind enough to supply. The remaining (repulsion and induction) parameters are obtained from the force-fitting procedure using the `MINUIT` minimization library [136].

Our initial results showed a very large error value for the ion-dipole error function $\chi^2_{ion-dip} \simeq 1$ in the case of cations. We were unable to reproduce the induced dipoles on the ions by fitting the damping parameters for the (ion) dipole - (water) charge interactions. We believe this is due to the relatively low values of the induced dipoles on the cations, which is a consequence of their small polarizability. Therefore, we have chosen not to represent the cations as polarizable species. Fortunately, this does not seem to have a negative impact on our final results, as we are able to accurately reproduce the (*ab-initio* DFT) forces on the ions. With this simplification of non-polarizable cations, our fitting procedure contains only four free parameters: the ion - water (oxygen) repul-

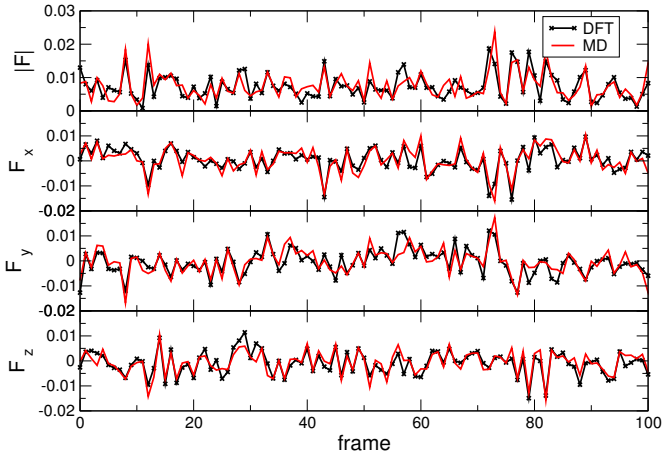

(a) force

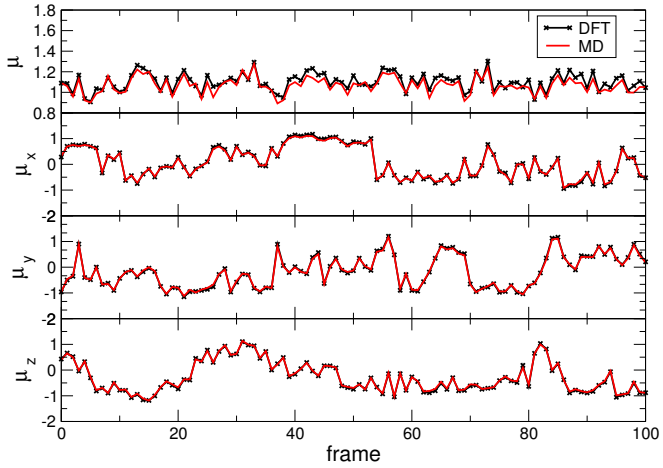

(b) dipole

Figure 4.8: Comparison between the *ab-initio* (DFT) and the fitted (MD) forces and dipoles of an individual water molecule, over a sample trajectory of 100 configurations (frames). The forces and dipoles are given in atomic units, E_h/a_0 and ea_0, respectively.

sion parameters A^{ij} and B^{ij} and the water (dipole) - ion (charge) damping parameters c_I^{ij} and b_I^{ij}. Since the DFT forces do not include the dispersion contributions, the fitting procedure does not allow for the parametrization of the dispersion damping parameters b_D^{ij}. We have thus taken the same value for all the ions $b_D^{ij} = 3.0\ a_0$, except for Cs^+, for which we have used a lower value $b_D^{ij} = 1.8\ a_0$. These values were transferred from a separate parametrization of the ion-ion potentials designed to reproduce the crystalline structure of the chloride compounds. We thus assume that the effective size of the cation's electron density does not vary considerably upon solvation. This is supported by the small difference in ion polarizability between the gas and liquid phases described above.

The actual error function minimized is then given by Equation (4.53) with $\gamma_1 = \gamma_3 = 0.5$ and $\gamma_2 = 0$. The final parameters for our proposed ion-water potentials are summarized in Table 4.3. Although the exact values obtained from the minimization will depend on the weights γ_X, this dependence will be very small, since there is a difference of two orders of magnitude between the error functions for the ion forces and the water dipoles. As long as the relative weights are of the same order of magnitude

we have $\chi^2_{\text{total}} \simeq \chi^2_{\text{ion-frc}}$. An illustration of the type of agreement that can be achieved is given in Figure 4.7 for the case Rb^+, where the fitted (MD) forces are compared to the reference (DFT) values. Figure 4.8 shows the corresponding comparison for the forces and dipoles of a single water molecule for this same system (Rb^+ in water). The dipoles are seen to be in very good agreement, while a considerable difference is observed for the force felt by the water molecule. This disagreement is a consequence of the missing dispersion interactions in the DFT calculations. Note that we have not attempted to fit the forces on the water molecules, but only their dipoles (through the water-ion polarization damping). Finally, we note that there was no observable difference between "hydration" and "bulk" waters: fitting the dipole of the water molecules inside the ion's first hydration sphere gave essentially the same result as using all the water molecules. A plot of the ion-water repulsion potential is presented in Figure 4.9.

Ion	$A^{ij} \times 10^{-2}$ $^{(a)}$	B^{ij} $^{(b)}$	$C_6^{ij} \times 10^{-1}$ $^{(c)}$	$C_8^{ij} \times 10^{-2}$ $^{(d)}$	b_I^{ij} $^{(b)}$	c_I^{ij}	$\chi^2_{\text{ion-force}}$	$\chi^2_{\text{wat-dip}} \times 10^2$
Li^+	0.247	4.094	0.050	0.016	4.010	2.950	0.156	0.176
Na^+	7.111	5.061	0.013	0.001	1.562	0.683	0.225	0.800
K^+	1.256	3.734	3.429	1.960	1.314	0.462	0.111	0.279
Rb^+	1.578	3.656	5.580	3.687	1.248	0.476	0.102	0.235
Cs^+	2.694	3.635	9.291	7.553	2.524	2.950	0.228	0.300

Table 4.3: Parameters for the ion-water interactions obtained using our parametrization method, as well as the minimized error functions χ^2 ($^{(a)}: E_h$, $^{(b)}: \text{Å}^{-1}$, $^{(c)}: \text{Å}^6$, $^{(d)}: \text{Å}^8$). The repulsion and dispersion parameters correspond to the ion - oxygen interactions, while the damping parameters are for the water (dipole) - ion (charge) interactions.

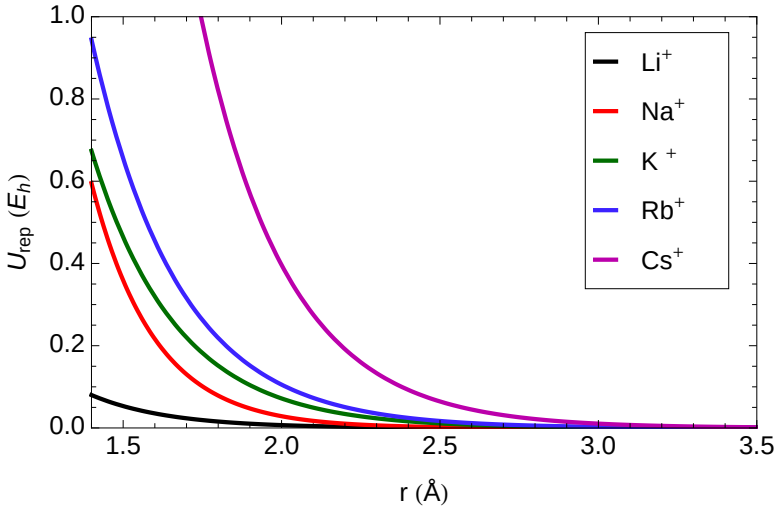

Figure 4.9: Ion-water repulsion potential obtained from the fit to the *ab-initio* forces.

Ion-Ion

The ion-ion parameters for the cations considered above where obtained by considering the series of chloride crystalline compounds. These parametrization where performed by Sami Tazi, and should be published soon; we include his results in order to provide a complete set of force-fields for chloride salts in solution. The chloride-water potential parameters are given in Table 4.4, and the ion-ion parameters in Table 4.5.

	$A^{ij} \times 10^{-2}$	B^{ij}	$C_6^{ij} \times 10^{-1}$	$C_8^{ij} \times 10^{-2}$	b_I^{ij}	c_I^{ij}
Cl^--OW	4.996	3.559	9.285	6.986	–	–
Cl^--HW	–	–	–	–	4.793	1.093
Cl^--MW	–	–	–	–	2.444	−1.900

Table 4.4: Parameters for the chloride-water interactions. The units are the same as in Table 4.3. The damping parameters (b_I^{ij} and c_I^{ij}) correspond to the ion (dipole) - water (charge) interactions. There is no need to damp the water dipoles in this case.

System	Ion Pair	$A^{ij} \times 10^{-2}$	B^{ij}	$C_6^{ij} \times 10^{-1}$	$C_8^{ij} \times 10^{-2}$	b_d^{ij}	b_I^{ij}	c_I^{ij}
Li-Cl	Li^+-Li^+	4.818	6.958	0.001	$\simeq 0$	6.958	–	–
	Li^+-Cl^-	0.155	3.000	0.108	0.041	3.000	3.128	1.4326
	Cl^--Cl^-	6.984	3.777	27.095	20.901	1.65	–	–
Na-Cl	Na^+-Na^+	$\simeq 0$	4.964	0.132	0.022	4.9648	–	–
	Na^+-Cl^-	0.444	3.000	1.353	0.615	3.000	2.7746	2.0398
	Cl^--Cl^-	6.983	3.776	27.095	20.901	1.65	–	–
K-Cl	K^+-K^+	1.747	4.9989	3.266	1.506	4.9989	–	–
	K^+-Cl^-	0.829	3.000	0.898	5.443	3.000	1.2816	0.90587
	Cl^--Cl^-	6.983	3.7767	27.095	20.901	1.65	–	–
Rb-Cl	Rb^+-Rb^+	$\simeq 0$	3.4849	10.180	6.355	3.4849	–	–
	Rb^+-Cl^-	1.079	3.000	17.100	11.748	3.000	1.46	0.98248
	Cl^--Cl^-	6.983	3.7767	27.095	20.901	1.65	–	–
Cs-Cl	Cs^+-Cs^+	3.529	3.7819	33.360	30.322	3.7819	–	–
	Cs^+-Cl^-	1.501	3.000	33.420	27.578	1.8	1.541	0.46651
	Cl^--Cl^-	6.983	3.776	27.095	20.901	1.65	–	–

Table 4.5: Ion-Ion potentials parameters. The units are the same as in Table 4.3. The damping parameters (b_I^{ij} and c_I^{ij}) correspond to the chloride (dipole) - cation (charge) interactions.

Validation of the Method

In order to test the force-fields we have developed, we proceed to compare various structural, thermodynamic, and dynamic properties with the corresponding values obtained from experiments. To this end, additional MD simulations have been performed. All the systems consist of one ion and 215 water molecules (DCW), in a periodically replicated cubic simulations box $L = 18.65$ Å. The total simulation time was 3 ns, with 0.25 ns of equilibration. A Nosé-Hoover chain of length three, with a time constant of 1 ns, was used as a thermostat at $T = 298.15$ K. The electrostatic interactions were computed using a dipolar Ewald sum. An Ewald convergence parameter of $\alpha = 0.3646$ was used, with 17 total grid point in each direction, and a real-space cutoff equal to $L/2$. A tolerance of 1×10^{-7} was used to obtain the self-consistent dipole moments. The simulations were performed using the `CP2K` simulation package [137]. The ion-water radial distribution functions are given in Figure 4.10. The distance to the first peak in the $g_{ij}(r)$, as well as the coordination number, are summarized in Table 4.6, where the corresponding experimental values are also given. The agreement of our results with experiments is seen to be excellent, considering the large errors reported for the latter.

The infinite dilution diffusion coefficients for the ions are obtained from the particle's mean-squared displacement, using the well-known Einstein relation (see Section 3.1.5). A plot of $\langle r^2 \rangle$ as a function of time is given in Figure 4.11. As this is a single ion property, it is very slow to converge and relatively long rung are needed. The statistical errors were computed using block averages, with a (optimal) block length of 256 (see AppendixB). The onset of the linear regime appears around $t \simeq 2$ ns in all cases, and although the statistical errors increase considerably with time, a weighted least-squares fit is seen to correspond very well with the measured data. These values give the same

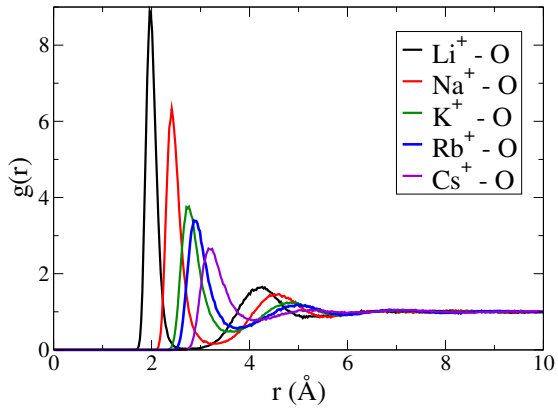

Figure 4.10: Ion-Water radial distribution functions obtained from simulations of a single ion with 215 water molecules.

Ion	r_{peak}	N_{coord}
Li^+	$1.96(1.90-2.25)$	$4(4)$
Na^+	$2.41(2.41-2.5)$	$5.9(4-8)$
K^+	$2.74(2.60-2.92)$	$7.2(4-8)$
Rb^+	$2.88(-)$	$7.5(-)$
Cs^+	$3.2(2.95-3.15)$	$9.6(-)$

Table 4.6: Distance to the first peak and coordination number obtained from the ion-water radial distribution functions (Figure 4.10). Experimental values, where available, are provided in parenthesis.

results, within error bars, to those obtained from the integral of the velocity auto-correlation function (not shown). The final results for D_0 were computed by averaging the values obtained from the mean-squared displacements in the x, y, and z directions , as they each provide an independent measure of the diffusion coefficient. These values are given in Table 4.7. It was recently noticed that when computing diffusion coefficients

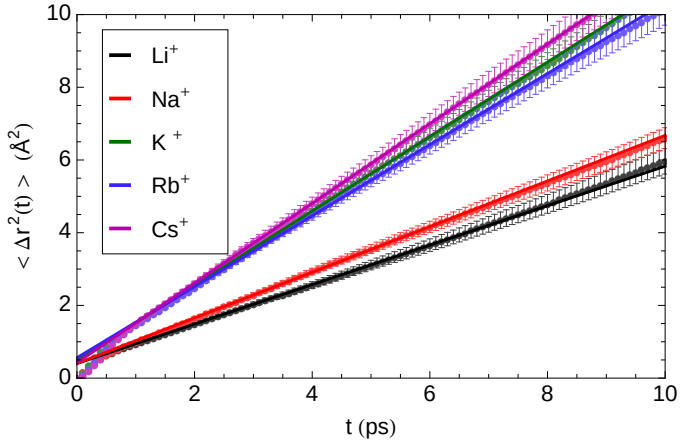

Figure 4.11: The mean-squared displacement as a function of time obtained for the series of cations using our force field parameters. The circles represent the simulation data, the error is computed using a block analysis, and the solid lines are obtained by performing a weighted least-squares fit to a linear function.

in systems with periodic boundary conditions, a considerable dependence on the system size is observed [138, 139]. In order to correct for the hydrodynamic self-interaction at the origin of this size-dependence, a $1/L$ correction must be added to the simulation results, effectively extrapolating to an infinite system size

$$D_0 = D_{0_{\mathrm{PBC}}} + 2.837297 k_{\mathrm{B}} T/(6\pi\eta L) \tag{4.54}$$

where η is the shear viscosity of the solvent. For the systems we have considered, $L = 18.65$Å and $T = 298.15$ K, the correction is of the order of $\simeq 0.44$. This amounts to roughly 50% of the value of the uncorrected diffusion coefficient for Li^+, and 20% for water, which shows how important it is to take this effect into account. Since neither the diffusion coefficient $D_0^{\mathrm{DCW}} = 2.74 \times 10^{-9}$m/s nor the viscosity $\eta = 7.4 \times 10^{-4}$Pa.s of our water model correspond to the experimental values ($D_0^{\mathrm{water}} = 2.3 \times 10^{-9}$m/s and $\eta^{\mathrm{water}} = 8.9 \times 10^{-4}$Pa.s), it makes little sense to compare our results directly with experiments. Instead, it is more instructive to compare the ratio of ion/water diffusion coefficients (with the appropriate system-size correction), since it provides a measure of how fast the ion moves with respect to the solvent. These ratios are also provided in Table 4.7.

Ion	$\mathrm{D}_{0_{\mathrm{PBC}}}^{\mathrm{ion}}$ $(10^{-9}m^2/s)$	$(D_0^{\mathrm{ion}}/D_0^{\mathrm{water}})$	$(D_0^{\mathrm{ion}}/D_0^{\mathrm{water}})^{\mathrm{EXP}}$
Li^+	0.90(4)	0.48(1)	0.44
Na^+	1.04(1)	0.54(1)	0.57
K^+	1.7(1)	0.78(3)	0.84
Rb^+	1.6(1)	0.74(3)	0.89
Cs^+	1.8(1)	0.81(3)	0.89

Table 4.7: Infinite dilution diffusion coefficients obtained from molecular dynamics simulations under periodic boundary conditions. The ratio of ion/water diffusion coefficients (with the appropriate system-size correction) is also shown, along with the corresponding experimental values.

Finally, to test the thermodynamic properties given by our potentials, we have also measured the relative hydration free energy $\Delta\Delta F$ among adjacent cations in the series of alkalines $Li^+ \rightarrow Na^+$, $Na^+ \rightarrow K^+$, $K^+ \rightarrow Rb^+$, and $Rb^+ \rightarrow Cs^+$ as well the change in the free energy of hydration between Li^+ and Cs^+. Computationally, it is more convenient to measure these relative free energies, since we need not worry about the numerous corrections [140, 141] (for system size, boundary conditions, and treatment of electrostatic interactions) that need to be included when comparing the solvation free energies ΔF to experiments. We can safely assume that the correction term is the same for all the cations, and is thus canceled out when computing the difference between the energies $\Delta\Delta F$. The measurements were carried out using the standard λ-coupling parameter techniques (see Section 3.1.4). A 6-point Gaussian quadrature was used to perform the integration[12]. The data needed for each point in the quadrature was obtained from separate (NVT) MD simulations of 0.3 ns, with 0.25 ns of equilibration (the simulation protocol is the same as before). Since experiments are performed at constant temperature and pressure, we only have the reference values for the change in the Gibbs free

[12]For the $Li^+ \rightarrow Cs^+$ transmutation, an 8-point Gaussian quadrature was used instead

energy of solvation $\Delta\Delta G$; however, we can effectively ignore the volume term[13] and consider that $\Delta\Delta G = \Delta\Delta F$. Our results, which are summarized in Table 4.8, show good quantitative agreement with experiments, except for the transmutations involving K^+, which appear to bee too "close" to Na^+ and too "far" from Rb^+.

$A^+ \longrightarrow B^+$	$\Delta\Delta G$	$(\Delta\Delta G)^{EXP}$
$Li^+ \longrightarrow Na^+$	110	106
$Na^+ \longrightarrow K^+$	57	71
$K^+ \longrightarrow Rb^+$	13	21
$Rb^+ \longrightarrow Cs^+$	32	25
$Li^+ \longrightarrow Cs^+$	215	225

Table 4.8: The change in hydration free energies $\Delta\Delta F$ along the series of alkalines. All values are given in kJ/mole.

4.6 Conclusions

In this chapter, we have shown how to implement a systematic procedure to derive classical force-fields for ions in solutions, from purely *ab-initio* calculations. The method relies primarily on the study of the MLWF. This representation presents a twofold advantage: (1) The MLWF provide a localized description of the electronic density and (2) they allow us to correct for the missing dispersion terms in a consistent manner. We have shown how this method can be used to obtain dipole polarizabilites for ions in condensed phases, for which there is no experimental data. Comparing our results with the corresponding gas phase values, we appreciate the importance of properly taking into account the environmental effects due to the solvent, as these can reduce the polarizabilities of anions by up to $50 \sim 70\%$. Remarkably, our predicted values are in very good agreement with those used in most polarizable potentials, which have been "adjusted" to reproduce the experimental data that *is* available. Although we have only presented the results of monovalent ions in this work, the method can just as easily be applied to multivalent or molecular ions [128].

Using the dispersion corrected DFT results, a simple-force matching procedure was then used to determine the best possible classical force-fields. Although we cannot claim perfect quantitative agreement with experiments (obviously), we nonetheless manage to obtain results, for a variety of equilibrium and dynamical properties, which are in good agreement with the experimental values (in some cases very good agreement) and which reproduce the expected ion specific behaviour. The main advantage of our method, is the fact that it does not require any type of (experimental) input data: All the necessary parameters are obtained from *ab-initio* calculations. Furthermore, the method is easily generalized and improved upon; whether it be to include a new and improved exchange-correlation functional or to consider higher-order multipole moments.

[13]The basic thermodynamic relation between the potentials gives $G = F + PV$ ($\Delta G = \Delta F + P\Delta V$), and since $P\Delta V << \Delta F$, and the change in volume is expected to be roughly the same among the cations ($\Delta\Delta V \approx 0$), we can safely assume that $\Delta\Delta G = \Delta\Delta F$.

Chapter 5

Implicit Solvent Molecular Descriptions of Ions in Solution

Summary

5.1 Introduction

In the previous chapter we have seen how to derive atomic scale interaction potentials for ions in solution directly from *ab-initio* calculations. Once these potentials are known, explicit solvent Molecular Dynamics simulations can be performed to study the ion specific properties. This method provides a convenient approach to the study of electrolytes in bulk and at interfaces, since the microscopic properties of the system are directly accessible. In particular, the solvent-ion properties, such as the free-energies of solvation or the self-diffusion coefficients can be easily calculated, as we have shown. However, the ion-ion properties, such as the ion activities or osmotic coefficients, are notoriously difficult to obtain. This is due to the separation between the characteristic length and time scales of the "fast" water molecules and the "slow" ions. A simulation that properly accounts for both of these regimes must use a time step that is small enough to probe the fast water dynamics, which makes the calculation of the ion properties very time consuming.

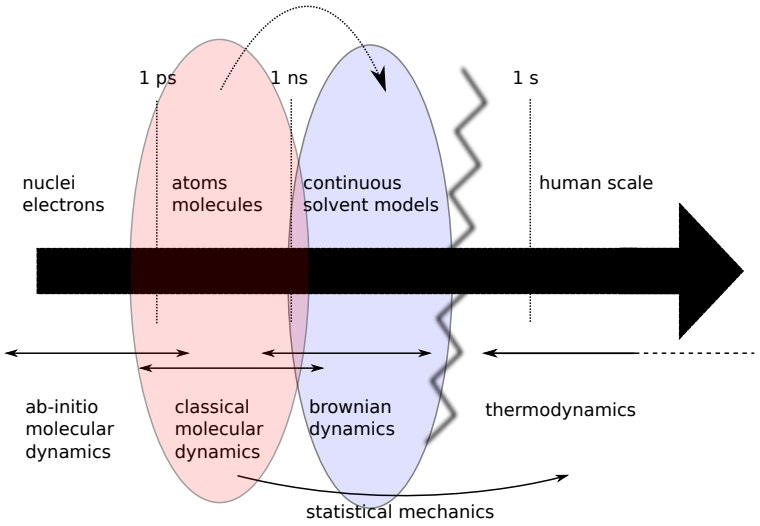

Figure 5.1: The second step in the multi-scale description of electrolyte solutions: Deriving implicit solvent models from classical molecular dynamics simulations of explicit solvent solutions.

Fortunately, the McMillan-Mayer theory of electrolyte solutions allows us to safely ignore the solvent degrees of freedom, and to focus our attention solely on the ions. Instead of using an explicit solvent (atomistic) description, we can use an implicit solvent model, that of a solute gas, whose interactions are determined by the McMillan-Mayer effective potentials. These effective particles move within a dielectric continuum, which takes the place of the solvent. Computing the properties of this reduced system is evidently much easier. Here we will only consider the equilibrium thermodynamic properties of electrolyte solutions, and in particular the osmotic coefficients ϕ. This collective property is very sensitive to the type of salt used, and is therefore a prime candidate to characterize the ion-specificity. Furthermore, as experimental data for this quantity is usually easy to obtain (at least for simple systems), it serves as a stringent benchmark during force-field development.

In this chapter we present the second step in our multi-scale description, by deriving effective (implicit solvent) interaction potentials for ions in solution from MD simulations of the explicit solvent system. These effective potentials will then be used to carry out Monte-Carlo simulations that will allow us to easily measure the thermodynamic properties our system, notable the free energy and the osmotic coefficients. Finally, we show the results obtained from this coarse graining procedure on two types of systems, alkaline salts (simple $1-1$ electrolytes) and lanthanoid salts (strongly charged asymmetric $3-1$ electrolytes), and compare our results with available experimental data.

5.2 McMillan-Mayer Ion-Ion Potentials

5.2.1 Computing the Effective Interactions

The Closure

Although the McMillan-Mayer theory is rigorously exact, it is seldom used directly, as it relies on the knowledge of the n-body potentials of mean force (PMF). To say that this is impractical is a gross understatement. In order to render the simulations feasible, we introduce two approximations for the PMF. First, we assume that three-body and higher order contributions can be neglected, rendering the potentials pairwise additive. Second, in order to avoid the substantial computational effort required to measure the infinite dilution PMF [142], we use an approximate inversion scheme to obtain the potentials from radial distribution functions measured in finite concentration simulations.

Normally, one knows the interaction potentials, and uses simulations or one of the many integral equations to study the thermodynamic and structural properties of the system. In this case, we are faced with the inverse problem. Namely, that of inverting the radial distribution function $g_{ij}(r)$, in order to obtain a two-body potential $v_{ij}(r)$ which accurately reproduces the measured structure. The existence and uniqueness of such a potential is guaranteed by a theorem due to Chayes and Chayes [143, 144], but the inversion procedure is left unspecified. Methods based on integral equation theories [145, 146], inverse Monte Carlo simulations [147], and Maximum Entropy principles [148] have been employed to study a wide variety of systems, with varying degrees of success. If this inversion is carried out at a sufficiently low concentration, we can assume that n-body effects are negligible, and this effective pair potential will be equal to the infinite dilution PMF.

Due to its simplicity, and the accuracy with which it describes electrolyte solutions, we use the HNC approximation (Eqs. 3.48 and 3.53), together with the Ornstein-Zernicke relation (Eq. 3.44), to perform the inversion. For a multi-component system, the HNC closure is given by

$$\beta v_{ij}(r) = h_{ij}(r) - c_{ij}(r) - \ln\left[h_{ij} + 1\right] \tag{5.1}$$

and the Ornstein-Zernicke by Eq. (3.46)

$$h_{ij}(\boldsymbol{r}_{ij}) = c_{ij}(\boldsymbol{r}_{ij}) + \sum_k \int \mathrm{d}\boldsymbol{r}_k \, c_{ik}(\boldsymbol{r}_{ik}) \rho_k h_{kj}(\boldsymbol{r}_{kj}) \tag{5.2a}$$

which, in Fourier space, is written as

$$\widetilde{h}_{ij}(k) = \widetilde{c}_{ij}(k) + \sum_k \widetilde{c}_{ik}(k) \rho_k \widetilde{h}_{kj}(k) \tag{5.2b}$$

Notice that only the pair correlation function $h_{ij}(r) = g_{ij}(r) - 1$ would need to be computed during a simulation. Once these distribution functions are known, the two equations can be directly solved for $v_{ij}(r)$. However, the OZ equation requires that the $g_{ij}(r)$ be known over the whole range of inter-particle distances $0 < r < \infty$, or at least up to distances over which it has converged to its asymptotic value of zero.

Unfortunately, the values of r over which the $h_{ij}(r)$ can be measured are limited due to the finite size of the simulation box L. Additionally, the long range nature of the interaction potential makes it very difficult to obtain accurate measurements of $g_{ij}(r)$ at long distances. This is especially true for the cation-cation and anion-anion interactions, which are dominated by the strong electrostatic repulsion.

Special care must be taken when extracting effective potentials from distribution functions, since the latter depend on the ensemble in which they are measured, and the OZ relation, as given in Eq. (5.2), is only valid in the grand-canonical ensemble [21]. Exact relations for the corrections which need to be applied to canonical radial distribution functions exist, but they involve the isothermal compressibility of the solution, as well as the partial molar volumes of the solutes [18]. Lyubartsev and Marčelja [145] used the (simpler) correction of a single-component system, in the strong coupling limit; while Kalcher and Dzubiella [142] have fitted the large-r behaviour of the PMF to a Debye-Hückel potential, in order to determine the correction factor. The procedure we use, which fits the small-k values of the pair correlation functions provides a convenient alternative to the latter method. Furthermore, our procedure is exact, in the sense that the Stillinger-Lovett conditions used in the fit are a consequence of the electro-neutrality and the long-range behaviour of the direct correlation functions (which is just determined by the charged nature of the system) [149].

Recovering the Asymptotic Coulomb Behaviour

In order to properly treat the long-range correlations, and unambiguously determine the effective pair potentials $v_{ij}(r)$, we use some exact results regarding the distribution functions of charged systems. This allows us to extrapolate the measured $h_{ij}(r)$ at long distances, in such a way that the asymptotic value of the effective (Coulomb) potential is recovered. For ionic liquids, the Stillinger-Lovett conditions establish two exact relations, which the set of $h_{ij}(r)$ must satisfy, regardless of the specific short-range interactions among the particles [17]

$$\rho_N \sum_j \int \mathrm{d}\boldsymbol{r}\, x_j z_j g_{ij}(\boldsymbol{r}) = -z_i \tag{5.3a}$$

$$\rho_N \sum_i x_i z_i \sum_j x_j z_j \int \mathrm{d}\boldsymbol{r}\, r^2 g_{ij}(\boldsymbol{r}) = -6\Lambda_D^2 \sum_i x_i z_i^2 \tag{5.3b}$$

where $\rho_N = \sum_i \rho_i$ is the total number density, $x_i = \rho_i/\rho_N$ is the density fraction of species i, and Λ_D is the Debye screening length, which depends on the dielectric constant of the solvent (Equation (3.91)). Notice that the first equation is just a consequence of the electro-neutrality of the system. Again, as with the OZ equation, these two relations are easier to work with in Fourier space

$$\rho_N \sum_j x_j z_j \widetilde{h}_{ij}(k=0) = -z_i \tag{5.4a}$$

$$\rho_N \sum_i x_i z_i \sum_j x_j z_j \left(\nabla_{\boldsymbol{k}}^2 \widetilde{h}_{ij}(k)\right)\Big|_{k=0} = 6\Lambda_D^2 \sum_i x_i z_i^2 \tag{5.4b}$$

where $\nabla_{\boldsymbol{k}}^2$ is the Laplacian with respect to the wave-vector $\boldsymbol{k}$. The second of these equations is easily derived from the properties of the Fourier transform: The Laplacian

$\nabla^2_{\boldsymbol{k}}$ gives a factor of $-r^2$, and by evaluating the resulting expression at $k = 0$, we obtain an equation analogous to Eq.(5.3), but for $h_{ij}(r)$ instead of $g_{ij}(r) = h_{ij}(r) + 1$. The missing (divergent) terms ($\sim \int \mathrm{d}\boldsymbol{r} r^2$) can be safely introduced, since electro-neutrality guarantees that the sum of these contributions is exactly zero ($\sum_i x_i z_i = 0$).

Our inversion procedure follows the one used in Ref [150]; it is based on the long-wavelength (short wavenumber) asymptotic behaviour of $\widetilde{h}_{ij}(k)$, given by Equation 5.4. Expanding the distribution functions in even powers of k, at small k, we obtain

$$h_{ij}^{\mathrm{mod}}(k) = a_{ij}^{(0)} + a_{ij}^{(2)}k^2 + a_{ij}^{(4)}k^4 + a_{ij}^{(6)}k^6 + a_{ij}^{(8)}k^8 + \mathcal{O}(k^{10}) \tag{5.5}$$

where the expansion coefficients $a_{ij}^{(n)}$ are related to the moments of order $(2n + 1)$ of $h_{ij}(r)$

$$a_{ij}^{(n)} = 4\pi \frac{(-1)^n}{(2n+1)!} \int_0^\infty \mathrm{d}r\, h_{ij}(r) r^{2n+1}$$

which are finite as long as the $h_{ij}(r)$ decays sufficiently rapidly to 0 at large r. Inserting Equation (5.5) into Equation (5.4), we obtain the following two relations for the expansion coefficients $a_{ij}^{(0)}$ and $a_{ij}^{(2)}$

$$\rho_N \sum_i x_i z_i a_{ij}^{(0)} = -z_i \tag{5.6a}$$

$$\rho_N \sum_i x_i z_i \sum_j a_{ij}^{(2)} = \Lambda_D^2 \sum_i x_i z_i^2 \tag{5.6b}$$

For the two-component systems considered here, these two relations reduce the number of fitting parameters in Eq. (5.5) from 15 to 12.

When computing $\widetilde{h}_{ij}(k)$, it is important to remove any discontinuities in the MD generated $h_{ij}(r)$, so as to minimize the numerical artifacts when using the Fast Fourier Transform routines. Considering the fact that the long range values of $h_{ij}(r)$ are also not known with high accuracy, we have chosen to truncate the functions at the nodes r_c closest to $L/2$. If $h_{ij}^{md}(r)$ represents the raw MD values, we set

$$\widetilde{h}_{ij}(k) = \begin{cases} \widetilde{h}_{ij}^{\mathrm{mod}}(k) & k \le \widetilde{k} \\ \widetilde{h}_{ij}^{\mathrm{dat}}(k) & k > \widetilde{k} \end{cases} \tag{5.7a}$$

with

$$h_{ij}^{\mathrm{dat}}(r) = \begin{cases} h_{ij}^{\mathrm{md}}(r) & r < r_c \\ 0 & r \ge r_c \end{cases} \tag{5.7b}$$

where $\widetilde{h}_{ij}^{\mathrm{fit}}(k)$ is obtained by fitting $\widetilde{h}_{ij}^{\mathrm{dat}}$ (the FT of the truncated MD values) to the functional form given in Eq (5.5). It is worth mentioning that for the systems considered here, the change to $h_{ij}(r)$ in real space, compared to the initial MD values, is negligible. The actual $\widetilde{h}_{ij}(k)$ used in the HNC inversion procedure (Eq. (5.1)) are those defined by Eq. (5.7).

The advantage of this method can be appreciated by inspecting the Bhatia-Thornton structure factors [151, 17]

$$S_{NN}(k) = \sum_i \sum_j S_{ij}(k) \tag{5.8a}$$

$$S_{NZ}(k) = \sum_i \sum_j z_j S_{ij}(k) \tag{5.8b}$$

$$S_{ZZ}(k) = \sum_i \sum_j z_i z_j S_{ij}(k) \tag{5.8c}$$

where $S_{ij}(k) = \delta_{ij} + \sqrt{\rho_i \rho_j}\widetilde{h}_{ij}(k)$ is the partial structure factor of a multi-component system. These functions, which give information on the density and concentration correlations within the fluid, possess well-defined long-wavelength limits, which are independent of the specific short-range potentials (i.e. they are a consequence of the long-range Coulomb interactions). Specifically, at small k, we have $S_{NN}(k) \sim k^0$, $S_{NZ}(k) \sim k^2$, and $S_{ZZ}(k) \sim k^2$, with $S_{ZZ} > 0$ for all values of k [17]. The inversion procedure we have detailed above, in which we enforce the Stillinger-Lovett sum rules, gives modified pair distribution functions $\widetilde{h}_{ij}(k)$ which obey these asymptotic limits [152].

5.2.2 Short-Range Solvent Averaged Interactions

When dealing with charged systems, it is convenient to separate the interaction potentials into a short-range and a long-range contribution

$$v_{ij}(r) = v_{ij}^{\mathrm{lr}}(r) + v_{ij}^{\mathrm{sr}}(r) \tag{5.9}$$

with

$$\beta v_{ij}(r) = \frac{L_{\mathrm{B}} z_i z_j}{r}$$

such that at long distances we recover the expected Coulomb interaction $v_{ij}(r) \underset{r\longrightarrow\infty}{=} v_{ij}^{\mathrm{lr}}(r)$. The short-range contribution to the potential will contain the average solvent effects. It is this term which gives the ion specific effects; in essence, all that is not due to the charge of the ions. A corresponding separation can thus be performed for the thermodynamic properties which depend only on the pair potentials, namely the McMillan-Mayer energy

$$U = U^{\mathrm{sr}} + U^{\mathrm{lr}} \tag{5.10}$$

$$U = \left\langle \sum_{i\neq j} v_{ij}^{\mathrm{lr}} \right\rangle + \left\langle \sum_{i\neq j} v_{ij}^{\mathrm{sr}} \right\rangle \tag{5.11}$$

and osmotic coefficient, which are computed using the pressure-energy relation for ionic systems [153]

$$\phi = \phi^{\mathrm{sr}} + \frac{\beta U^{\mathrm{lr}}}{3N} \tag{5.12}$$

where the short range part is calculated using the virial equation [14]

$$\phi^{\mathrm{sr}} = 1 - \frac{1}{6N}\left\langle \sum_{i\neq j} r_{ij}\frac{\partial v_{ij}^{\mathrm{sr}}}{\partial r_{ij}} \right\rangle \tag{5.13}$$

Computationally, the only term that requires some care is the evaluation of the long range energy U^{lr}, but this is easily taken care of by using the standard Ewald summation techniques (see Section 4.3.3).

5.2.3 Ion Association

For electrolyte solutions with high charges, or with low dielectric constants, the ions will tend to form pairs which behave as a chemically distinct species. The degree (strength) of this association, which determines the fraction of free and paired ions, is given by a mass action law, characterized by an equilibrium association constant K. Since the definition of a "pair" is completely arbitrary, the values for these constants cannot be considered independently of the model used to derive them. This was pointed out by Onsager, in discussing the Bjerrum association, when he said that *"The distinction between the free ions and associated pairs depends on an arbitrary convention ... In a complete theory this would not matter; what we remove from one page of the ledger would be entered elsewhere with the same effect"*. As long as we consistently use the same criteria to evaluate the association of all our systems, we can safely talk about ion pairs, and compare the relative strength of the "pairing" for the different systems. It is important to keep this consideration in mind, since the $1-1$ electrolytes we study here are not generally considered to be associated salts.

To characterize the degree of ion association, we employ the Bjerrum model, which uses a distance criteria to define the pair as two ions within a distance d of each other. At infinite dilution, the association constant K_0 can then be expressed as [154]

$$K_0(d) \equiv \frac{\rho_3}{\rho_1\rho_2} = \int_0^d \mathrm{d}r\, 4\pi r^2 e^{-\beta v_{12}(r)} \tag{5.14}$$

where the cations and anions are labelled as 1 and 2, respectively, and the pair as species 3. Again, the choice of d is completely arbitrary. The expression which appears in the integral ($r^2 \exp(-\beta v(r))$) essentially gives the conditional probability for observing the anion at a distance r from the cation (or vice versa). For purely Coulombic potentials, this function will present a minimum at the crossover point between the decreasing Boltzmann factor ($\exp -\beta v(r)$) and the increasing entropic term (r^2). For more complicated interactions, such as our McMillan-Mayer potentials, several local minima will appear, but the overall behaviour remains the same. We will thus use this (first) minimum in the integrand as the cutoff distance d[1].

[1]This cutoff distance can also be defined as the inflexion point in integrated function $K_0(d)$.

5.3 Results

5.3.1 Simple Electrolytes

We study the nine alkali-halide electrolyte solutions obtained from combinations of Li^+, Na^+, and K^+ cations with Cl^-, Br^-, and I^- anions. Finite concentration (non-polarizable) MD simulations are performed in order to compute the radial distribution functions $g_{ij}(r)$ needed to obtain the MM effective potentials. Once the potentials are known, we use implicit solvent MC simulations to measure the thermodynamic properties of the systems.

Simulation Details

ion/water	σ_{io} (Å)	ϵ_{io} (KJ mol^{-1})	charge (e)
Cl^-	3.785	0.5216	-1
Br^-	3.854	0.5216	-1
I^-	4.168	0.5216	-1
Li^+	2.337	0.6700	$+1$
Na^+	2.876	0.5216	$+1$
K^+	3.250	0.5216	$+1$
SPC/E	σ_{oo} (Å)	ϵ_{oo}(KJ mol^{-1})	charge (e)
O(H_2O)	3.169	0.6502	-0.8476
H(H_2O)	–	–	$+0.4238$

Table 5.1: Lennard-Jones force-field parameters used in molecular dynamics simulations.

All the systems consist of 2000 water molecules and 24 ion pairs, within a periodically replicated cubic simulation box, which corresponds to a salt concentration of $c = \rho_N/2 \simeq 0.6$ M (1M = 1mol.L^{-1}). The simulations are performed using the `Tinker` code [107] within the NPT ensemble, at standard temperature $T = 298.15$ K and pressure $P = 1$ atm. We use the Berendsen thermostat and barostat [101], with a coupling constant of 2 ps and 0.1 ps, respectively. The Beeman algorithm [20] is used to integrate the equations of motion with a timestep of 1 fs. Electrostatic interactions are evaluated using the particle mesh Ewald method [155], under tinfoil boundary conditions. The rattle algorithm [95] is used to handle the molecular constraints on the water molecules. A total of five simulations, each starting from a different random initial configuration, are performed for all nine systems. The final "converged" results are obtained by averaging the partial results measured during each of these five simulations; statistics are gathered during a 0.6 ns simulation, after a 0.25 ns equilibration run. In practice, the only results that are of interest to us, are the radial distribution functions $g_{ij}(r)$ we use to extract the effective pair interaction potentials $v_{ij}(r)$.

We model the ions as non-polarizable charged Lennard-Jones (LJ) particles, and the rigid non-polarizable SPC/E model [111] is used to represent the water molecules. The LJ parameters, ϵ_{ij} and σ_{ij}, for the ion-water interactions are those of Dang and coworkers [109, 156, 157], which are reported in Table 5.1. The ion-ion parameters are

obtained using the usual Lorentz-Berthelot mixing rules

$$\sigma_{ij} = \frac{1}{2}\left(\sigma_{ii} + \sigma_{jj}\right) \qquad \epsilon_{ij} = \sqrt{\epsilon_{ii}\epsilon_{jj}} \tag{5.15}$$

These force-field potentials have been extensively studied, both for ion thermodynamic and dynamic properties [158, 158, 159], as well as for electrolyte structure and thermodynamics [142, 160]. The $g_{ij}(r)$ obtained from these simulations are shown in Figure 5.2 as a function of the cation C^+ for a fixed anion A^-. Comparing with the results obtained by Kalcher and Dzubiella [142] (using considerably longer simulation times) for Na^+-Cl^-, K^+-Cl^-, Li^+-Cl^-, and Na^+-Cl^-, we find good agreement, although we obtain a higher value for the first peak of the Li^+-Cl^- $g_{ij}(r)$.

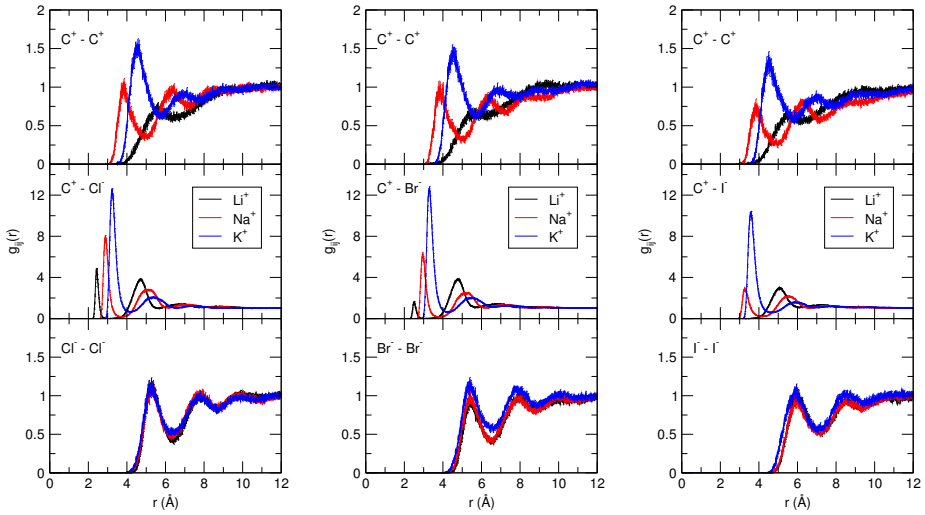

Figure 5.2: Radial distribution functions $g_{ij}(r)$ obtained from MD simulations at $c \simeq 0.6$ M for the Cl^-, Br^-, and I^- salts as a function of the cation C^+=Li^+, Na^+, K^+.

A brief justification for the MD force-fields used to obtain the effective MM pair-potentials is called for, as we have not used those obtained in the previous chapter from *ab-initio* considerations. Although the presentation of this work can be considered to be in a logical or conceptual ordering, where a systematic coarse graining procedure is performed at each level, in order to derive the model parameters used at the next level; the work was actually carried out (chronologically) in the inverse order. That is to say, that we actually started our work by trying to derive mesoscopic models, using already existing classical force-fields (the commonly used Dang Chang non-polarizable potentials). This was done in an effort to maximize the time and computing resources available, by working on both parts of the project simultaneously. However, since each step of the procedure can be considered to be independent of the others (once we have the model parameters, we do not *need* to know how they were derived). Therefore, this inconsistency regarding the MD force-fields will in no way effect our overall results or conclusions, nor will it alter the method we have developed.

Effective Pair Potentials

The radial distribution functions measured during the MD simulations are used within our HNC inversion scheme, to obtain the effective ion-ion interaction potentials. As

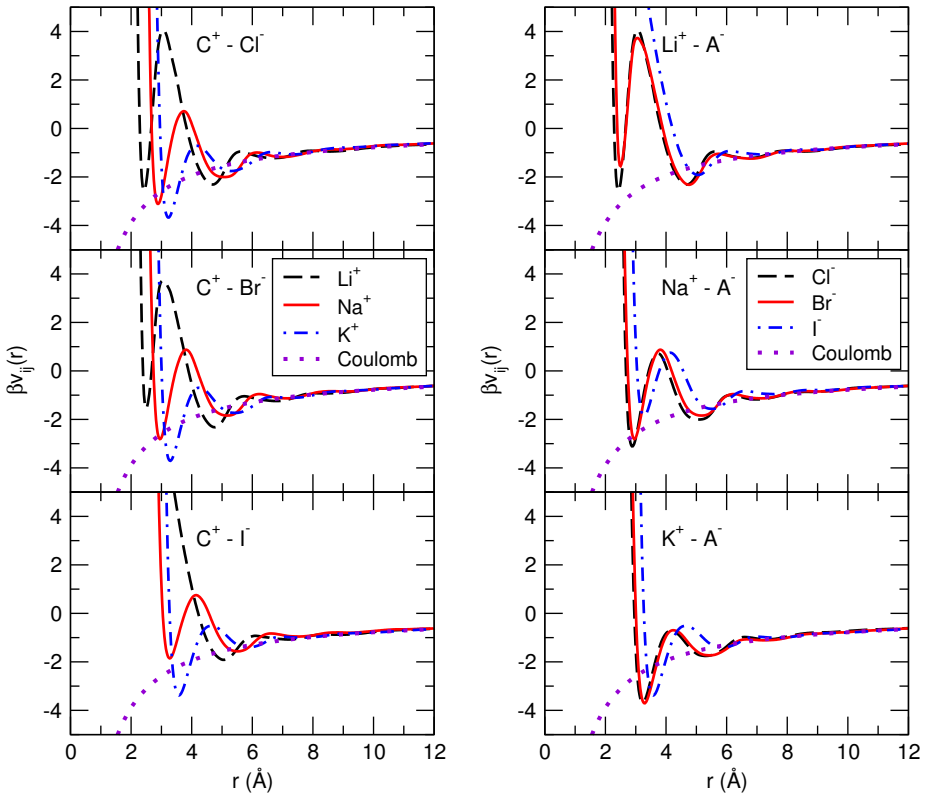

Figure 5.3: Effective McMillan-Mayer cation-anion (C^+-A^-) pair potentials $v_{ij}(r)$ obtained from the HNC closure using MD generated radial distribution functions. The left (right) panel shows the potential as a function of the cation (anion) for a given anion (cation).

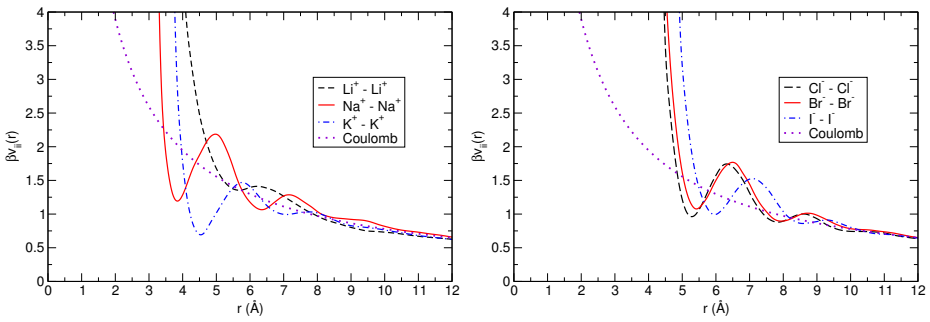

Figure 5.4: Effective McMillan-Mater cation-cation (left) and anion-anion (right) pair potentials $v_{ij}(r)$ obtained from the HNC closure using MD generated radial distribution functions.

mentioned before, the only parameter that needs to be specified is the dielectric constant of the solvent ϵ_r. We use the value of bulk water for the SPC/E model we have used $\epsilon_r = 72$ [161]. The effective cation-anion potentials we obtain are presented in Figure 5.3. We observe the existence of two distinct regimes in the potentials: at short distances $r \lesssim 7$ Å the potentials are strongly oscillating, while at long distances $r \gtrsim 7$ Å we recover the Coulomb attraction. These results support the separation of the potential into a long-range electrostatic contribution and a short-range, solvent averaged interaction, which contains the ion-specific effects. Furthermore, within this short-range region, we identify two clear minima for all the systems considered, except for Li^+-I^-. The first

minimum, which appears in the region $2 < r/\text{Å} < 4$, corresponds to configurations which we identify with the Contact Ion Pair (CIP); while the second minimum, which appears around $4 < r/\text{Å} < 6$, corresponds to the Solvent Separated Ion Pair (SSIP). We note that a potential barrier of at least $k_\text{B}T$ separates the SSIP from the CIP. It is immediately clear that a simple representation, in terms of charged hard-spheres cannot accurately represent such systems, since a single contact distance (or distance of minimum approach) cannot describe these two (stable) configurations.

When comparing the effective potentials to the asymptotic Coulomb attraction, an interesting trend is revealed for the relative stability of the CIP: It is unstable for Li^+ salts (non-existent for Li^+-I^-) and very stable for K^+ salts; with Na^+ salts presenting an intermediate case, in which the first and second minima deviate only slightly from the Coulomb potential. The variations in the potentials, as a function of the cation C^+, are roughly the same for all anions A^-. A larger contact distance, and a more stable contact minimum, is observed when transversing the series of alkali cations (Li^+, Na^+, K^+). A similar, though less noticeable effect is obtained when comparing the cation-anion potentials as a function of the anion, but in this case the energy at contact increases along the series (Cl^-, Br^-, I^-). We notice that the difference between chloride Cl^- and bromide Br^- salts is seen to be very small, and an inversion in the (expected) ordering is observed for K^+-Cl^- and K^+-Br^-. However, this is likely due to the limited accuracy of the inversion procedure, as the corresponding radial distribution functions (Figure 5.2) are practically indistinguishable, especially withing the CIP region. In general, the ordering observed in these effective potentials, in terms of the contact distance and the strength of the interaction at contact, provides a clear and quantitative description of the salt-specificity (i.e. how the cation-anion interactions are modified by the solvation effects depending on the type of the ions). Finally, the averages of the effective cation-cation and anion-anion potentials[2] are given in Figure 5.4. In this case, we see that a hard-core repulsion plus a long-range Coulomb tail is a very good approximation to the effective potential, as the energy oscillations (with respect to the Coulomb repulsion) are always less than $k_\text{B}T$. Comparing our results to those obtained by Kalcher [142] and Fennel [162], the latter from infinite dilution PMF calculations, we again observe good agreement; although we seem to have systematically overestimated the cation-anion attraction in the case of Li^+ salts, probably due to an incomplete sampling in our initial MD simulations.

The McMillan-Mayer effective potentials, for each of the nine alkali-halide salts specified above, are used to carry out Monte Carlo simulations. These are performed in the NVT ensemble, within a periodically replicated cubic simulation box, for 14 different values of the salt concentration c, within the range $0 < c < 2$ M. The concentration values are chosen to obtain an equally spaced distribution of points for $\sqrt{c}$. We assume that the potentials are concentration independent, and the same effective potential is used for simulations at all the concentrations. The dielectric constant was that of the bulk system $\epsilon_r = 72$. The simulated systems all contain the same number of particles $N = 216$, the volume is determined by the concentration c, and the temperature is the same as in the original MD simulations $T = 298.15$ K. The systems are equilibrated over 5×10^5 steps, and subsequent data gathering runs of 10^6 steps are performed. One MC step consists in attempting a random displacement of all the particles, with each move

[2]For each ion we have three different counter-ions, and each provides an independent measurement for the ion-ion potential.

being accepted/rejected according to the Metropolis scheme. Partial averages are sampled every step for the pressure and energy, and every 25 steps for the radial distribution function; a subsequent block averaging is performed every 100 steps.

Validation of the Inversion Procedure

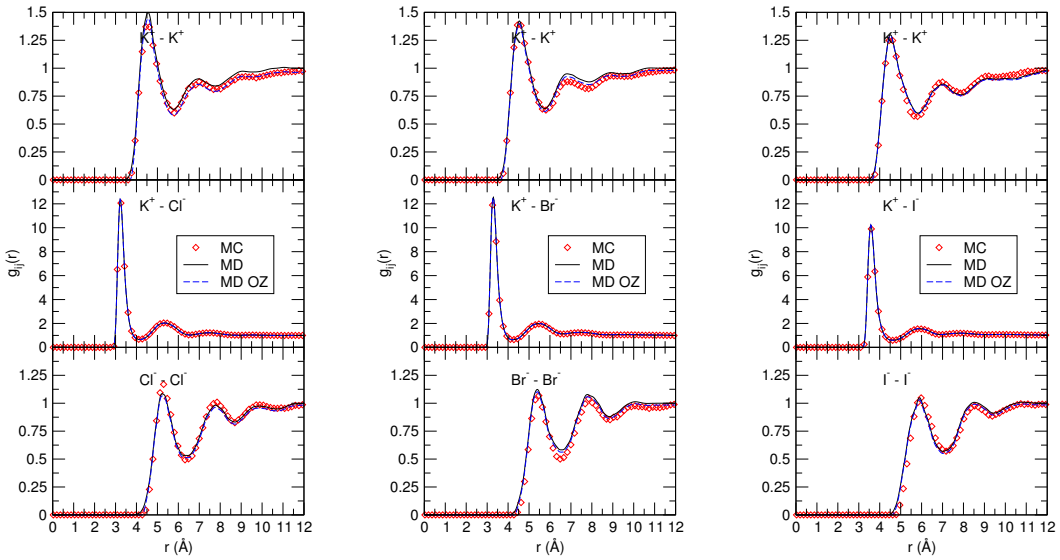

Figure 5.5: Comparison between the MD (raw and OZ "corrected" results) and the MC radial distribution functions for the K^+ salts at $c = 0.64$ M.

In order to test our inversion procedure, we have compared the radial distribution functions obtained from the original (explicit solvent) MD simulations, with those obtained from implicit solvent MC simulations (at the same concentration) using the effective ion-ion potentials. For all the systems considered, we obtain very good agreement, in particular for the cation-anion distributions. Although a slight difference is observed in the cation-cation and anion-anion $g_{ij}(r)$, this is probably due to the fact that we have used the average potential for the like-ion interactions. However, this effect is secondary, as it is the cation-anion interactions which give the dominant contributions to the thermodynamics. In addition, we have also compared the "raw" (MD) data to the "corrected" (MD OZ) data actually used in the inversion (the $g_{ij}(r)$ fitted to satisfy the OZ equations). As expected, the difference in real space is barely noticeable. These comparisons, for the case of the K^+ salts, are shown in Figure 5.5.

Finally, we note that the validity of the inversion procedure we have used relies on one basic assumption: that the effective potentials derived from finite concentration simulations accurately represent the infinite dilution PMF. Given that the PMF are expected to be concentration-independent up to molar concentrations [142], and the fact that the dielectric constant of the solution at 0.6 M is essentially that of bulk (SPC/E) water $\epsilon_r = 72$ [142, 161], we expect this approximation to be valid.

Thermodynamics of the Solute Gas

The two basic thermodynamic properties that we measure during the implicit solvent MC simulations are the McMillan-Mayer internal energy U and pressure P. As

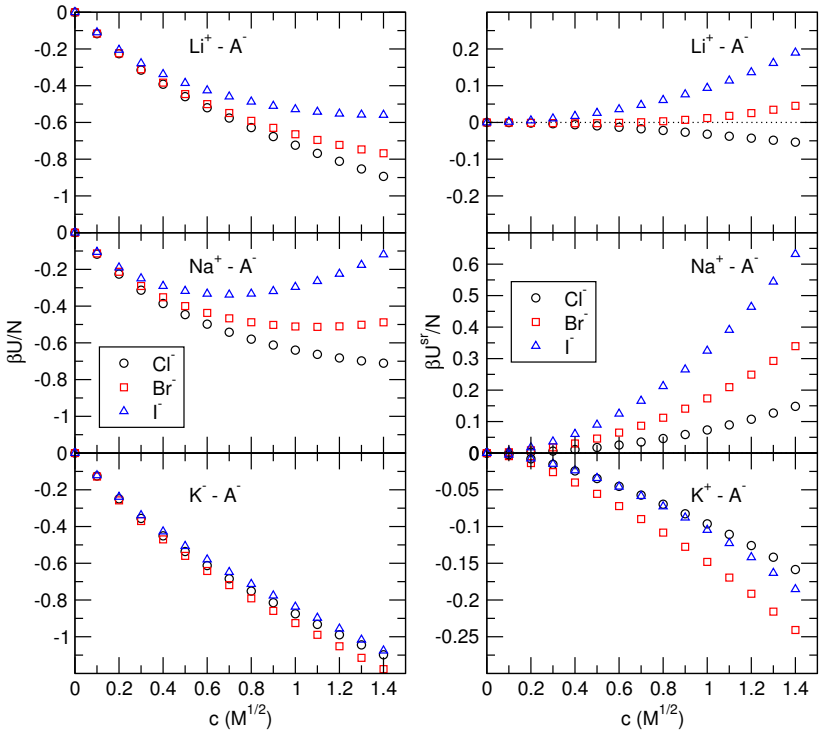

Figure 5.6: Total U (left) and short-range U^{sr} (right) McMillan-Mayer internal energy obtained from implicit solvent Monte-Carlo simulations as a function of the anion (A^-=Cl^-, Br^-, I^-), for the Li^+, Na^+, and K^+ cations.

mentioned before, this pressure corresponds to the osmotic pressure of the solute gas $P = P_{\mathrm{osm}}$, in equilibrium with the pure solvent (see Section 3.4.3). The data is presented in the form of an osmotic coefficient $\phi = \beta P/\rho_N$, as this is the quantity that is usually measured experimentally. The values for the total- and short-range energy per particle are given in Figure 5.6. The long-range Coulomb energy (not shown) is essentially the same for all the systems, confirming our previous assertion, that it is short-range solvent averaged interactions which determine the salt specificity. The following order is observed in the MM energies: $U^{\mathrm{sr}}_{\mathrm{Na^+\text{-}A^-}} > 0$, $U^{\mathrm{sr}}_{\mathrm{Li^+\text{-}A^-}} \simeq 0$, and $U_{\mathrm{K^+\text{-}A^-}} < 0$. It's worth pointing out that although the CIP is unstable for the Li^+ salts, when compared to Na^+ (as seen in Figure 5.3), the energy (total or short-range) is actually lower for Li^+. This is due to the depth of the minimum in the SSIP region, with respect to the CIP, which is seen to be more stable for Li^+. Since the pair is only marginally stable for Na^+ salts, it is the SSIP that gives the dominant contribution in both cases. For the K^+ salts, the solvent averaged contributions give rise to a considerably lower internal energy, compared to both Li^+ and Na^+ salts. It is easy to see that the CIP gives the dominant contribution in this case.

The osmotic coefficients ϕ are shown in Figure 5.7, along with the experimental values. The ordering in the series, as a function of the anion, $\phi_{\mathrm{C^+\text{-}Cl^-}} > \phi_{\mathrm{C^+\text{-}Br^-}} > \phi_{\mathrm{C^+\text{-}I^-}}$ is the same ordering obtained for the total internal energy U. This series corresponds very well with experimental observations, except for the inversion of the K^+-Br^- and K^+-Cl^- osmotic coefficients. This inversion was already present in the cation-anion potentials, although the energy difference at the first minimum is barely noticeable

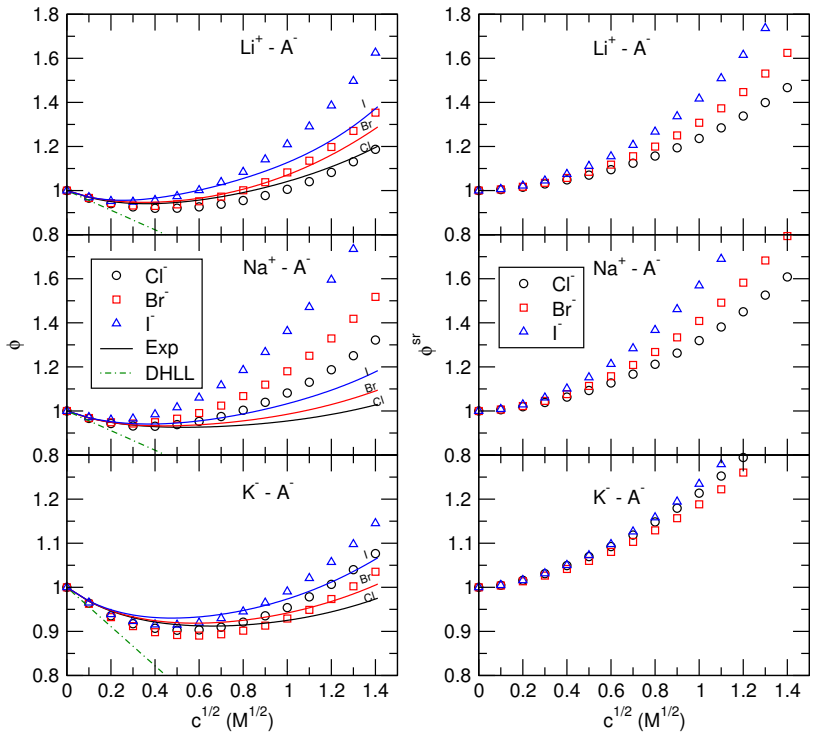

Figure 5.7: Total ϕ (left) and short-range $\phi^{\rm sr}$ contributions to the osmotic coefficient obtained from implicit solvent Monte-Carlo simulations as a function of the anion (A^-=Cl^-, Br^-, I^-), for the Li^+, Na^+, K^+ cations. Experimental values for the osmotic coefficient, as well as the Debye-Hückel limiting law (DHLL), are also shown. All values are given in the McMillan-Mayer frame of reference.

($\lesssim 0.1 k_{\rm B}T$)[3]. The small difference in the osmotic coefficients obtained for Na^+-Cl^-, with respect to our previously published results [163], is due to a difference in the effective potentials used in the simulations. This is just a consequence of the different inversion methods we have used: initially we tried to directly fit the long-r behaviour of the potentials (as done by Kalcher et al. [142]), instead of the small-k fit for the pair-correlation functions we have used here.

The direct comparison between osmotic coefficients obtained from simulations and experiments is seen to be less than perfect, but this is not unexpected, as it is well known that the effective potentials will strongly depend on the underlying atomistic force-fields used in the MD simulations [162, 164]. Given the fact that the ion-water potentials are generally fitted to reproduce single-ion properties, and that the ion-ion potentials are obtained using simple mixing rules, it is not evident *a priori*, that they will be able to provide a suitable description for macroscopic thermodynamic properties. In fact, it was recently shown that it is not always possible, using Lennard-Jones potentials with additive diameters, to parametrize such force-fields to give both the solvation free energies and the osmotic coefficients [165]. The inversion procedure must also be considered, since small variations in the effective potentials are known to lead to relatively large differences in the osmotic coefficients (which is why they serve as a good benchmarking parameter) [166], as our results also indicate.

As mentioned above, we assume that both the short-range solvent averaged potential

[3]The difference in the anion-anion interaction potentials is of the same order of magnitude $\simeq 0.1 k_{\rm B}T$.

and the solvent dielectric constant are concentration independent. Although many-body contributions are not negligible over the concentration range we have studied, bringing into question the use of concentration independent pair-wise additive potentials, Kalcher and Dzubiella [142] and Vrbka et al. [160] have shown that osmotic coefficients obtained through the compressibility (exact) and the virial routes (with a concentration dependent dielectric permittivity [166, 167]) are equal to each other (within error bars). However, since this *correction* does not necessarily improve the agreement with experiments, and since we are interested in deriving implicit solvent primitive models, we do not consider such a concentration dependence. In what follows, we assume that the effective potentials we have derived represent the exact two-body potentials. This is not a bad approximation, as the variations among the different salts are globally reproduced, and the error with respect to the experimental values is not greater than what could be expected using more "exact" representations.

Ion Association

		Li^+	Na^+	K^+
	Cl^-	0.12	0.48	1.40
k_0 (L.mol^{-1})	Br^-	0.04	0.39	1.51
	I^-	0.00	0.25	1.47

Table 5.2: Equilibrium Bjerrum association constants derived from the cation-anion effective potentials.

The monovalent salts we have studied are not generally considered to form electrostatic ion pairs; however, this does not prevent us from using the Bjerrum concept to estimate the degree of association. The values for the equilibrium association constant K_0, computed using Eq. (5.14), are given in Table 5.2. These values allow us to quantify the observations made previously on the stability of the CIP. Namely, that the Li^+ salts are the least associated, the K^+ salts the most associated, and the Na^+ salts present an intermediate behaviour. In terms of the anions, the variation is not as clear, the chloride Cl^- and bromide Br^- salts give comparable results, although the former seems to be slightly more associated, and the I^- salts can be considered to be the least associated. However, this is contradicted by the results shown for the K^+ salts, but we must take into account the inversion of the Cl^- and Br^- seen in the effective potentials. Quantitatively, we also observe an order of magnitude difference between the Li^+ and the K^+ salts. The variation of K_0 among salts with the same cation C^+ is seen to vary only slightly, at least compared to the variation seen for salts with a fixed anion A^-.

Within the literature [154], one can find references to multi-step ion association constants, used to describe the association mechanism between a cation and an anion: from a configuration in which the solvation spheres of both ions are intact, to one in which the solvation shell is shared among the two (overlaps), and finally, to a configuration in which the ions are at contact. However, from the simplified description provided by the Bjerrum association model, with the MM effective potentials, we can only make a clear distinction between ions at contact (with no water molecules between them) and those which are separated by one or more water molecules. In fact, the Bjerrum model we use essentially defines the pair as a cation and an anion within the CIP region.

5.3.2 Highly Charged Asymmetric Electrolytes

To test the validity of our coarse-graining procedure, we have also studied a series of highly-charged asymmetric electrolytes: the lanthanoid - chloride Ln^{3+}-Cl^{-} salt solutions. In order to obtain a clear picture of the cation specificity, we have chosen five representative lanthanoids Ln^{3+}= La^{3+}, Nd^{3+}, Eu^{3+}, Dy^{3+}, and Lu^{3+}; which span the entire series (see Figure 5.8). These systems present important industrial applications, as the lanthanoids Ln^{3+} are commonly used as actinoid An^{3+} salt analogues, for which experimental data is difficult to obtain. This work was done in collaboration with Magali Duvail and Philippe Guilbaud, who kindly provided us with all their MD simulation results.

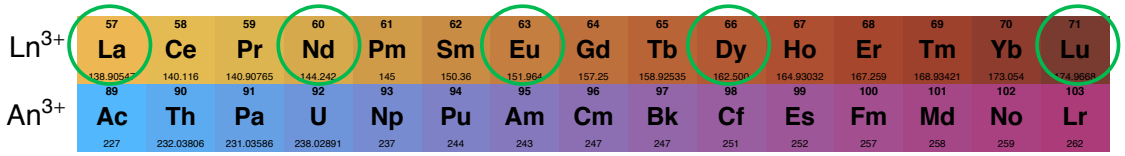

Figure 5.8: Elemental data for the actinoid and lanthanoid series. The lanthanoid elements considered in this work are circled in green.

Simulation Details

ion/water	σ_{io} (Å)	ϵ_{io} (KJ mol^{-1})	charge (e)	α(Å^3)
Cl^{-}	3.827	0.4187	-1	3.250
La^{3+}	3.384	0.4215	$+3$	1.134
Nd^{3+}	3.317	0.4404	$+3$	0.955
Eu^{3+}	3.237	0.4586	$+3$	0.823
Dy^{3+}	3.161	0.4649	$+3$	0.728
Lu^{3+}	3.045	0.4822	$+3$	0.623
POL3	σ_{oo} (Å)	ϵ_{oo}(KJ mol^{-1})	charge (e)	α(Å^3)
O(H_2O)	3.204	0.6531	-0.7300	0.528
H(H_2O)	–	–	$+0.3650$	0.170

Table 5.3: Lennard-Jones force-field parameters used in molecular dynamics simulations.

Simulations for the five binary lanthanoid-chloride aqueous solutions are performed at two different concentrations, c = 0.5 and 1.0 mol kg^{-1}, within the NPT ensemble, using the `AMBER 10` code module, `Sander` [168]. The long-range interactions are computed using the particle-mesh Ewald method [169], the temperature and pressure (T = 298.15 K and P = 1 atm) are controlled using a Berendsen thermostat and barostat [101] (coupling constant τ = 1 ps.). A 1 fs time step is used to integrate the equations of motion, with the Beeman algorithm [20]. All systems are equilibrated during at least 100 ps, with the lanthanoid salts initialized as first shell dissociated (i.e. chloride anions are outside the first solvation sphere of the lanthanoid cation), and subsequent production runs of 2 ns are then performed. The molecules (atoms) are considered to be polarizable species, the pair interactions are modelled with the usual Lennard-Jones

potentials, and the Lorenz-Berthelot mixing rules are used to determine the cross interactions. The POL3 model is used to represent the water molecules [170, 171], the model of Smith and Dang [172] is used for the Cl^- anion, and the potential parameters of Duvail et al. [173, 152] are used for the Ln^{3+} cations. The ion-water and water-water LJ parameters are summarized in Table 5.3. A cubically replicated cubic simulation box with 887 (1498) water molecules, 8 (27) Ln^{3+} cations, and 24 (81) Cl^- anions is used for the simulations at 0.5 (1.0) mol kg^{-1}.

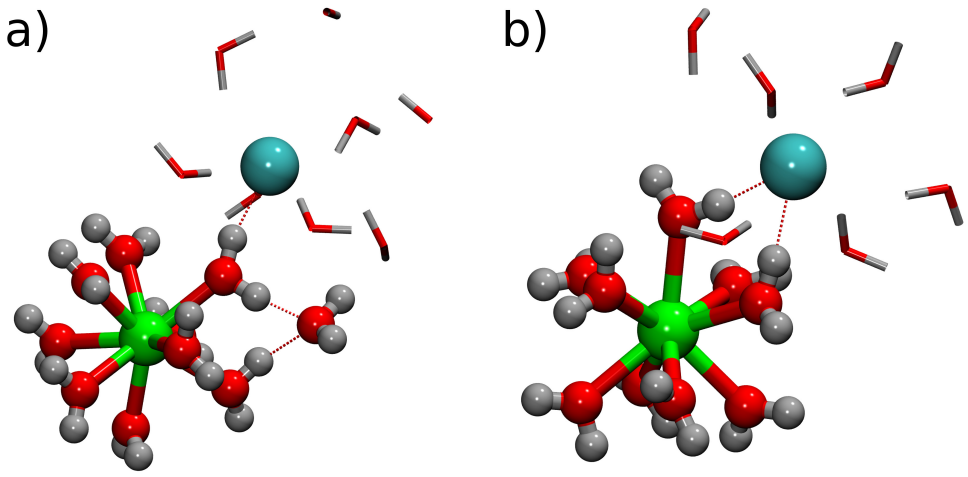

Figure 5.9: The two characteristic hydrogen bonded structures of Cl^- anions with water molecules in the Ln^{3+} first solvation shell.

As before, the output required from these MD simulations is the radial distribution functions. We use those obtained at $c = 0.5$ mol kg^{-1} to perform the inversion procedure, where we have again assumed that the dielectric constant of the solution is that of bulk water for the POL3 model $\epsilon_r^{\mathrm{POL3}} = 106$. These distribution functions are shown in Figure 5.10, where a decrease in the Ln^{3+}-Cl^- "contact" distance is observed across the series ($La^{3+} > Nd^{3+} > Eu^{3+} > Dy^{3+} > Lu^{3+}$), which is accompanied by a decrease in the average size of the cation's solvation sphere [152]. In contrast to the $1-1$ electrolytes, the first peak in this cation-anion $g_{ij}(r)$ actually corresponds to the SSIP, and not the CIP [174]. As previous experimental and computational studies have shown, there is no inner-sphere complexation (CIP) between Ln^{3+} and Cl^- at this concentration. This outer sphere complex presents two preferred locations for the Cl^- anion, corresponding to two distinct hydrogen-bond formations between the anion and the water molecules of the (first) hydration sphere [174]. A snapshot from the MD simulations illustrating these two configurations is provided in Figure 5.9. This internal structure within the SSIP is clearly reproduced in the distribution functions, where the first peak is seen to be composed of two sub-peaks.

Effective Pair Potentials

The effective potentials obtained from the MD generated $g_{ij}(r)$ are given in Figure 5.11. The cation-cation potentials clearly present a hard-core repulsion at short distances, which reproduces the expected ordering in the series $La^{3+} < Nd^{3+} < Eu^{3+} < Dy^{3+} < Lu^{3+}$. The long-range, small energy fluctuations, which become attractive for Eu^{3+} and Lu^{3+}, are likely a consequence of the errors inherent to the inversion procedure,

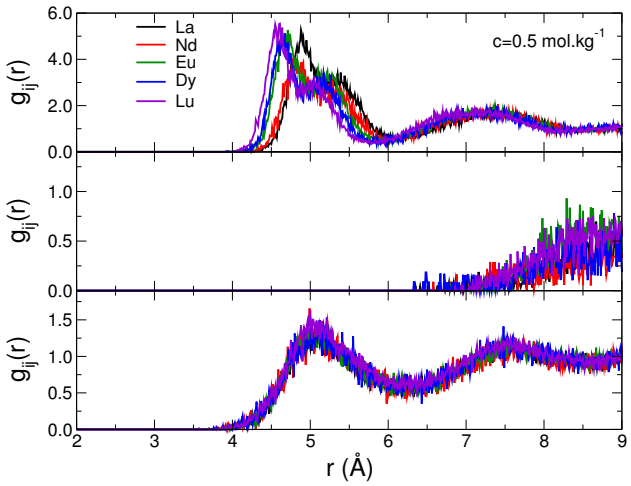

Figure 5.10: Radial distribution functions obtained from explicit solvent Molecular Dynamics simulations of a series of Ln^{3+}-Cl^- salt solutions at $c = 0.5$ mol kg^{-1}. Ln^{3+}= La^{3+}, Nd^{3+}, Eu^{3+}, Dy^{3+}, and Lu^{3+}.

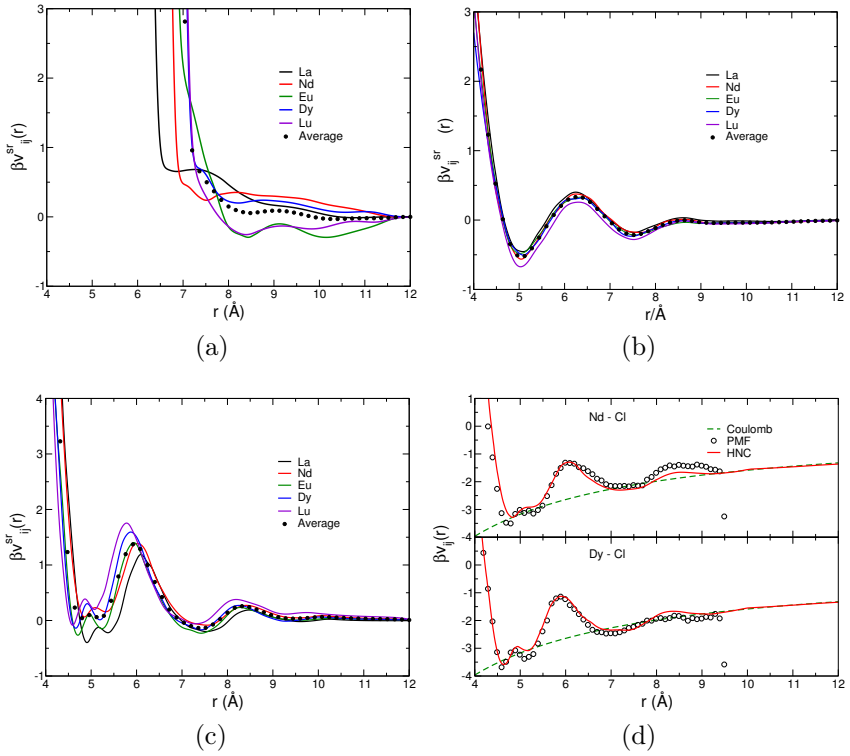

Figure 5.11: Effective McMillan-Mayer (a) cation-cation, (b) anion-anion, and (c) cation-anion pair potentials $v_{ij}(r)$ obtained from the HNC closure using MD generated radial distribution functions. (d) A comparison between the "exact" infinite dilution PMF, our effective potential, and the asymptotic Coulomb potential is also shown, for the case of Nd^{3+}-Cl^- and Dy^{3+}-Cl^-.

which are magnified by the noise present in the original radial distribution functions (Figure 5.10). The cation-anion potentials also reproduce the same ordering, for both the height (depth) and the position of the first maxima (minima), with the exception of the Nd^{3+}-Cl^- potential, which completely underestimates the ion association. This anomaly can already be seen in the original $g_{ij}(r)$, which leads us to believe that this is due, either

to an incomplete sampling (the simulation time was too short), or to an inadequate force field. The Cl^--Cl^- potential is essentially the same for all the salts considered, and the average of the five estimates is the potential that will be used for the implicit solvent MC simulations. The figures also report the average cation-cation Ln^{3+}-Ln^{3+} and cation-anion Ln^{3+}-Cl^- potentials. These fictitious potentials are used in additional simulations, in order to evaluate the sensitivity of the measured thermodynamic data to variations in the potentials, allowing us to measure the propagation of errors throughout the coarse-graining procedure.

These potentials are then used in implicit solvent MC simulations. The details of the simulation protocol are the same as in the previous case, for the alkali-halide salts. The effective potentials used are those obtained from the MD simulation results at the lowest concentration available $c = 0.5$ mol kg^{-1}($\simeq 0.51$ M). Again, these are assumed to be concentration independent and used for all the MC simulations ($0 \leq c \leq 1.44$ M). As before, we use a concentration independent dielectric constant which corresponds to that of the bulk water, $\epsilon_r = 106$ for the POL3 water model used in this case.

Validation of the Inversion Procedure

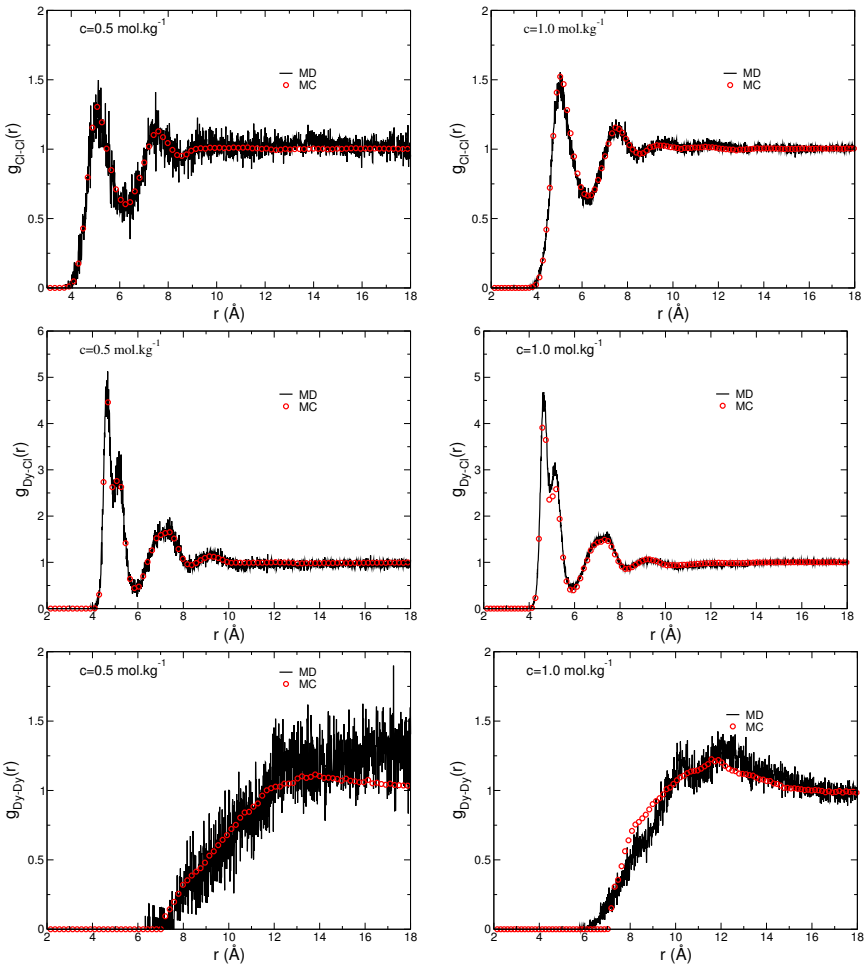

Figure 5.12: Comparison between the MD (explicit solvent) and MC (implicit solvent) radial distribution functions for Dy^{3+}-Cl^- at $c = 0.5$ (left) and 1.0 mol kg^{-1} (right).

A comparison between the effective HNC potentials and the *exact* infinite dilution

PMF (obtained by Duvail et al. [173] from umbrella sampling simulations of two ions in water is given in Figure 5.11(d), where the PMF have been shifted to align with the first-peak in the HNC potential. Very good agreement is obtained, particularly at short distances, which shows that the concentration dependence of the effective potentials is still very weak at $c \simeq 0.5$ M(which is not to say that these difference are insignificant, as relatively small variations in the effective potentials can give rise to considerable differences in the osmotic coefficients). The poor asymptotic behavior of the PMF, which is unable to reproduce the Coulombic tail, is due to the uncertainty in the Umbrella sampling simulations, as well as artifacts arising from the periodic boundary conditions. The former is due to the limited sampling that can be achieved for large ion-ion separations, while the latter results from the self interactions of the ions with all their periodic replicas.

The advantage of the approximate HNC closure we have used is to allow us to recover the expected long-range Coulomb behaviour. The main drawback of our procedure is obviously the fact that we ignore all correlations beyond the cutoff distance r_c (used to truncate the distribution functions, in order to avoid discontinuities when computing the Fourier transforms). Inspection of the radial distribution functions (Figure 5.10) leads us to believe that this effect will only be important for the cation-cation interactions, since the cation-anion and anion -anion $g_{ij}(r)$ have already converged to their asymptotic values at $r_c \gtrsim 10$ Å. We note that this problem was not encountered when computing the effective potentials of the $1-1$ electrolytes, since there was no apparent structuring at large distances. This could be improved upon by considering independent measurements for $h_{ij}(r)$ and $\widetilde{h}_{ij}(k)$, as has been done in Ref [150].

The radial distribution functions obtained from the implicit solvent simulations of Dy^{3+}-Cl^{-} at two concentrations, are given in Figure 5.12, where they are compared to the corresponding explicit solvent functions. At $c = 0.5$ mol kg^{-1}($\simeq 0.51$ M) the agreement is seen to be excellent for the cation-anion and anion-anion $g_{ij}(r)$. The cation-cation comparison is less favorable, particularly at long distances, but this was to be expected, since we have truncated the cation-cation radial distribution functions at a node $r_c \sim 11$ Å (where significant structuring can still be observed) in order to perform the potential inversion. We obtain essentially the same results at the higher concentration $c = 1.00$ mol kg^{-1}($\simeq 1.06$ M), although there is a slight underestimation of the cation-anion pairing. This difference is most noticeable in the second maxima of the first peak. These results validate the coarse-graining strategy, although they indicate the onset of n-body effects at molar concentrations.

Thermodynamics of the Solute Gas

The osmotic coefficients obtained from the implicit solvent MC simulations are compared to the experimental values in Figure 5.13. It is evident at first sight that our results overestimate (underestimate) the repulsion (attraction); however, this is due (in large part) to the fact that the dielectric constant of our water model $\epsilon_{\text{POL3}} = 106$ significantly overestimates that of real water $\epsilon_{\text{exp}} = 78.4$. Given that the thermodynamics of the system is (to first order) determined by the cation-anion attraction, a screened Coulomb potential will lead to a decrease in the ion association, and thus to an increase in the osmotic coefficient. This is verified by the MC results obtained using the dielectric constant of pure water $\epsilon_r = 78.4$, with the same short-range (solvent averaged) potentials

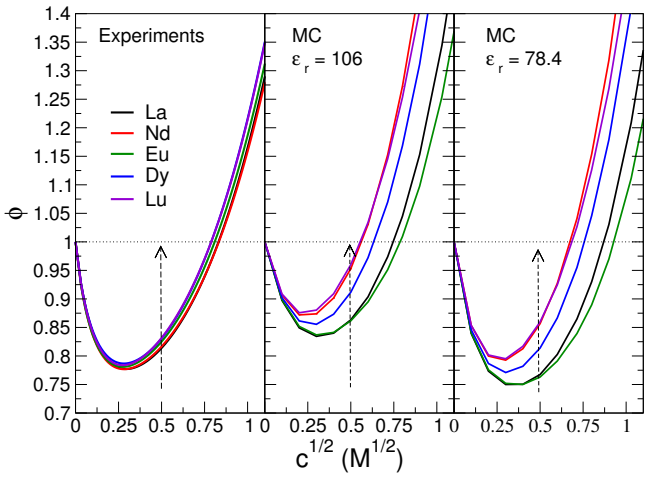

Figure 5.13: Comparison between the experimental and the MC osmotic coefficients. (left) experiments, (center) MC at $\epsilon_r = 106$, (right) MC at $\epsilon_r = 78.4$

as before. These results are also shown in Figure 5.13, where it can be clearly seen that this reduction in the dielectric constant produces a shift in the osmotic coefficients, which is salt independent. The agreement with respect to the experimental values is improved, especially at low concentrations, as expected.

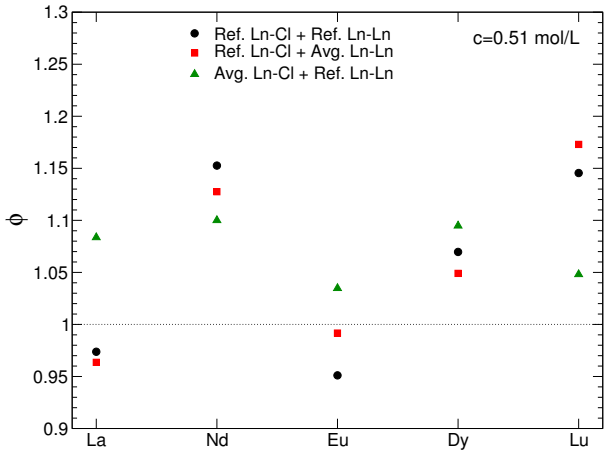

Figure 5.14: Variation of the osmotic coefficient at $c = 0.51$ M due to changes in the cation-cation and cation-anion effective potentials: (circles) salts-specific reference potentials, (squares) reference Ln^{3+}-Cl^- with average Ln^{3+}-Ln^{3+} potentials, and (triangles) average Ln^{3+}-Cl^- with reference Ln^{3+}-Ln^{3+} potentials.

In order to provide an estimate of the intrinsic error in the inversion procedure, we have performed additional MC simulations with two different set of effective potentials: For the first, the salt-specific (reference) Ln^{3+}-Cl^- potentials are replaced by the average Ln^{3+}-Cl^- potential, with all other potentials being left unchanged; while for the second, the corresponding substitution is performed for the Ln^{3+}-Ln^{3+} interaction potentials. The osmotic coefficients computed from MC simulations at $c = 0.51$ M, using these modified potentials, are given in Figure 5.14. The results obtained using the average Ln^{3+}-Cl^- potential (varying only the Ln^{3+}-Ln^{3+} potential) are seen to be essentially equivalent for all the lanthanoids, with a relative error of $\simeq 5\%$ with respect to the average value of ϕ; even though the energy differences among the cation-cation

potentials can be as large as $k_{\mathrm{B}}T$, and the onset of the hard-core repulsion can vary by up to 1 Å. Given the fact that the energy fluctuations present in the Ln^{3+}-Ln^{3+} potentials are largely introduced during the inversion procedure, this variation in ϕ (as a function of the cation-cation potential) can be considered to provide an estimate of the error due to the uncertainty in the interactions. This small variation is nonetheless surprising, since the short-range energy fluctuations are roughly an order of magnitude weaker than the Coulomb repulsion which dominates the cation-cation interactions. The reason for this is simple: as the concentration is increased, packing effects become important, and the solvent averaged cation-cation potentials start to play a role, despite the dominant electrostatic repulsion. A simple calculation can help illustrate this situation. We imagine a hard-sphere representation of the system, with the hard-core diameters σ_{ij} given by the steep repulsive barriers in the effective potentials $v_{ij}(r)$. Let $\sigma_{22} = 4.5$ Å ($v_{22}(\sigma_{22}) \simeq 1k_{\mathrm{B}}T$) and $\sigma_{12} = 6$ Å (SSIP), this gives $\sigma_{11} = 7.5$ Å for the diameter of the hydrated cation. The packing fraction of this hard-sphere system, at $c = 1$ M, is 22%.

Ion Association

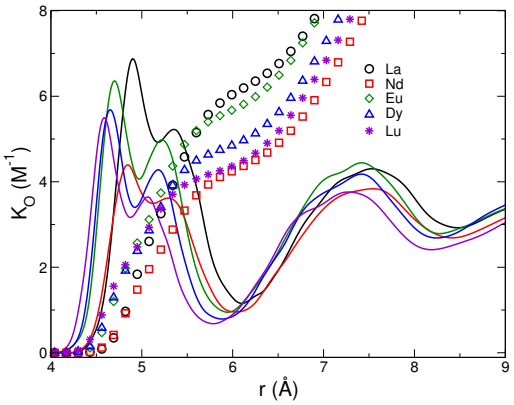

Figure 5.15: Bjerrum association constants obtained from the effective cation-anion potentials. The open symbols show the values of K_0 as a function of the cutoff distance, and the solid lines show the value of the integrand ($4\pi r^2 \exp\left[-\beta v_{12}(r)\right]$) as a function of r.

Our estimates for the association constants K_0 of the different lanthanoid salts are given in Table 5.4, where we compare our results to those obtained by Ruas et al [6], who considers them as fitting parameters (along with the cation diameters and the concentration dependent dielectric permittivity) within a BIMSA model adjusted to reproduce the experimental osmotic coefficients. Although we use a vastly different approach, starting from an approximate molecular description of the system, we are able, without any fitting parameters, to reproduce the same variation across the series of lanthanoids. Our final values for K_0 differ only by a factor of two from the fitted values of Ruas and coworkers.

Ln^{3+}	K_0(HNC)	K_0(BIMSA)
La^{3+}	6.1	3.05
Nd^{3+}	4.2	2.59
Eu^{3+}	5.6	2.55
Dy^{3+}	4.7	2.39
Lu^{3+}	4.2	2.08

Table 5.4: Associations Constants K_0 (L.mol^{-1}) obtained from the cation-anion effective HNC potentials and from BIMSA fits to the experimental osmotic coefficients. The BIMSA values are taken from Ref [6].

5.4 Conclusions

We have shown how a coarse-grained description of electrolyte solutions can be derived which allows for a relatively simple calculation of the osmotic (or activity) coefficients of ions in solution. Although we manage to obtain results which are in qualitative agreement with experimental data, it is clear that obtaining accurate quantitative results is very difficult, as this would require very precise fine-tuning of the effective potentials. The problem is clearly seen when inspecting the variation for the osmotic coefficients of the lanthanoid-chloride salts, as a function of the cation, since the difference is never more than a few percentage points. In contrast, our effective potentials predict a rather large variation, which is extremely sensitive to the relative stability of the contact (CIP) and solvent separated ion pair (SSIP).

Even though the reduction in computational complexity provided by such an implicit solvent description is remarkable, compared to what would have been required to compute the osmotic coefficients directly from explicit solvent MD simulations (using the Kirkwood-Buff theory), the calculations are still relatively long. For engineering applications, this remains prohibitively expensive, and it is necessary to look for further simplifications. The work we have presented in this chapter can thus be considered as an intermediate step, between the fully atomistic description used previously, and the primitive (analytically solvable) model we derive in the next chapter. Finally, we note that all the results obtained from the MC simulations on the alkali-halide and lanthanoid-chloride salts are given in Appendix E.

Chapter 6

From Molecular Descriptions to Primitive Models

Summary

6.1 Introduction

In the last chapter, we have seen how to use the McMillan-Mayer theory to easily measure the thermodynamic properties of ions in solution, from a completely atomistic description. Explicit solvent MD simulations were performed in order to measure the ion-ion correlations, which were then used to define effective ion-ion potentials. Once these potentials are known, implicit solvent Monte-Carlo simulations allow us obtain the ion thermodynamic properties with a reasonable computational investment. However, such a description still requires the use of numerical simulations, since the effective potentials are still too complicated to attempt any sort of analytical solution. This is an important

issue when considering industrial applications, where analytic solutions are required (even the relatively fast implicit solvent MC simulations are considered too expensive and time consuming). Furthermore, the study of complex systems, such as porous or electrochemical materials, requires simple implicit solvent models. Usually, these have been fitted to reproduce experimental data, providing little microscopic insight into the relevant physical phenomena. Our job is to derive these models from molecular simulations. These problems can be addressed by performing yet another coarse-graining procedure, effectively deriving a simple (analytic) model from molecular considerations. The question that must be asked, is then: What is the best possible (simple) model of electrolytes?

6.2 Deriving the Simplest Implicit Solvent Model: A perturbation approach

As mentioned above (Section 3.1.4), thermodynamic perturbation theory provides a convenient way of approximating the free energy of a given (model) system, in terms of the free energy of a well-known (reference) system. We recall the expression for the second-order expansion of the Helmholtz Free energy (Eq. (3.55))

$$\beta F = \beta F^{(0)} + \beta\langle\delta\mathcal{V}\rangle_0 - \frac{1}{2}\beta^2\left(\left\langle\delta\mathcal{V}^2\right\rangle_0 - \langle\delta\mathcal{V}\rangle_0^2\right) + \mathcal{O}(\beta^3) \tag{6.1}$$

where $\mathcal{V} = \mathcal{V}^{(0)} + \delta\mathcal{V}$ and $\mathcal{V}^{(0)}$ are the potentials for the model and reference systems, respectively ($\delta\mathcal{V}$ is the perturbation), and the ensemble averages are all computed in the reference system ensemble. For a multi-component system with pair-wise additive potentials, the first order approximation, which also provides a rigorous upper bound (analogous to Eq. (3.63)), is given by

$$\beta f \lesssim \beta f^{(0)} + \frac{1}{2}\beta\sum_i\sum_j \rho_i\rho_j \int \mathrm{d}\boldsymbol{r}\, g_{ij}^{(0)}(r)\left[v_{ij}(r) - v_{ij}^{(0)}(r)\right] \tag{6.2}$$

where $f = F/V$ is the free energy density. For the binary $1-1$ electrolytes we have considered, the obvious reference to choose for a perturbation calculation is the two-component charged hard-sphere (HS) system, specified by the diameter σ_i and density ρ_i of the cation and anion. The advantage of such a representation, is the fact that it presents a clear one-to-one mapping to our model system. In principle, we have all that is needed to perform the calculations, as the reference free energy and radial distribution functions, $f^{(0)}$ and $g_{ij}^{(0)}$, can be taken from the MSA solution (see Section 3.3.2), and the perturbation is simply given by the short-range MM potentials

$$\delta v_{ij} \equiv v_{ij}(r) - v_{ij}^{(0)}(r) = v_{ij}^{\mathrm{sr}}(r) \tag{6.3}$$

We can perform this substitution since the long-range Coulomb interaction is the same for both systems, and the HS divergence in $v_{ij}^{(0)}(r)$ is cancelled by the $g_{ij}^{(0)}(r)$ (which are exactly zero in the overlap region).

However, there are two fundamental problems with this approach. First, the MSA solution for the $g_{ij}(r)$ is known to yield unphysical (i.e. negative) regions at distances

close to contact for small diameters. Since the perturbation approach we use is defined as a minimization procedure, we must correct for this artificial behaviour[1]. To this end, we have used an exponential approximation to the $g_{ij}(r)$ given by the MSA solution

$$g_{ij}(r) = \Theta(\sigma_{ij}) \exp\left[g_{ij}^{\mathrm{MSA}}(r) - 1\right] \tag{6.4}$$

which removes any unphysical regions, and has the added benefit of improving the comparison with HNC calculations. In this equation, $\Theta(\sigma_{ij})$ is the Heaviside step function ($\sigma_{ij} = (\sigma_i + \sigma_j)/2$), which ensures that $g_{ij}(r)$ vanishes within the HS overlap regions ($r < \sigma_{ij}$). All references to the MSA radial distribution functions $g_{ij}(r)$ are understood to refer to this "corrected" version, unless stated otherwise. The second problem, which is much more severe, relates to the inherent inability of such a reference to accurately represent the strong non-additive nature of our system. As we have already mentioned when discussing the effective MM potentials, an additive two-component reference system is not able to describe both the CIP and the SSIP configurations. For comparison purposes, we have nonetheless performed the perturbation calculations using this "flawed" reference system. The results obtained using this approximation are labelled MSA2.

In what follows, we show why a three component system, in which an ion pair is explicitly introduced (representing the CIP interaction), is able to provide a better description for our systems. We demonstrate how a perturbation theory with this artificial three-component reference system can be performed, by deriving relations which relate the free energy and the interaction potentials of the two systems (the two-component model system and the three-component reference system). We then apply this method to study the series of alkali-halide salts considered previously (for which we know the MM effective potentials), in order to obtain an analytical solution to the thermodynamic and structural properties of these systems. Our final model shows very good agreement with the *exact* MC data and has no free parameters.

6.3 Choosing the Reference System: the importance of the pair

6.3.1 Singular Reference Potentials

When performing perturbation calculations with singular reference potentials (i.e hard-spheres), an intrinsic error is introduced which must be taken into account to obtain the best approximation to the free energy[2]. This error is due to the difference in the configuration space that is available to the model and reference systems, Ω and Ω_{HS}, respectively. Fortunately, the error has the "correct" sign, so that the Gibbs-Bogoluibov inequality is always satisfied, whether or not the error is corrected for. This was recognized by Mon [175, 176, 177], who showed that a correction term $\Delta F = \ln \epsilon$ should be added to the right hand side of Eq. (6.1), where ϵ is defined as the following ratio of

[1] Otherwise, the negative portions in the $g_{ij}(r)$ will give rise to a large (negative) perturbation term, which drives the minimization to the edges of the parameter space.

[2] Strictly speaking, it is not the singularity of the reference potentials which poses a problem, but the singularity in the perturbation (i.e. when the singularity is *only* present in the reference potential)

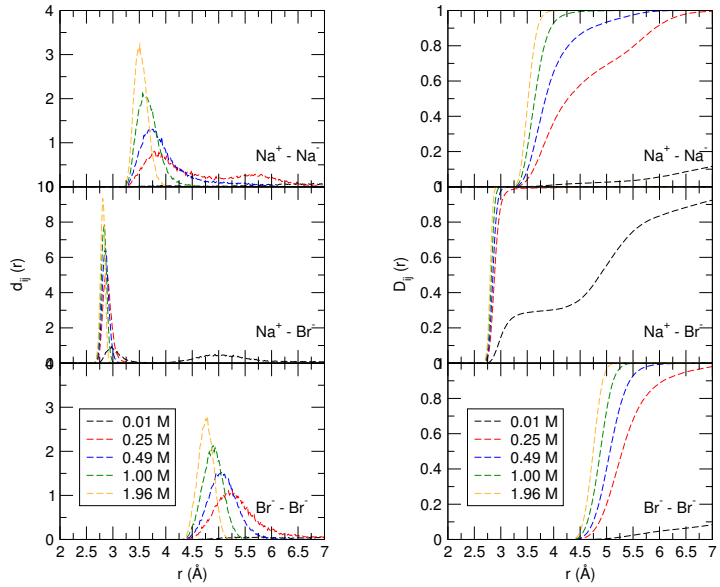

Figure 6.1: Minimum distance probability distribution functions obtained from MC simulations of Na^+-Br^-.

configuration integrals

$$\epsilon = \frac{\int_{\Omega_{\mathrm{HS}}} \exp\left[-\beta\mathcal{V}\right]}{\int_{\Omega} \exp\left[-\beta\mathcal{V}\right]} \tag{6.5}$$

This gives the fraction of configurations generated by the model Boltzmann distribution $\exp\left[-\beta\mathcal{V}\right]$ with no hard-sphere overlaps.

Although the hard-sphere configuration space Ω_{HS} depends on the specific diameters chosen for the HS reference system, the correction term can (in principle) be computed for all such possible values in just one MC simulation. This is accomplished by computing the minimum distance distributions $d_{ij}(r)$, i.e. the histograms of the distances of minimal approach for each of the pair interactions. These are defined such that $d_{ij}(r)\mathrm{d}r$ is the probability, for a configuration sampled within the model ensemble, to have a minimum $i-j$ particle distance between r and $r+\mathrm{d}r$. These functions are computed in a similar manner to the $g_{ij}(r)$[3]: At a given step (n) during our simulation we compute the minimum pair distances $r_{ij}^{\min} = \min(\{r_{ij}\})$ and update the distributions as follows

$$d_{ij}^{(n+1)}(k) = \begin{cases} d_{ij}^{(n)}(k) + 1 & \text{if} \quad (k-1)\Delta r \leq r_{ij}^{\min} < k\Delta r \\ d_{ij}^{(n)}(k) & \text{otherwise} \end{cases} \tag{6.6}$$

where $k = (1, 2, \ldots)$ is the bin index (Δr the bin width) for the discretized histogram. The normalized $d_{ij}(k)$ will thus give the fraction of configurations (generated during the simulation) for which the minimum distance, between particles of type i and j, was between $(k-1)\Delta r$ and $k\Delta r$.

We now define the cumulative probability distribution $D_{ij}(r)$

$$D_{ij}(r) = \int_0^r \mathrm{d}r'\, d_{ij}(r') \tag{6.7}$$

[3]The $d_{ij}(r)$ can be considered as non-normalized radial distribution functions for the distances of closes approach.

which gives the probability that the minimum $i-j$ distance is less than or equal to r. For a given HS reference system, the fraction of configurations with no $i-j$ HS overlap (those for which the minimum pair distance is greater than the contact distance) is $\epsilon_{ij} = 1 - D_{ij}(\sigma_{ij})$. For a one-component system, ϵ can thus be determined directly from the $D(r)$. However, for multi-component systems this is no longer valid, since the inter-particle overlaps cannot be considered independently (i.e. ϵ cannot be recovered form the various $\epsilon_{ij}(r)$). Fortunately, for the charged binary systems considered here, the cation-anion contribution is dominant, and a single-pair approximation can be made

$$\epsilon \simeq \epsilon_{12} = [1 - D_{12}(\sigma_{12})] \tag{6.8}$$

The distribution functions $d_{ij}(r)$ and $D_{ij}(r)$ obtained from MC simulations of Na^+-Br^-, at several concentrations, are shown in Figure 6.1. These functions allow us to establish upper limits on the values of σ_{ij} that would produce an adequate sampling of the model configuration space ($\epsilon \simeq 1$). For this particular example, we see that $\sigma_{11} \lesssim 3.5$ Å, $\sigma_{22} \lesssim 4.75$ Å, and $\sigma_{12} \lesssim 2.75$ Å. If our HS reference system does not satisfy these constraints, a portion of the model system's configuration space will by systematically ignored. It seems reasonable to take the limiting values for σ_{ij}, since the MC simulations show that these are in fact the minimum inter-particle separations (varying only slightly with concentrations) and can thus be considered as "effective" hard-core diameters. However, this would clearly result in a non-additive model $\sigma_{12} \neq (\sigma_{11} + \sigma_{22})/2$, for which no analytic solution is known: the MSA theory (as well as PY) requires additivity in the hard-sphere diameters. Furthermore, we note that Mon's first order correction is of little practical use for us, given the fact that it diverges for the "interesting" values of σ_{ij}, since the correction factor ϵ is essentially a step function

$$\epsilon = \begin{cases} 1 & \sigma_{12} \lesssim 3 \text{ Å} \\ 0 & \sigma_{12} \gtrsim 3 \text{ Å} \end{cases} \tag{6.9}$$

If we take a value of $\sigma_{12} < 3$ Å, the additivity constraint will give cation and anion diameters which are too small, leading to an increased perturbation term $\langle \delta v \rangle_0$[4], and to a reference hard-sphere model that samples regions of the configuration space not available to the model system[5]. However, taking a value of $\sigma_{12} > 3$ Å gives a divergent correction.

Since it is the cation-anion interactions which give the dominant contributions to the thermodynamics, a possible solution to this problem is to treat the CIP interactions and the "free" cation-anion interactions (corresponding to the SSIP) separately. This distinction between the two states is clearly shown in the $d_{12}(r)$ at low concentrations $c \lesssim 0.1$ M, where a bimodal distribution for the minimum cation-anion distance is observed (see Figure 6.1). Since there is a considerable potential barrier separating the two regions $\delta v_{12} \gtrsim 1\ k_B T$, we can consider a representations in which a part of the ions are "paired" together, and the remaining ions are represented as "free", and prevented from coming too close to each other. This will help reduce the intrinsic errors in a PFT calculation, since the HS overlap configurations discussed before, corresponding to the strong cation-anion interactions, are now incorporated into the reference system in the form of an ion

[4]The peak in the $g_{ij}(r)$ will lie in a region where the perturbation potential is very repulsive

[5]This is relevant, since the first order perturbation theory we use, assumes that the structure of the fluid is unaffected by the perturbation in the potential.

pair. This results in a more accurate sampling of the relevant configuration space. However, this approximation will only be valid at moderate concentrations $c \lesssim 1$ M, where higher-order clustering can be safely ignored. Although the previous analysis is based on the Na^+-Br^- simulation results, the same observations can be made for all the $1-1$ salts which we have considered (see Appendix E.4).

6.3.2 The Three - Component Model

We now introduce the *paired* three-component models that will be used as reference in the perturbation calculations. These new systems consist of free ions and neutral pairs, which are in chemical equilibrium with each other. We consider two distinct families of reference models, which differ in the manner in which the internal structure of the pair is taken into account: (1) as a neutral-sphere or (2) as a dipolar dumbbell. In both cases, the free ions are represented as charged hard spheres. We now detail how the free energies and radial distribution functions of these three-component systems are calculated, and in the next section, we answer the question of how to relate the properties of this auxiliary system, to those of the *real* two-component system we are actually interested in.

The Pair as a Neutral Sphere

If the pair is represented as a neutral sphere, the system can be characterized by specifying the diameters σ_i and densities ρ_i of the three components, where $i = 1, 2, 3$ for cations, anions, and pairs, respectively. Note that the charges are fixed parameters. As we mentioned before, the free energy of such a system is naturally divided into ideal, excluded volume, and electrostatic contributions

$$\beta f = \beta f^{\mathrm{id}} + \beta f^{\mathrm{ev}} + \beta f^{\mathrm{el}} \tag{6.10}$$

The ideal term is given by the free energy of a corresponding ideal gas, the excluded volume term is computed using the BMCSL approximation, and the electrostatic term by the MSA solution. The radial distribution functions $g_{ij}(r)$ are also those given by MSA (see Section 3.3.2). We refer to this representation as MSA3.

The Pair as a Dipolar Dumbbell

If the pair is represented as a dipolar dumbbell, we require an additional degree of freedom to represent the internal structure of the pair. We must specify the densities of the three components, as well as four diameters: those of the free ions, σ_1 and σ_2, as well as those of the cation and anion which form the pair, σ_C and σ_A, respectively. Since we are dealing with the pair at contact (CIP), we expect these last two diameters to differ from those of the free ions, which will correspond to the hydrated sizes. However, in order to simplify the perturbation calculations, we consider only symmetric dumbbells ($\sigma_C = \sigma_A$).

For these systems, we must add an additional association term f^{as} to Eq. (6.10), such that the free energy is now given by

$$\beta f = \beta f^{\mathrm{id}} + \beta f^{\mathrm{ev}} + \beta f^{\mathrm{el}} + \beta f^{\mathrm{as}} \tag{6.11}$$

The ideal term is exactly the same as before. The excluded volume term is computed using the same BMCSL approximation, with the free and paired cations and anions

treated independently (i.e. considering we have a four component system). The electrostatic and association terms are now given by the BIMSA solution (see Section 3.3.3).

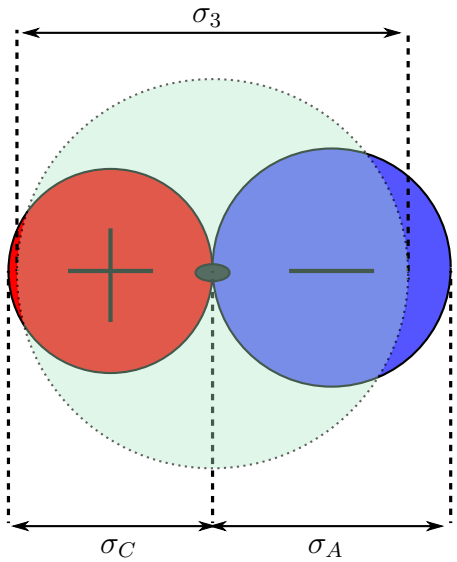

Figure 6.2: Schematic representation of the effective dumbbell size.

Unfortunately, the BIMSA theory does not provide tractable, analytic expressions for the radial distribution functions. For this reason, we have adopted a mixed representation, in which the pair is treated as a dumbbell when computing f and as an effective hard sphere when computing $g_{ij}(r)$. This allows us to use the same MSA solution for the $g_{ij}(r)$ as before. However, we are forced to introduce an additional diameter into the system, that of the effective dumbbell size σ_3 (as shown in Figure 6.2). We use four simple geometric criteria to define this effective diameter in terms of σ_C (the dumbbell ion diameters), the resulting models are referred to as BIMSAi ($i = 1, 2, 3, 4$).

σ_3/σ_C	Model
$\frac{4}{\pi}$ ($\simeq 1.37$)	BIMSA1
$\frac{3\sqrt{3}}{\pi}$ ($\simeq 1.65$)	BIMSA2
$\frac{4\sqrt{2}}{\pi}$ ($\simeq 1.80$)	BIMSA3
2	BIMSA4

Table 6.1: Transformation rules to obtain the effective dumbbell size from the cation(anion) dumbbell diameter.

6.4 The Free Energy of the Paired System

We proceed to show how the free energies of the paired three-component system can be related to those of the *original* two-component system. Consider an open binary system of charged point particles, with chemical potentials μ_1 and μ_2, at temperature T and volume V; as before, 1 and 2, refer to the cation and anion, respectively. The

grand-canonical partition for this system $\Xi(\mu_1, \mu_2, V, T)$ is given by

$$\Xi(\mu_1, \mu_2, V, T) = \sum_{N_1, N_2} \frac{z_1^{N_1} z_2^{N_2}}{N_1! N_2!} \int \mathrm{d}\boldsymbol{r}_1^{N_1} \mathrm{d}\boldsymbol{r}_2^{N_2} \, \exp\left(-\beta \mathcal{V}\right), \tag{6.12}$$

where $\mathcal{V} = \mathcal{V}(\{\boldsymbol{r}_1\}, \{\boldsymbol{r}_2\})$ is the potential energy of the $N_1 + N_2$ particle system. We recall the definitions of the activity z_i and thermal wavelength Λ_i of species i: $z_i = \exp\left(\beta \mu_i\right)/\Lambda_i^3$ and $\Lambda_i = h/\sqrt{2\pi m_i k_\mathrm{B} T}$ (m_i is the mass of species i). The free energy of this system $F(N_1, N_2, V, T)$ is obtained from the grand-potential Ω through a Legendre transformation

$$F(N_1, N_2, V, T) = \Omega(\mu_1, \mu_2, V, T) + N_1 \mu_1 + N_1 \mu_1 \tag{6.13}$$

Using a purely geometrical criteria to define an ion pair, as a cation and anion at a distance less than or equal to d, we wish to rewrite Eq. (6.12) as a partition function for a three component system (composed of free cations (1) and anions (2), along with neutral "pair" particles (3))

$$\Xi'(\mu_1', \mu_2', \mu_3', V, T) = \sum_{N_1, N_2, N_3} \frac{z_1'^{N_1} z_2'^{N_2} z_3'^{N_3}}{N_1! N_2! N_3!} \int \mathrm{d}\boldsymbol{r}_1^{N_1} \mathrm{d}\boldsymbol{r}_2^{N_2} \mathrm{d}\boldsymbol{r}_3^{N_3} \, \exp\left(-\beta \mathcal{V}'\right) \tag{6.14}$$

where primed variables are used for the three-component quantities. This system is characterized by an effective potential $\mathcal{V}'$, which determines the interactions among the free ions and the effective pairs. In writing Eq. (6.14), we have assumed that this potential only depends on the positions of the different species $\mathcal{V}' = \mathcal{V}'(\{\boldsymbol{r}_1\}, \{\boldsymbol{r}_2\}, \{\boldsymbol{r}_3\})$; any dependence on the internal degrees of freedom of the pair must have been averaged out. The free energy of this "new" system is given by

$$F'(N_1', N_2', N_3', V, T) = \Omega'(\mu_1', \mu_2', \mu_3', V, T) + N_1' \mu_1' + N_2' \mu_2' + N_3' \mu_3' \tag{6.15}$$

All that remains to be done is to relate Eqs. (6.13) and (6.15).

In what follows, we use a characteristic function formalism [178, 179] to obtain an expression relating the free energies of the two systems, which is exact at infinite dilution. Define the following cluster functions, $\mathcal{P}_{k_1 k_2}$ and $\overline{P}_{k_1 k_2} = 1 - \mathcal{P}_{k_1 k_2}$,

$$\mathcal{P}_{k_1 k_2} = \begin{cases} 1, & \text{if } k_1 \text{ and } k_2 \text{ are associated: } ||\boldsymbol{r}_{1_{k_1}} - \boldsymbol{r}_{2_{k_2}}|| \leq d \\ 0, & \text{if } k_1 \text{ and } k_2 \text{ are not associated: } ||\boldsymbol{r}_{1_{k_1}} - \boldsymbol{r}_{2_{k_2}}|| > d \end{cases} \tag{6.16}$$

such that $\prod_{k_1, k_2} (\mathcal{P}_{k_1 k_2} + \overline{\mathcal{P}}_{k_1 k_2}) = 1$, where k_1 and k_2 refer to the indices of the cations and anions, respectively. We note that this geometric distance criteria, used to define the pair, is completely arbitrary; any other choice is valid, but this is the most natural one. Introducing this last relation in Eq. (6.12) gives

$$\Xi(\mu_1, \mu_2, V, T) = \sum_{N_1, N_2} \frac{z_1^{N_1} z_2^{N_2}}{N_1! N_2!} \int \mathrm{d}\boldsymbol{r}_1^{N_1} \mathrm{d}\boldsymbol{r}_2^{N_2} \, \exp\left(-\beta \mathcal{V}\right) \prod_{k_1, k_2} (\mathcal{P}_{k_1 k_2} + \overline{\mathcal{P}}_{k_1 k_2}). \tag{6.17}$$

At infinite dilution, for the systems we are considering, contributions from clusters of order higher than 2 are negligible (i.e. each ion belongs to at most one ion pair), and

the product inside the integral can be expanded to give

$$\Xi(\mu_1,\mu_2,V,T) \underset{\rho_1,\rho_2\to 0}{=} \sum_{N_1,N_2} \frac{z_1^{N_1} z_2^{N_2}}{N_1!N_2!} \int \mathrm{d}\boldsymbol{r}_1^{N_1}\mathrm{d}\boldsymbol{r}_2^{N_2}\, \exp\left(-\beta\mathcal{V}\right) \times \sum_{N_3=0}^{\min(N_1,N_2)} C(N_3|N_1,N_2)\overline{\mathcal{Q}}(N_3|N_1,N_2)\mathcal{Q}(N_3) \tag{6.18}$$

with

$$\mathcal{Q}(N_3) = \prod_{k=1}^{N_3} \mathcal{P}_{kk} \tag{6.19a}$$

$$\overline{\mathcal{Q}}(N_3|N_1,N_2) = \prod_{k_1}^{N_1} \prod_{k_2}^{N_2\,\prime} \overline{\mathcal{P}}_{k_1k_2} \tag{6.19b}$$

where the prime indicates a product over all pairs (k_1,k_2), except those for which $k_1 = k_2 \leq N_3$, such that

$$\overline{\mathcal{Q}}(N_3|N_1,N_2) = \begin{cases} 1, & \text{all pairs except } (1,1),\ldots,(N_3,N_3) \text{ are unassociated} \\ 0, & \text{otherwise.} \end{cases}$$

In writing Eqs. (6.18) and (6.19), we have used the fact that the cations (anions) are indistinguishable, allowing us to permute the particle numbers in such a way that the cluster functions $P_{k_1k_2}$ have the lowest possible indices (i.e. the cation and the anion of a given pair have the same label: $k_1 = k_2 = k$). The factor $C(N_3|N_1,N_2)$ counts the distinct number of ways of forming N_3 pairs from N_1 cations and N_2 anions: there are $\binom{N_3}{N_1}$ ways of choosing the N_3 cations, $\binom{N_3}{N_2}$ ways of choosing the N_3 anions, and $N_3!$ equivalent ways of pairing them, which gives

$$C(N_3|N_1,N_2) = \frac{N_1!N_2!}{(N_1-N_3)!(N_2-N_3)!N_3!}$$

The grand-canonical partition function, Eq. (6.18), can then be expressed as

$$\Xi(\mu_1,\mu_2,V,T) = \sum_{N_1,N_2,N_3} \frac{z_1^{N_1} z_2^{N_2} z_3^{N_3}}{N_1!N_2!N_3!} \int \mathrm{d}\boldsymbol{r}_1^{(N_1+N_3)}\mathrm{d}\boldsymbol{r}_2^{(N_2+N_3)} \times \exp\left(-\beta\mathcal{V}\right)\mathcal{Q}(N_3)\overline{Q}(N_3|N_1+N_3,N_2+N_3) \tag{6.20}$$

where $z_3 = z_1z_2$. This relation between the activities of the free and paired ions is just an expression of the mass-action law which must be satisfied at equilibrium.

Next, we perform a transformation on the pair coordinates, in order to distinguish between its translational and internal degrees of freedom. If $\boldsymbol{r}_1 = (r_1^x, r_1^y, r_1^z)$ and $\boldsymbol{r}_2 = (r_2^x, r_2^y, r_2^z)$ are the coordinates for the cation and anion of a given pair, of bond length l, we define (for each pair) the vectors $\boldsymbol{r}_3 = (\boldsymbol{r}_1+\boldsymbol{r}_2)/2$ and $\boldsymbol{r}_l = (\boldsymbol{r}_1-\boldsymbol{r}_2)/2$. Expressing $\boldsymbol{r}_l$ in spherical coordinates (in the molecular reference frame, with origin at the charge barycenter) $\boldsymbol{r}_l = (l/2,\theta,\phi)$, we obtain

$$\Xi(\mu_1,\mu_2,V,T) = \sum_{N_1,N_2,N_3} \frac{z_1^{N_1} z_2^{N_2} z_3^{N_3}}{N_1!N_2!N_3!} \int \mathrm{d}\boldsymbol{r}_1^{N_1}\mathrm{d}\boldsymbol{r}_2^{N_2}\mathrm{d}\boldsymbol{r}_3^{N_3} \int \mathrm{d}(\cos\theta)^{N_3}\mathrm{d}\phi^{N_3} \times \int \prod_i^{N_3} \left(l_i^2\mathrm{d}l_i\right) \exp(-\beta\mathcal{V})\mathcal{Q}(N_3)\overline{\mathcal{Q}}(N_3|N_1+N_3,N_2+N_3)$$

Comparing this last equation with (6.14), we see that

$$z_3'^{N_3} \exp\left(-\beta\mathcal{V}'\right) = z_3^{N_3} \int \mathrm{d}(\cos\theta)^{N_3} \mathrm{d}\phi^{N_3} \int \prod_i^{N_3} (l_i^2 \mathrm{d}l_i) \exp\left(-\beta\mathcal{V}\right) \times \mathcal{Q}(N_3)\overline{\mathcal{Q}}(N_3|N_1+N_3, N_2+N_3) \tag{6.21}$$

At infinite dilution, $\mathcal{V}' = 0$ and $\mathcal{V} = \mathcal{V}_{\text{ext}} + \mathcal{V}_{\text{int}} = \mathcal{V}_{\text{int}}$ (the inter-pair interactions are negligible $\mathcal{V}_{\text{ext}} = 0$), and the internal and external degrees of freedom are uncoupled, so that

$$z_3' = 4\pi z_3 z_{\text{int}} \tag{6.22}$$

with

$$z_{\text{int}} = \int l^2 \mathrm{d}l \, \exp\left(-\beta v_{\text{int}}(l)\right) \tag{6.23}$$

where $v_{\text{int}}(r)$ is the interaction potential for a paired cation and anion. This internal partition function is, by definition of Eq. (5.14), proportional to the association constant K_0

$$z_{\text{int}} = K_0/4\pi \tag{6.24}$$

We obtain the following for the effective potential of the paired system $\mathcal{V}'$

$$\exp\left(-\beta\mathcal{V}'\right) = \frac{\int \mathrm{d}(\cos\theta)^{N_3} \mathrm{d}\phi^{N_3} \int \prod_i^{N_3} (l_i^2 \mathrm{d}l_i) \exp\left(-\beta\mathcal{V}\right) \mathcal{Q}(N_3)\overline{\mathcal{Q}}(N_3|N_1+N_3, N_2+N_3)}{(4\pi z_{\text{int}})^{N_3}} \tag{6.25}$$

The equilibrium condition for the activities (Eq. (6.22)) establishes the following condition on the chemical potential of the pair

$$\mu_3' = \mu_1 + \mu_2 + k_{\text{B}}T \ln\left(4\pi z_{\text{int}}\right) + 3k_{\text{B}}T \ln\left(\frac{\Lambda_3'}{\Lambda_1\Lambda_2}\right) \tag{6.26}$$

Finally, since $\Omega = \Omega'$, as they are describing the same system (the separation between free and paired ions being completely arbitrary), Eqs. (6.13) and (6.15) give the following relationship between the free energies in both representations

$$F = F' - k_{\text{B}}TN_3 \ln K_0 - 3k_{\text{B}}TN_3 \ln\left(\frac{\Lambda_3'}{\Lambda_1\Lambda_2}\right) \tag{6.27}$$

where we have assumed that the chemical potentials of the free ions are unchanged, i.e $\mu_1' = \mu_1$ and $\mu_2' = \mu_2$. From the definition of the ideal free energy (Eq. (3.94)), and the fact that $N_1' + N_3 = N_1$ and $N_2' + N_3 = N_2$ (for a $1-1$ electrolyte), we see that the last term on the right hand side of Eq. (6.27) will exactly cancel an equivalent term coming from the ideal part of F'. Therefore, in order to simplify the calculations, this term can be ignored, provided that it is also set to zero in F'. We thus obtain

$$F = F'(\Lambda_3' = \Lambda_1\Lambda_2) - k_{\text{B}}TN_3 \ln K_0 \tag{6.28}$$

As expected, we see that the difference in the free energies (the second term on the right hand side of Eq. (6.28)) is given by the shift in the standard chemical potential of the pair (the energy required to create the pair).

6.5 The Effective Interactions of the Paired System

We have just seen how to relate the free energies of the two-and three-component systems; all that remains to be done is to determine the effective ion-ion, pair-ion, and pair-pair interaction potentials $v'_{ij}(r)$ for the *auxiliary* paired system from the original potentials $v_{ij}(r)$. Since we only allow for uncharged cation-anion pairs, the like-charge interactions are not modified with respect to the two-component model, $v_{11}(r)' = v_{11}(r)$ and $v_{22}(r) = v'_{22}(r)$, leaving only four unspecified potentials: the pair-ion potentials v'_{31} and v'_{32}, the pair-pair potential v'_{33}, and the internal potential of the pair v_{int}.

As we discussed previously, the cation-anion effective potentials $v_{12}(r)$ present a strong potential barrier ($\gtrsim k_{\text{B}}T$) between the CIP and the SSIP; a fact which is used to unambiguously define the ion pair. Furthermore, given the height of the barrier, the probability of observing a pair in the transition state is considerably less than the probability of the pair being in either of the two local minima. As such, the interaction between free (paired) cations and anions can be approximated by extrapolating v_{12}^{sr}, at the barrier, to an exponential function. An example of this separation procedure is given in Figure 6.3 for the Na^+-Br^- MM effective potential. In what follows, we show how to approximate the pair-ion and pair-pair potentials.

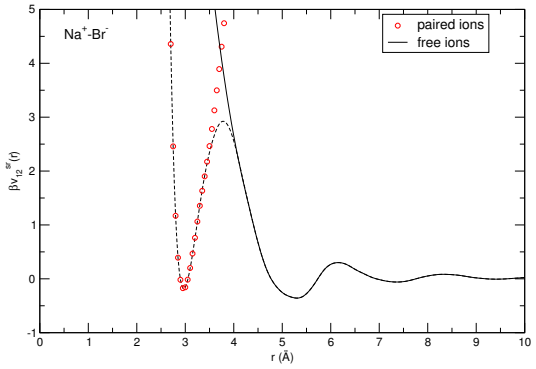

Figure 6.3: Separation of the paired ($v_{\text{int}}(r)$) and free ($v'_{12}(r)$) cation-anion interactions for the case of Na^+-Br^-.

6.5.1 The Pair-Ion Potential

Without loss of generality, we can consider the coordinate origin to coincide with the charge barycenter of the pair, let $+\boldsymbol{l}/2$ and $-\boldsymbol{l}/2$ be the position vectors of the positive (q_1) and negative (q_2) charges of the dipole (pair), and $\boldsymbol{r}$ be the position vector of the "free" ion (charge q_i). The probability of finding a charge q_i at $\boldsymbol{r}$ and a "dipole" of length l, with solid angle $\Omega(\theta, \phi)$, at the origin, is simply

$$P(l, \Omega, \boldsymbol{r}) = \frac{\exp\left[-\beta v(l, \Omega, \boldsymbol{r})\right] l^2 \mathrm{d}l \mathrm{d}\Omega \mathrm{d}\boldsymbol{r}}{\int \mathrm{d}\boldsymbol{r} \int \mathrm{d}\Omega \int \mathrm{d}l\, l^2 \exp\left[-\beta v(l, \Omega, \boldsymbol{r})\right]} \tag{6.29}$$

where $\mathrm{d}\Omega = \sin\theta \mathrm{d}\theta \mathrm{d}\phi$ and $v(l, \Omega, \boldsymbol{r}) = v_{\text{int}}(l) + v_{\text{ext}}(l, \Omega, \boldsymbol{r})$, with v_{int} the internal (charge–charge) potential of the dipole and v_{ext} the external (dipole–charge) potential energy. The probability of finding the charge at $\boldsymbol{r}$ and the dipole at an orientation Ω (irrespective

of the distance between the charges of the pair) is then

$$P(\Omega,\boldsymbol{r}) = \frac{\mathrm{d}\boldsymbol{r}\mathrm{d}\Omega \int \mathrm{d}l\, l^2 \exp\left[-\beta v(l,\Omega,\boldsymbol{r})\right]}{\int \mathrm{d}\boldsymbol{r} \int \mathrm{d}\Omega \int \mathrm{d}l\, l^2 \exp\left[-\beta v(l,\Omega,\boldsymbol{r})\right]} \tag{6.30}$$

which leads us to define the following effective dipole-charge potential

$$\exp\left[-\beta v''_{3i}(\Omega,\boldsymbol{r})\right] = \left\langle \exp\left[-\beta v_{\mathrm{ext}}(l,\Omega,\boldsymbol{r})\right]\right\rangle_l \tag{6.31a}$$

$$P(\Omega,\boldsymbol{r}) = \frac{\exp\left[-\beta v''_{3i}(\Omega,\boldsymbol{r})\right]\mathrm{d}\Omega\mathrm{d}\boldsymbol{r}}{\int \mathrm{d}\boldsymbol{r} \int \mathrm{d}\Omega\, \exp\left[-\beta v''_{3i}(\Omega,\boldsymbol{r})\right]} \tag{6.31b}$$

where

$$\langle \mathcal{A} \rangle_l = \int \mathrm{d}l\, l^2 \mathcal{A} \exp\left[-\beta v_{int}(l)\right]/z_{\mathrm{int}} \tag{6.32}$$

with z_{int} given by Eq. (6.23).

Performing a first order Taylor expansion of $\exp\left[-\beta v''_{3i}\right]$ and $\exp\left[-\beta v_{\mathrm{ext}}\right]$, in Eq. (6.31a), and separating the external potential into short-range and long-range (electrostatic) contributions, we arrive at

$$v''^{\,\mathrm{sr}}_{3i}(\Omega,\boldsymbol{r}) = \langle v^{\mathrm{sr}}_{\mathrm{ext}}(l,\Omega,\boldsymbol{r})\rangle_l \tag{6.33a}$$

$$v''^{\,\mathrm{lr}}_{3i}(\Omega,\boldsymbol{r}) = \left\langle v^{\mathrm{lr}}_{\mathrm{ext}}(l,\Omega,\boldsymbol{r})\right\rangle_l \tag{6.33b}$$

Again, without loss of generality, we can set the z-axis parallel to $\boldsymbol{r}$, and assuming that the long-range potential v^{lr}_{ext} is that of a (point) dipole-charge interaction [180],

$$v_{\mathrm{dip-charge}} = \frac{q_i}{4\pi\epsilon_0\epsilon_r}\boldsymbol{p}.\hat{\boldsymbol{r}} \tag{6.34}$$

we have

$$v''^{\,lr}_{3i}(\Omega,\boldsymbol{r}) = \frac{q_i\langle p\rangle_l \cos\theta}{4\pi\epsilon_0\epsilon_r r^2} \tag{6.35}$$

where $\boldsymbol{p}$ is the "pair" dipole.

Since we would like to derive effective potentials between point particles, and this effective pair–charge potential $v''_{3i}(\Omega,\boldsymbol{r})$ still makes reference to the internal degrees of freedom of the pair (the dipole orientation Ω), it is natural to perform a subsequent average over Ω, which serves as the definition of $v'_{3i}(\boldsymbol{r})$

$$\exp\left[-\beta v'_{3i}(\boldsymbol{r})\right] = \left\langle \exp\left[-\beta v''_{3i}(\Omega,\boldsymbol{r})\right]\right\rangle_\Omega \tag{6.36a}$$

$$P(\boldsymbol{r}) = \frac{\exp\left[-\beta v'_{3i}(\boldsymbol{r})\right]}{\int \mathrm{d}\boldsymbol{r}\, \exp\left[-\beta v'_{3i}(\boldsymbol{r})\right]} \tag{6.36b}$$

with

$$\langle \mathcal{A} \rangle_\Omega = \frac{1}{4\pi}\int \mathrm{d}\Omega\, \mathcal{A} = \frac{1}{4\pi}\int \mathrm{d}\phi \int \mathrm{d}\theta\, \sin\theta \mathcal{A} \tag{6.37}$$

Again, we perform a Taylor expansion of $\exp\left[-\beta v''_{3i}\right]$ and separate the short-range and long-range contributions of the potential, which gives, to second order

$$\begin{aligned}\exp\left[-\beta v'_{3i}(\boldsymbol{r})\right] = 1 &- \beta\langle v''^{\,\mathrm{sr}}_{3i}(\Omega,\boldsymbol{r})\rangle_\Omega - \beta\left\langle v''^{\,\mathrm{lr}}_{3i}(\Omega,\boldsymbol{r})\right\rangle_\Omega \\ &+ \frac{1}{2}\beta^2\left\langle \left(v''^{\,\mathrm{sr}}_{3i}(\Omega,\boldsymbol{r})\right)^2\right\rangle_\Omega + \frac{1}{2}\beta^2\left\langle \left(v''^{\,\mathrm{lr}}_{3i}(\Omega,\boldsymbol{r})\right)^2\right\rangle_\Omega \\ &+ \beta^2\left\langle v''^{\,\mathrm{sr}}_{3i}(\Omega,\boldsymbol{r})v''^{\,\mathrm{lr}}_{3i}(\Omega,\boldsymbol{r})\right\rangle_\Omega\end{aligned} \tag{6.38}$$

From Eq. (6.35), we see that the first order long-range contribution is exactly zero ($\langle\cos\theta\rangle_\Omega = 0$). Therefore, taking the lowest (non-vanishing) short- and long-range contributions to the potential, we obtain

$$\exp\left[-\beta v'_{3i}(\boldsymbol{r})\right] = 1 - \beta\langle v''^{\,\mathrm{sr}}_{3i}(\Omega,\boldsymbol{r})\rangle_\Omega + \frac{1}{2}\beta^2\left\langle \left(v''^{\,\mathrm{lr}}_{3i}(\Omega,\boldsymbol{r})\right)^2\right\rangle_\Omega \tag{6.39}$$

Finally, a first order series expansion of the left hand side of Eq. (6.39), allows us to define the corresponding short-range and long-range contributions to $v'_{3i}(\boldsymbol{r}) = v'^{\,\mathrm{sr}}_{3i}(\boldsymbol{r}) + v'^{\,\mathrm{lr}}_{3i}(\boldsymbol{r})$

$$v'^{\,\mathrm{sr}}_{3i}(\boldsymbol{r}) = \int \mathrm{d}\boldsymbol{l}\, w(\boldsymbol{l}) v^{\mathrm{sr}}_{\mathrm{ext}}(l,\Omega,\boldsymbol{r}) \tag{6.40a}$$

$$v'^{\,\mathrm{lr}}_{3i}(\boldsymbol{r}) = -\frac{\beta}{6}\left(\frac{q_i\langle p\rangle_l}{4\pi\epsilon_0\epsilon_r r^2}\right)^2 \tag{6.40b}$$

where $i = 1, 2$ and $w(\boldsymbol{l})$ is defined as

$$w(\boldsymbol{l}) = (4\pi z_{\mathrm{int}})^{-1}\exp\left[-\beta v_{\mathrm{int}}(l)\right] \tag{6.41}$$

The integral in Eq. (6.40a) can be written in a simpler form in k-space, since

$$v'^{\,\mathrm{sr}}_{3i}(\boldsymbol{r}) = \int \mathrm{d}\boldsymbol{l}\, w(\boldsymbol{l})\left[v^{\mathrm{sr}}_{1i}(\boldsymbol{r}-\boldsymbol{l}/2) + v^{\mathrm{sr}}_{2i}(\boldsymbol{r}+\boldsymbol{l}/2)\right]$$

performing a change of variables, and using the fact that $w(l)$ is an even function of l, we obtain

$$\begin{aligned}v'^{\,\mathrm{sr}}_{3i}(\boldsymbol{r}) &= \int \mathrm{d}\boldsymbol{l}\, w(\boldsymbol{l})\left[v^{sr}_{1i} + v^{\mathrm{sr}}_{2i}\right](\boldsymbol{r}-\boldsymbol{l}/2) \\ &= \frac{1}{(2\pi)^3}\int \mathrm{d}\boldsymbol{k}\, \exp\left(i\boldsymbol{k}.\boldsymbol{r}\right)\widetilde{w}(\boldsymbol{k}/2)\left[\widetilde{v}^{\mathrm{sr}}_{1i} + \widetilde{v}^{\mathrm{sr}}_{2i}\right](\boldsymbol{k})\end{aligned} \tag{6.42}$$

with $\widetilde{w}(\boldsymbol{k})$ and $\widetilde{v}^{\mathrm{sr}}_{ij}(\boldsymbol{k})$ the 3-dimensional Fourier transforms of $w(\boldsymbol{r})$ and $v^{\mathrm{sr}}_{ij}(\boldsymbol{r})$, respectively.

6.5.2 The Pair-Pair Potential

To obtain the effective pair-pair potentials, we proceed in the same manner as above. Consider two pairs, A and B, without loss of generality, we can take the coordinate origin at the charge barycenter of pair A. Let $\boldsymbol{r}$ be the vector to the charge center of pair B. First, we define a potential $v''_{33}(\Omega_A,\Omega_B,\boldsymbol{r})$ averaged over the bond lengths of the

two dipoles l_A and l_B; we then average over the angular degrees of freedom $\Omega_A(\theta_A, \phi_A)$ and $\Omega_B(\theta_B, \phi_B)$, to obtain an effective pair-pair potential $v'_{33}(\boldsymbol{r})$, which only depends on the distance r between the two pairs. Let $v''_{33}(\Omega_A, \Omega_B, \boldsymbol{r})$ be defined as

$$\exp\left[-\beta v''_{33}(\Omega_A, \Omega_B, \boldsymbol{r})\right] = \langle \exp\left[-\beta v_{\text{ext}}(l_A, l_B, \Omega_A, \Omega_B, \boldsymbol{r})\right]\rangle_{l_A, l_B} \tag{6.43a}$$

$$P(\Omega_A, \Omega_B, \boldsymbol{r}) = \frac{\exp\left[-\beta v_{33''}(\Omega_A, \Omega_B, \boldsymbol{r})\right] \mathrm{d}\Omega_A \mathrm{d}\Omega_B \mathrm{d}\boldsymbol{r}}{\int \mathrm{d}\boldsymbol{r} \int \mathrm{d}\Omega_A \int \mathrm{d}\Omega_B \exp\left[-\beta v''_{33}(\Omega_A, \Omega_B, \boldsymbol{r})\right]} \tag{6.43b}$$

where

$$\langle \mathcal{A} \rangle_{l_A, l_B} = \int l_A^2 \mathrm{d}l_A \int l_B^2 \mathrm{d}l_B \, \mathcal{A} \exp\left[-\beta \left(v_{\text{int}}(l_A) + v_{\text{int}}(l_B)\right)\right] / \left(z_{\text{int}}\right)^2 \tag{6.44}$$

Separating $v_{\text{ext}}(l_A, l_B, \Omega_A, \Omega_B, \boldsymbol{r})$ into a short- and long-range potential, and performing a series expansion of Eq. (6.43a), allows us to define the corresponding short and long range contributions to $v''_{33}(\Omega_A, \Omega_B, \boldsymbol{r})$. Assuming that the long-range pair-pair interaction is that of two point dipoles [180]

$$v_{\text{dip-dip}} = \frac{1}{4\pi\epsilon_0\epsilon_r r^3} \left[\boldsymbol{p}_A.\boldsymbol{p}_B - 3\left(\boldsymbol{p}_A.\hat{\boldsymbol{r}}\right)\left(\boldsymbol{p}_B.\hat{\boldsymbol{r}}\right)\right] \tag{6.45}$$

with $\hat{\boldsymbol{r}} = \boldsymbol{r}/||\boldsymbol{r}||$, we obtain

$$v''^{\,\text{sr}}_{33}(\Omega_A, \Omega_B, \boldsymbol{r}) = \langle v^{\text{sr}}_{\text{ext}}(l_A, l_B, \Omega_A, \Omega_B, \boldsymbol{r})\rangle_{l_A, l_B} \tag{6.46a}$$

$$v''^{\,\text{lr}}_{33}(\Omega_A, \Omega_B, \boldsymbol{r}) = \frac{\langle p \rangle_l^2}{4\pi\epsilon_0\epsilon_r r^3} \left(\sin\theta_A \sin\theta_B \cos\left(\phi_B - \phi_A\right) - 2\cos\theta_A \cos\theta_B\right) \tag{6.46b}$$

where we have set the $z - axis$ parallel to $\boldsymbol{r}$. Averaging over the angular degrees of freedom gives the desired effective potential $v'_{33}(\boldsymbol{r})$

$$\exp\left[-\beta v'_{33}(\boldsymbol{r})\right] = \langle \exp\left[-\beta v''_{33}(\Omega_A, \Omega_B, \boldsymbol{r})\right]\rangle_{\Omega_A, \Omega_B} \tag{6.47a}$$

$$P(\boldsymbol{r}) = \frac{\exp -\beta v'_{33}(\boldsymbol{r})}{\int \mathrm{d}\boldsymbol{r} \exp\left[-\beta v'_{33}(\boldsymbol{r})\right]} \tag{6.47b}$$

with

$$\langle \mathcal{A} \rangle_{\Omega_A, \Omega_B} = \frac{1}{(4\pi)^2} \int \mathrm{d}\Omega_A \int \mathrm{d}\Omega_B \, \mathcal{A} \tag{6.48}$$

In the same way we derived Eq. (6.40), we perform a series expansion of Eq. (6.47a) and keep the lowest order (non-vanishing) terms; as before, the first order long-range contribution $\left\langle v''^{\,\text{lr}}_{33}\right\rangle_{\Omega_A, \Omega_B}$ vanishes, and we neglect the cross correlation term $\beta^2 \left\langle v''^{\,\text{sr}}_{33}\, v''^{\,\text{lr}}_{33}\right\rangle_{\Omega_A, \Omega_B}$, since it will be negligible compared to $\beta \langle v''^{\,\text{sr}}_{33}\rangle_{\Omega_A, \Omega_B}$. Finally, we obtain the following for $v'_{33}(\boldsymbol{r}) = v'^{\,\text{sr}}_{33}(\boldsymbol{r}) + v'^{\,\text{lr}}_{33}(\boldsymbol{r})$

$$\begin{aligned} v'^{\,\text{sr}}_{33}(\boldsymbol{r}) &= \langle v''^{\,\text{sr}}_{33}(\Omega_A, \Omega_B, \boldsymbol{r})\rangle_{\Omega_A, \Omega_B} \\ &= \int \mathrm{d}\boldsymbol{l}_A \int \mathrm{d}\boldsymbol{l}_B \, w(\boldsymbol{l}_A) w(\boldsymbol{l}_B) v^{\text{sr}}_{\text{ext}}(l_A, l_B, \Omega_A, \Omega_B, \boldsymbol{r}) \end{aligned} \tag{6.49a}$$

$$\begin{aligned} v'^{\,\text{lr}}_{33}(\boldsymbol{r}) &= -\frac{\beta}{2} \left\langle \left(v''^{\text{lr}}_{33}(\Omega_A, \Omega_B, \boldsymbol{r})\right)^2 \right\rangle_{\Omega_A, \Omega_B} \\ &= -\frac{\beta}{3} \left(\frac{\langle p \rangle_l^2}{4\pi\epsilon_0\epsilon_r r^3}\right)^2 \end{aligned} \tag{6.49b}$$

In the last step, we have used the following relation

$$\left\langle (\sin\theta_1 \sin\theta_2 \cos(\phi_2 - \phi_1) - 2\cos\theta_1 \cos\theta_2)^2 \right\rangle_{\Omega_1,\Omega_2} = \frac{2}{3}$$

As before, the short-range contribution is given as a convolution product, and it is therefore natural to express it in k-space

$$\begin{aligned} v'^{\mathrm{sr}}_{33}(\boldsymbol{r}) &= \int \mathrm{d}\boldsymbol{l}_A \int \mathrm{d}\boldsymbol{l}_B \, w(\boldsymbol{l}_A) w(\boldsymbol{l}_B) \\ &\quad \times \Big[v^{\mathrm{sr}}_{11}(\boldsymbol{r} - \boldsymbol{l}_A/2 + \boldsymbol{l}_B/2) + v^{\mathrm{sr}}_{12}(\boldsymbol{r} - \boldsymbol{l}_A/2 - \boldsymbol{l}_B/2) \\ &\quad + v^{\mathrm{sr}}_{21}(\boldsymbol{r} + \boldsymbol{l}_A/2 + \boldsymbol{l}_B/2) + v^{\mathrm{sr}}_{22}(\boldsymbol{r} + \boldsymbol{l}_A/2 - \boldsymbol{l}_B/2) \Big] \\ &= \int \mathrm{d}\boldsymbol{l}_A \int \mathrm{d}\boldsymbol{l}_B w(\boldsymbol{l}_A) w(\boldsymbol{l}_B) \left[v^{\mathrm{sr}}_{11} + 2v^{\mathrm{sr}}_{12} + v^{\mathrm{sr}}_{22} \right] (\boldsymbol{r} - \boldsymbol{l}_A/2 - \boldsymbol{l}_B/2) \\ &= \frac{1}{(2\pi)^3} \int \mathrm{d}\boldsymbol{k} \, \exp(i\boldsymbol{k}.\boldsymbol{r}) \, [w(\boldsymbol{k}/\boldsymbol{2})]^2 \left[\widetilde{v}^{\mathrm{sr}}_{11} + 2\widetilde{v}^{\mathrm{sr}}_{12} + \widetilde{v}^{\mathrm{sr}}_{22} \right] (\boldsymbol{k}) \end{aligned} \tag{6.50}$$

6.5.3 Summary

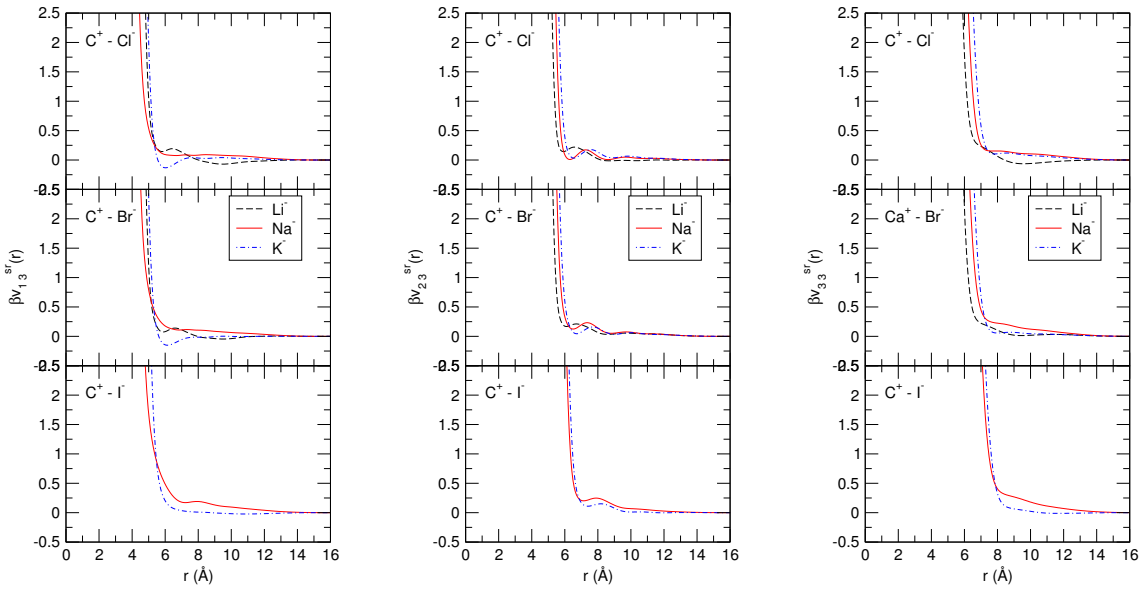

Figure 6.4: Effective pair-ion $v'^{\mathrm{sr}}_{i3}(r)$ $(i = 1, 2)$ and pair-pair v'^{sr}_{33} short-range potentials used in the PFT calculations with a paired reference system.

We have shown that at infinite dilution, the effective pair–ion and pair–pair interactions can be naturally decomposed into short-range and long-range contributions

$$v'_{3j}(\boldsymbol{r}) = v'^{\mathrm{sr}}_{3j}(\boldsymbol{r}) + v'^{\mathrm{lr}}_{3j} \qquad j = 1, 2, 3 \tag{6.51}$$

which are easily obtained as averages over the corresponding potentials of the two-

component system

$$v'^{\mathrm{sr}}_{3i}(\boldsymbol{r}) = \frac{1}{(2\pi)^3}\int \mathrm{d}\boldsymbol{k}\, \exp\left(i\boldsymbol{k}.\boldsymbol{r}\right)\widetilde{w}(\boldsymbol{k}/2)\left[\widetilde{v}^{\mathrm{sr}}_{1i} + \widetilde{v}^{\mathrm{sr}}_{2i}\right](\boldsymbol{k}) \tag{6.52a}$$

$$v'^{\mathrm{sr}}_{33}(\boldsymbol{r}) = \frac{1}{(2\pi)^3}\int \mathrm{d}\boldsymbol{k}\, \exp\left(i\boldsymbol{k}.\boldsymbol{r}\right)\left[\widetilde{w}(\boldsymbol{k}/2)\right]^2\left[\widetilde{v}^{\mathrm{sr}}_{11} + 2\widetilde{v}^{\mathrm{sr}}_{12} + \widetilde{v}^{\mathrm{sr}}_{22}\right](\boldsymbol{k}) \tag{6.52b}$$

$$v'^{\mathrm{lr}}_{3i}(\boldsymbol{r}) = -\frac{k_{\mathrm{B}}T}{6}\left(\frac{z^2 a L_{\mathrm{B}}}{r^2}\right)^2 \tag{6.52c}$$

$$v'^{\mathrm{lr}}_{33}(\boldsymbol{r}) = -\frac{k_{\mathrm{B}}T}{3}\left(\frac{z^2 a^2 L_{\mathrm{B}}}{r^3}\right)^2 \tag{6.52d}$$

We have assumed that our system corresponds to a symmetric electrolyte, such that $\langle p\rangle_l = eza$, where $a = \langle l\rangle_l$ is the average "intra-molecular" pair distance (z is the valence charge of the ions $q_i = \pm ze$). For non-symmetric case, the same procedure can be performed, but an additional long-range term would need to be added to the pair–ion and pair–pair interactions, since the pair would now be a charged species. The effective (short-range) pair-pair and pair-ion potentials of the eight salts (Li^+-I^- is not included since no CIP was obtained in the MM potential $v_{12}(r)$) we have considered are shown in Figure 6.4. It is seen that all the interactions are essentially those of soft-spheres, since the energy oscillations are now considerably lower than the thermal energy $k_{\mathrm{B}}T$. As we have also removed the large energy fluctuations from the cation-anion potential $v_{12}(r)$, by removing the portion corresponding to the CIP, we can expect that a (charged) hard-sphere perturbation theory will provide a good approximation for these paired systems. Finally, we note that the theory defined by Eqs. (6.20), (6.25), and (6.28) is exact, whatever the criteria used for the definition of the pair. However, these expressions are only valid in the dilute limit, since correlations between rotation and translation have been neglected.

6.6 The Structure of the Paired System

We have seen how to derive effective potentials for a system which includes the ion pair as a distinct species. If the potentials for this three component system are used to generate radial distribution functions, it is important to be able to *recover* the distribution functions corresponding to the original two-component system. The procedure is very similar to that used in deriving the effective potentials.

We start by considering a two-component system of N total particles, with $N_1 = N/2$ particles of type 1 (cation) and $N_2 = N/2$ particles of type 2 (anion). Let a fraction of these N_1 (N_2) particles be paired together. Assuming that a particle can belong to at most one pair (which is a valid approximation at very low dilution), we can decompose the two-body probability density as follows

$$\rho_{ij}(\boldsymbol{r}_1, \boldsymbol{r}_2) = \rho^{ff}_{ij}(\boldsymbol{r}_1, \boldsymbol{r}_2) + \rho^{fp}_{ij}(\boldsymbol{r}_1, \boldsymbol{r}_2) + \rho^{pf}_{ij}(\boldsymbol{r}_1, \boldsymbol{r}_2) + \rho^{pp}_{ij}(\boldsymbol{r}_1, \boldsymbol{r}_2), \qquad i = 1, 2 \tag{6.53}$$

where $\rho^{ff}_{ij}(\boldsymbol{r}_1, \boldsymbol{r}_2)$ gives the probability of finding a (free) particle of type i at $\boldsymbol{r}_1$ and a (free) particle of type j at $\boldsymbol{r}_2$; with the three remaining distribution functions ρ^{fp}_{ij}, ρ^{pf}_{ij}, and ρ^{pp}_{ij} defined in an analogous manner for free - paired (fp), paired - free (pf), and paired-paired (pp) ions.

Free ion - Free ion

The first term in Eq. (6.53) is easily evaluated, since, by definition

$$\rho_{ij}^{ff}(\boldsymbol{r}_1, \boldsymbol{r}_2) \equiv \rho_i' \rho_j' g_{ij}'(\boldsymbol{r}_1, \boldsymbol{r}_2) \tag{6.54}$$

where $g_{ij}'(\boldsymbol{r}_1, \boldsymbol{r}_2)$ is the distribution function obtained from the effective three component system (i and j refer to the free ions).

Free ion - Paired ion

At infinite dilution, the second term on the right-hand side of Eq. (6.53) is evaluated by considering a three particle system, composed of a free ion of type i and paired ion of type j. Let j^* denote the ion type for the remaining particle in the pair, such that

$$j^* = \begin{cases} 1 & \text{if } j = 2 \\ 2 & \text{if } j = 1 \end{cases}$$

The (canonical) configuration integral for this system is given by

$$Z_{ijj^*} = \int \mathrm{d}\boldsymbol{r}_i \mathrm{d}\boldsymbol{r}_j \mathrm{d}\boldsymbol{r}_{j^*} e^{-\beta \mathcal{V}} \tag{6.55}$$

where $\mathcal{V} = \mathcal{V}_{\text{int}}(\boldsymbol{r}_j, \boldsymbol{r}_{j^*}) + \mathcal{V}_{\text{ext}}(\boldsymbol{r}_i, \boldsymbol{r}_j, \boldsymbol{r}_{j^*})$ is the total potential energy, which is naturally separated into an internal contribution (due to the pair) and an external contribution (due to the interactions between the free i particle and the (j, j^*) pair). The two-body distribution function takes the following form

$$\rho_{ij}^{fp}(\boldsymbol{r}_1, \boldsymbol{r}_2) = \frac{1}{Z_{ijj^*}} \int \mathrm{d}\boldsymbol{r}_i \mathrm{d}\boldsymbol{r}_j \mathrm{d}\boldsymbol{r}_{j^*} \exp\left[-\beta \mathcal{V}\right] \delta(\boldsymbol{r}_i - \boldsymbol{r}_1) \delta(\boldsymbol{r}_j - \boldsymbol{r}_2)$$

and since $\mathcal{V}_{\text{int}}(\boldsymbol{r}_j, \boldsymbol{r}_j) = \mathcal{V}_{\text{int}}(\boldsymbol{l} = \boldsymbol{r}_{j^*} - \boldsymbol{r}_j) = v_{int}(l)$, we have, after a change of variables

$$\rho_{ij}^{fp}(\boldsymbol{r}_1, \boldsymbol{r}_2) = \frac{4\pi z_{\text{int}}}{Z_{ijj^*}} \int \mathrm{d}\boldsymbol{l} w(\boldsymbol{l}) \exp\left[-\beta \mathcal{V}_{\text{ext}}(\boldsymbol{r}_1, \boldsymbol{r}_2 + \boldsymbol{l}/2; \boldsymbol{l}/2)\right] \tag{6.56}$$

where $\mathcal{V}_{\text{ext}}(\boldsymbol{r}_1, \boldsymbol{r}_2 + \boldsymbol{l}/2; \boldsymbol{l}/2)$ is the potential between a free particle (type i) located at $\boldsymbol{r}_1$ and a pair centered at $\boldsymbol{r}_3 = \boldsymbol{r}_2 + \boldsymbol{l}/2$ (with charges at $\boldsymbol{r}_2$ and $\boldsymbol{r}_2 + \boldsymbol{l}$). Using a mean-field approximation, we replace the exponential factor appearing in this expression with its average value

$$\exp\left[-\beta \mathcal{V}_{\text{ext}}(\boldsymbol{r}_1, \boldsymbol{r}_2 + \boldsymbol{l}/2; \boldsymbol{l}/2)\right] \simeq \exp\left[-\beta v_{i3}'(\boldsymbol{r}_1, \boldsymbol{r}_2 + \boldsymbol{l}/2)\right] \tag{6.57}$$

Finally, since we are considering the infinite dilution limit, where the translational and rotational degrees of freedom are uncoupled, the configuration integral for this system can be separated according to

$$Z_{ijj^*} \simeq Z_{i3} \times (4\pi z_{\text{int}})$$

where Z_{i3} is the configuration integral of an effective two body system, composed of a free ion (i) and a pair (3), which is given (under the same mean-field approximation) as

$$Z_{i3} = \int \mathrm{d}\boldsymbol{r}_i \mathrm{d}\boldsymbol{r}_3 e^{-\beta v_{i3}'(\boldsymbol{r}_i, \boldsymbol{r}_3)}$$

This allows us to write the distribution function, Eq. (6.56), as

$$\rho_{ij}^{fp}(\boldsymbol{r}_1, \boldsymbol{r}_2) \simeq \int \mathrm{d}\boldsymbol{l} w(\boldsymbol{l}) \left(\frac{\exp\left[-\beta v'_{i3}(\boldsymbol{r}_1, \boldsymbol{r}_2 + \boldsymbol{l}/2)\right]}{Z_{i3}} \right) \tag{6.58}$$

but by definition, the term in parenthesis is just the two-body distribution function for the primed system, such that

$$\rho_{ij}^{fp}(\boldsymbol{r}_1, \boldsymbol{r}_2) = \int \mathrm{d}\boldsymbol{l} w(\boldsymbol{l}) \rho'_{i3}(\boldsymbol{r}_1, \boldsymbol{r}_2 + \boldsymbol{l}/2) \tag{6.59}$$

Paired ion - Paired ion

The last term on the right hand side of Eq. (6.53) is computed using the same mean-field, infinite dilution, approximation used before. To begin with, we assume that the i and j particles belong to different pairs. At infinite dilution, we need only consider two such pairs, (i, i^*) and (j, j^*); the configuration integral for this four particle system is given by

$$Z_{ii^*jj^*} = \int \mathrm{d}\boldsymbol{r}_i \mathrm{d}\boldsymbol{r}_j \mathrm{d}\boldsymbol{r}_{i^*} \mathrm{d}\boldsymbol{r}_{j^*} \exp\left[-\beta \mathcal{V}\right] \tag{6.60}$$

where the potential $\mathcal{V}$ is again separated into an internal contribution $\mathcal{V}_{\mathrm{int}} = v_{\mathrm{int}}(\boldsymbol{r}_i, \boldsymbol{r}_{i^*}) + v_{\mathrm{int}}(\boldsymbol{r}_j, \boldsymbol{r}_{j^*})$ (interactions among the ions belonging to the same pair) and an external contribution $\mathcal{V}_{\mathrm{ext}}(\boldsymbol{r}_1 + \boldsymbol{l}_1/2, \boldsymbol{r}_2 + \boldsymbol{l}_2/2; \boldsymbol{l}_1/2, \boldsymbol{l}_2/2)$, due to interactions between the two pairs, located at $\boldsymbol{r}_1 + \boldsymbol{l}_1/2$ and $\boldsymbol{r}_2 + \boldsymbol{l}_2/2$, with a pair distance of $\boldsymbol{l}_1$ and $\boldsymbol{l}_2$, respectively. The pair distribution function takes the form

$$\rho_{ij}^{pp}(\boldsymbol{r}_1, \boldsymbol{r}_2) = \frac{2}{Z_{ii^*jj^*}} \int \mathrm{d}\boldsymbol{r}_i \mathrm{d}\boldsymbol{r}_{i^*} \mathrm{d}\boldsymbol{r}_j \mathrm{d}\boldsymbol{r}_{j^*} e^{-\beta \mathcal{V}} \delta(\boldsymbol{r}_i - \boldsymbol{r}_1) \delta(\boldsymbol{r}_j - \boldsymbol{r}_2) \tag{6.61}$$

where the factor of two is needed to count the possible ways of choosing the (i, j) particles from two pairs. Separating the internal and external contributions to the potential, and changing the integration variables to the pair lengths $\boldsymbol{l}_1$ and $\boldsymbol{l}_2$, we have

$$\begin{aligned} \rho_{ij}^{pp}(\boldsymbol{r}_1, \boldsymbol{r}_2) = 2 \frac{(4\pi z_{\mathrm{int}})^2}{Z_{ii^*jj^*}} \int \mathrm{d}\boldsymbol{l}_1 \mathrm{d}\boldsymbol{l}_2 w(\boldsymbol{l_1}) w(\boldsymbol{l_2}) \\ \times \exp\left[-\beta \mathcal{V}_{\mathrm{ext}}(\boldsymbol{r}_1 + \boldsymbol{l}_1/2, \boldsymbol{r}_2 + \boldsymbol{l}_2/2, \boldsymbol{l}_1/2, \boldsymbol{l}_2/2)\right] \end{aligned} \tag{6.62}$$

Again, we replace the external potential with its average value v'_{33}, and we take the configuration integral to be separable

$$Z_{ii^*jj^*} \simeq Z'_{33} (4\pi z_{\mathrm{int}})^2 \tag{6.63}$$

$$Z'_{33} = \int \mathrm{d}\boldsymbol{r}_3 \mathrm{d}\boldsymbol{r}'_3 e^{-\beta v'_{33}(\boldsymbol{r}_1 + \boldsymbol{l}_1/2, \boldsymbol{r}_2 + \boldsymbol{l}_2/2)} \tag{6.64}$$

Equation (6.62) then becomes

$$\rho_{ij}^{pp} = \int \mathrm{d}\boldsymbol{l}_1 \mathrm{d}\boldsymbol{l}_2 w(\boldsymbol{l}_2) w(\boldsymbol{l}_2) \left(2 \frac{\exp\left[-\beta v'_{33}(\boldsymbol{r}_1 + \boldsymbol{l}_1/2, \boldsymbol{r}_2 + \boldsymbol{l}_2/2)\right]}{Z_3} \right) \tag{6.65}$$

but, as before, the term in parenthesis is just the pair-pair distribution function (in the primed system), so that

$$\rho_{ij}^{pp} = \int \mathrm{d}\boldsymbol{l}_1 \mathrm{d}\boldsymbol{l}_2 w(\boldsymbol{l}_1) w(\boldsymbol{l}_2) \rho'_{33}(\boldsymbol{r}_1 + \boldsymbol{l}_1/2, \boldsymbol{r}_2 + \boldsymbol{l}_2/2) \tag{6.66}$$

In deriving this equation, we have assumed that the i and j particles belong to different pairs; in the case that they belong to the same pair, the probability is given directly by the distribution function of the pair $\rho'_3 w(\boldsymbol{l})$.

The transformation

Finally, the distribution function for the original two-component system can be expressed in terms of the Fourier transforms of the corresponding functions for the effective three component system as

$$\begin{aligned} \rho_i \rho_j g_{ij}(\boldsymbol{r}_1, \boldsymbol{r}_2) &= \rho'_i \rho'_j g'_{ij}(\boldsymbol{r}_1, \boldsymbol{r}_2) + \rho'_3 w(\boldsymbol{r})(1 - \delta_{ij}) \\ &+ \rho'_3 \frac{1}{(2\pi)^3} \int \mathrm{d}\boldsymbol{k} \exp\left[i\boldsymbol{k}.\boldsymbol{r}\right] \widetilde{w}(\boldsymbol{k}/2) \Big\{ \rho'_i g'_{i3}(\boldsymbol{k}) + \rho'_j g'_{j3}(\boldsymbol{k}) + \rho'_3 w(\boldsymbol{k}/2) g'_{33}(\boldsymbol{k}) \Big\} \end{aligned} \tag{6.67}$$

We recall that this is has been derived within a mean-field approximation, at infinite dilution; so that it can only be expected to give a rough approximation to the radial distribution function of the two-component system. However, as we shall see below, comparison with the exact MC results shows relatively good agreement up to molar concentrations.

6.7 The Minimization Procedure

Model	Pert. Energy	Pert. Terms	Min. Parameters	Solution
MSA3	$\delta v'_{ij}(r) = v'^{\mathrm{sr}}_{ij}(r) \quad i,j = 1,2$	$\Delta f'^{\mathrm{id}}$	ρ'_3	ideal gas
	$\delta v'_{3i}(r) = v'^{\mathrm{sr}}_{3i}(r) + v'^{\mathrm{lr}}_{3i}(r)$	f'^{ev}	$\sigma_1, \sigma_2, \sigma_3, \rho'_3$	BMCSL
		$f'^{\mathrm{el}}, g'_{ij}(r)$	$\sigma_1, \sigma_2, \sigma_3, \rho'_3$	MSA
BIMSAi	$\delta v'_{ij}(r) = v'^{\mathrm{sr}}_{ij}(r)$	$\Delta f'^{\mathrm{id}}$	ρ'_3	ideal gas
		f'^{ev}	$\sigma_1, \sigma_2, \sigma_C, \rho'_3$	BMCSL
		$f'^{\mathrm{el}}, f^{\mathrm{as}}$	$\sigma_1, \sigma_2, \sigma_C, \rho'_3$	BIMSA
		$g'_{ij}(r)$	$\sigma_1, \sigma_2, \sigma_3(\sigma_C), \rho'_3$	MSA

Table 6.2: Summary of the different terms appearing in the perturbation calculations, Eq. (6.68), their dependence on the minimization parameters, and the solutions that have been employed.

From Eqs. (6.2) and (6.28), we can write the first order perturbation expansion for the excess free energy density of a binary electrolyte, using a three-component (associated) reference system, as

$$\beta f^{\mathrm{ex}} \lesssim \Delta f'^{\mathrm{id}} + \beta f'^{\mathrm{ex}} - \rho'_3 \ln K_0 + \frac{1}{2}\beta \sum_{i=1}^{3}\sum_{j=1}^{3} \rho'_i \rho'_j \int \mathrm{d}\boldsymbol{r}\, g'_{ij}(r) \delta v'_{ij}(r) \tag{6.68}$$

where $\Delta f'^{\mathrm{id}} = f'^{\mathrm{id}} - f^{\mathrm{id}}$ gives the difference in the ideal free energies (between the reference three-component system and the model two-component system). The solutions

used for the excess free energy f'^{ex} and radial distribution functions $g'_{ij}(r)$ will depend on the model used to represent the reference system (MSA3 or one of the BIMSA models), as detailed in Section 6.3.2. A summary of the different terms contributing to the perturbation calculation, along with the relevant minimization diameters and the solution that has been used, is given in Table 6.2. All the models that are considered have four minimization parameters: the two diameters for the free ions (σ_1 and σ_2), the diameter of the pair (sphere σ_3 or dumbbell σ_C), and the pair fraction or density (ρ'_3).

We note that the perturbation potential $\delta v'_{ij}(r)$ that should be used will depend on the representation of the pair. For hard-spheres (MSA3), the long-range dipolar contributions should be included, as they are not part of the reference system. When the pair is represented as a dipolar dumbbell (BIMSAi), these long-range contributions are (in theory) already included in the reference, and should therefore not appear in the perturbation. However, one should keep in mind that the BIMSA solution we use for f^{el}, which is computed by averaging over the internal energy, using a linearized radial distribution function, does not properly account for these terms. In practice, including the long-range potentials within the perturbation should improve the results, but for consistency reasons, we show only the "uncorrected" results[6].

The PFT calculations are performed for the nine alkali-halide electrolytes, using the MM potentials derived above, over a range of concentrations $0 < c < 2$ M. As before, we take a concentration independent dielectric permittivity of $\epsilon_r = 72$ (corresponding to the bulk value of the SPC/E water model used in the original MD simulations). The results are fitted to the following limiting form [9]

$$\beta f^{\text{ex}} = Ac^{3/2} + b_0 c^2 \ln c + b_2 c^2 + b_3 c^{5/2} + b_4 c^3 + b_5 c^{7/2} \tag{6.69}$$

allowing us to obtain the osmotic coefficients ϕ, since

$$\phi^{\text{ex}} = \frac{1}{2}\left(\frac{\partial \beta f^{\text{ex}}}{\partial c} - \frac{\beta f^{\text{ex}}}{c}\right) \tag{6.70}$$

The inverse fit is also carried out on the MC results for ϕ, in order to compare our PFT predictions with the exact results, for both the free energy and the pressure.

6.8 Results

Case Study: K^+-Br^-

We proceed to give a detailed account of the results obtained for K^+-Br^-. The excess free energy densities f for the six reference systems we have used are shown in Figure 6.5, where they are compared to the *exact* MC results; also shown are the osmotic coefficients ϕ and the relative error $|f^{\text{ex}} - f^{\text{ex}}_{\text{MC}}|/|f^{\text{ex}}_{\text{MC}}|$. The first thing to note is the fact that the Gibbs-Bogoliubov inequality is satisfied in all cases. Since we use approximate solutions for the (reference) free energies and radial distribution functions,

[6] We have performed the PFT calculations for the BIMSA models, with the long-range potentials included in the perturbation term, and we indeed obtain better agreement; however, this is only appreciable at high concentrations, where our approximations are no longer justified.

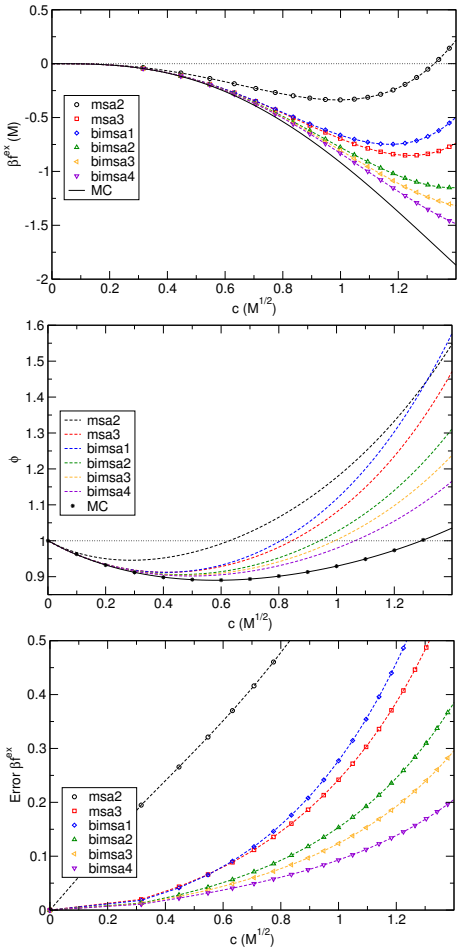

Figure 6.5: The excess free energy density f^{ex}, osmotic coefficient $\phi = 1 + \phi^{\text{ex}}$, and relative error (with respect to the MC results), as a function of the reference system used in the PFT calculations, for K^+–Br^-. The *exact* MC results are shown in solid black lines.

it is not clear *a priori* whether we will actually satisfy this rigorous condition. As expected, the two-component representation is seen to yield very poor results, showing only moderate agreement with the exact values at very low concentrations. The passage to a three-component representation provides a marked improvement, reducing the relative error by almost an order of magnitude (for the best model). At low concentrations $c \lesssim 0.5$ M, the various three-component representations are essentially equivalent, the differences only become apparent at molar concentrations. For these paired systems, we identify the following relations among our different representations: MSA3$\simeq$BIMSA1 and BIMSA2$\simeq$BIMSA3$\simeq$BIMSA4. It is clear that a representation of the pair as a dumbbell provides the best description. Among the six different dumbbell representations we have used (BIMSAi), it is seen that a better (lower) estimate is obtained for larger values of the effective hard-sphere diameter σ_3 (σ_C), with the BIMSA4 model providing the best approximation (the relative error is less than 10% at $c = 1.0$ M). The same global behaviour is seen in the osmotic coefficients, although they provide for a more sensitive comparison, since they depend on both the value of f, as well as its derivative.

The fraction of pairs (given directly by the minimization) is shown in Figure 6.6.

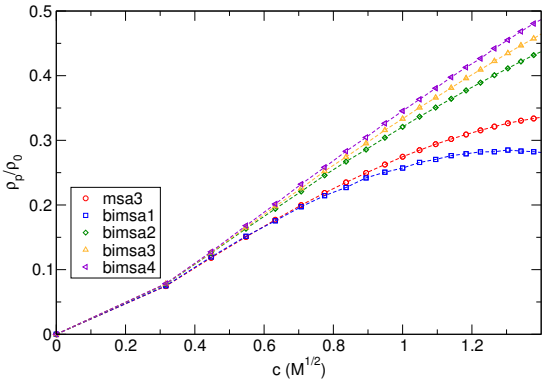

Figure 6.6: Fraction of pairs obtained from the PFT calculations for K^+-Br^-.

There is a strong dependence on the criteria used to define the ion pair, but again, the variation only becomes important at high concentrations $c \gtrsim 1.0$ M. The optimal diameters, expressed in terms of the cation–anion contact distance $\sigma_{12} = \frac{1}{2}(\sigma_1 + \sigma_2)$ and size difference $\overline{\sigma}_{12} = \sigma_2 - \sigma_1$, and the dumbbell ion size σ_C, are given in Figure 6.7. Fortunately, the minimization diameters are seen to vary only very little with the concentration, and the size of the (free) ions is essentially independent of the model used in the PFT calculation. For comparison purposes, we have also fitted the MC free energy to a two-component MSA model. These are the *fit* values referenced in the figures. The

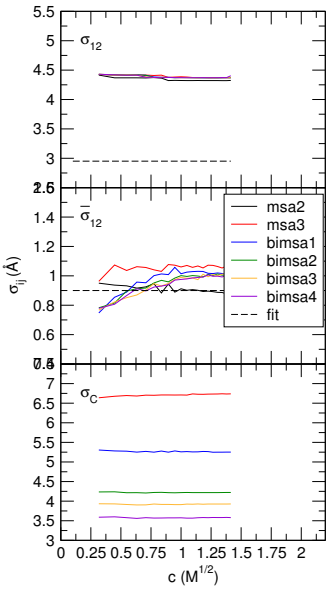

Figure 6.7: Minimization diameters obtained from the PFT calculations for K^+-Br^-.

comparison between both sets of data, the PFT results and the (MC) fits, is seen to be considerable, especially for σ_{12}. For the potassium salts, where the CIP is dominant, the favoured cation-anion distance will correspond to this CIP region; this is precisely what we obtain from the fits, but not at all what is obtained from the PFT calculations. Although one would have expected the PFT results corresponding to the two-component reference system (MSA2) to yield the same diameters as the fit, the non-additivity in the effective potentials would have resulted in an increased perturbation term for the cation-cation and anion-anion terms. The value for σ_{12} that is obtained from the PFT calculations corresponds to the SSIP. By construction, the CIP configuration is repre-

sented by the ion pair. This can be clearly seen by inspecting the radial distribution functions, which are shown in Figure 6.8. Here is where we can appreciate the advantage of our method, since we have been able to describe a strongly non-additive system, in terms of additive hard-sphere models, by introducing the concept of ion association.

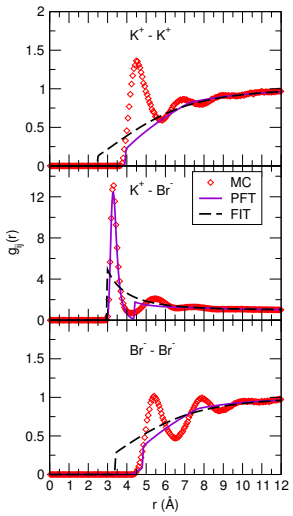

Figure 6.8: Comparison between radial distribution functions obtained from MC simulations (exact) and our PFT calculations (using the BIMSA4 model) for K^+-Br^- at $c = 0.5$ M, . The results obtained from a fit to a two component model (using the MSA solution with concentration independent diameters) are also shown.

Similar results are obtained for the other salts we have studied (See Appendix F), with the BIMSA4 model always providing the best approximation to the free energy, with a relative error $\lesssim 20\%$ at molar concentrations. We thus consider this to be our *final* model; except for Li^+-I^-, for which we use the MSA2 model, since no contact ion pair is formed.

Final Results

Our PFT predictions for the excess free energies of the nine salts are shown in Figure 6.9, where they are compared to the exact MC values. We note that the ordering seen in the MC values is preserved in the PFT results: I^->Br^->Cl^- and Na^+>Li^+>K^+. This is the same ordering given by the association constant K_0, except for an inversion of Na^+ and Li^+; which, as we mentioned before, is due to the more stable SSIP configuration of Li^+.

The average minimization diameters given by the PFT calculations are summarized in Table 6.3. The two- and three-component free ion diameters are seen to be essentially equivalent, supporting our previous observation, that the inclusion of the pair is just a way of renormalizing the cation-anion interactions, in order to account for the portion of the configuration space that is neglected by a two-component representation (the non-additive region). These diameters can be given a clear physical interpretation, by inspecting the cation-anion effective potentials $v_{12}(r)$. The values we have obtained for σ_{12} are seen to correspond to the distance for which the potential energy difference, with respect to the second minimum (SSIP), is $\simeq k_{\mathrm{B}}T$.

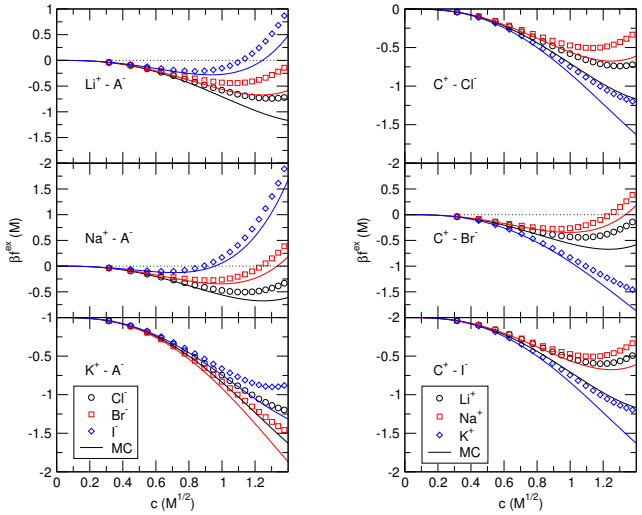

Figure 6.9: Excess free energy densities f^{ex} as a function of concentration, obtained from PFT calculations, for the series of anions A^- (left) and cations C^+ (right). The exact MC results are also shown.

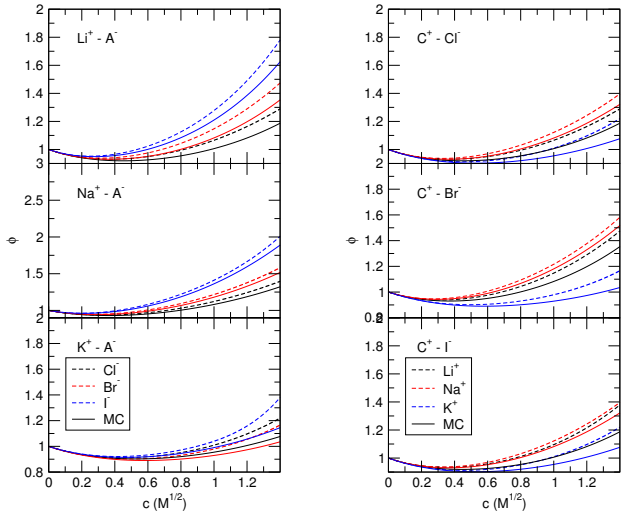

Figure 6.10: Osmotic coefficients ϕ as a function of concentration, obtained from PFT calculations, for the series of anions A^- (left) and cations C^+ (right). The *exact* MC results ore also shown.

		Li^+	Na^+	K^+
σ_1/Å	Cl^-	3.92(3.92)	3.71(3.67)	3.86(3.88)
	Br^-	3.94(3.94)	3.80(3.75)	3.91(3.88)
	I^-	– (3.98)	4.09(4.01)	4.09(3.87)
σ_2/Å	Cl^-	4.39(4.40)	4.75(4.78)	4.71(4.66)
	Br^-	4.46(4.46)	4.88(4.92)	4.85(4.79)
	I^-	– (4.94)	5.27(5.31)	5.32(5.13)
σ_{12}/Å	Cl^-	4.16(4.16)	4.23(4.23)	4.28(4.27)
	Br^-	4.20(4.20)	4.34(4.33)	4.38(4.34)
	I^-	– (4.46)	4.68(4.66)	4.71(4.50)
$\overline{\sigma}_{12}$/Å	Cl^-	0.47(0.48)	1.03(1.10)	0.84(0.78)
	Br^-	0.51(0.52)	1.07(1.16)	0.94(0.90)
	I^-	– (0.96)	1.18(1.30)	1.23(1.25)
σ_3/Å	Cl^-	6.62	6.76	7.1
	Br^-	6.71	6.94	7.15
	I^-	–	7.80	7.90
σ_C/Å	Cl^-	3.30	3.38	3.55
	Br^-	3.35	3.47	3.57
	I^-	–	3.90	3.95

Table 6.3: Optimal three-component reference system parameters obtained from our final PFT calculations, using an associated reference system. The two-component MSA2 parameters are shown in parenthesis.

6.9 Conclusions

We have shown how to successfully derive an analytical model of electrolytes in solution, from the effective McMillan-Mayer ion-ion potentials obtained from explicit solvent MD simulations. To do this, we have used the standard fluid perturbation theory to relate the properties of our system of interest (characterized by the complicated MM effective potentials) to a primitive-type model, in which the ions are represented as charged hard-spheres. The reason for choosing this particular reference system is simple: there exist well known analytical (approximate) solutions, such as the MSA and the BIMSA, which provide an accurate description for the thermodynamics. In the case of the MSA solution (within an exponential approximation), we also have a relatively good description of the structure of the fluid. However, the perturbation calculations are not as straightforward as one could have imagined, because of the strong non-additive nature of electrolytes: the cation-anion contact distance σ_{12} does not correspond to the average of the cation-cation σ_1 and anion-anion σ_2 contact distances. Due to the strong electrostatic attraction, the cation-anion contact distance is significantly reduced ($\sigma_{12} < (\sigma_1 + \sigma_2)/2$) with respect to the additive value. This poses a considerable problem, since the MSA solution we use requires additive diameters for the hard-spheres. As expected, PFT calculations performed using a *naive* two-component hard-sphere reference system show very poor results when compared to the exact MC calculations.

We have proposed to treat this troublesome non-additivity by allowing for the association of (oppositely charged) ions. We thus consider the contact ion pair (CIP), which corresponds to the first peak in the cation-anion radial distribution function, as a distinct chemical species. The chemical equilibrium between the free ions and the pair is characterized with the help of the Bjerrum association constant K_0, which is determined by the effective potentials. The interactions between free ions in this auxiliary three-

component system remain unchanged[7], and the interactions involving the pair can be easily calculated (to first order) by considering the average dipole-ion and dipole-dipole interactions at infinite dilution. A similar calculation was used to relate the structure of the three-component fluid to that of the original two-component system. Finally, we have shown how to relate the free energies of both representations; where the difference between them is due to the standard chemical potential of the pair.

We have considered the free ions as charged hard-spheres, and we have adopted two representations for the pair: as a neutral sphere or as a dipolar dumbbell. In the first case, we can use the MSA solution to compute the free energy and radial distribution functions of the system. In the second case, we use a mixed representation, in which the free energy is computed using the BIMSA solution, and the radial distribution functions are obtained from the MSA solution for an equivalent system of hard-spheres (where the dumbbell is treated as a sphere)[8]. We have considered four different parametrizations for the pair, for a total of five distinct associated reference systems (MSA3 and the four BIMSA models). The PFT calculations obtained using these systems show very good agreement with the exact results; the improvement with respect to the PFT calculations for the two-component reference systems show the importance of properly accounting for the CIP. Furthermore, it is clearly shown that the exact parametrization of the pair is not important, with all reference systems yielding essentially the same results up to molar concentrations. Also, the minimization diameters are practically independent of the concentration.

In order to understand why our method works, and why the CIP should be treated independently, it is instructive to compare the radial distribution functions predicted by our theory and those obtained by a simple fit of the *exact* free energy (MC) to a two-component charged hard-sphere system (within the MSA approximation). By construction, the fit will give excellent agreement with the exact free energy; however, due to the non-additivity of the *real* system, the additive MSA solution gives radial distribution functions which are in very poor agreement with the MC values. Here we identify two distinct scenarios, depending on the relative stability of the CIP: For the weakly associated electrolytes (Li^+ and Na^+ salts) the fit will give a cation-anion distance which corresponds to the SSIP configuration. For the strongly associated electrolytes (K^+ salts), on the other hand, this contact distance will correspond to the CIP. In the first case, an additive system will severely underestimate the diameters of the free ions; while in the second case, the enforcement of additivity will cause us to completely ignore the CIP. Our model separates the CIP, which is responsible for the non-additivity, from the additive interactions of the free (hydrated) ions. The next step in our work, would be to consider a non-additive reference model, as this would allow us to use the simpler two-component system as a reference. Preliminary results for the development of such non-additive systems are presented in the next chapter.

[7]Except for the cation-anion potentials, which have been modified to remove the minimum corresponding to the CIP, which itself defines the internal potential of the pair

[8]We were forced to do this because BIMSA does not provide tractable expression for the radial distribution functions.

Chapter 7

Perspective I: Towards a Non-Additive Primitive Model

Summary

7.1 Motivation

One of the main problems we encountered when attempting to derive a primitive model description of electrolyte solutions, was how to adequately represent their strong non-additivity using additive models. We overcame this difficulty by introducing the CIP as an additional chemical species. This allowed us to separate the strong cation-anion attraction at short-distances, responsible for the non-additivity, from the remaining interactions (those of the "free" ions). This auxiliary three-component system allowed for a simple representation in terms of (additive) charged hard-spheres, for which the MSA (BIMSA) solutions are well suited.

In this chapter, we propose to develop an alternative route: that of treating the non-additivity directly. We thus seek to generalize the thermodynamic perturbation theory

developed recently by Sillren and Hansen [7, 8], which allows one to obtain the properties of a non-additive hard-sphere system from those of an additive reference system. We use an approach similar to that employed by Andersen, Weeks, and Chandler to develop their "blip-function" formalism, only we wish to evaluate the first order correction to the radial distribution function (the second order correction to the free energy)[1]. We follow the derivation given by Barker and Henderson [36, 181] for the case of a one-component system[2], and generalize their theory to the multi-component case. We will present no *new* results in this chapter, as Henderson is supposed to have already published such a theory; however, his work was presented in an obscure Canadian journal of applied mathematics (*Utilitas Mathematica* 1, 211, (1972)), which we were unable to obtain.

As mentioned before, we expect that a perturbation theory which uses non-additive reference systems could provide a good description of electrolyte solutions without having to include the concept of ion association (i.e. a binary electrolyte could be well represented by a two-component system of non-additive charged hard-spheres). The free energy of our system would be determined by Eq. (6.2),

$$\beta F \lesssim \beta F^{\mathrm{NA}} + \frac{1}{2}\sum_i \sum_j \rho_i \rho_j \int \mathrm{d}\boldsymbol{r}\, g_{ij}^{\mathrm{NA}}(r) \left[v_{ij}(r) - v_{ij}^{\mathrm{NA}}(r)\right] \tag{7.1}$$

where the $v_{ij}(r)$ are the MM effective ion-ion potentials and the reference is now a system of non-additive (NA) charged hard-spheres. Since we only have analytical solutions for additive models (MSA), the reference free energies and radial distribution functions would themselves be computed by yet another perturbation calculation. Thus, the non-additive reference free energy would be given by

$$\beta F^{\mathrm{NA}} = \beta F^{(0)} + \frac{1}{2}\sum_i \sum_j \rho_i \rho_j \int \mathrm{d}\boldsymbol{r}\, g_{ij}^{(0)} \left[v_{ij}^{\mathrm{NA}}(r) - v_{ij}^{(0)}(r)\right] \tag{7.2}$$

where $F^{(0)}$ and $g_{ij}^{(0)}$ are the free energies and radial distribution functions of an *additive* system. With a similar expression for the non-additive radial distribution function g_{ij}^{NA}. In this chapter we focus on the development of Eq. (7.2): i.e. how to obtain the properties of a non-additive hard-sphere system from an additive hard-sphere representation. As we shall see below, the difficulty is in the calculation of $g_{ij}^{\mathrm{NA}}(r)$, since this is a second order term. We begin by defining the formalism and the notation that will be used in the remainder of the chapter. We then present the second-order perturbation theory needed to compute the corrections to the radial distribution functions, and we end by showing a simple application of this theory. We note that this is a work in progress, which is not yet applicable to charged system, but we believe it is prudent to start by studying hard-spheres before introducing any further complications.

7.2 Definitions

In order to simplify the equations, we have adopted a notation which is more suitable for the description of multi-component systems, but differs slightly from that used in

[1] The AWC theory chooses the reference system in such a way that the first order correction to the free energy is exactly zero.

[2] This is the version presented in most textbooks

the rest of this work. In what follows, we redefine the basic quantities needed for our derivations, which have been previously introduced in Section 3.1 for the case of a one-component system. We now consider an m-component system, with N_ν particles of species ν, with $\nu = 1, \ldots, m$. Let $\boldsymbol{N} = (N_1, N_2, \ldots, N_m)$ be an m-dimensional vector representing the particle numbers of each species, with $N = \sum_\nu N_\nu$ the total number of particles. The position vectors for the particles are denoted as

$$\begin{aligned} \{\boldsymbol{N}\} &= \{N_1\}_1, \{N_2\}_2, \ldots, \{N_m\}_m \\ \{i\}_\nu &= \boldsymbol{r}_{1_\nu}, \boldsymbol{r}_{2_\nu}, \ldots, \boldsymbol{r}_{i_\nu} \end{aligned}$$

and the corresponding volume elements as

$$\begin{aligned} \mathrm{d}\{\boldsymbol{N}\} &= \mathrm{d}\{N_1\}_1 \mathrm{d}\{N_2\}_2 \cdots \mathrm{d}\{N_m\}_m \\ \mathrm{d}\{i\}_\nu &= \mathrm{d}\boldsymbol{r}_{1_\nu} \mathrm{d}\boldsymbol{r}_{2_\nu} \cdots \mathrm{d}\boldsymbol{r}_{i_\nu} \end{aligned}$$

Assuming that the total potential energy $\mathcal{V}(\{\boldsymbol{N}\})$ is pair-wise additive, we have

$$\mathcal{V}\left(\{\boldsymbol{N}\}\right) = \sum_{\nu=1}^{m} \sum_{i=1}^{N_\nu} \sum_{j>i}^{N_\nu} v_{\nu\nu}\left(\boldsymbol{r}_{i_\nu}, \boldsymbol{r}_{j_\nu}\right) + \sum_{\nu=1}^{m} \sum_{\eta>\nu}^{m} \sum_{i=1}^{N_\nu} \sum_{j=1}^{N_\eta} v_{\nu\eta}\left(\boldsymbol{r}_{i_\nu}, \boldsymbol{r}_{j_\eta}\right) \tag{7.3}$$

where $v_{\nu\eta}$ is the $\nu - \eta$ pair interaction potential. The corresponding Boltzmann factor can be written as

$$\exp\left[-\beta \mathcal{V}(\{\boldsymbol{N}\})\right] = \prod_{\substack{\langle \nu,\eta \rangle \\ \langle i,j \rangle}}{}' e_{\nu\eta}(r_{i_\nu}, r_{j_\eta}) \tag{7.4}$$

where $< \eta, \nu >$ is used to denote all possible (η, ν) pairs (likewise for $< i, j >$), and the prime indicates that only the terms $i_\nu \neq j_\eta$ should be included. We thus have

$$\exp\left[-\beta \mathcal{V}(\{\boldsymbol{N}\})\right] = \left(\prod_{\nu=1}^{m} \prod_{i=1}^{N_\nu} \prod_{j>i}^{N_\nu} e_{\nu\nu}\left(\boldsymbol{r}_{i_\nu}, \boldsymbol{r}_{j_\nu}\right) \right) \left(\prod_{\nu=1}^{m} \prod_{\eta>\nu}^{m} \prod_{i=1}^{N_\nu} \prod_{j=1}^{N_\eta} e_{\nu\eta}\left(\boldsymbol{r}_{i_\nu}, \boldsymbol{r}_{j_\eta}\right) \right) \tag{7.5}$$

with $e_{\nu\eta}(\boldsymbol{r}, \boldsymbol{r}') = \exp\left[-\beta v_{\nu\eta}(\boldsymbol{r}, \boldsymbol{r}')\right]$.

Canonical Ensemble

Using this notation, the canonical partition function $Q(\boldsymbol{N}, V, T)$ of an $\boldsymbol{N}$-particle system, at constant volume V and temperature T, is given in terms of the configuration integral $Z(\boldsymbol{N})$ by (Eq. (3.16))

$$\begin{aligned} Q(\boldsymbol{N}) &= \prod_{\nu=1}^{m} \left(\frac{1}{\Lambda_\nu^{3N_\nu}\, N_\nu!} \right) Z(\boldsymbol{N}) \\ Z(\boldsymbol{N}) &= \int \cdots \int \mathrm{d}\{\boldsymbol{N}\} \exp\left[-\beta V(\{\boldsymbol{N}\})\right] \end{aligned} \tag{7.6}$$

The n-particle distribution function (Eq. (3.33)),

$$\rho_{\boldsymbol{N}}^{(\boldsymbol{n})}(\{\boldsymbol{n}\}) = \prod_{\nu=1}^{m} \left(\frac{N_\nu!}{(N_\nu - n_\nu)!} \right) \frac{1}{Z_{\boldsymbol{N}}} \int \cdots \int \mathrm{d}\{\boldsymbol{N} - \boldsymbol{n}\} \exp\left[-\beta V(\{\boldsymbol{N}\})\right] \tag{7.7}$$

gives the probability of observing $n = \sum_\nu n_\nu$ particles, n_ν of which are of species ν, at positions $\{\boldsymbol{n}\}$, irrespective of the positions of the remaining $N - n$ particles.

Grand-Canonical Ensemble
The grand partition function of an open system, at constant chemical potential $\boldsymbol{\mu}$, volume V, and temperature T, is given by (Eq (3.22))

$$\Xi(\boldsymbol{\mu}) = \sum_{\boldsymbol{N}=0}^{\infty} \prod_{\nu=1}^{m} \left(\frac{z_\nu^{N_\nu}}{N_\nu!} \right) \int \cdots \int \mathrm{d}\{\boldsymbol{N}\} \exp\left[-\beta V(\{\boldsymbol{N}\})\right] \tag{7.8}$$

$$\tag{7.9}$$

and the n-particle density is now defined as

$$\begin{aligned} \varrho^{(\boldsymbol{n})}(\{\boldsymbol{n}\}) &= \frac{1}{\Xi} \sum_{\boldsymbol{N}=\boldsymbol{n}}^{\infty} \prod_{\nu=1}^{m} \left(\frac{z_\nu^{N_\nu}}{(N_\nu - n_\nu)!} \right) \int \cdots \int \mathrm{d}\{\boldsymbol{N} - \boldsymbol{n}\} \exp\left[-\beta V\left(\{\boldsymbol{N}\}\right)\right] \\ &= \frac{1}{\Xi} \sum_{\boldsymbol{N}=0}^{\infty} \prod_{\nu=1}^{m} \left(\frac{z_\nu^{N_\nu+n_\nu}}{N_\nu!} \right) \int \cdots \int \mathrm{d}\{\boldsymbol{N}\} \exp\left[-\beta V\left(\{\boldsymbol{N} + \boldsymbol{n}\}\right)\right] \end{aligned} \tag{7.10}$$

We note the different variables used to represent the canonical and grand-canonical distribution functions, ρ and ϱ, respectively.

7.3 Second-Order Perturbation Theory

For generality, it is convenient to consider the partition functions as functionals of the $e_{\nu\mu}$. If ϕ is an arbitrary function of $\boldsymbol{N}, V, T$ and a functional of the $e_{\nu\eta}$ (or $v_{\nu\eta}$), the functional series expansion in powers of $\Delta e_{\eta\nu} = e_{\eta\nu} - e_{\eta\nu}^{(0)}$ is given by

$$\phi(\boldsymbol{N}, V, T) = \sum_{j=0}^{\infty} \left[\frac{1}{j!} \left(\sum_{\nu=1}^{m} \sum_{\eta \geq \nu}^{m} \delta_{\nu\eta} \right)^j \phi \right]_{e=e^{(0)}} \tag{7.11}$$

$$\delta_{\nu\eta} = \iint \mathrm{d}\boldsymbol{r}_{1_\nu} \mathrm{d}\boldsymbol{r}_{2_\eta}\, \Delta e_{\nu\eta}(\boldsymbol{r}_{1_\nu}, \boldsymbol{r}_{2_\eta})\, \frac{\delta}{\delta e_{\nu\eta}(\boldsymbol{r}_{1_\nu}, \boldsymbol{r}_{2_\eta})} \bigg|_{\boldsymbol{N},V,T} \tag{7.12}$$

where the functional derivatives are taken at constant number of particles (as well as constant volume and temperature). The standard formulation of PFT seeks to evaluate the changes in ϕ as a function of the perturbation; however, this is clearly not applicable when the perturbation diverges, which is why we use $\delta e_{\nu\mu}$ and not $v_{\nu\mu}$ directly.

For a 1-component system, this functional expansion yields, to second order

$$\begin{aligned} \phi(N, V, T) = \phi_0 &+ \iint \mathrm{d}\boldsymbol{r}_1 \mathrm{d}\boldsymbol{r}_2 \Delta e(\boldsymbol{r}_1, \boldsymbol{r}_2)\, \frac{\delta\phi}{\delta e(\boldsymbol{r}_1, \boldsymbol{r}_2)} \bigg|_{\boldsymbol{N}, e=e^{(0)}} \\ &+ \frac{1}{2!} \iiiint \mathrm{d}\boldsymbol{r}_1 \mathrm{d}\boldsymbol{r}_2 \mathrm{d}\boldsymbol{r}_3 \mathrm{d}\boldsymbol{r}_4\, \Delta e(\boldsymbol{r}_1, \boldsymbol{r}_2) \Delta e(\boldsymbol{r}_3, \boldsymbol{r}_4)\, \frac{\delta^2\phi}{\delta e(\boldsymbol{r}_1, \boldsymbol{r}_2) \delta e(\boldsymbol{r}_3, \boldsymbol{r}_4)} \bigg|_{\boldsymbol{N}, e=e^{(0)}} \end{aligned} \tag{7.13}$$

and for a two-component (AB) system, with arbitrary and independent perturbations

in the three pair potentials AA, AB, and BB, we have

$$\begin{aligned}\phi(N_A,N_B,V,T) = \phi_0 &+ \iint \mathrm{d}\boldsymbol{r}_1\mathrm{d}\boldsymbol{r}_2\,\Delta e_{AA}(\boldsymbol{r}_1,\boldsymbol{r}_2)\,\frac{\delta\phi}{\delta e_{AA}(\boldsymbol{r}_1,\boldsymbol{r}_2)}\bigg|_{\boldsymbol{N},e=e^{(0)}} \\ &+ \iint \mathrm{d}\boldsymbol{r}_1\mathrm{d}\boldsymbol{s}_1\,\Delta e_{AB}(\boldsymbol{r}_1,\boldsymbol{s}_1)\,\frac{\delta\phi}{\delta e_{AB}(\boldsymbol{r}_1,\boldsymbol{s}_1)}\bigg|_{\boldsymbol{N},e=e^{(0)}} \\ &+ \iint \mathrm{d}\boldsymbol{s}_1\mathrm{d}\boldsymbol{s}_2\,\Delta e_{BB}(\boldsymbol{s}_1,\boldsymbol{s}_2)\,\frac{\delta\phi}{\delta e_{BB}(\boldsymbol{s}_1,\boldsymbol{s}_2)}\bigg|_{\boldsymbol{N},e=e^{(0)}} \\ &+ \frac{1}{2}\iiint \mathrm{d}\boldsymbol{r}_1\mathrm{d}\boldsymbol{r}_2\mathrm{d}\boldsymbol{r}_3\mathrm{d}\boldsymbol{r}_4\,\Delta e_{AA}(\boldsymbol{r}_1,\boldsymbol{r}_2)\Delta e_{AA}(\boldsymbol{r}_3,\boldsymbol{r}_4)\,\frac{\delta^2\phi}{\delta e_{AA}(\boldsymbol{r}_1,\boldsymbol{r}_2)\delta e_{AA}(\boldsymbol{r}_3,\boldsymbol{r}_4)}\bigg|_{\boldsymbol{N},e=e^{(0)}} \\ &+ \frac{1}{2}\iiint \mathrm{d}\boldsymbol{s}_1\mathrm{d}\boldsymbol{s}_2\mathrm{d}\boldsymbol{s}_3\mathrm{d}\boldsymbol{s}_4\,\Delta e_{BB}(\boldsymbol{s}_1,\boldsymbol{s}_2)\Delta e_{BB}(\boldsymbol{s}_3,\boldsymbol{s}_4)\,\frac{\delta^2\phi}{\delta e_{BB}(\boldsymbol{s}_1,\boldsymbol{s}_2)\delta e_{BB}(\boldsymbol{s}_3,\boldsymbol{s}_4)}\bigg|_{\boldsymbol{N},e=e^{(0)}} \\ &+ \frac{1}{2}\iiint \mathrm{d}\boldsymbol{r}_1\mathrm{d}\boldsymbol{r}_2\mathrm{d}\boldsymbol{s}_1\mathrm{d}\boldsymbol{s}_2\Delta e_{AB}(\boldsymbol{r}_1,\boldsymbol{s}_1)\Delta e_{AB}(\boldsymbol{r}_2,\boldsymbol{s}_2)\,\frac{\delta^2\phi}{\delta e_{AB}(\boldsymbol{r}_1,\boldsymbol{s}_1)\delta e_{AB}(\boldsymbol{r}_2,\boldsymbol{s}_2)}\bigg|_{\boldsymbol{N},e=e^{(0)}} \\ &+ \iiint \mathrm{d}\boldsymbol{r}_1\mathrm{d}\boldsymbol{r}_2\mathrm{d}\boldsymbol{s}_1\mathrm{d}\boldsymbol{s}_2\Delta e_{AA}(\boldsymbol{r}_1,\boldsymbol{r}_2)\Delta e_{BB}(\boldsymbol{s}_1,\boldsymbol{s}_2)\,\frac{\delta^2\phi}{\delta e_{BB}(\boldsymbol{s}_1,\boldsymbol{s}_2)e_{AA}(\boldsymbol{r}_1,\boldsymbol{r}_2)}\bigg|_{\boldsymbol{N},e=e^{(0)}} \\ &+ \iiint \mathrm{d}\boldsymbol{r}_1\mathrm{d}\boldsymbol{r}_2\mathrm{d}\boldsymbol{r}_3\mathrm{d}\boldsymbol{s}_1\Delta e_{AA}(\boldsymbol{r}_2,\boldsymbol{r}_3)\Delta e_{AB}(\boldsymbol{r}_1,\boldsymbol{s}_1)\,\frac{\delta^2\phi}{\delta e_{AA}(\boldsymbol{r}_2,\boldsymbol{r}_3)e_{AB}(\boldsymbol{r}_1,\boldsymbol{s}_1)}\bigg|_{\boldsymbol{N},e=e^{(0)}} \\ &+ \iiint \mathrm{d}\boldsymbol{r}_1\mathrm{d}\boldsymbol{s}_1\mathrm{d}\boldsymbol{s}_2\mathrm{d}\boldsymbol{s}_3\Delta e_{BB}(\boldsymbol{s}_2,\boldsymbol{s}_3)\Delta e_{AB}(\boldsymbol{r}_1,\boldsymbol{s}_1)\,\frac{\delta^2\phi}{\delta e_{BB}(\boldsymbol{s}_2,\boldsymbol{s}_3)\delta e_{AB}(\boldsymbol{r}_1,\boldsymbol{s}_1)}\bigg|_{\boldsymbol{N},e=e^{(0)}}\end{aligned} \tag{7.14}$$

As pointed out by Henderson and Barker, such a series expansion for F, derived in the canonical ensemble, is "not useful for numerical computation ... because it is valid only for a finite system. To obtain results which are useful, one must take the *thermodynamic limit*, and unfortunately, this involves [for the second order term] the unknown asymptotic behaviour of the four-body distribution function when two of the molecules involved are remote from the other two" [181]. For this reason, we will seek to express the functional derivative in the canonical ensemble, in terms of their grand-canonical counterparts, where the asymptotic behaviour of the n-body distribution functions presents no difficulties. We therefore require a relationship between partial derivatives taken at constant number of particles to those taken at constant chemical potential.

7.4 Ensemble Transformation

In deriving the relationships between derivatives in the different ensembles, we have not used the functional formalism introduced above, but this is just a matter of notational convenience; the results derived here for the partial derivatives are trivially extended to the case of functional derivatives. We therefore consider a system in which the pair potentials $v_{\nu\eta}(r;\gamma_{\nu\eta})$ depend on a parameter $\gamma_{\nu\eta}$, such that $\gamma_{\nu\eta} = 0$ corresponds to a reference potential and $\gamma_{\nu\eta} = 1$ to the potential of the system we wish to study. Relations between derivatives in the different ensembles can easily be found by treating the $\gamma_{\nu\mu}$ as additional thermodynamic variables. The procedure is similar to that used in deriving the Kirkwood-Buff theory (Section 3.4.2), only now we want to establish a relationship between the $(\boldsymbol{\mu}VT)$ and $(\boldsymbol{N}VT)$ ensembles, instead of $(\boldsymbol{\mu}VT)$ and $(\boldsymbol{N}PT)$.

For simplicity, we denote the $m(m+1)/2$ perturbation parameters (one for each distinct pair-potential) as the "vector" $\boldsymbol{\gamma}$. In order, to distinguish the $\boldsymbol{\gamma}$ vector from the m-dimensional vectors ($\boldsymbol{N}$, $\boldsymbol{n}$, $\boldsymbol{\mu}$) we use capital non-Greek letters to represent the individual components, i.e. γ_X, γ_Y.

7.4.1 Basic Properties

From the basic properties of partial derivatives, we have

- $\boldsymbol{N}, V, \boldsymbol{\gamma} \longrightarrow \boldsymbol{\mu}, V, \boldsymbol{\gamma}$

$$\left.\frac{\partial}{\partial N_\nu}\right|_{\boldsymbol{N}/N_\nu,V,\boldsymbol{\gamma}} \longrightarrow \sum_\eta \left(\frac{\partial \mu_\eta}{\partial N_\nu}\right)_{\boldsymbol{N}/N_\nu,V,\boldsymbol{\gamma}} \left.\frac{\partial}{\partial \mu_\eta}\right|_{\boldsymbol{\mu}/\mu_\eta,V,\boldsymbol{\gamma}} \tag{7.15a}$$

$$\left.\frac{\partial}{\partial V}\right|_{\boldsymbol{N},\boldsymbol{\gamma}} \longrightarrow \left.\frac{\partial}{\partial V}\right|_{\boldsymbol{\mu},\boldsymbol{\gamma}} + \sum_\eta \left(\frac{\partial \mu_\eta}{\partial V}\right)_{\boldsymbol{N},\boldsymbol{\gamma}} \left.\frac{\partial}{\partial \mu_\eta}\right|_{\boldsymbol{\mu}/\mu_\eta,V,\boldsymbol{\gamma}} \tag{7.15b}$$

$$\left.\frac{\partial}{\partial \gamma_X}\right|_{\boldsymbol{N},V,\boldsymbol{\gamma}/\gamma_X} \longrightarrow \left.\frac{\partial}{\partial \gamma_X}\right|_{\boldsymbol{\mu},V,\boldsymbol{\gamma}/\gamma_X} + \sum_\eta \left(\frac{\partial \mu_\eta}{\partial \gamma_X}\right)_{\boldsymbol{N},V,\boldsymbol{\gamma}/\gamma_X} \left.\frac{\partial}{\partial \mu_\eta}\right|_{\boldsymbol{\mu}/\mu_\eta,V,\boldsymbol{\gamma}} \tag{7.15c}$$

- $\boldsymbol{\mu}, V, \boldsymbol{\gamma} \longrightarrow \boldsymbol{N}, V, \boldsymbol{\gamma}$

$$\left.\frac{\partial}{\partial \mu_\nu}\right|_{\boldsymbol{\mu}/\mu_\nu,V,\boldsymbol{\gamma}} \longrightarrow \sum_\eta \left(\frac{\partial \overline{N}_\eta}{\partial \mu_\nu}\right)_{\boldsymbol{\mu}/\mu_\nu,V,\boldsymbol{\gamma}} \left.\frac{\partial}{\partial N_\eta}\right|_{\boldsymbol{N}/N_\eta,V,\boldsymbol{\gamma}} \tag{7.16a}$$

$$\left.\frac{\partial}{\partial V}\right|_{\boldsymbol{\mu},\boldsymbol{\gamma}} \longrightarrow \left.\frac{\partial}{\partial V}\right|_{\boldsymbol{N},\boldsymbol{\gamma}} + \sum_\eta \left(\frac{\partial \overline{N}_\eta}{\partial V}\right)_{\boldsymbol{\mu},\boldsymbol{\gamma}} \left.\frac{\partial}{\partial N_\eta}\right|_{\boldsymbol{N}/N_\eta,V,\boldsymbol{\gamma}} \tag{7.16b}$$

$$\left.\frac{\partial}{\partial \gamma_X}\right|_{\boldsymbol{\mu},V,\boldsymbol{\gamma}/\gamma_X} \longrightarrow \left.\frac{\partial}{\partial \gamma_X}\right|_{\boldsymbol{N},V,\boldsymbol{\gamma}/\gamma_X} + \sum_\eta \left(\frac{\partial \overline{N}_\eta}{\partial \gamma_X}\right)_{\boldsymbol{\mu},V,\boldsymbol{\gamma}/\gamma_X} \left.\frac{\partial}{\partial N_\eta}\right|_{\boldsymbol{N}/N_\eta,V,\boldsymbol{\gamma}} \tag{7.16c}$$

Where $\overline{N}_\eta$ denotes the average number of particles of type η in the grand-canonical ensemble ($\overline{N}_\eta = \langle N_\eta \rangle = k_\mathrm{B}T\partial \ln \Xi/\partial \mu_\eta$).

The following preliminary results will prove to be useful. Inserting μ_α into Eq. (7.16a)

$$\begin{aligned}\left(\frac{\partial \mu_\alpha}{\partial \mu_\nu}\right)_{\boldsymbol{\mu}/\mu_\nu,V,\boldsymbol{\gamma}} &= \sum_\eta \left(\frac{\partial \overline{N}_\eta}{\partial \mu_\nu}\right)_{\boldsymbol{\mu}/\mu_\nu,V,\boldsymbol{\gamma}} \left(\frac{\partial \mu_\alpha}{\partial N_\eta}\right)_{\boldsymbol{N}/N_\eta,V,\boldsymbol{\gamma}} \\ \delta_{\alpha\nu} &= \sum_\eta \mathrm{A}_{\alpha\eta}\mathrm{B}_{\eta\nu}\end{aligned} \tag{7.17}$$

we obtain a simple matrix equation which relates the derivatives of N and μ with respect to each other. Inserting N_ν into Eq. (7.15b) we have

$$\left(\frac{\partial N_\nu}{\partial V}\right)_{\boldsymbol{N},\boldsymbol{\gamma}} = \left(\frac{\partial \overline{N}_\nu}{\partial V}\right)_{\boldsymbol{\mu},\boldsymbol{\gamma}} + \sum_\eta \left(\frac{\partial \overline{N}_\nu}{\partial \mu_\eta}\right)_{\boldsymbol{\mu}/\mu_\eta,V,\boldsymbol{\gamma}} \left(\frac{\partial \mu_\eta}{\partial V}\right)_{\boldsymbol{N},\boldsymbol{\gamma}}$$

but the term on the lhs is zero, and the last term on the rhs can be expressed as a function of the pressure, by using the definition of μ_η and P (Eq. (3.20))

$$\begin{aligned}\left(\frac{\partial\overline{N}_\nu}{\partial V}\right)_{\boldsymbol{\mu},\boldsymbol{\gamma}} &= \sum_\eta \left(\frac{\partial P}{\partial N_\eta}\right)_{\boldsymbol{N}/N_\eta,V,\boldsymbol{\gamma}} \left(\frac{\partial\overline{N}_\nu}{\partial\mu_\eta}\right)_{\boldsymbol{\mu}/\mu_\eta,V,\boldsymbol{\gamma}} \\ \varrho_\nu &= \sum_\eta \left(\frac{\partial P}{\partial N_\eta}\right)_{\boldsymbol{N}/N_\eta,V,\boldsymbol{\gamma}} \left(\frac{\partial\overline{N}_\nu}{\partial\mu_\eta}\right)_{\boldsymbol{\mu}/\mu_\eta,V,\boldsymbol{\gamma}}\end{aligned} \tag{7.18}$$

with $\varrho_\nu = \overline{N}_\nu/V$. Finally, if we insert μ_ν into Eq. (7.16c), we obtain the following relationship

$$\begin{aligned}\left(\frac{\partial\mu_\nu}{\partial\gamma_X}\right)_{\boldsymbol{\mu},V,\boldsymbol{\gamma}/\gamma_X} &= \left(\frac{\partial\mu_\nu}{\partial\gamma_X}\right)_{\boldsymbol{N},V,\boldsymbol{\gamma}/\gamma_X} + \sum_\eta \left(\frac{\partial\overline{N}_\eta}{\partial\gamma_X}\right)_{\boldsymbol{\mu},V,\boldsymbol{\gamma}/\gamma_X} \left(\frac{\partial\mu_\nu}{\partial N_\eta}\right)_{\boldsymbol{N}/N_\eta,V,\boldsymbol{\gamma}} \\ \left(\frac{\partial\mu_\nu}{\partial\gamma_X}\right)_{\boldsymbol{N},V,\boldsymbol{\gamma}/\gamma_X} &= -\sum_\eta \left(\frac{\partial\mu_\nu}{\partial N_\eta}\right)_{\boldsymbol{N}/N_\eta,V,\boldsymbol{\gamma}} \left(\frac{\partial^2 k_\mathrm{B}T\ln\Xi}{\partial\mu_\eta\,\partial\gamma_X}\right)_{\boldsymbol{\mu}/\mu_\eta,V,\boldsymbol{\gamma}/\gamma_X}\end{aligned} \tag{7.19}$$

Summary:

$$\mathrm{A}_{\nu\eta} = \left(\frac{\partial\mu_\nu}{\partial N_\eta}\right)_{\boldsymbol{N}/N_\nu} \tag{7.20a}$$

$$\mathrm{B}_{\nu\eta} = \left(\frac{\partial\overline{N}_\nu}{\partial\mu_\eta}\right)_{\boldsymbol{\mu}/\mu_\nu} \tag{7.20b}$$

with A B = I, where I is the unit matrix, so that

$$\mathrm{A}_{\nu\eta} = (\mathrm{B}^{-1})_{\nu\eta} = \frac{1}{|\mathrm{B}|}B^\dagger_{\eta\nu} \tag{7.20c}$$

where $|\mathrm{B}|$ and $\mathrm{B}^\dagger$ are the determinant and the cofactor matrix of B, respectively.

$$\varrho_\nu = V^{-1}\sum_\eta \mathrm{B}_{\nu\eta}\left(\frac{\partial P}{\partial\rho_\eta}\right)_{\boldsymbol{N}/N_\eta} \tag{7.20d}$$

$$\left(\frac{\partial\mu_\nu}{\partial\gamma_X}\right)_{\boldsymbol{N}} = -k_\mathrm{B}T\sum_\eta \mathrm{A}_{\nu\eta}\left(\frac{\partial^2\ln\Xi}{\partial\mu_\eta\,\partial\gamma_X}\right)_{\boldsymbol{\mu}/\mu_\eta} \tag{7.20e}$$

Example: In the case of a 1-component system, Eq. (7.16a) reduces to

$$\frac{\partial}{\partial\mu} = \left(\frac{\partial\varrho}{\partial\mu}\right)\frac{\partial}{\partial\rho} \tag{7.21a}$$

and Eq. (7.20) takes the following simplified form

$$\left(\frac{\partial P}{\partial\rho}\right) = \varrho\left(\frac{\partial\mu}{\partial\varrho}\right) \equiv \frac{1}{\varrho\chi_T} = k_{\mathrm{B}}TS^{-1}(0) \tag{7.21b}$$

$$\left(\frac{\partial\mu}{\partial\gamma}\right)_N = -\frac{k_{\mathrm{B}}T}{V}\left(\frac{\partial^2\ln\Xi}{\partial\rho\,\partial\gamma}\right) \tag{7.21c}$$

where $S(k)$ is the structure factor.

7.4.2 Free Energy Derivatives

We now use the results previously derived to compute the first and second-order free energy derivatives needed in the perturbation calculations

First Order

Using the definition of the Legendre transformation between F and Ω (Eq. (3.26)), we have

$$\left(\frac{\partial F}{\partial\gamma_X}\right)_{\boldsymbol{N},V,\boldsymbol{\gamma}/\gamma_X} = -\left(\frac{\partial k_{\mathrm{B}}T\ln\Xi}{\partial\gamma_X}\right)_{\boldsymbol{N},V,\boldsymbol{\gamma}/\gamma_X} + \sum_\nu N_\nu\left(\frac{\partial\mu_\nu}{\partial\gamma_X}\right)_{\boldsymbol{N},V,\boldsymbol{\gamma}/\gamma_X}$$

and using Eq. (7.15c) we obtain

$$\begin{aligned}
&= -\left(\frac{\partial k_{\mathrm{B}}T\ln\Xi}{\partial\gamma_X}\right)_{\boldsymbol{\mu},V,\boldsymbol{\gamma}/\gamma_X} - \sum_\nu\left(\frac{\partial\mu_\nu}{\partial\gamma_X}\right)_{\boldsymbol{N},V,\boldsymbol{\gamma}/\gamma_X}\left(\frac{\partial k_{\mathrm{B}}T\ln\Xi}{\partial\mu_\nu}\right)_{\boldsymbol{\mu}/\mu_\nu,V,\boldsymbol{\gamma}} \\
&\quad + \sum_\nu N_\nu\left(\frac{\partial\mu_\nu}{\partial\gamma_X}\right)_{\boldsymbol{N},V,\boldsymbol{\gamma}/\gamma_X} \\
&= -k_{\mathrm{B}}T\left(\frac{\partial\ln\Xi}{\partial\gamma_X}\right)_{\boldsymbol{\mu},V,\boldsymbol{\gamma}/\gamma_X}
\end{aligned}$$

where we have assumed that $\overline{N}_\nu = N_\nu$.

Second Order

By definition

$$\left(\frac{\partial^2 F}{\partial\gamma_Y\,\partial\gamma_X}\right)_{\boldsymbol{N},V,\boldsymbol{\gamma}/\{\gamma_X,\gamma_Y\}} = -k_{\mathrm{B}}T\frac{\partial}{\partial\gamma_Y}\left[\left(\frac{\partial\ln\Xi}{\partial\gamma_X}\right)_{\boldsymbol{\mu},V,\boldsymbol{\gamma}/\gamma_X}\right]_{\boldsymbol{N},V,\boldsymbol{\gamma}/\gamma_Y}$$

using Eq. (7.15c), we obtain

$$\begin{aligned}
&= -k_{\mathrm{B}}T\left(\frac{\partial^2\ln\Xi}{\partial\gamma_Y\,\partial\gamma_X}\right)_{\boldsymbol{\mu},V,\boldsymbol{\gamma}/\{\gamma_X,\gamma_Y\}} \\
&\quad - k_{\mathrm{B}}T\sum_\nu\left(\frac{\partial\mu_\nu}{\partial\gamma_Y}\right)_{\boldsymbol{N},V,\boldsymbol{\gamma}/\gamma_Y}\left(\frac{\partial^2\ln\Xi}{\partial\mu_\nu\,\partial\gamma_X}\right)_{\boldsymbol{\mu}/\mu_\nu,V,\boldsymbol{\gamma}/\gamma_X}
\end{aligned}$$

and finally, from Eq. (7.20e), we arrive at

$$
\begin{aligned}
&= -k_{\mathrm{B}}T \left(\frac{\partial^2 \ln \Xi}{\partial \gamma_Y \, \partial \gamma_X} \right)_{\boldsymbol{\mu},V,\boldsymbol{\gamma}/\{\gamma_X,\gamma_Y\}} \\
&\quad + (k_{\mathrm{B}}T)^2 \sum_{\nu\eta} \left(\mathrm{B}^{-1}\right)_{\nu\eta} \left(\frac{\partial^2 \ln \Xi}{\partial \mu_\nu \, \partial \gamma_X} \right)_{\boldsymbol{\mu}/\mu_\nu,V,\boldsymbol{\gamma}/\gamma_X} \\
&\qquad \times \left(\frac{\partial^2 \ln \Xi}{\partial \mu_\eta \, \partial \gamma_Y} \right)_{\boldsymbol{\mu}/\mu_\eta,V,\boldsymbol{\gamma}/\gamma_Y}
\end{aligned}
$$

Summary:

$$
\left(\frac{\partial F}{\partial \gamma_X} \right)_{\boldsymbol{N}} = -k_{\mathrm{B}}T \left(\frac{\partial \ln \Xi}{\partial \gamma_X} \right)_{\boldsymbol{\mu}} \tag{7.22a}
$$

$$
\begin{aligned}
\left(\frac{\partial^2 F}{\partial \gamma_Y \, \partial \gamma_X} \right)_{\boldsymbol{N}} &= -k_{\mathrm{B}}T \left(\frac{\partial^2 \ln \Xi}{\partial \gamma_Y \, \partial \gamma_X} \right)_{\boldsymbol{\mu}} \\
&\quad + (k_{\mathrm{B}}T)^2 \sum_{\nu\eta} \left(\mathrm{B}^{-1}\right)_{\nu\eta} \left(\frac{\partial^2 \ln \Xi}{\partial \mu_\nu \, \partial \gamma_X} \right)_{\boldsymbol{\mu}/\mu_\nu} \left(\frac{\partial^2 \ln \Xi}{\partial \mu_\eta \, \partial \gamma_Y} \right)_{\boldsymbol{\mu}/\mu_\nu}
\end{aligned} \tag{7.22b}
$$

Example: In the case of a 1-component system, Eqs. (7.22) take the following form

$$
\left(\frac{\partial F}{\partial \gamma} \right)_{N} = -k_{\mathrm{B}}T \left(\frac{\partial \ln \Xi}{\partial \gamma} \right)_{\mu} \tag{7.23a}
$$

$$
\left(\frac{\partial^2 F}{\partial \gamma^2} \right)_{N} = -k_{\mathrm{B}}T \left(\frac{\partial^2 \ln \Xi}{\partial \gamma^2} \right)_{\mu} + (k_{\mathrm{B}}T)^2 \frac{\varrho}{V} \left(\frac{\partial \rho}{\partial P} \right) \left(\frac{\partial}{\partial \rho} \frac{\partial \ln \Xi}{\partial \gamma} \right)^2 \tag{7.23b}
$$

where we have used Eqs. (7.21a) and (7.21b) to relate $\frac{\partial}{\partial \mu}$ to $\frac{\partial}{\partial \rho}$. Furthermore, since $-k_{\mathrm{B}}T \frac{\partial \ln \Xi}{\partial \gamma} = \frac{1}{2} V \varrho^2 \int \mathrm{d}\boldsymbol{r} g(r) \frac{\partial v(r)}{\partial \gamma}$, we have

$$
\begin{aligned}
&= -k_{\mathrm{B}}T \left(\frac{\partial^2 \ln \Xi}{\partial \gamma^2} \right)_{\mu} + \overline{N} \left(\frac{\partial \rho}{\partial P} \right) \left[\frac{\partial}{\partial \rho} \left(\frac{1}{2} \varrho^2 \int \mathrm{d}\boldsymbol{r} g(r) \frac{\partial v(r)}{\partial \gamma} \right) \right]^2 \\
&= -k_{\mathrm{B}}T \left(\frac{\partial^2 \ln \Xi}{\partial \gamma^2} \right)_{\boldsymbol{\mu}} + \frac{1}{4} \beta \overline{N} S(0) \left[\frac{\partial}{\partial \rho} \left(\varrho^2 \int \mathrm{d}\boldsymbol{r} \, g(r) \frac{\partial v(r)}{\partial \gamma} \right) \right]^2
\end{aligned}
$$

7.4.3 Grand-Potential Derivatives

As mentioned before, the results given in Eqs. (7.20) and (7.22) can be directly expressed in terms of functional derivatives by identifying $\frac{\partial}{\partial \gamma_X} \longleftrightarrow \frac{\delta}{\delta e_X(\boldsymbol{r},\boldsymbol{s})}$. We are thus left with the task of evaluating the first and second order functional derivatives of $\ln \Xi$ with respect to the $e_X(\boldsymbol{r},\boldsymbol{s})$. These computation is straightforward, but care must be taken to correctly count all the terms appearing in the derivatives.

First Order:
By definition (Eq. (7.8)), the first order functional derivative of the grand potential is given by

$$e_{\alpha\beta}(\boldsymbol{r},\boldsymbol{s})\frac{\delta \ln \Xi}{\delta e_{\alpha\beta}(\boldsymbol{r},\boldsymbol{s})} = \frac{1}{\Xi}\sum_{\boldsymbol{N}=0}^{\infty}\left(\prod_{\nu=1}^{m}\frac{z_\nu^{N_\nu}}{N_\nu!}\right)\int\cdots\int \mathrm{d}\{\boldsymbol{N}\}\left(\prod_{\substack{\langle\nu,\eta\rangle/(\alpha,\beta)\\ \langle i,j\rangle}} e_{\nu\eta}(\boldsymbol{r}_{i_\nu},\boldsymbol{r}_{j_\eta})\right)$$
$$\times\, e_{\alpha\beta}(\boldsymbol{r},\boldsymbol{s})\frac{\delta}{\delta e_{\alpha\beta}(\boldsymbol{r},\boldsymbol{s})}\left(\prod_{\langle i,j\rangle} e_{\alpha\beta}(\boldsymbol{r}_{i_\alpha},\boldsymbol{r}_{j_\beta})\right)$$

The functional derivative appearing inside the integral will produce a delta function in both variables, for each one of the $e_{\alpha\beta}$ functions; and since, upon integration, all terms of the resulting sum are equivalent, we need only take one of them into account. If $\alpha=\beta$ we have $N_\alpha(N_\alpha-1)/2$ equivalent terms, and if not we we have $N_\alpha N_\beta$ terms

$$e_{\alpha\beta}(\boldsymbol{r},\boldsymbol{s})\tfrac{\delta}{\delta e_{\alpha\beta}(\boldsymbol{r},\boldsymbol{s})}\left(\textstyle\prod_{\langle i,j\rangle} e_{\alpha\beta}(\boldsymbol{r}_{1_\alpha},\boldsymbol{r}_{1_\beta})\right) = \prod_{\langle i,j\rangle} e_{\alpha\beta}(\boldsymbol{r}_{1_\alpha},\boldsymbol{r}_{2_\beta})$$
$$\times\begin{cases}\frac{N_\alpha(N_\alpha-1)}{2}\delta(\boldsymbol{r}_{1_\alpha}-\boldsymbol{r})\delta(\boldsymbol{r}_{2_\alpha}-\boldsymbol{s}) & \alpha=\beta\\ N_\alpha N_\beta\delta(\boldsymbol{r}_{1_\alpha}-\boldsymbol{r})\delta(\boldsymbol{r}_{1_\beta}-\boldsymbol{s}) & \alpha\neq\beta\end{cases}$$

This can be expressed in terms of the two-body distribution function, Eq. (7.10), as

$$\frac{\delta \ln \Xi}{\delta e_{\alpha\beta}(\boldsymbol{r},\boldsymbol{s})} = c_{\alpha\beta}\, e_{\alpha\beta}^{-1}(\boldsymbol{r},\boldsymbol{s})\varrho_{\alpha\beta}^{(2)}(\boldsymbol{r},\boldsymbol{s}) \tag{7.25}$$

where

$$c_{\alpha\beta} = \begin{cases}\frac{1}{2} & ,\alpha=\beta\\ 1 & ,\alpha\neq\beta\end{cases} \tag{7.26}$$

Second Order
By definition, the second order derivatives are given by

$$\begin{aligned}&\frac{\delta^2 \ln \Xi}{\delta e_{\nu\eta}(\boldsymbol{p},\boldsymbol{q})\,\delta e_{\alpha\beta}(\boldsymbol{r},\boldsymbol{s})}\\ &\equiv \frac{1}{\Xi}\left(\frac{\delta^2\Xi}{\delta e_{\nu\eta}(\boldsymbol{p},\boldsymbol{q})\,\delta e_{\alpha\beta}(\boldsymbol{r},\boldsymbol{s})}\right) - \left(\frac{\delta \ln \Xi}{\delta e_{\alpha\beta}(\boldsymbol{r},\boldsymbol{s})}\right)\left(\frac{\delta \ln \Xi}{\delta e_{\nu\eta}(\boldsymbol{p},\boldsymbol{q})}\right)\\ &= \frac{1}{\Xi}\left[\frac{\delta}{\delta e_{\nu\eta}(\boldsymbol{p},\boldsymbol{q})}\left(\Xi\, c_{\alpha\beta}\, e_{\alpha\beta}^{-1}(\boldsymbol{r},\boldsymbol{s})\varrho_{\alpha\beta}^{(2)}(\boldsymbol{r},\boldsymbol{s})\right)\right]\\ &\quad - c_{\alpha\beta}c_{\nu\eta}e_{\alpha\beta}^{-1}(\boldsymbol{r},\boldsymbol{s})e_{\nu\eta}^{-1}(\boldsymbol{p},\boldsymbol{q})\varrho_{\alpha\beta}^{(2)}(\boldsymbol{r},\boldsymbol{s})\varrho_{\nu\eta}^{(2)}(\boldsymbol{p},\boldsymbol{q})\\ &= -\delta_{\alpha\nu}\delta_{\beta\eta}\delta(\boldsymbol{r}-\boldsymbol{p})\delta(\boldsymbol{s}-\boldsymbol{q})c_{\alpha\beta}e_{\alpha\beta}^{-2}(\boldsymbol{r},\boldsymbol{s})\varrho_{\alpha\beta}^{(2)}(\boldsymbol{r},\boldsymbol{s}) + c_{\alpha\beta}e_{\alpha\beta}^{-1}(\boldsymbol{r},\boldsymbol{s})\frac{\delta\varrho_{\alpha\beta}^{(2)}(\boldsymbol{r},\boldsymbol{s})}{\delta e_{\nu\eta}(\boldsymbol{p},\boldsymbol{q})}\end{aligned} \tag{7.27}$$

In total, we must evaluate seven different combinations (for the general case when $m\geq 4$) for the functional derivatives of $\varrho_{\alpha\beta}^{(2)}$ with respect to variations in $e_{\nu\eta}$. We assume that

$\alpha \neq \beta \neq \nu \neq \eta$, and to simplify the expressions, we will only explicitly write the part of the configuration integral which is affected by the functional differentiation.

In what follows, all functional derivatives are taken with respect to the natural variables for the grand-canonical ensemble, i.e. at constant μ, V, and T, unless stated otherwise.

1. $\alpha\alpha - \alpha\alpha$
By definition,

$$\frac{\delta \varrho^{(2)}_{\alpha\alpha}(\boldsymbol{r},\boldsymbol{s})}{\delta e_{\alpha\alpha}(\boldsymbol{p},\boldsymbol{q})} = \frac{\delta}{\delta e_{\alpha\alpha}(\boldsymbol{p},\boldsymbol{q})}\left[\frac{1}{\Xi}\sum_{N_\alpha>2}\frac{1}{(N_\alpha-2)!}\int \mathrm{d}\{N_\alpha-2\}_\alpha \prod_{i<j}^{N_\alpha} e_{\alpha\alpha}(\boldsymbol{r}_{i_\alpha},\boldsymbol{r}_{j_\alpha})\right]_{\substack{r_{1_\alpha}\to r\\ r_{2_\alpha}\to s}}$$

where the integral runs over all variables, except r_{1_α} and r_{2_α}, which are held at $\boldsymbol{r}$ and $\boldsymbol{s}$, respectively. The derivative will give two global terms: (1) from acting on the partition function in the denominator and (2) from acting on the product of Boltzmann factors inside the integral. Each of these can easily be expressed in terms of an n-body distribution function (Eq. (7.10)) as follows

$$\begin{aligned}\frac{\delta \varrho^{(2)}_{\alpha\alpha}(\boldsymbol{r},\boldsymbol{s})}{\delta e_{\alpha\alpha}(\boldsymbol{p},\boldsymbol{q})} = &\left[\frac{1}{\Xi}\sum_{N_\alpha>2}\frac{1}{(N_\alpha-2)!}\int \mathrm{d}\{N_\alpha-2\}_\alpha \frac{\delta}{\delta e_{\alpha\alpha}(\boldsymbol{p},\boldsymbol{q})}\prod_{i<j}^{N_\alpha} e_{\alpha\alpha}(\boldsymbol{r}_{i_\alpha},\boldsymbol{r}_{j_\alpha})\right]_{\substack{r_{1_\alpha}\to r\\ r_{2_\alpha}\to s}}\\ &- c_{\alpha\alpha}e^{-1}_{\alpha\alpha}(\boldsymbol{p},\boldsymbol{q})\varrho^{(2)}_{\alpha\alpha}(\boldsymbol{p},\boldsymbol{q})\varrho^{(2)}_{\alpha\alpha}(\boldsymbol{r},\boldsymbol{s})\end{aligned}$$

The terms inside square brackets will give four distinct contributions, depending on whether or not the variables r_{i_α} and r_{j_α} are integration variables: (a) one term for $(r_{1_\alpha}, r_{2_\alpha})$, (b) $(N_\alpha - 2)$ terms for $(r_{1_\alpha}, r_{j_\alpha\geq 3})$, (c) $(N_\alpha - 2)$ terms for $(r_{2_\alpha}, r_{j_\alpha\geq 3})$, and (d) $(N_\alpha - 2)(N_\alpha - 3)/2$ terms for all pairs $(r_{i_\alpha\geq 3}, r_{j_\alpha>i_\alpha})$.

$$\begin{aligned}e_{\alpha\alpha}(\boldsymbol{p},\boldsymbol{q})\frac{\delta \varrho^{(2)}_{\alpha\alpha}(\boldsymbol{r},\boldsymbol{s})}{\delta e_{\alpha\alpha}(\boldsymbol{p},\boldsymbol{q})} = &\,\delta(\boldsymbol{r}-\boldsymbol{p})\delta(\boldsymbol{s}-\boldsymbol{q})\varrho^{(2)}_{\alpha\alpha}(\boldsymbol{r},\boldsymbol{s}) + \left[\delta(\boldsymbol{r}-\boldsymbol{p})+\delta(\boldsymbol{s}-\boldsymbol{p})\right]\varrho^{(3)}_{\alpha\alpha\alpha}(\boldsymbol{r},\boldsymbol{s},\boldsymbol{q})\\ &+ c_{\alpha\alpha}\left(\varrho^{(4)}_{\alpha\alpha\alpha\alpha}(\boldsymbol{r},\boldsymbol{s},\boldsymbol{p},\boldsymbol{q}) - \varrho^{(2)}_{\alpha\alpha}(\boldsymbol{r},\boldsymbol{s})\varrho^{(2)}_{\alpha\alpha}(\boldsymbol{p},\boldsymbol{q})\right) \qquad (7.28)\end{aligned}$$

The density derivatives for the other six cases can be computed in roughly the same manner.

2. $\alpha\alpha - \alpha\beta$

$$\frac{\delta\varrho^{(2)}_{\alpha\alpha}(\boldsymbol{r},\boldsymbol{s})}{\delta e_{\alpha\beta}(\boldsymbol{p},\boldsymbol{q})} = \frac{\delta}{\delta e_{\alpha\beta}(\boldsymbol{p},\boldsymbol{q})}\left[\frac{1}{\Xi}\sum_{N_\alpha\geq 2}\sum_{N_\beta\geq 0}\frac{1}{(N_\alpha-2)!N_\beta!}\right.$$
$$\left.\times\int \mathrm{d}\{N_\alpha-2\}_\alpha \mathrm{d}\{N_\beta\}_\beta \prod_{i=1}^{N_\alpha}\prod_{j=1}^{N_\beta} e_{\alpha\beta}(\boldsymbol{r}_{i_\alpha},\boldsymbol{r}_{j_\beta})\right]_{\substack{r_{1_\alpha}\to r\\ r_{2_\alpha}\to s}}$$
$$= \left[\frac{1}{\Xi}\sum_{N_\alpha\geq 2}\sum_{N_\beta\geq 0}\frac{1}{(N_\alpha-2)!N_\beta!}\right.$$
$$\left.\times\int \mathrm{d}\{N_\alpha-2\}_\alpha \mathrm{d}\{N_\beta\}_\beta \frac{\delta}{\delta e_{\alpha\beta}(\boldsymbol{p},\boldsymbol{q})}\prod_{i=1}^{N_\alpha}\prod_{j=1}^{N_\beta} e_{\alpha\beta}(\boldsymbol{r}_{i_\alpha},\boldsymbol{r}_{j_\beta})\right]_{\substack{r_{1_\alpha}\to r\\ r_{2_\alpha}\to s}}$$
$$- c_{\alpha\beta}e^{-1}_{\alpha\beta}(\boldsymbol{p},\boldsymbol{q})\varrho^{(2)}_{\alpha\beta}(\boldsymbol{p},\boldsymbol{q})\varrho^{(2)}_{\alpha\alpha}(\boldsymbol{r},\boldsymbol{s})$$

The functional derivative will give three distinct contributions: (a) N_β terms for $(r_{1_\alpha}, r_{j_\beta\geq 1})$, (b) N_β terms for $(r_{2_\alpha}, r_{j_\beta\geq 1})$, and (c) $N_\beta(N_\alpha-2)$ terms for the pairs $(r_{i_\alpha\geq 3}, r_{j_\alpha\geq 1})$

$$e_{\alpha\beta}(\boldsymbol{p},\boldsymbol{q})\frac{\delta\varrho^{(2)}_{\alpha\alpha}(\boldsymbol{r},\boldsymbol{s})}{\delta e_{\alpha\beta}(\boldsymbol{p},\boldsymbol{q})} = [\delta(\boldsymbol{r}-\boldsymbol{p})+\delta(\boldsymbol{s}-\boldsymbol{p})]\,\varrho^{(3)}_{\alpha\alpha\beta}(\boldsymbol{r},\boldsymbol{s},\boldsymbol{q}) \tag{7.29}$$
$$+ c_{\alpha\beta}\left(\varrho^{(4)}_{\alpha\alpha\alpha\beta}(\boldsymbol{r},\boldsymbol{s},\boldsymbol{p},\boldsymbol{q}) - \varrho^{(2)}_{\alpha\alpha}(\boldsymbol{r},\boldsymbol{s})\varrho^{(2)}_{\alpha\beta}(\boldsymbol{p},\boldsymbol{q})\right)$$

3. $\alpha\alpha-\beta\beta$

$$\frac{\delta\varrho^{(2)}_{\alpha\alpha}(\boldsymbol{r},\boldsymbol{s})}{\delta e_{\beta\beta}(\boldsymbol{p},\boldsymbol{q})} = \frac{\delta}{\delta e_{\beta\beta}(\boldsymbol{p},\boldsymbol{q})}\left[\frac{1}{\Xi}\sum_{N_\alpha\geq 2}\sum_{N_\beta\geq 0}\frac{1}{(N_\alpha-2)!N_\beta!}\right.$$
$$\left.\times\int \mathrm{d}\{N_\alpha-2\}_\alpha \mathrm{d}\{N_\beta\}_\beta \prod_{i<j}^{N_\beta} e_{\beta\beta}(\boldsymbol{r}_{i_\beta},\boldsymbol{r}_{j_\beta})\right]_{\substack{r_{1_\alpha}\to r\\ r_{2_\alpha}\to s}}$$
$$= \left[\frac{1}{\Xi}\sum_{N_\alpha\geq 2}\sum_{N_\beta\geq 0}\frac{1}{(N_\alpha-2)!N_\beta!}\right.$$
$$\left.\times\int \mathrm{d}\{N_\alpha-2\}_\alpha \mathrm{d}\{N_\beta\}_\beta \frac{\delta}{\delta e_{\beta\beta}(\boldsymbol{p},\boldsymbol{q})}\prod_{i<j}^{N_\beta} e_{\beta\beta}(\boldsymbol{r}_{i_\beta},\boldsymbol{r}_{j_\beta})\right]_{\substack{r_{1_\alpha}\to r\\ r_{2_\alpha}\to s}}$$
$$- c_{\beta\beta}e^{-1}_{\beta\beta}\varrho^{(2)}_{\beta\beta}(\boldsymbol{p},\boldsymbol{q})\varrho^{(2)}_{\alpha\alpha}(\boldsymbol{r},\boldsymbol{s})$$

This time, the functional derivative only gives one contribution, the $N_\beta(N_\beta-1)/2$ terms for the pairs $(r_{1_{\beta\geq 1}}, r_{j_\beta>i_\beta})$

$$e_{\beta\beta}(\boldsymbol{p},\boldsymbol{q})\frac{\delta\varrho^{(2)}_{\alpha\alpha}(\boldsymbol{r},\boldsymbol{s})}{\delta e_{\beta\beta}(\boldsymbol{p},\boldsymbol{q})} = c_{\beta\beta}\left(\varrho^{(4)}_{\alpha\alpha\beta\beta}(\boldsymbol{r},\boldsymbol{s},\boldsymbol{p},\boldsymbol{q}) - \varrho^{(2)}_{\alpha\alpha}(\boldsymbol{r},\boldsymbol{s})\varrho^{(2)}_{\beta\beta}(\boldsymbol{p},\boldsymbol{q})\right) \tag{7.30}$$

4. $\alpha\beta - \alpha\beta$

$$\begin{aligned}\frac{\delta\varrho^{(2)}_{\alpha\beta}(\boldsymbol{r},\boldsymbol{s})}{\delta e_{\alpha\beta}(\boldsymbol{p},\boldsymbol{q})} &= \frac{\delta}{\delta e_{\alpha\beta}(\boldsymbol{p},\boldsymbol{q})}\Bigg[\frac{1}{\Xi}\sum_{N_\alpha\geq 1}\sum_{N_\beta\geq 1}\frac{1}{(N_\alpha-1)!(N_\beta-1)!} \\ &\qquad\times\int \mathrm{d}\{N_\alpha-1\}_\alpha \mathrm{d}\{N_\beta-1\}_\beta \prod_{i=1}^{N_\alpha}\prod_{j=1}^{N_\beta} e_{\alpha\beta}(\boldsymbol{r}_{i_\alpha},\boldsymbol{r}_{j_\beta})\Bigg]_{\substack{r_{1_\alpha}\to r\\ r_{1_\beta}\to s}} \\ &= \Bigg[\frac{1}{\Xi}\sum_{N_\alpha\geq 1}\sum_{N_\beta\geq 1}\frac{1}{(N_\alpha-1)!(N_\beta-1)!} \\ &\qquad\times\int \mathrm{d}\{N_\alpha-1\}_\alpha \mathrm{d}\{N_\beta-1\}_\beta \frac{\delta}{\delta e_{\alpha\beta}(\boldsymbol{p},\boldsymbol{q})}\prod_{i=1}^{N_\alpha}\prod_{j=1}^{N_\beta} e_{\alpha\beta}(\boldsymbol{r}_{i_\alpha},\boldsymbol{r}_{j_\beta})\Bigg]_{\substack{r_{1_\alpha}\to r\\ r_{1_\beta}\to s}} \\ &\quad - c_{\alpha\beta}e^{-1}_{\alpha\beta}(\boldsymbol{q},\boldsymbol{q})\varrho^{(2)}(\boldsymbol{p},\boldsymbol{q})\varrho^{(2)}_{\alpha\beta}(\boldsymbol{r},\boldsymbol{s})\end{aligned}$$

The functional derivatives will give rise to four distinct terms: (a) a single term for the pair $(r_{1_\alpha}, r_{1_\beta})$, (b) $(N_\beta - 1)$ terms for the pairs $(r_{1_\alpha}, r_{j_{\beta\geq 2}})$, (c) $(N_\alpha - 1)$ terms for the pairs $(r_{i_{\alpha\geq 2}}, r_{1_\beta})$, and (d) $(N_\alpha - 1)(N_\beta - 1)$ terms for the pairs $(r_{i_{\alpha\geq 2}}, r_{j_{\beta\geq 2}})$

$$\begin{aligned}e_{\alpha\beta}(\boldsymbol{p},\boldsymbol{q})\frac{\delta\varrho^{(2)}_{\alpha\beta}(\boldsymbol{r},\boldsymbol{s})}{\delta e_{\alpha\beta}(\boldsymbol{p},\boldsymbol{q})} &= \delta(\boldsymbol{r}-\boldsymbol{p})\delta(\boldsymbol{s}-\boldsymbol{q})\varrho^{(2)}_{\alpha\beta}(\boldsymbol{r},\boldsymbol{s}) \\ &\quad + \delta(\boldsymbol{r}-\boldsymbol{p})\varrho^{(3)}_{\alpha\beta\beta}(\boldsymbol{r},\boldsymbol{s},\boldsymbol{q}) + \delta(\boldsymbol{s}-\boldsymbol{q})\varrho^{(3)}_{\alpha\beta\alpha}(\boldsymbol{r},\boldsymbol{s},\boldsymbol{p}) \\ &\quad + c_{\alpha\beta}\left(\varrho^{(4)}_{\alpha\beta\alpha\beta}(\boldsymbol{r},\boldsymbol{s},\boldsymbol{p},\boldsymbol{q}) - \varrho^{(2)}_{\alpha\beta}(\boldsymbol{r},\boldsymbol{s})\varrho^{(2)}_{\alpha\beta}(\boldsymbol{p},\boldsymbol{q})\right)\end{aligned} \tag{7.31}$$

5. $\alpha\alpha - \beta\nu$

$$\begin{aligned}\frac{\delta\varrho^{(2)}_{\alpha\alpha}(\boldsymbol{r},\boldsymbol{s})}{\delta e_{\beta\nu}(\boldsymbol{p},\boldsymbol{q})} &= \frac{\delta}{\delta e_{\beta\nu}(\boldsymbol{p},\boldsymbol{q})}\Bigg[\frac{1}{\Xi}\sum_{N_\alpha\geq 2}\sum_{N_\beta\geq 0}\sum_{N_\nu\geq 0}\frac{1}{(N_\alpha-2)!N_\beta!N_\nu!} \\ &\qquad\times\int \mathrm{d}\{N_\alpha-2\}_\alpha \mathrm{d}\{N_\beta\}_\beta \mathrm{d}\{N_\nu\}_\nu \prod_{i=1}^{N_\beta}\prod_{j=1}^{N_\nu} e_{\beta\nu}(\boldsymbol{r}_{i_\beta},\boldsymbol{r}_{j_\nu})\Bigg]_{\substack{r_{1_\alpha}\to r\\ r_{2_\alpha}\to s}} \\ &= \Bigg[\frac{1}{\Xi}\sum_{N_\alpha\geq 2}\sum_{N_\beta\geq 0}\sum_{N_\nu\geq 0}\frac{1}{(N_\alpha-2)!N_\beta!N_\nu!} \\ &\qquad\times\int \mathrm{d}\{N_\alpha-2\}_\alpha \mathrm{d}\{N_\beta\}_\beta \mathrm{d}\{N_\nu\}_\nu \frac{\delta}{\delta e_{\beta\nu}(\boldsymbol{p},\boldsymbol{q})}\prod_{i=1}^{N_\beta}\prod_{j=1}^{N_\nu} e_{\beta\nu}(\boldsymbol{r}_{i_\beta},\boldsymbol{r}_{j_\nu})\Bigg]_{\substack{r_{1_\alpha}\to r\\ r_{2_\alpha}\to s}} \\ &\quad - c_{\beta\nu}e^{-1}_{\beta\nu}(\boldsymbol{p},\boldsymbol{q})\varrho^{(2)}_{\beta\nu}(\boldsymbol{p},\boldsymbol{q})\varrho^{(2)}_{\alpha\alpha}(\boldsymbol{r},\boldsymbol{s})\end{aligned}$$

As with case (3), we only obtain one contribution from the functional derivative, the

$N_\beta N_\nu$ terms corresponding to the pairs $(r_{i_\beta \geq 1}, r_{j_\nu \geq 1})$

$$e_{\beta\nu}(\boldsymbol{p},\boldsymbol{q})\frac{\delta\varrho^{(2)}_{\alpha\alpha}(\boldsymbol{r},\boldsymbol{s})}{\delta e_{\beta\nu}(\boldsymbol{p},\boldsymbol{q})} = c_{\beta\nu}\left[\varrho^{(4)}_{\alpha\alpha\beta\nu}(\boldsymbol{r},\boldsymbol{s},\boldsymbol{p},\boldsymbol{q}) - \varrho^{(2)}_{\alpha\alpha}(\boldsymbol{r},\boldsymbol{s})\varrho^{(2)}_{\beta\nu}(\boldsymbol{p},\boldsymbol{q})\right] \tag{7.32}$$

6. $\alpha\beta - \alpha\nu$

$$\begin{aligned}\frac{\delta\varrho^{(2)}_{\alpha\beta}(\boldsymbol{r},\boldsymbol{s})}{\delta e_{\alpha\nu}(\boldsymbol{p},\boldsymbol{q})} &= \frac{\delta}{\delta e_{\alpha\nu}(\boldsymbol{p},\boldsymbol{q})}\left[\frac{1}{\Xi}\sum_{N_\alpha\geq 1}\sum_{N_\beta\geq 1}\sum_{N_\nu\geq 0}\frac{1}{(N_\alpha-1)!(N_\beta-1)!N_\nu!}\right.\\ &\qquad\left.\times\int \mathrm{d}\{N_\alpha-1\}_\alpha\mathrm{d}\{N_\beta-1\}_\beta\mathrm{d}\{N_\nu\}_\nu\prod_{i=1}^{N_\alpha}\prod_{j=1}^{N_\nu}e_{\alpha\nu}(\boldsymbol{r}_{i_\alpha},\boldsymbol{r}_{j_\nu})\right]_{\substack{r_{1_\alpha}\to r\\ r_{1_\beta}\to s}}\\ &= \left[\frac{1}{\Xi}\sum_{N_\alpha\geq 1}\sum_{N_\beta\geq 1}\sum_{N_\nu\geq 0}\frac{1}{(N_\alpha-1)!(N_\beta-1)!N_\nu!}\right.\\ &\qquad\left.\times\int \mathrm{d}\{N_\alpha-1\}_\alpha\mathrm{d}\{N_\beta-1\}_\beta\mathrm{d}\{N_\nu\}_\nu\frac{\delta}{\delta e_{\alpha\nu}(\boldsymbol{p},\boldsymbol{q})}\prod_{i=1}^{N_\alpha}\prod_{j=1}^{N_\nu}e_{\alpha\nu}(\boldsymbol{r}_{i_\alpha},\boldsymbol{r}_{j_\nu})\right]_{\substack{r_{1_\alpha}\to r\\ r_{1_\beta}\to s}}\\ &\quad - c_{\alpha\nu}e^{-1}_{\alpha\nu}(\boldsymbol{p},\boldsymbol{q})\varrho^{(2)}_{\alpha\nu}(\boldsymbol{p},\boldsymbol{q})\varrho^{(2)}_{\alpha\beta}(\boldsymbol{r},\boldsymbol{s})\end{aligned}$$

The functional derivative will give two distinct contributions: (a) N_ν terms for the pairs $(r_{1_\alpha}, r_{j_\nu\geq 1})$ and (b) $(N_\alpha - 1)N_\nu$ terms for the pairs $(r_{i_\alpha\geq 2}, r_{j_\nu\geq 1})$

$$\begin{aligned}e_{\alpha\nu}(\boldsymbol{p},\boldsymbol{q})\frac{\delta\varrho^{(2)}_{\alpha\beta}(\boldsymbol{r},\boldsymbol{s})}{\delta e_{\alpha\nu}(\boldsymbol{p},\boldsymbol{q})} &= \delta(\boldsymbol{r}-\boldsymbol{p})\varrho^{(3)}_{\alpha\beta\nu}(\boldsymbol{r},\boldsymbol{s},\boldsymbol{q})\\ &\quad + c_{\alpha\nu}\left[\varrho^{(4)}_{\alpha\beta\alpha\nu}(\boldsymbol{r},\boldsymbol{s},\boldsymbol{p},\boldsymbol{q}) - \varrho^{(2)}_{\alpha\beta}(\boldsymbol{r},\boldsymbol{s})\varrho^{(2)}_{\alpha\nu}(\boldsymbol{p},\boldsymbol{q})\right]\end{aligned} \tag{7.33}$$

7. $\alpha\beta - \nu\eta$

$$\begin{aligned}\frac{\delta\varrho^{(2)}_{\alpha\beta}(\boldsymbol{r},\boldsymbol{s})}{\delta e_{\nu\eta}(\boldsymbol{p},\boldsymbol{q})} &= \frac{\delta}{\delta e_{\nu\eta}(\boldsymbol{p},\boldsymbol{q})}\left[\frac{1}{\Xi}\sum_{N_\alpha\geq 1}\sum_{N_\beta\geq 1}\sum_{N_\nu\geq 0}\sum_{N_\eta\geq 0}\frac{1}{(N_\alpha-1)!(N_\beta-1)!N_\nu!N_\eta!}\right.\\ &\qquad\left.\times\int \mathrm{d}\{N_\alpha-1\}_\alpha\mathrm{d}\{N_\beta-1\}_\beta\mathrm{d}\{N_\nu\}_\nu\mathrm{d}\{N_\eta\}_\eta\prod_{i=1}^{N_\nu}\prod_{j=1}^{N_\eta}e_{\nu\eta}(\boldsymbol{r}_{i_\nu},\boldsymbol{r}_{j_\eta})\right]_{\substack{r_{1_\alpha}\to r\\ r_{1_\beta}\to s}}\\ &= \left[\frac{1}{\Xi}\sum_{N_\alpha\geq 1}\sum_{N_\beta\geq 1}\sum_{N_\nu\geq 0}\sum_{N_\eta\geq 0}\frac{1}{(N_\alpha-1)!(N_\beta-1)!N_\nu!N_\eta!}\right.\\ &\qquad\int \mathrm{d}\{N_\alpha-1\}_\alpha\mathrm{d}\{N_\beta-1\}_\beta\mathrm{d}\{N_\nu\}_\nu\\ &\qquad\left.\times\,\mathrm{d}\{N_\eta\}_\eta\frac{\delta}{\delta e_{\nu\eta}(\boldsymbol{p},\boldsymbol{q})}\prod_{i=1}^{N_\nu}\prod_{j=1}^{N_\eta}e_{\nu\eta}(\boldsymbol{r}_{i_\nu},\boldsymbol{r}_{j_\eta})\right]_{\substack{r_{1_\alpha}\to r\\ r_{1_\beta}\to s}}\\ &\quad - c_{\nu\eta}e^{-1}_{\nu\eta}(\boldsymbol{p},\boldsymbol{q})\varrho^{(2)}_{\nu\eta}(\boldsymbol{p},\boldsymbol{q})\varrho^{(2)}_{\alpha\beta}(\boldsymbol{r},\boldsymbol{s})\end{aligned}$$

As with cases (3) and (5), we only obtain one distinct contribution from the functional derivatives, the $N_\beta N_\nu$ terms for the pairs $(r_{i_\beta \geq 1}, r_{j_\nu \geq 1})$, so that

$$e_{\nu\eta}(\boldsymbol{p},\boldsymbol{q})\frac{\delta \varrho^{(2)}_{\alpha\beta}(\boldsymbol{r},\boldsymbol{s})}{\delta e_{\nu\eta}(\boldsymbol{p},\boldsymbol{q})} = c_{\nu\eta}\left(\varrho^{(4)}_{\alpha\beta\nu\eta}(\boldsymbol{r},\boldsymbol{s},\boldsymbol{p},\boldsymbol{q}) - \varrho^{(2)}_{\alpha\beta}(\boldsymbol{r},\boldsymbol{s})\varrho^{(2)}_{\nu\eta}(\boldsymbol{p},\boldsymbol{q})\right) \tag{7.34}$$

Summary:
Finally, Eqs. (7.25), (7.27), and (7.28) – (7.34), can be expressed in the following generalized form

$$\frac{e_{\nu\mu}(\boldsymbol{p},\boldsymbol{q})}{c_{\nu\mu}}\left.\frac{\delta \ln \Xi}{\delta e_{\nu\mu}(\boldsymbol{p},\boldsymbol{q})}\right|_{\boldsymbol{\mu}} = \varrho^{(2)}_{\nu\mu}(\boldsymbol{p},\boldsymbol{q}) \tag{7.35a}$$

$$\begin{aligned}\frac{e_{\alpha\beta}(\boldsymbol{r},\boldsymbol{s})}{c_{\nu\eta}c_{\alpha\beta}}\left.\frac{\delta^2 \ln \Xi}{\delta e_{\nu\eta}(\boldsymbol{p},\boldsymbol{q})\,\delta e_{\alpha\beta}(\boldsymbol{r},\boldsymbol{s})}\right|_{\boldsymbol{\mu}} &= c^{-1}_{\nu\eta}\frac{\delta \varrho^{(2)}_{\alpha\beta}(\boldsymbol{r},\boldsymbol{s})}{\delta e_{\nu\eta}(\boldsymbol{p},\boldsymbol{q})} \\ &\quad - \delta_{\alpha\nu}\delta_{\beta\eta}\delta(\boldsymbol{r}-\boldsymbol{p})\delta(\boldsymbol{s}-\boldsymbol{q})e^{-1}_{\alpha\beta}(\boldsymbol{r},\boldsymbol{s})\varrho^{(2)}_{\alpha\beta}(\boldsymbol{r},\boldsymbol{s}) \\ &\quad - \delta_{\alpha\eta}\delta_{\beta\nu}\delta(\boldsymbol{r}-\boldsymbol{q})\delta(\boldsymbol{s}-\boldsymbol{p})e^{-1}_{\alpha\beta}(\boldsymbol{r},\boldsymbol{s})\varrho^{(2)}_{\alpha\beta}(\boldsymbol{r},\boldsymbol{s})\end{aligned} \tag{7.35b}$$

$$\begin{aligned}\frac{e_{\nu\eta}(\boldsymbol{p},\boldsymbol{q})}{c_{\nu\eta}}\left.\frac{\delta \varrho^{(2)}_{\alpha\beta}(\boldsymbol{r},\boldsymbol{s})}{\delta e_{\nu\eta}(\boldsymbol{p},\boldsymbol{q})}\right|_{\boldsymbol{\mu}} &= \varrho^{(4)}_{\alpha\beta\nu\eta}(\boldsymbol{r},\boldsymbol{s},\boldsymbol{p},\boldsymbol{q}) - \varrho^{(2)}_{\alpha\beta}(\boldsymbol{r},\boldsymbol{s})\varrho^{(2)}_{\nu\eta}(\boldsymbol{p},\boldsymbol{q}) \\ &\quad + \delta_{\alpha\nu}\delta_{\beta\eta}\delta(\boldsymbol{r}-\boldsymbol{p})\delta(\boldsymbol{s}-\boldsymbol{q})\varrho^{(2)}_{\alpha\beta}(\boldsymbol{r},\boldsymbol{s}) \\ &\quad + \delta_{\alpha\eta}\delta_{\beta\nu}\delta(\boldsymbol{r}-\boldsymbol{q})\delta(\boldsymbol{s}-\boldsymbol{p})\varrho^{(2)}_{\alpha\beta}(\boldsymbol{r},\boldsymbol{s}) \\ &\quad + \left(\delta_{\alpha\nu}\delta(\boldsymbol{r}-\boldsymbol{p}) + \delta_{\beta\nu}\delta(\boldsymbol{s}-\boldsymbol{p})\right)\varrho^{(3)}_{\alpha\beta\eta}(\boldsymbol{r},\boldsymbol{s},\boldsymbol{q}) \\ &\quad + \left(\delta_{\alpha\eta}\delta(\boldsymbol{r}-\boldsymbol{q}) + \delta_{\beta\eta}\delta(\boldsymbol{s}-\boldsymbol{q})\right)\varrho^{(3)}_{\alpha\beta\nu}(\boldsymbol{r},\boldsymbol{s},\boldsymbol{p})\end{aligned} \tag{7.35c}$$

$$\frac{e_{\nu\eta}(\boldsymbol{p},\boldsymbol{q})}{c_{\nu\eta}}\left.\frac{\delta \varrho^{(2)}_{\alpha\beta}(\boldsymbol{r},\boldsymbol{s})}{\delta e_{\nu\eta}(\boldsymbol{p},\boldsymbol{q})}\right|_{\boldsymbol{\mu}} = \frac{e_{\alpha\beta}(\boldsymbol{r},\boldsymbol{s})}{c_{\alpha\beta}}\left.\frac{\delta \varrho^{(2)}_{\nu\eta}(\boldsymbol{p},\boldsymbol{q})}{\delta e_{\alpha\beta}(\boldsymbol{r},\boldsymbol{s})}\right|_{\boldsymbol{\mu}} \tag{7.35d}$$

where $c_{\alpha\beta} = 1 - \delta_{\alpha\beta}/2$.
Practically the same results could have been obtained using the γ-perturbation representation (which we used to derive the relationships between derivatives in both ensembles), instead of considering the thermodynamic functions as functionals of the interaction potentials. We have basically treated the two representations as interchangeable (we derived Eq. (7.22) assuming a perturbation given by the γ parameter); however, the results that are obtained for the second order derivative are not exactly the same (an additional term involving the second order derivative of the interaction potentials appears). This should be taken into account when comparing our results with those given by Barker and Henderson [36, 181], for the one-component case.

7.5 Case Study: A Two Component system (AB non-additivity)

7.5.1 Model

We now focus on the two-component hard-sphere system with non-additive AB interactions considered in Ref [7]. Let σ_A and σ_B be the hard-sphere diameters, the distances

of closest approach for the three pairs are

$$\begin{aligned}\sigma_{\mathrm{AA}} &= \sigma_{\mathrm{A}} \\ \sigma_{\mathrm{BB}} &= \sigma_{\mathrm{B}} \\ \sigma_{\mathrm{AB}} &= \frac{1}{2}(\sigma_{\mathrm{A}} + \sigma_{\mathrm{B}})(1+\Delta)\end{aligned} \tag{7.36}$$

where $\Delta > 0$ is the dimensionless non-additivity parameter. The hard sphere potentials are given by

$$v_{\nu\eta} = \begin{cases}\infty, & r < \sigma_{\mathrm{AB}} \\ 0, & r > \sigma_{\mathrm{AB}}; \quad \nu, \eta = \text{A or B}\end{cases} \tag{7.37}$$

For a perturbation calculation, the natural reference is evidently the additive hard-sphere system ($\Delta = 0$). The perturbation[3] in the AB interactions is then

$$w_{\mathrm{AB}}(r) = \begin{cases}0, & r < \frac{1}{2}(\sigma_{\mathrm{A}} + \sigma_{\mathrm{B}}) \\ \infty, & \frac{1}{2}(\sigma_{\mathrm{A}} + \sigma_{\mathrm{B}}) < r < \sigma_{\mathrm{AB}} \\ 0, & r > \sigma_{\mathrm{AB}}\end{cases} \tag{7.38}$$

and the so-called blip function is given by

$$\Delta e_{\mathrm{AB}}(r) = \begin{cases}0, & r < \frac{1}{2}(\sigma_{\mathrm{A}} + \sigma_{\mathrm{B}}) \\ -1, & \frac{1}{2}(\sigma_{\mathrm{A}} + \sigma_{\mathrm{B}}) < r < \sigma_{\mathrm{AB}} \\ 0, & r > \sigma_{\mathrm{AB}}\end{cases} \tag{7.39}$$

For what follows, we define the following functions

$$f_{\mathrm{AB}}(\boldsymbol{r}, \boldsymbol{r}') = \frac{\Delta e_{\mathrm{AB}}(\boldsymbol{r}, \boldsymbol{r}')}{e^{(0)}(\boldsymbol{r}, \boldsymbol{r}')} = e^{-\beta w_{\mathrm{AB}}(\boldsymbol{r}, \boldsymbol{r}')} - 1 \tag{7.40a}$$

$$\Theta_{\mathrm{AB}}(\boldsymbol{r}, \boldsymbol{r}') = f_{\mathrm{AB}}(\boldsymbol{r}, \boldsymbol{r}') g_{\mathrm{AB}}(\boldsymbol{r}, \boldsymbol{r}') \tag{7.40b}$$

7.5.2 Functional Expansion

For convenience, we will use $\boldsymbol{r}$ and $\boldsymbol{s}$ to denote the position vectors of A and B particles, respectively, and $\boldsymbol{p}$ and $\boldsymbol{q}$ for arbitrary particles. To second order, the functional Taylor expansion of the free energy for this non-additive AB system is given by (Eq. (7.14))

$$\begin{aligned}F = F_0 &+ \iint \mathrm{d}\boldsymbol{r}_1' \mathrm{d}\boldsymbol{s}_1' \Delta e_{AB}(\boldsymbol{r}_1', \boldsymbol{s}_1') \left.\frac{\delta F}{\delta e_{AB}(\boldsymbol{r}_1', \boldsymbol{s}_1')}\right|_{\boldsymbol{N}, e=e^{(0)}} \\ &+ \frac{1}{2} \iiiint \mathrm{d}\boldsymbol{r}_1' \mathrm{d}\boldsymbol{r}_2' \mathrm{d}\boldsymbol{s}_1' \mathrm{d}\boldsymbol{s}_2' \Delta e_{AB}(\boldsymbol{r}_1', \boldsymbol{s}_1') \Delta e_{AB}(\boldsymbol{r}_2', \boldsymbol{s}_2') \\ &\times \left.\frac{\delta^2 F}{\delta e_{AB}(\boldsymbol{r}_2', \boldsymbol{s}_2')\, \delta e_{AB}(\boldsymbol{r}_1', \boldsymbol{s}_1')}\right|_{\boldsymbol{N}, e=e^{(0)}}\end{aligned} \tag{7.41}$$

[3]For clarity, and following Ref [7], we use w and not δv to denote the perturbation, so as to differentiate it from a functional derivative.

the corresponding expansion for the pair densities, to first order, is

$$\rho_X(\boldsymbol{p},\boldsymbol{q}) = \rho_X^{(0)}(\boldsymbol{p},\boldsymbol{q}) + \iint \mathrm{d}\boldsymbol{r}_1'\mathrm{d}\boldsymbol{s}_1' \Delta e_{\mathrm{AB}}(\boldsymbol{r}_1',\boldsymbol{s}_1') \left.\frac{\delta\rho_X(\boldsymbol{p},\boldsymbol{q})}{\delta e_{AB}(\boldsymbol{r}_1',\boldsymbol{s}_1')}\right|_{\boldsymbol{N},e=e^{(0)}} \tag{7.42}$$

where $X = \mathrm{AA}, \mathrm{BB}, \mathrm{AB}$. The functional derivatives appearing here will be evaluated in the grand-canonical ensemble, allowing us to express the perturbation in terms of the two, three, and four-body density functions of an open system. From Equations (7.35), we have

$$e_{\mathrm{AB}}(\boldsymbol{r}_1,\boldsymbol{s}_1) \left.\frac{\delta \ln \Xi}{\delta e_{\mathrm{AB}}(\boldsymbol{r}_1,\boldsymbol{s}_1)}\right|_{\boldsymbol{\mu}} = \varrho_{\mathrm{AB}}(\boldsymbol{r}_1,\boldsymbol{s}_1) \tag{7.43a}$$

$$\begin{aligned} e_{\mathrm{AB}}(\boldsymbol{r}_1',\boldsymbol{s}_1') \left.\frac{\delta \varrho_{\mathrm{AA}}(\boldsymbol{r}_1,\boldsymbol{r}_2)}{\delta e_{\mathrm{AB}}(\boldsymbol{r}_1',\boldsymbol{s}_1')}\right|_{\boldsymbol{\mu}} &= \big(\delta(\boldsymbol{r}_1-\boldsymbol{r}_1') + \delta(\boldsymbol{r}_2-\boldsymbol{r}_1')\big)\, \varrho_{\mathrm{AAB}}(\boldsymbol{r}_1,\boldsymbol{r}_2,\boldsymbol{s}_1') \\ &\quad + \varrho_{\mathrm{AAAB}}(\boldsymbol{r}_1,\boldsymbol{r}_2,\boldsymbol{r}_1',\boldsymbol{s}_1') - \varrho_{\mathrm{AA}}(\boldsymbol{r}_1,\boldsymbol{r}_2)\varrho_{\mathrm{AB}}(\boldsymbol{r}_1',\boldsymbol{s}_1') \end{aligned} \tag{7.43b}$$

$$\begin{aligned} e_{\mathrm{AB}}(\boldsymbol{r}_1',\boldsymbol{s}_1') \left.\frac{\delta \varrho_{\mathrm{BB}}(\boldsymbol{s}_1,\boldsymbol{s}_2)}{\delta e_{\mathrm{AB}}(\boldsymbol{r}_1',\boldsymbol{s}_1')}\right|_{\boldsymbol{\mu}} &= \big(\delta(\boldsymbol{s}_1-\boldsymbol{s}_1') + \delta(\boldsymbol{s}_2-\boldsymbol{s}_1')\big)\, \varrho_{\mathrm{BBA}}(\boldsymbol{s}_1,\boldsymbol{s}_2,\boldsymbol{r}_1') \\ &\quad + \varrho_{\mathrm{BBAB}}(\boldsymbol{s}_1,\boldsymbol{s}_2,\boldsymbol{r}_1',\boldsymbol{s}_1') - \varrho_{\mathrm{BB}}(\boldsymbol{s}_1,\boldsymbol{s}_2)\varrho_{\mathrm{AB}}(\boldsymbol{r}_1',\boldsymbol{s}_1') \end{aligned} \tag{7.43c}$$

$$\begin{aligned} e_{\mathrm{AB}}(\boldsymbol{r}_1',\boldsymbol{s}_1') \left.\frac{\delta \varrho_{\mathrm{AB}}(\boldsymbol{r}_1,\boldsymbol{s}_1)}{\delta e_{\mathrm{AB}}(\boldsymbol{r}_1',\boldsymbol{s}_1')}\right|_{\boldsymbol{\mu}} &= \delta(\boldsymbol{r}_1-\boldsymbol{r}_1')\delta(\boldsymbol{s}_1-\boldsymbol{s}_1')\varrho_{\mathrm{AB}}(\boldsymbol{r}_1,\boldsymbol{s}_1) \\ &\quad + \delta(\boldsymbol{r}_1-\boldsymbol{r}_1')\varrho_{\mathrm{ABB}}(\boldsymbol{r}_1,\boldsymbol{s}_1,\boldsymbol{s}_1') \\ &\quad + \delta(\boldsymbol{s}_1-\boldsymbol{s}_1')\varrho_{\mathrm{ABA}}(\boldsymbol{r}_1,\boldsymbol{s}_1,\boldsymbol{r}_1') \\ &\quad + \varrho_{\mathrm{ABAB}}(\boldsymbol{r}_1,\boldsymbol{s}_1,\boldsymbol{r}_1',\boldsymbol{s}_1') - \varrho_{\mathrm{AB}}(\boldsymbol{r}_1,\boldsymbol{s}_1)\varrho_{\mathrm{AB}}(\boldsymbol{r}_1',\boldsymbol{s}_1') \end{aligned} \tag{7.43d}$$

$$\begin{aligned} e_{\mathrm{AB}}(\boldsymbol{r}_1,\boldsymbol{s}_1) \left.\frac{\delta^2 \ln \Xi}{\delta e_{\mathrm{AB}}(\boldsymbol{r}_1',\boldsymbol{s}_1')\,\delta e_{\mathrm{AB}}(\boldsymbol{r}_1,\boldsymbol{s}_1)}\right|_{\boldsymbol{\mu}} &= -\delta(\boldsymbol{r}_1-\boldsymbol{r}_1{}')\delta(\boldsymbol{s}_1-\boldsymbol{s}_1')e_{\mathrm{AB}}^{-1}(\boldsymbol{r}_1,\boldsymbol{s}_1)\varrho_{\mathrm{AB}}(\boldsymbol{r}_1,\boldsymbol{s}_1) \\ &\quad + \left.\frac{\delta \varrho_{\mathrm{AB}}(\boldsymbol{r}_1,\boldsymbol{s}_1)}{\delta e_{\mathrm{AB}}(\boldsymbol{r}_1',\boldsymbol{s}_1')}\right|_{\boldsymbol{\mu}} \end{aligned} \tag{7.43e}$$

Using Eqs. (7.15c), (7.20), and (7.43a) the functional derivatives of the two-particle density (for a closed system) can be expressed as

$$\begin{aligned} \left.\frac{\delta\rho_X(\boldsymbol{p},\boldsymbol{q})}{\delta e_{AB}(\boldsymbol{r}_1,\boldsymbol{s}_1)}\right|_{\boldsymbol{N}} &= \left.\frac{\delta\varrho_X(\boldsymbol{p},\boldsymbol{q})}{\delta e_{\mathrm{AB}}(\boldsymbol{r}_1,\boldsymbol{s}_1)}\right|_{\boldsymbol{\mu}} \\ &\quad - k_{\mathrm{B}}T e_{\mathrm{AB}}^{-1}(\boldsymbol{r}_1,\boldsymbol{s}_1) \sum_{\nu=\mathrm{A,B}} \sum_{\eta=\mathrm{A,B}} (B^{-1})_{\nu\eta} \left(\frac{\partial}{\partial\mu_\nu}\varrho_X(\boldsymbol{p},\boldsymbol{q})\right)\left(\frac{\partial}{\partial\mu_\eta}\varrho_{\mathrm{AB}}(\boldsymbol{r}_1,\boldsymbol{s}_1)\right) \end{aligned}$$

and the functional derivatives of the free energy are given by Eq. (7.22), which in this case reduces to

$$\left.\frac{\delta F}{\delta e_{AB}(\boldsymbol{r}_1,\boldsymbol{s}_1)}\right|_{\boldsymbol{N}} = -k_{\mathrm{B}}T e_{\mathrm{AB}}^{-1}(\boldsymbol{r}_1,\boldsymbol{s}_1)\varrho_{\mathrm{AB}}(\boldsymbol{r}_1,\boldsymbol{s}_1) \tag{7.44}$$

and

$$\begin{aligned} &\left.\frac{\delta^2 F}{\delta e_{AB}(\boldsymbol{r}_2,\boldsymbol{s}_2)\,\delta e_{AB}(\boldsymbol{r}_1,\boldsymbol{s}_1)}\right|_{\boldsymbol{N}} \\ &\quad = k_{\mathrm{B}}T e_{\mathrm{AB}}^{-1}(\boldsymbol{r}_1,\boldsymbol{s}_1)\Bigg\{\delta(\boldsymbol{r}_1-\boldsymbol{r}_1)\delta(\boldsymbol{s}_1-\boldsymbol{s}_2)e_{\mathrm{AB}}^{-1}(\boldsymbol{r}_1,\boldsymbol{s}_1)\varrho_{\mathrm{AB}}(\boldsymbol{r}_1,\boldsymbol{s}_1) - \left.\frac{\delta\varrho_{\mathrm{AB}}(\boldsymbol{r}_1,\boldsymbol{s}_1)}{\delta e_{\mathrm{AB}}(\boldsymbol{r}_2,\boldsymbol{s}_2)}\right|_{\boldsymbol{\mu}} \\ &\quad + k_{\mathrm{B}}T e_{\mathrm{AB}}^{-1}(\boldsymbol{r}_2,\boldsymbol{s}_2) \sum_{\nu=A,B} \sum_{\eta=A,B} (B^{-1})_{\nu\mu} \left(\frac{\partial\varrho_{\mathrm{AB}}(\boldsymbol{r}_1,\boldsymbol{s}_1)}{\partial\mu_\nu}\right)\left(\frac{\partial\varrho_{\mathrm{AB}}(\boldsymbol{r}_2,\boldsymbol{s}_2)}{\partial\mu_\eta}\right)\Bigg\} \end{aligned} \tag{7.45}$$

where

$$\mathrm{B} = \begin{pmatrix} \left(\frac{\partial \overline{N}_A}{\partial \mu_A}\right)_{\mu_B} & \left(\frac{\partial \overline{N}_A}{\partial \mu_B}\right)_{\mu_A} \\ \left(\frac{\partial \overline{N}_B}{\partial \mu_A}\right)_{\mu_B} & \left(\frac{\partial \overline{N}_B}{\partial \mu_B}\right)_{\mu_A} \end{pmatrix}$$

Let $\Delta_1\rho_X$ be the first order correction to the canonical two-particle density, such that

$$\begin{aligned} \Delta_1\rho_X(\boldsymbol{p},\boldsymbol{q}) &= \iint \mathrm{d}\boldsymbol{r}_1'\mathrm{d}\boldsymbol{s}_1'\Delta e_{AB}(\boldsymbol{r}_1',\boldsymbol{s}_1')\left.\frac{\delta\rho_X(\boldsymbol{p},\boldsymbol{q})}{\delta e_{AB}(\boldsymbol{r}_1',\boldsymbol{s}_1')}\right|_{\boldsymbol{N},e=e^{(0)}} \qquad (7.46)\\ &= \iint \mathrm{d}\boldsymbol{r}'\mathrm{d}\boldsymbol{s}'\Delta e_{\mathrm{AB}}(\boldsymbol{r}_1',\boldsymbol{s}_1')\left.\frac{\delta\varrho_X(\boldsymbol{p},\boldsymbol{q})}{\delta e_{\mathrm{AB}}(\boldsymbol{r}_1',\boldsymbol{s}_1')}\right|_{\boldsymbol{\mu},e=e^{(0)}} \\ &\quad - k_{\mathrm{B}}T\sum_\nu\sum_\eta (B^{-1})_{\nu\eta}\left(\frac{\partial\varrho_X^{(0)}(\boldsymbol{p},\boldsymbol{q})}{\partial\mu_\nu}\right) \\ &\quad\quad \times\left(\frac{\partial}{\partial\mu_\eta}\iint \mathrm{d}\boldsymbol{r}_1'\mathrm{d}\boldsymbol{s}_1' f_{\mathrm{AB}}(\boldsymbol{r}_1',\boldsymbol{s}_1')\varrho_X^{(0)}(\boldsymbol{p},\boldsymbol{q})\right) \\ &\equiv \Delta_1\varrho_X(\boldsymbol{p},\boldsymbol{q}) + \Delta_\infty\varrho_X(\boldsymbol{p},\boldsymbol{q}) \qquad (7.47) \end{aligned}$$

which we write in terms of its grand-canonical counterpart $\Delta_1\varrho_X(\boldsymbol{p},\boldsymbol{q})$ plus a correction term $\Delta_\infty\varrho_X(\boldsymbol{p},\boldsymbol{q})$

$$\Delta_1\varrho_X(\boldsymbol{p},\boldsymbol{q}) = \iint \mathrm{d}\boldsymbol{r}_1'\mathrm{d}\boldsymbol{s}_1'\Delta e_{\mathrm{AB}}(\boldsymbol{r}_1',\boldsymbol{s}_1')\left.\frac{\delta\varrho_X(\boldsymbol{p},\boldsymbol{q})}{\delta e_{\mathrm{AB}}(\boldsymbol{r}_1',\boldsymbol{s}_1')}\right|_{\boldsymbol{\mu},e=e^{(0)}} \qquad (7.48)$$

$$\begin{aligned} \Delta_\infty\varrho_X(\boldsymbol{p},\boldsymbol{q}) &= -k_{\mathrm{B}}T\sum_\nu\sum_\nu (B^{-1})_{\nu\mu}\left(\frac{\partial\varrho_X^{(0)}(\boldsymbol{p},\boldsymbol{q})}{\partial\mu_\nu}\right) \qquad (7.49)\\ &\quad\quad \times\left(\frac{\partial}{\partial\mu_\eta}\iint \mathrm{d}\boldsymbol{r}_1'\mathrm{d}\boldsymbol{s}_1' f_{\mathrm{AB}}(\boldsymbol{r}_1',\boldsymbol{s}_1')\varrho_X^{(0)}(\boldsymbol{p},\boldsymbol{q})\right) \end{aligned}$$

The perturbation expansion for the free energy (Eq. (7.41)) can be expressed as $F = F^{(0)} + F_1 + F_2$, with

$$F_1 = -k_{\mathrm{B}}T\iint \mathrm{d}\boldsymbol{r}_1\mathrm{d}\boldsymbol{s}_1 f_{\mathrm{AB}}(\boldsymbol{r}_1,\boldsymbol{s}_1)\varrho_{\mathrm{AB}}^{(0)}(\boldsymbol{r}_1,\boldsymbol{s}_1) \qquad (7.50a)$$

$$\begin{aligned} F_2 = \frac{1}{2}k_{\mathrm{B}}T\iint \mathrm{d}\boldsymbol{r}_1\mathrm{d}\boldsymbol{s}_1 f_{\mathrm{AB}}(\boldsymbol{r}_1,\boldsymbol{s}_1)\Big[& f_{\mathrm{AB}}(\boldsymbol{r}_1,\boldsymbol{s}_1)\varrho_{\mathrm{AB}}^{(0)}(\boldsymbol{r}_1,\boldsymbol{s}_1) - \Delta_1\varrho_{\mathrm{AB}}(\boldsymbol{r}_1,\boldsymbol{s}_1) \\ & - \Delta_\infty\varrho_{\mathrm{AB}}(\boldsymbol{r}_1,\boldsymbol{s}_1)\Big] \qquad (7.50b) \end{aligned}$$

and that for the two particle density as $\rho_X(\boldsymbol{p},\boldsymbol{q}) = \rho_X^{(0)}(\boldsymbol{p},\boldsymbol{q}) + \Delta_1\varrho_X(\boldsymbol{p},\boldsymbol{q}) + \Delta_\infty\varrho_X(\boldsymbol{p},\boldsymbol{q})$. All the results given up to this point are exact; however, they are of no use since they require the three and four-particle density functions. Therefore, we use the standard Kirkwood superposition approximation to approximate these functions, in terms of the two-particle densities ϱ_{AA}, ϱ_{BB}, and ϱ_{AB}.

We need to evaluate the first-order correction to the two-body distribution function $\Delta_1\varrho_X(\boldsymbol{p},\boldsymbol{q})$, which appears in both the free energy (second order) and pair distribution

function expansion (first order). From Eqs. (7.48) and (7.43) we have

$$\begin{aligned}
\frac{\Delta_1 \varrho_{\mathrm{AA}}(\boldsymbol{r}_1, \boldsymbol{r}_2)}{\varrho_{\mathrm{A}}^2} &= \varrho_{\mathrm{B}} g_{\mathrm{AA}}(\boldsymbol{r}_1, \boldsymbol{r}_2) \int \mathrm{d}\boldsymbol{s}_1' \Theta_{\mathrm{AB}}(\boldsymbol{r}_1, \boldsymbol{s}_1') g_{\mathrm{AB}}(\boldsymbol{r}_2, \boldsymbol{s}_1') \qquad (7.51a) \\
&\quad + \varrho_{\mathrm{B}} g_{\mathrm{AA}}(\boldsymbol{r}_1, \boldsymbol{r}_2) \int \mathrm{d}\boldsymbol{s}_1' \Theta_{\mathrm{AB}}(\boldsymbol{r}_2, \boldsymbol{s}_1') g_{\mathrm{AB}}(\boldsymbol{r}_1, \boldsymbol{s}_1') \\
&\quad + \varrho_{\mathrm{A}} \varrho_{\mathrm{B}} g_{\mathrm{AA}}(\boldsymbol{r}_1, \boldsymbol{r}_2) \iint \mathrm{d}\boldsymbol{r}_1' \mathrm{d}\boldsymbol{s}_1' \Theta_{\mathrm{AB}}(\boldsymbol{r}_1', \boldsymbol{s}_1') \\
&\qquad \times \Big[g_{\mathrm{AA}}(\boldsymbol{r}_1, \boldsymbol{r}_1') g_{\mathrm{AB}}(\boldsymbol{r}_1, \boldsymbol{s}_1') g_{\mathrm{AB}}(\boldsymbol{r}_2, \boldsymbol{s}_1') g_{\mathrm{AA}}(\boldsymbol{r}_2, \boldsymbol{r}_1') - 1 \Big] \\
\frac{\Delta_1 \varrho_{\mathrm{BB}}(\boldsymbol{s}_1, \boldsymbol{s}_2)}{\varrho_{\mathrm{B}}^2} &= \varrho_{\mathrm{A}} g_{\mathrm{BB}}(\boldsymbol{s}_1, \boldsymbol{s}_2) \int \mathrm{d}\boldsymbol{r}_1' \Theta_{\mathrm{AB}}(\boldsymbol{r}_1', \boldsymbol{s}_1) g_{\mathrm{AB}}(\boldsymbol{r}_1', \boldsymbol{s}_s) \qquad (7.51b) \\
&\quad + \varrho_{\mathrm{A}} g_{\mathrm{BB}}(\boldsymbol{s}_1, \boldsymbol{s}_2) \int \mathrm{d}\boldsymbol{r}_1' \Theta_{\mathrm{AB}}(\boldsymbol{r}_1', \boldsymbol{s}_2) g_{\mathrm{AB}}(\boldsymbol{r}_1', \boldsymbol{s}_1) \\
&\quad + \varrho_{\mathrm{A}} \varrho_{\mathrm{B}} g_{\mathrm{BB}}(\boldsymbol{s}_1, \boldsymbol{s}_2) \iint \mathrm{d}\boldsymbol{r}_1' \mathrm{d}\boldsymbol{s}_1' \Theta_{\mathrm{AB}}(\boldsymbol{r}_1', \boldsymbol{s}_1') \\
&\qquad \times \Big[g_{\mathrm{BB}}(\boldsymbol{s}_1, \boldsymbol{s}_1') g_{\mathrm{AB}}(\boldsymbol{r}_1', \boldsymbol{s}_1) g_{\mathrm{AB}}(\boldsymbol{r}_1', \boldsymbol{s}_2) g_{\mathrm{BB}}(\boldsymbol{s}_2, \boldsymbol{s}_1') - 1 \Big] \\
\frac{\Delta_1 \varrho_{\mathrm{AB}}(\boldsymbol{r}_1, \boldsymbol{s}_1)}{\varrho_{\mathrm{A}} \varrho_{\mathrm{B}}} &= \Theta_{\mathrm{AB}}(\boldsymbol{r}_1, \boldsymbol{s}_1) \qquad (7.51c) \\
&\quad + \varrho_{\mathrm{B}} g_{\mathrm{AB}}(\boldsymbol{r}_1, \boldsymbol{s}_1) \int \mathrm{d}\boldsymbol{s}_1' \Theta_{\mathrm{AB}}(\boldsymbol{r}_1, \boldsymbol{s}_1') g_{\mathrm{BB}}(\boldsymbol{s}_1, \boldsymbol{s}_1') \\
&\quad + \varrho_{\mathrm{A}} g_{\mathrm{AB}}(\boldsymbol{r}_1, \boldsymbol{s}_1) \int \mathrm{d}\boldsymbol{r}_1' \Theta_{\mathrm{AB}}(\boldsymbol{r}_1', \boldsymbol{s}_1) g_{\mathrm{AA}}(\boldsymbol{r}_1, \boldsymbol{r}_1') \\
&\quad + \varrho_{\mathrm{A}} \varrho_{\mathrm{B}} g_{\mathrm{AB}}(\boldsymbol{r}_1, \boldsymbol{s}_1) \iint \mathrm{d}\boldsymbol{r}_1' \mathrm{d}\boldsymbol{s}_1' \Theta_{\mathrm{AB}}(\boldsymbol{r}_1', \boldsymbol{s}_1') \\
&\qquad \times \Big[g_{\mathrm{AA}}(\boldsymbol{r}_1, \boldsymbol{r}_1') g_{\mathrm{AB}}(\boldsymbol{r}_1, \boldsymbol{s}_1') g_{\mathrm{AB}}(\boldsymbol{r}_1', \boldsymbol{s}_1) g_{\mathrm{BB}}(\boldsymbol{s}_1, \boldsymbol{s}_1') - 1 \Big]
\end{aligned}$$

where the terms in square bracket can be expanded in terms of h-bonds as

- AA

$$\begin{aligned}
&\Big[g_{\mathrm{AA}}(\boldsymbol{r}_1, \boldsymbol{r}_1') g_{\mathrm{AB}}(\boldsymbol{r}_1, \boldsymbol{s}_1') g_{\mathrm{AB}}(\boldsymbol{r}_2, \boldsymbol{s}_1') g_{\mathrm{AA}}(\boldsymbol{r}_2, \boldsymbol{r}_1') - 1 \Big] \\
&= h_{\mathrm{AA}}(\boldsymbol{r}_1, \boldsymbol{r}_1') + h_{\mathrm{AB}}(\boldsymbol{r}_1, \boldsymbol{s}_1') + h_{\mathrm{AB}}(\boldsymbol{r}_2, \boldsymbol{s}_1') + h_{\mathrm{AA}}(\boldsymbol{r}_2, \boldsymbol{r}_1') \\
&\quad + h_{\mathrm{AA}}(\boldsymbol{r}_1, \boldsymbol{r}_1') h_{\mathrm{AB}}(\boldsymbol{r}_1, \boldsymbol{s}_1') + h_{\mathrm{AA}}(\boldsymbol{r}_1, \boldsymbol{r}_1') h_{\mathrm{AB}}(\boldsymbol{r}_2, \boldsymbol{s}_1') + h_{\mathrm{AA}}(\boldsymbol{r}_1, \boldsymbol{r}_1') h_{\mathrm{AA}}(\boldsymbol{r}_2, \boldsymbol{r}_1') \\
&\quad + h_{\mathrm{AB}}(\boldsymbol{r}_1, \boldsymbol{s}_1') h_{\mathrm{AB}}(\boldsymbol{r}_2, \boldsymbol{s}_1') + h_{\mathrm{AB}}(\boldsymbol{r}_1, \boldsymbol{s}_1') h_{\mathrm{AA}}(\boldsymbol{r}_2, \boldsymbol{r}_1') + h_{\mathrm{AB}}(\boldsymbol{r}_2, \boldsymbol{s}_1') h_{\mathrm{AA}}(\boldsymbol{r}_2, \boldsymbol{r}_1') \\
&\quad + h_{\mathrm{AA}}(\boldsymbol{r}_1, \boldsymbol{r}_1') h_{\mathrm{AB}}(\boldsymbol{r}_1, \boldsymbol{s}_1') h_{\mathrm{AB}}(\boldsymbol{r}_2, \boldsymbol{s}_1') + h_{\mathrm{AA}}(\boldsymbol{r}_1, \boldsymbol{r}_1') h_{\mathrm{AB}}(\boldsymbol{r}_1, \boldsymbol{s}_1') h_{\mathrm{AA}}(\boldsymbol{r}_2, \boldsymbol{r}_1') \\
&\quad + h_{\mathrm{AA}}(\boldsymbol{r}_1, \boldsymbol{r}_1') h_{\mathrm{AB}}(\boldsymbol{r}_2, \boldsymbol{s}_1') h_{\mathrm{AA}}(\boldsymbol{r}_2, \boldsymbol{r}_1') + h_{\mathrm{AB}}(\boldsymbol{r}_1, \boldsymbol{s}_1') h_{\mathrm{AB}}(\boldsymbol{r}_2, \boldsymbol{s}_1') h_{\mathrm{AA}}(\boldsymbol{r}_2, \boldsymbol{r}_1') \\
&\quad + h_{\mathrm{AA}}(\boldsymbol{r}_1, \boldsymbol{r}_1') h_{\mathrm{AB}}(\boldsymbol{r}_1, \boldsymbol{s}_1') h_{\mathrm{AB}}(\boldsymbol{r}_2, \boldsymbol{s}_1') h_{\mathrm{AA}}(\boldsymbol{r}_2, \boldsymbol{r}_1')
\end{aligned}$$

- BB

$$
\begin{aligned}
&\Big[g_{\mathrm{BB}}(\boldsymbol{s}_1,\boldsymbol{s}_1')g_{\mathrm{AB}}(\boldsymbol{r}_1',\boldsymbol{s}_1)g_{\mathrm{AB}}(\boldsymbol{r}_1',\boldsymbol{s}_2)g_{\mathrm{BB}}(\boldsymbol{s}_2,\boldsymbol{s}_1')-1\Big]\\
&=h_{\mathrm{BB}}(\boldsymbol{s}_1,\boldsymbol{s}_1')+h_{\mathrm{AB}}(\boldsymbol{r}_1',\boldsymbol{s}_1)+h_{\mathrm{AB}}(\boldsymbol{r}_1',\boldsymbol{s}_2)+h_{\mathrm{BB}}(\boldsymbol{s}_2,\boldsymbol{s}_1')\\
&+h_{\mathrm{BB}}(\boldsymbol{s}_1,\boldsymbol{s}_1')h_{\mathrm{AB}}(\boldsymbol{r}_1',\boldsymbol{s}_1)+h_{\mathrm{BB}}(\boldsymbol{s}_1,\boldsymbol{s}_1')h_{\mathrm{AB}}(\boldsymbol{r}_1',\boldsymbol{s}_2)+h_{\mathrm{BB}}(\boldsymbol{s}_1,\boldsymbol{s}_1')h_{\mathrm{BB}}(\boldsymbol{s}_2,\boldsymbol{s}_1')\\
&+h_{\mathrm{AB}}(\boldsymbol{r}_1',\boldsymbol{s}_1)h_{\mathrm{AB}}(\boldsymbol{r}_1',\boldsymbol{s}_2)+h_{\mathrm{AB}}(\boldsymbol{r}_1',\boldsymbol{s}_1)h_{\mathrm{BB}}(\boldsymbol{s}_1',\boldsymbol{s}_2)+h_{\mathrm{AB}}(\boldsymbol{r}_1',\boldsymbol{s}_2)h_{\mathrm{BB}}(\boldsymbol{s}_2,\boldsymbol{s}_1')\\
&+h_{\mathrm{BB}}(\boldsymbol{s}_1,\boldsymbol{s}_1')h_{\mathrm{AB}}(\boldsymbol{r}_1',\boldsymbol{s}_1)h_{\mathrm{AB}}(\boldsymbol{r}_1',\boldsymbol{s}_2)+h_{\mathrm{BB}}(\boldsymbol{s}_1,\boldsymbol{s}_1')h_{\mathrm{AB}}(\boldsymbol{r}_1',\boldsymbol{s}_1)h_{\mathrm{BB}}(\boldsymbol{s}_2,\boldsymbol{s}_1')\\
&+h_{\mathrm{BB}}(\boldsymbol{s}_1,\boldsymbol{s}_1')h_{\mathrm{AB}}(\boldsymbol{r}_1',\boldsymbol{s}_2)h_{\mathrm{BB}}(\boldsymbol{s}_2,\boldsymbol{s}_1')+h_{\mathrm{AB}}(\boldsymbol{r}_1',\boldsymbol{s}_1)h_{\mathrm{AB}}(\boldsymbol{r}_1',\boldsymbol{s}_2)h_{\mathrm{BB}}(\boldsymbol{s}_2,\boldsymbol{s}_1')\\
&+h_{\mathrm{BB}}(\boldsymbol{s}_1,\boldsymbol{s}_1')h_{\mathrm{AB}}(\boldsymbol{r}_1',\boldsymbol{s}_1)h_{\mathrm{AB}}(\boldsymbol{r}_1',\boldsymbol{s}_2)h_{\mathrm{BB}}(\boldsymbol{s}_2,\boldsymbol{s}_1')
\end{aligned}
$$

- AB

$$
\begin{aligned}
&\Big[g_{\mathrm{AA}}(\boldsymbol{r}_1,\boldsymbol{r}_1')g_{\mathrm{AB}}(\boldsymbol{r}_1,\boldsymbol{s}_1')g_{\mathrm{AB}}(\boldsymbol{r}_1',\boldsymbol{s}_1)g_{\mathrm{BB}}(\boldsymbol{s}_1,\boldsymbol{s}_1')-1\Big]\\
&=h_{\mathrm{AA}}(\boldsymbol{r}_1,\boldsymbol{r}_1')+h_{\mathrm{AB}}(\boldsymbol{r}_1,\boldsymbol{s}_1')+h_{\mathrm{AB}}(\boldsymbol{r}_1',\boldsymbol{s}_1)+h_{\mathrm{BB}}(\boldsymbol{s}_1,\boldsymbol{s}_1')\\
&+h_{\mathrm{AA}}(\boldsymbol{r}_1,\boldsymbol{r}_1')h_{\mathrm{AB}}(\boldsymbol{r}_1,\boldsymbol{s}_1')+h_{\mathrm{AA}}(\boldsymbol{r}_1,\boldsymbol{r}_1')h_{\mathrm{AB}}(\boldsymbol{r}_1',\boldsymbol{s}_1)+h_{\mathrm{AA}}(\boldsymbol{r}_1,\boldsymbol{r}_1')h_{\mathrm{BB}}(\boldsymbol{s}_1,\boldsymbol{s}_1')\\
&+h_{\mathrm{AB}}(\boldsymbol{r}_1,\boldsymbol{s}_1')h_{\mathrm{AB}}(\boldsymbol{r}_1',\boldsymbol{s}_1)+h_{\mathrm{AB}}(\boldsymbol{r}_1,\boldsymbol{s}_1')h_{\mathrm{BB}}(\boldsymbol{s}_1,\boldsymbol{s}_1')+h_{\mathrm{AB}}(\boldsymbol{r}_1',\boldsymbol{s}_1)h_{\mathrm{BB}}(\boldsymbol{s}_1,\boldsymbol{s}_1')\\
&+h_{\mathrm{AA}}(\boldsymbol{r}_1,\boldsymbol{r}_1')h_{\mathrm{AB}}(\boldsymbol{r}_1,\boldsymbol{s}_1')h_{\mathrm{AB}}(\boldsymbol{r}_1',\boldsymbol{s}_1)+h_{\mathrm{AA}}(\boldsymbol{r}_1,\boldsymbol{r}_1')h_{\mathrm{AB}}(\boldsymbol{r}_1,\boldsymbol{s}_1')h_{\mathrm{BB}}(\boldsymbol{s}_1,\boldsymbol{s}_1')\\
&+h_{\mathrm{AA}}(\boldsymbol{r}_1,\boldsymbol{r}_1')h_{\mathrm{AB}}(\boldsymbol{r}_1',\boldsymbol{s}_1)h_{\mathrm{BB}}(\boldsymbol{s}_1,\boldsymbol{s}_1')+h_{\mathrm{AB}}(\boldsymbol{r}_1,\boldsymbol{s}_1')h_{\mathrm{AB}}(\boldsymbol{r}_1',\boldsymbol{s}_1)h_{\mathrm{BB}}(\boldsymbol{s}_1,\boldsymbol{s}_1')\\
&+h_{\mathrm{AA}}(\boldsymbol{r}_1,\boldsymbol{r}_1')h_{\mathrm{AB}}(\boldsymbol{r}_1,\boldsymbol{s}_1')h_{\mathrm{AB}}(\boldsymbol{r}_1',\boldsymbol{s}_1)h_{\mathrm{BB}}(\boldsymbol{s}_1,\boldsymbol{s}_1')
\end{aligned}
$$

7.5.3 Diagrammatic Representation

For convenience, we express Eqs.(7.51) using the standard diagrammatic representation, in terms of g, h, and Θ bonds. We adopt the following notation, assuming that a colored circle carries with it a density factor ρ_ν and an integration over the position of the corresponding particle.

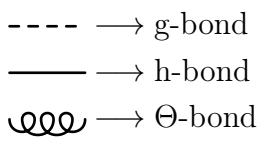

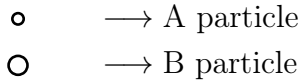

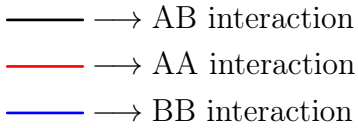

- AB

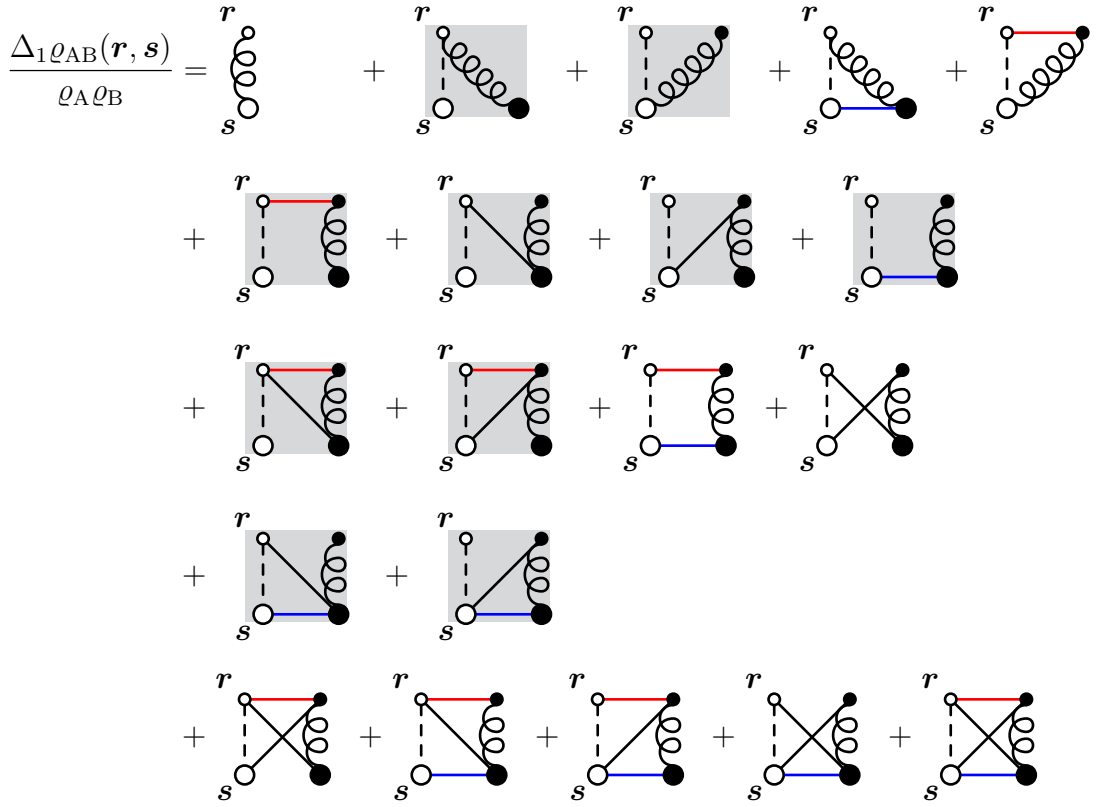

where the reducible cluster diagrams are shaded in gray. Following Henderson and Barker [181], we ignore these contributions, since one of the functions of the correction term $\Delta_\infty \varrho_{\mathrm{AB}}$ is to cancel these reducible cluster integrals. We have then

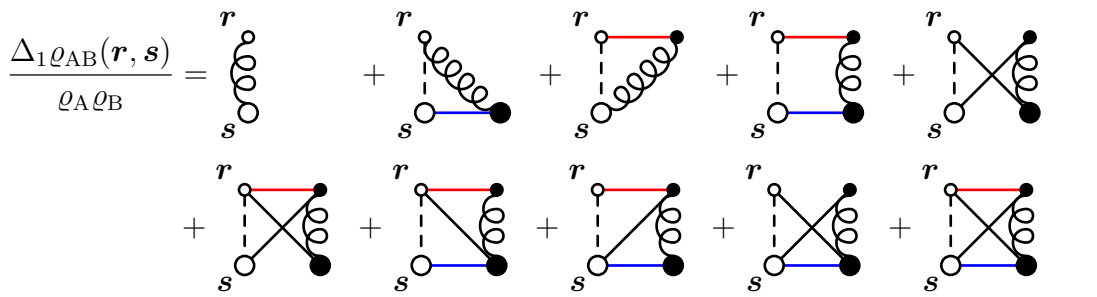

- AA

$$\frac{\Delta_1 \varrho_{\mathrm{AA}}(\boldsymbol{r}_1, \boldsymbol{r}_2)}{\varrho_{\mathrm{A}}^2} =$$

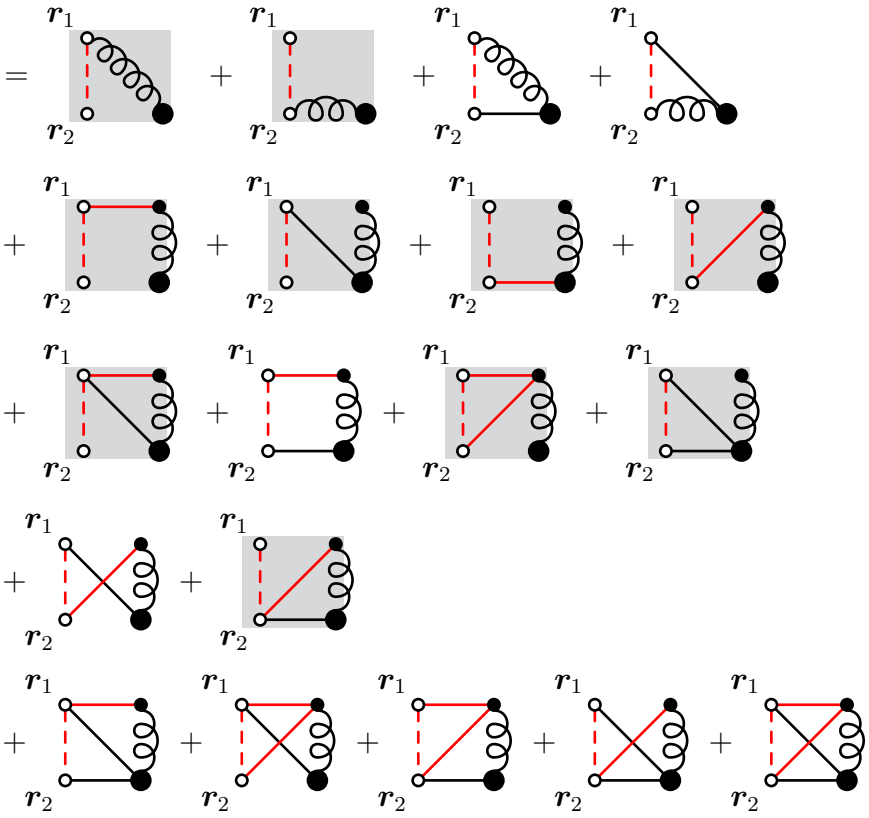

eliminating the reducible cluster integrals we obtain

$$\frac{\Delta_1 \varrho_{\mathrm{AA}}(\boldsymbol{r}_1, \boldsymbol{r}_2)}{\rho_{\mathrm{A}}^2} =$$

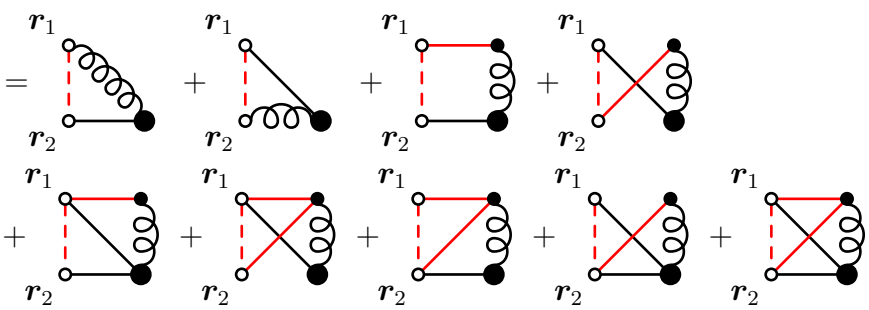

- BB

$$\frac{\Delta_1 \varrho_{\mathrm{BB}}(\boldsymbol{s}_1, \boldsymbol{s}_2)}{\rho_{\mathrm{B}}^2} =$$

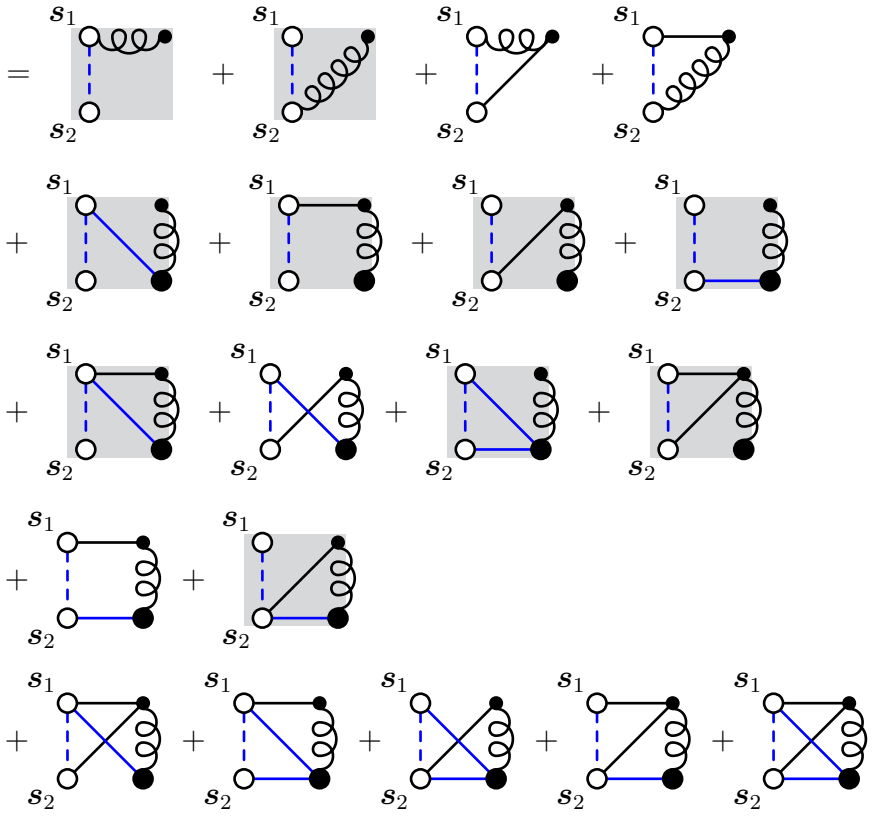

again, eliminating the reducible cluster diagrams gives

$$\frac{\Delta_1 \varrho_{\mathrm{BB}}(\boldsymbol{s}_1, \boldsymbol{s}_2)}{\rho_{\mathrm{B}}^2} =$$

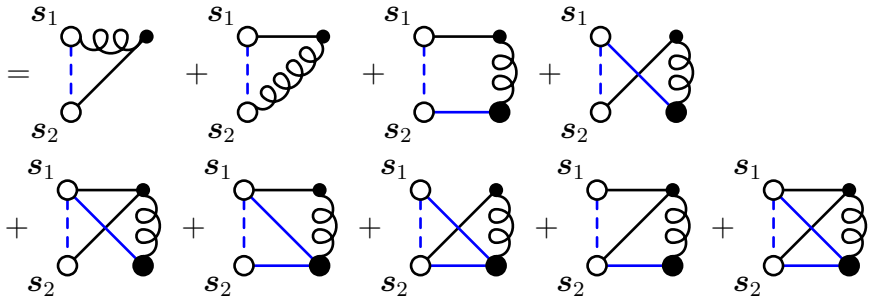

These high-dimensional cluster integrals can be evaluated with the method of Attard and Patey [182, 183, 184], who use a series expansion in terms of Legendre polynomials, which significantly reduces the complexity of the calculations.

7.6 Conclusions

Motivated by the results obtained in the previous chapter, we have attempted to develop a perturbation theory which would allow us to compute the free energies and radial distribution functions of a non-additive hard-sphere system (to first order). We have re-derived the second order perturbation theory of Barker and Henderson, for the general case of a multi-component system and have shown how such a theory could be used to compute the first(second)-order correction to the free energy (radial distribution functions) of a two-component system (A and B particles) with non-additive A-B interactions. The long-term goal of this project is to derive non-additive corrections to the

standard MSA theory used to describe charged systems. We expect this to be of great use, in particular for electrolyte mixtures, where the non-additivity provides a natural description for the specific interactions among distinct cation-anion pairs.

Chapter 8

Perspective II: Towards a Simple Theory for the Viscosity of Electrolytes - A Mode Coupling Approach

Summary

8.1 Introduction

So far we have been primarily interested with the equilibrium thermodynamic and structural properties of electrolyte solutions. In this chapter we propose to study the transport properties, in particular the viscosity. Among the different transport coefficients of ionic solutions, the viscosity is probably the most interesting, as it is the least understood. One could go as far as to say that no significant improvements have been made to the pioneering work presented by Onsager, Fuoss, and Falkenhagen almost a century ago (1930s) [9]; contrary to the other dynamic properties, such as the mutual- and self-diffusion or the conductivity. These classical theories, based on the simple point-charge model of Debye and Hückel, provide exact limiting laws for the concentration variation of the transport properties, which correctly predict the increase in the diffusion, conductivity, and viscosity of electrolyte solutions as a function of the salt concentration c.

However, these laws are only valid in the very dilute regime, and are unable to properly describe the ion specificity (in particular, because the influence of the ion size is not considered). As mentioned before, the limiting laws only provide for the $\sqrt{c}$ dependence of the transport properties (consequence of the charged nature of the system). Several successful attempts at extending the validity of such implicit solvent descriptions have been made over the years: The effect of the ion size on the conductance was studied by Onsager and Fuoss (1950s) [185], and Turq and Micheletti have done the same for the self-diffusion (1970s) [186, 187]. More recently (2005), a study by Dufrêche et al [188], which coupled the Smoluchowsky theory to the MSA solution for the equilibrium pair correlation, has provided simple analytical expressions for the mutual- and self-diffusion coefficients, as well as for the electric conductivity coefficient, which are in very good agreement with the experimental values up to molar concentrations. A similar theory for the viscosity has yet to be proposed.

For a symmetric electrolyte, the Onsager-Fuoss-Falkenhagen Limiting Law is given by

$$\eta(c) = \eta^{(0)} + \frac{\kappa_D(c)\zeta_0}{480\pi} \tag{8.1}$$

where $\eta^{(0)}$ is the viscosity of the pure solvent, κ_D is the inverse Debye screening length, and ζ_0 is the friction coefficient at infinite dilution. This last term can be related to the (infinite dilution) diffusion coefficient, by means of the well known Einstein relation $\zeta_0 = k_{\mathrm{B}}T/D_0$. This contribution is seen to be particularly small, due to the factor of 480π which appears in the denominator. As expected, experimental measurements show that this term is only relevant at very low concentrations. At higher concentrations (from 10^{-2} M to molar concentrations) the dominant contribution is linear in c, so that

$$\eta^{\mathrm{ex}} \equiv \eta(c) - \eta^{(0)} = A\sqrt{c} + Bc \tag{8.2}$$

It is this B term, the so-called Jones-Dole coefficient [189], which proves to be problematic, as no satisfactory (microscopic) theory has been proposed which manages to explain the experimental values. This B term, which is observed to be additive (i.e. $B = B_+ + B_-$ for a simple electrolyte), is a fundamental property of the ion specificity. In particular, no quantitative explanation has been given for the fact that this B coefficient is negative for some ions, and positive for others [1, 42, 154, 190]. This specificity in the B coefficient is interpreted on the basis of the structure breaking nature of the former, and the structure making effect of the latter; but again, no theory has been able to explanation such a simple experimental observation. The experimental values of B for Li^+, Na^+, K^+, and Cl^- are given in Table 8.1. We note that all the microscopic theories of the viscosity of electrolytes predict positive values for the Jones-Dole B coefficient, in stark contrast to the experimental results [42, 9, 10].

Ion	$B(\mathrm{dm}^3/\mathrm{mol})$
Li^+	0.146
Na^+	0.085
K^+	−0.009
Cl^-	−0.005

Table 8.1: Experimental Jones-Dole B coefficients [1].

In the case of neutral (colloidal) particles in suspension, the linear term for the excess viscosity (i.e. the B coefficient) was first calculated by Einstein in 1906 [191, 192], who showed that

$$\eta = \eta^{(0)}(1 + 2.5\phi) \tag{8.3}$$

where $\phi = \rho_i V_i$ is the volume fraction of the solute (ρ_i and V_i its density and volume, respectively)[1]. From this relation, we see that $B \propto V_i$. In the case of ions, this approach clearly fails, as ions with negative partial volumes (i.e Li^+ and Na^+) have positive B coefficients; and ions with positive partial volumes may have negative B coefficients (i.e. K^+). This apparent paradox for the viscosity of electrolytes is not yet fully understood.

A first step towards providing a clear microscopic description for the concentration dependence of the viscosity of electrolytes was taken by Chandra and Bagchi [10], who were able to recover (exactly) the Falkenhagen law using a Mode Coupling Theory (MCT) approach [17, 193]. In this chapter, we propose to use the same framework to study the ion-solvent contributions to the viscosity. In what follows, we give a brief introduction to the Mori-Zwanzig formalism [194, 195] which lies at the basis of MCT. Then, generalizing the work of Chandra and Bagchi [10], we show how this theory can be applied to study the ion-solvent contributions to the viscosity, in an attempt to provide a microscopic understanding of their ion specificity.

8.2 Mori-Zwanzig Projector Operator Formalism

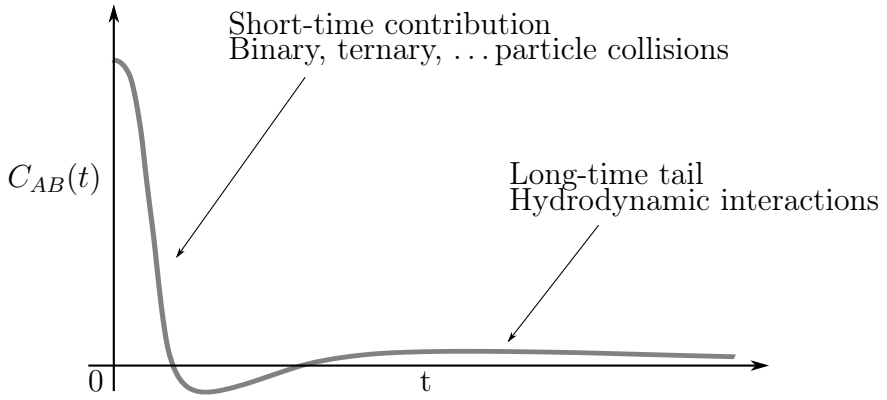

Figure 8.1: Schematic representation of the domain separation in a time correlation function, between the short-time (kinetic) and the long-time (hydrodynamic) contributions.

The Green-Kubo formula for the viscosity can be written in q-dependent form as [17]

$$\eta = \lim_{\epsilon \to 0} \lim_{q \to 0} \frac{1}{V k_{\mathrm{B}} T q^2} \int_0^\infty \mathrm{d}t \left\langle \dot{J}_x(q,t) \dot{J}_x(-q,0) \right\rangle e^{i\epsilon t} \tag{8.4a}$$

where $J_x = \sum_i m_i v_{i,x} e^{-i\boldsymbol{q}\cdot\boldsymbol{r}_i}$ is the transverse current (the projection of the particle current perpendicular to the wave-vector $\boldsymbol{q}$), assuming that $\boldsymbol{q} = q\hat{\boldsymbol{z}}$. What is missing is a

[1] The original publication [191], which appeared in 1906 (right after his *annus mirabilis*) does not give the correct numerical prefactor (1 instead of 2.5); the correct result was only published in 1911 [191].

theory that allows us to compute the time self-correlation functions (for the off-diagonal components of the shear-stress tensor or the transverse current) appearing in this integral. The simplest solution is to use a Taylor time series expansion around the value at $t = 0$, where the n-th term will give the contribution arising from n-body collisions [17]. This approach works well in the case of a gas, but it is entirely unsuitable for describing the behaviour of a liquid, in which the long-time, long-wavelength, hydrodynamic collective motion of the particles becomes important. This is represented by a persistent long-time tail in the time correlation functions, which is schematically represented in Figure 8.1. It is clear that while the short-time behaviour of the correlation functions can be represented in terms of kinetic contributions, arising from particle collisions, the long-time behaviour must be treated differently. One way of doing this, is to use the Mori-Zwanzig projector operator formalism, to which we now turn.

The Mori-Zwanzig technique, which is rigorously exact, allows us to rewrite the Liouville equation, for an arbitrary set of dynamical variables $\mathcal{A}$, in the form of a generalized Langevin equation (i.e. a Langevin equation with memory). This provides us with a convenient method for evaluating the time evolution of the dynamical variables $\mathcal{A}$, as well as their time correlation functions $C_{AA}(t)$. Furthermore, this approach naturally introduces the concept of a set of "fast" variables, at the origin of the random force in the Langevin equation, which evolve on a completely different time-scale from the "slow" variables $\mathcal{A}$. This is precisely the separation we are looking for in order to evaluate the long-time contributions to the viscosity. The only issue is to choose the appropriate "slow" variables contributing to the viscosity.

Let $\mathcal{A}$ be the dynamical variable of interest, its time evolution is governed by the Liouville equation (Eq. (3.8))

$$\mathcal{A}(t) = e^{i\mathcal{L}t}\mathcal{A}(0) \tag{8.5a}$$

$$\dot{\mathcal{A}}(t) = i\mathcal{L}\mathcal{A}(t) \tag{8.5b}$$

We define a projector P, over the subspace spanned by $\mathcal{A} = \mathcal{A}(0)$, by its action on another dynamical variable $B(t)$ as

$$P\mathcal{B}(t) \equiv \langle \mathcal{B}(t)\mathcal{A}^* \rangle \langle \mathcal{A}\mathcal{A}^* \rangle^{-1} \mathcal{A} \tag{8.6}$$

If $\mathbb{I}$ is the identity operator, we can also define the orthogonal operator Q by

$$Q \equiv \mathbb{I} - P \tag{8.7}$$

These projectors essentially separate out the parts of $\mathcal{B}(t)$ which depend on $\mathcal{A}$ from those which do not; we thus speak of the parallel and orthogonal components of $B(t)$ (with respect to $\mathcal{A}$) within the multi-dimensional Hilbert space of all possible dynamical variables.

Using this formalism, one can transform Eq. (8.5) into a generalized Langevin equation of the form [193, 194, 196]

$$\frac{\mathrm{d}\mathcal{A}(t)}{\mathrm{d}t} = i\Omega\mathcal{A}(t) - \int_0^t \mathrm{d}\tau\, K(\tau)\mathcal{A}(t-\tau) + f(t) \tag{8.8}$$

where the first two terms on the right hand side give the contributions to the time evolution of $\mathcal{A}(t)$ which depend on $\mathcal{A}$ itself (as well as its past values), while the last term

gives the contributions arising from the variables orthogonal to $\mathcal{A}$. We have introduced three new functions Ω, $K(t)$, and $f(t)$, which are the frequency, the memory function, and the random force[2], respectively. They are defined as

$$i\Omega \equiv \left\langle \dot{\mathcal{A}}, \mathcal{A}^* \right\rangle \langle \mathcal{A}, \mathcal{A}^* \rangle^{-1} \tag{8.9a}$$

$$K(t) \equiv \langle f(t), f^* \rangle \langle \mathcal{A}, \mathcal{A}^* \rangle^{-1} \tag{8.9b}$$

$$f(t) \equiv e^{iQ\mathcal{L}t} Q\dot{\mathcal{A}} = e^{iQ\mathcal{L}Qt} iQ\mathcal{L}\mathcal{A} \tag{8.9c}$$

Usually, Ω is equal to zero, unless we consider a set of dynamical variables $\mathcal{A}_i$ which exhibit collective oscillations (propagation) among themselves[3]. The definition of the random force $f(t)$, whose time evolution is dictated by the anomalous propagator $\exp[iQ\mathcal{L}t]$ (instead of the standard Liouville propagator $\exp[i\mathcal{L}t]$), guarantees that it is orthogonal to $\mathcal{A}$ at all times

$$\langle f(t), \mathcal{A}^* \rangle = 0 \tag{8.10}$$

Therefore, by multiplying Eq. (8.8) by $\mathcal{A}*$ and taking the ensemble average, we obtain the following formula for the time correlation function

$$\frac{\mathrm{d}C_{AA}}{\mathrm{d}t} = i\Omega\, C_{AA}(t) - \int_0^t \mathrm{d}\tau\, K(\tau) C_{AA}(t-\tau) \tag{8.11}$$

8.3 Mode - Coupling Theory for the Viscosity

We base our study on the MCT for the viscosity proposed by Geszti [197] to study the liquid-glass transition of simple liquids. This theory was later applied to electrolyte solutions by Chandra and Bagchi [10], who where able to exactly derive the Falkenhagen expression for the ionic contribution to the viscosity. We propose to do the same to study the concentration of the solvent-solvent contribution to the viscosity. We choose as the slow "modes" A_i the hydrodynamic variables for the particle density and current

$$A_{\mathcal{X}} = J_{\mathcal{X}} = \sum_i m_i v_{i,\alpha} e^{-i\boldsymbol{q}\cdot\boldsymbol{r}_i}, \qquad \mathcal{X} = x, y, z \tag{8.12a}$$

$$A_\alpha = \rho_\alpha(\boldsymbol{q}) = \sum_{i\in\alpha} e^{-i\boldsymbol{q}\cdot\boldsymbol{r}_i} \tag{8.12b}$$

where α runs over the different particle types (solvent and solute). This differs from the choice of Chandra and Bagchi, who use the total charge density (for an implicit solvent system) as a slow variable for the projection. Also, we consider the density of each species independently (solvent and solute particles). Thus, we are interested in studying the subspace $\boldsymbol{A}$ spanned by the six variables $\mathcal{A}$

$$\boldsymbol{A} = (A_x, A_y, A_z, A_0, A_1, A_2) \tag{8.13}$$

[2] Although not physically a force, $f(t)$ is referred to as one, in reference to the corresponding term appearing in the Langevin equation for the velocity of a Brownian particle.

[3] For simplicity we have only considered the single variable case, but the generalization to the many-variable case is straightforward: it suffices to write the equations in matrix form.

where the indices 0, 1, and 2 refer to the solute (water), the cation, and the anion, respectively. With this choice, Mori has shown that one can rewrite the Green-Kubo expression for the viscosity as

$$\begin{aligned}\eta &= \lim_{\epsilon\to 0}\lim_{q\to 0}\frac{1}{Vk_{\mathrm{B}}Tq^2}\int_0^\infty \mathrm{d}t\left\langle\left[Q\dot{J}_x(q,t)\right]\left[Q\dot{J}_x(-q,0)\right]\right\rangle e^{-\epsilon t} \\ &= \lim_{\epsilon\to 0}\lim_{q\to 0}\frac{1}{q^2V}\int \mathrm{d}t\,\langle[Q\mathcal{L}J_x(-q)][\,e^{iQ\mathcal{L}Qt-\epsilon t}Q\mathcal{L}J_x(q)\,]\rangle\end{aligned} \tag{8.14}$$

where, as before, $Q = \mathbb{I} - P$ is the projector onto the subspace orthogonal to $\boldsymbol{A}$, and P the projector onto $\boldsymbol{A}$.

The first approximation that is usually made is to replace the full evolution operator by its projection over the slow variables only, we thus take

$$\exp\left[iQ\mathcal{L}Qt - \epsilon t\right] \simeq P\exp\left[iQ\mathcal{L}Qt - \epsilon t\right]P$$

Furthermore, by using a Gaussian approximation[4], the resulting expression for η can be written solely in terms of binary products of the basic variables: $J_{\mathcal{X}}J_{\mathcal{X}'}$ and $\rho_\alpha\rho_\beta$. Finally, since the contribution from the density-density terms (the density modes) is expected to be much more important than those of the current-current terms (which decay much faster), the latter can be neglected, and then the viscosity can be expressed as

$$\eta^{\rho\rho} = \sum_{\alpha\beta}\eta^{\rho\rho}_{\alpha\beta} \tag{8.15}$$

with α, β referring to the particle species (in our case the water and the ions), and

$$\eta^{\rho\rho}_{\alpha\beta} = \frac{k_{\mathrm{B}}T}{60\pi^2}\int_0^\infty \mathrm{d}q\, q^4\frac{S'_{\alpha\alpha}(q)S'_{\beta\beta}(q)}{S^2_{\alpha\alpha}(q)S^2_{\beta\beta}(q)}\int_\tau^\infty \mathrm{d}t\, F^2_{\alpha\beta}(q,t) \tag{8.16}$$

where a prime denotes a partial derivative with respect to q, and the notation $\eta^{\rho\rho}_{\alpha\beta}$ is used to stress the fact that we only considered the density (ρ) modes within the MCT calculations. In this last equation, $S_{\alpha\beta}(q)$ and $F_{\alpha\beta}(q)$ refer to the structure factor and the intermediate scattering function, respectively. They are defined in terms of the density-density correlation functions as

$$S_{\alpha\beta}(\boldsymbol{q}) = \frac{1}{\sqrt{N_\alpha N_\beta}}\langle\delta\rho_\alpha(\boldsymbol{q})\delta\rho_\beta(-\boldsymbol{q})\rangle \tag{8.17a}$$

$$F_{\alpha\beta}(\boldsymbol{q},t) = \frac{1}{\sqrt{N_\alpha N_\beta}}\langle\delta\rho_\alpha(\boldsymbol{q},t)\delta\rho_\beta(-\boldsymbol{q},0)\rangle \tag{8.17b}$$

such that $F_{\alpha\beta}(\boldsymbol{q},0) = S_{\alpha\beta}(\boldsymbol{q})$. As mentioned before, this approach allows us to take into account the long-time (hydrodynamic) contributions to the viscosity; the short-time contributions due to the particle collisions, which give rise to a binary term η^B, must be computed separately. This is why the lower limit in the time integral is given by a characteristic time τ, which marks the transition between the kinetic and collective motion. Thus, the complete expression for the viscosity becomes

$$\begin{aligned}\eta &= \eta^B + \eta^{\rho\rho} \\ &= \eta^B + \eta^{\rho\rho}_{\text{solvent}-\text{solvent}} + \eta^{\rho\rho}_{\text{solvent}-\text{ion}} + \eta^{\rho\rho}_{\text{ion}-\text{ion}}\end{aligned} \tag{8.18}$$

[4]Assuming that the $J_{\mathcal{X}}$ and ρ_α variables are propagated independently of each other [17, 198].

The ion-ion contribution $\eta^{\rho\rho}_{\text{ion}-\text{ion}}$ is similar to the one studied in detail by Chandra and Bagchi [10], who show that the lowest order term (as given by the MCT calculations) is able to reproduce the correct limiting law. At higher concentrations, although they obtain a significant increase with respect to the limiting value, they still considerably underestimate the viscosity. We believe that this is due to the fact their theory only takes into account the ion/ion interactions. In order to provide a more suitable description of the excess viscosity, it is thus necessary to consider the molecular details of the solvent-solvent and solvent-ion correlations. As a first approximation, given the fact that we are interested in understanding the linear behaviour (the Jones-Dole B coefficient), we consider only the former[5], such that

$$\eta \simeq \eta^B + \eta^{\rho\rho}_{\text{solvent-solvent}} + \eta^{\rho\rho}_{\text{ion-ion}} \tag{8.19}$$

8.4 The Procedure

8.4.1 Calculation of the Binary Term

To compute the binary (collision) contributions to the viscosity, we use the standard kinetic theory of gases, within the Enskog approximation, to describe the molecular collisions. We thus assume that over these short time-scales, our system (water + cations + anions) can be represented as a dense hard-sphere fluid. As given originally by Enskog [199], the theory is only applicable to pure fluids, but Tham and Gubbins have provided a generalization for multi-component systems [200]. They obtain the following for the viscosity

$$\begin{aligned}\eta^B = \frac{1}{2}\sum_i \rho_i k_{\text{B}} T b_i^{(0)} \left(1 + \frac{4}{5}\sum_j M_{ji} b^*_{ij} g_{ij}\right) \\ + \frac{4}{15}\sum_{ij}\left[2\pi k_{\text{B}} T \frac{m_i m_j}{m_i + m_j}\right]^{\frac{1}{2}} \rho_i \rho_j g_{ij} \sigma_{ij}^4\end{aligned} \tag{8.20}$$

where i, j run over the distinct species in the system, M_{ij}, b^*_{ij}, σ_{ij} (the contact diameter), and g_{ij} (the radial distribution function at contact) are given by

$$\begin{aligned} M_{ij} &= \frac{m_i}{m_i + m_j} & \sigma_{ij} &= \frac{1}{2}(\sigma_i + \sigma_j) \\ b^*_{ij} &= \frac{2}{3}\pi \rho_j \sigma_{ij}^3 & g_{ij} &= g_{ij}(\sigma_{ij}) \end{aligned} \tag{8.21}$$

and b^0_j is defined through the following matrix equation

$$\sum_j H_{ij} b^0_j = K_i \tag{8.22}$$

[5] One can show that, to first order, $\eta^{\rho\rho}_{\text{ion-solvent}}$ is proportional to c^2 (where c is the salt concentration).

with

$$H_{ij} = \sum_k \frac{\sigma_{ik}^2 \rho_i \rho_k g_{ik}}{(m_i + m_k)^{\frac{3}{2}}} \left(\frac{2\pi k_\mathrm{B} T m_k}{m_i} \right)^{\frac{1}{2}} \times \left(\frac{40}{3} m_i \delta_{ij} + 8 m_k \delta_{ij} - \frac{16}{3} m_i \delta_{ik} \right) \tag{8.23}$$

$$k_i = 5\rho_i \left[1 + \frac{4}{5} \sum_j M_{ji} b_{ij}^* g_{ij} \right]$$

For a binary electrolyte, which is the case we will consider here, we must thus specify the effective hard-sphere diameters of the water (0), the cation (1), and the anion (2), as well as the values of the radial distribution functions at contact. These parameters are deduced from MD simulation results. The water-water and water-ion parameters are taken directly from the distance and height of the first peak in the corresponding radial distribution functions. Due to the difficulty of accurately measuring the ion-ion correlations at low concentrations, the ionic values are approximated by assuming additivity of the hard-sphere diameters and ignoring the ion-ion correlations, so that

$$\sigma_{ii} = 2\sigma_{0i} - \sigma_{00} \qquad i, j = 1, 2 \tag{8.24a}$$

$$\sigma_{12} = \frac{1}{2}(\sigma_{11} + \sigma_{12})$$

$$g_{ij} = 1 \tag{8.24b}$$

for the radial distribution functions at contact. As the dominant contributions will come from the water-water and water-ion collisions, Eq. (8.24) is easy enough to justify: it gives the correct water-ion contact distances (with respect to the simulations), under the additivity constraints imposed by the Enskog theory. For the low concentration regime we are interested in, the ion-ion collisions will be practically non-existent, which means that the exact values of the ion-ion g_{ij} should not be relevant.

8.4.2 Calculation of the Mode-Coupling Term

Solvent-Solvent Contribution

From Eq. (8.16), we see that the water-water contribution to the viscosity is given by

$$\eta_{00}^{\rho\rho} = \frac{k_\mathrm{B} T}{60\pi^2} \int_0^\infty \mathrm{d}q\, q^4 \left(\frac{S_{00}'^2(q)}{S_{00}^4(q)} \right) \int_\tau^\infty \mathrm{d}t\, F_{00}^2(q,t) \tag{8.25}$$

While the structure factors $S_{00}(q)$ are easily obtained during a simulation, we must resort to some approximate theory in order to compute the intermediate scattering function $F_{00}(q,t)$. To this end, we assume that the decay of the water-water density fluctuations is given by the following mean-field expression [198]

$$F_{00}(q,t) = S_{00}(q) \exp\left(-D_0(q) q^2 t\right) \tag{8.26}$$

where $D_0(q) = D_0/S_{00}(q)$ (D_0 is the self-diffusion coefficient of water). Under this approximation, the time integral in Eq. (8.25) can be performed analytically, and we are left with the following expression

$$\eta_{00}^{\rho\rho} = \frac{k_\mathrm{B} T}{60\pi^2} \int_0^\infty \mathrm{d}q\, q^4 \left(\frac{R_{00}(q)}{S_{00}(q)} \right)^2 \frac{\exp\left[-2D_0(q) q^2 \tau\right]}{2D_0(q) q^2} \tag{8.27}$$

where $R_{00} = S'_{00} = \partial S_{00}(q)/\partial q$. In order to study the dependence on the salt concentration c, we perform a series expansion of $S_{00}(q)$ around its value at infinite dilution $S^{(0)}_{00}(q)$

$$S_{00}(q) = S^{(0)}_{00}(q) + c\delta S_{00} + \mathcal{O}(c^2) \tag{8.28}$$

where, by definition, the first order correction is given by

$$\begin{aligned} \delta S_{00} &= \left.\frac{\partial S_{00}(q)}{\partial c}\right|_{c=0} \\ &= \left.\frac{\partial S_{00}(q)}{\partial c_1}\right|_{c_1=0} + \left.\frac{\partial S_{00}(q)}{\partial c_2}\right|_{c_2=0} \end{aligned} \tag{8.29}$$

with similar expressions for $R_{00}(q)$. Inserting these relations into Eq. (8.27), we obtain

$$\begin{aligned} \eta^{\rho\rho}_{00} = \frac{k_{\mathrm{B}}T}{60\pi^2}\int_0^\infty \mathrm{d}q\, q^4 \left(\frac{R^{(0)}_{00}(q)}{S^{(0)}_{00}(q)}\right)^2 \frac{\exp\left[-2D_0/S^{(0)}_{00}(q)q^2\tau\right]}{2D_0/S^{(0)}_{00}(q)q^2} \\ \times \left(1 + c(\Delta Q + \Delta F) + \mathcal{O}(c^2)\right) \end{aligned} \tag{8.30}$$

where ΔQ and ΔF give the (linear) correction terms due to the changes in the water density fluctuations, and the manner in which they decay, induced by the presence of the salt

$$\Delta Q = 2\frac{\delta R_{00}(q)}{R^{(0)}_{00}} - 4\frac{\delta S_{00}(q)}{S^{(0)}_{00}(q)} \tag{8.31a}$$

$$\Delta F = \frac{\delta S_{00}(q)}{S^{(0)}_{00}(q)}\left(3 + 2D_0/S^{(0)}_{00}(q)q^2\tau\right) \tag{8.31b}$$

Ion-Ion Contribution

The ion-ion contributions to the viscosity can be expressed as

$$\eta^{\rho\rho}_{\text{ion-ion}} = \sum_{i,j}\eta^{\rho\rho}_{ij} \qquad i,j = 1,2 \tag{8.32}$$

with $\eta^{\rho\rho}_{ij}$ given by Eq. (8.16). We follow the same method proposed by Chandra [10], and assume a continuum (implicit-solvent) model when computing these ion-ion terms. As before, we require some approximate theory to relate the intermediate scattering functions $F_{ij}(q,t)$ to the structure factors $S_{ij}(q)$. Using a time-dependent density-functional description, one obtains the following [10]

$$\sum_\gamma \left((s + q^2D_\alpha)\delta_{\alpha\gamma} - q^2D_\alpha\sqrt{\rho_\alpha\rho_\gamma}c_{\alpha\gamma}(q)\right)\widehat{F}_{\gamma\beta}(q,s) = S_{\alpha\beta}(q) \tag{8.33}$$

where $\widehat{F}(q,s)$ is the Laplace transform of $F(q,t)$. This matrix equation is trivially solved to yield

$$F(q,s) = M^{-1}(q,s)S(q) \tag{8.34}$$

with

$$M_{\alpha\beta} = (s + q^2D_\alpha)\delta_{\alpha\beta} - q^2D_\alpha\sqrt{\rho_\alpha\rho_\beta}c_{\alpha\beta}(q) \tag{8.35}$$

For the numerical calculations, we use the MSA solution for the structure factors, and the Laplace inversion required to obtain $F(q,t)$ is performed using the Gaver-Wynn-Rho method (see Appendix D). The parameters used for this charged hard-sphere model are the same as those used to compute the binary term (themselves derived from MD simulations).

8.5 Results

8.5.1 Molecular Dynamics Simulations

We have chosen to study the viscosity of three distinct chloride salts: Li^+-Cl^-, Na^+-Cl^-, and K^+-Cl^-. In order to determine the various parameters needed for our Mode-Coupling calculations, we have performed molecular dynamics simulations for the single-ion (Li^+, Na^+, K^+, and Cl^-) and binary salt (Li^+-Cl^-, Na^+-Cl^-, K^+-Cl^-) solutions at two distinct concentrations, as well as for bulk water. All the systems consists of 2048 total molecules (water + ions), with 0, 12, or 24 ions (ion pairs in the case of the binary salt simulations), corresponding to a concentration of $c = 0$ M, $c \simeq 0.32$ M, and $c \simeq 0.65$ M, respectively. The simulations are first equilibrated within the NPT ensemble, in order to fix the density of the solution, and a subsequent NVT simulation is performed for data gathering purposes[6]. We use the same force-fields as in Section 5.3.1 (Dang-Chang for the ions and SPC/E for the water molecules).

The simulation results can be divided into two sets: (1) those used to determine the hard-sphere parameters needed to compute the binary Enskog contribution to the viscosity (the densities, diameters, and radial distribution functions at contact) and (2) those used to determine the mode-coupling term (δR_{00} and δS_{00}). The former are obtained from the average densities of the NPT simulations and the radial distribution functions (NPT or NVT), while the latter can be estimated from the difference between the structure factors obtained at two different concentrations

Water Density

In Figure 8.2, we show the average water density obtained from NPT simulations at three different ion (salt) concentrations. Within this (low) salt concentration regime, the water density is seen to vary linearly with the salt concentration, as expected. Furthermore, by comparing the single-ion and binary salt results, we see that the variation can also be considered to be additive (with respect to the cation/anion values). If $\rho_{\text{wat}}^{(0)} = 55.14$ M is the density of bulk SPC/E water, then the water density (for a given salt concentration) will be given by the following linear relationship

$$\rho_{\text{wat}}(c) = \rho_{\text{wat}}^{(0)} + c\,\alpha \tag{8.36}$$

where α is a salt-specific parameter

$$\alpha = \begin{cases} -1.2 & Li^+\text{-}Cl^- \\ -1.1 & Na^+\text{-}Cl^- \\ -1.8 & K^+\text{-}Cl^- \end{cases} \tag{8.37}$$

[6] As expected, the results are (within error bars) the same in both ensembles.

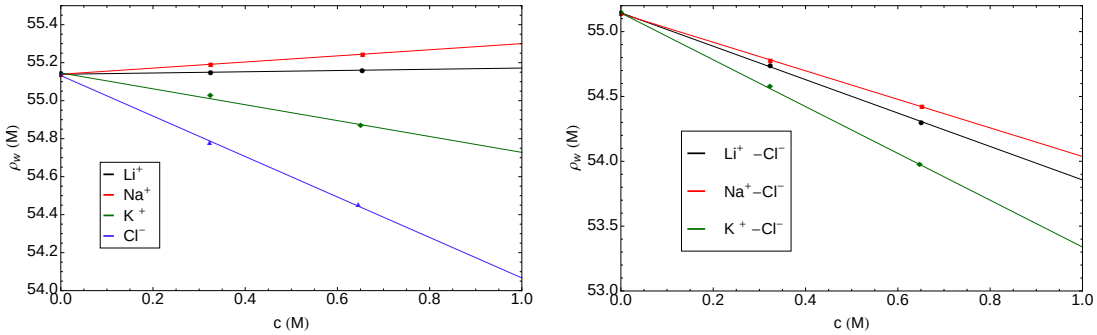

Figure 8.2: Average water density as a function of ion concentration obtained from NPT simulations. (right) single-ion and (left) binary X^+-Cl^- salt simulations.

Recalling the Euler relation for the partial (molar) volumes, Eq. (3.133), we have, for the single-ion case

$$V = n_{\text{wat}}\overline{V}_{\text{wat}} + n_{\text{ion}}\overline{V}_{\text{ion}} \tag{8.38}$$

where n_{wat} and n_{ion} are the number of moles of water and ions, respectively. Assuming that the partial volumes are concentration independent, such that $\overline{V}_{\text{wat}} = 1/\rho^{(0)}_{\text{wat}}$, our simulation data can be used to determine the $\overline{V}_{\text{ion}}$. The partial molar volumes of the salt $\overline{V}_{\text{salt}}$ (which are the experimentally measurable quantities) are then easily obtained, since $\overline{V}_{\text{salt}} = \overline{V}_{\text{cation}} + \overline{V}_{\text{anion}}$. The values we have obtained are given in Table 8.2, along with the experimental values given by Marcus [1]. We observe a shift for the single-ion values, since these depend on the reference state, but the values for the salt show good agreement.

Ion	$\overline{V}_{\text{MD}}$	$\overline{V}_{\text{EXP}}$
Li^+	−0.59	−7.3
Na^+	−2.92	−7.6
K^+	7.58	2.6
Cl^-	19.32	24.2

Salt	$\overline{V}_{\text{MD}}$	$\overline{V}_{\text{EXP}}$
Li^+-Cl^-	18.7	16.9
Na^+-Cl^-	16.4	16.6
K^+-Cl^-	26.9	26.8

Table 8.2: Single-ion (left) and salt (right) partial molar volumes computed from MD simulations. The experimental results were taken from Ref. [1]. All values are given in $\text{cm}^3.\text{mol}^{-1}$.

Radial Distribution Functions at Contact

In Figure 8.3, we give the variation of the water-water radial distribution functions at contact, as a function of the ion (salt) concentration, obtained from NVT simulations. As before, the values are seen to be linear and additive. If $g^{(0)}_{\text{wat-wat}}(\sigma_{\text{wat-wat}}) = 3.095$ is the value at contact for the pure solvent, the variation with respect to the salt concentration is given by

$$g_{\text{wat-wat}}(\sigma_{\text{wat-wat}}) = g^{(0)}_{\text{wat-wat}}(\sigma_{\text{wat-wat}}) + c\,\beta \tag{8.39}$$

with

$$\beta = \begin{cases} -0.10 & \text{Li}^+\text{-Cl}^- \\ -0.14 & \text{Na}^+\text{-Cl}^- \\ -0.08 & \text{K}^+\text{-Cl}^- \end{cases} \tag{8.40}$$

The value of the ion-water radial distribution functions $g_{\text{wat-ion}}(\sigma_{\text{wat-ion}})$ shows practically no variation at low salt concentration, and as a first approximation, we can consider them be equal to the infinite dilution limit

$$g_{\text{wat-ion}}(\sigma_{\text{wat-ion}}) = \begin{cases} 14.31 & \text{Li}^+ \\ 7.25 & \text{Na}^+ \\ 4.30 & \text{K}^+ \\ 3.80 & \text{Cl}^- \end{cases} \tag{8.41}$$

As mentioned before, given the difficulty in accurately measuring the ion-ion correlations within finite concentration simulations, and the fact that we are only interested in the linear corrections (at low concentrations), we take $g_{\text{ion-ion}} = 1$.

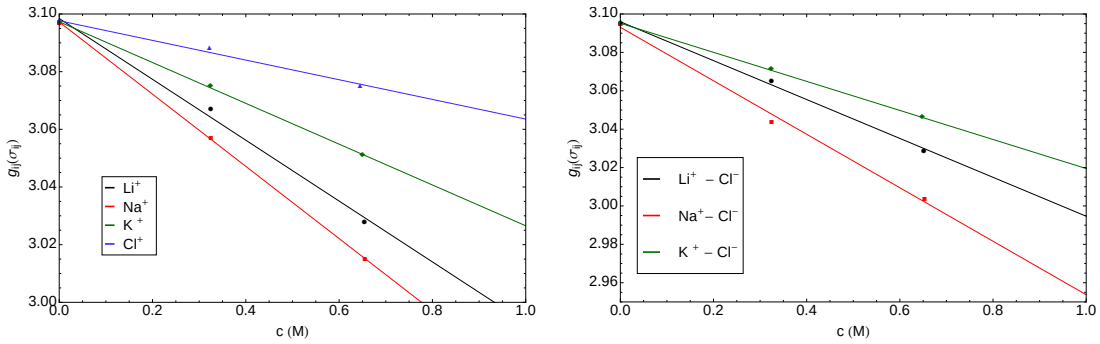

Figure 8.3: The water-water radial distribution function at contact as a function of ion (salt) concentration obtained from NVT simulations. (right) single-ion and (left) binary salt simulations.

Effective Hard-Sphere Diameters

The effective hard-sphere contact diameters are obtained from the distances to the first peaks in the radial distribution functions. These values show no considerable variation with salt concentration, allowing us to consider them as constant. A value of $\sigma_{\text{wat-wat}} = 2.745$ Å is obtained for the diameter of the water molecules (this corresponds to the distance between oxygen atoms). Finally, the ion diameters are deduced from the water-ion and water-water contact distances. These results are summarized in Table 8.3.

Ion	$\sigma_{\text{water-ion}}$	$\sigma_{\text{ion-ion}}$
Li^+	1.96	1.175
Na^+	2.45	2.155
K^+	2.82	2.895
Cl^-	3.21	3.675

Table 8.3: Ion-water and ion-ion contact distances obtained from MD simulations. The former are obtained directly from the simulations (through the radial distribution functions), while the latter are deduced assuming additivity of the contact diameters (Eq. (8.24)).

Structure Factors

In Figure 8.4 we show the structure factors obtained from the four different single-ion simulations at the lowest salt concentration considered ($c \simeq 0.32$ M). Both the results

obtained from the direct calculation, as well as those given by the Fourier transform of the radial distribution functions are presented. The agreement between the two is seen to be excellent, except for small values of k, where numerical errors start to become important. Fortunately, the dominant contribution of the density modes (water-water) we are interested in, comes from intermediate length scales $1.5 \leq k \leq 4$, at which the two routes give the same results.

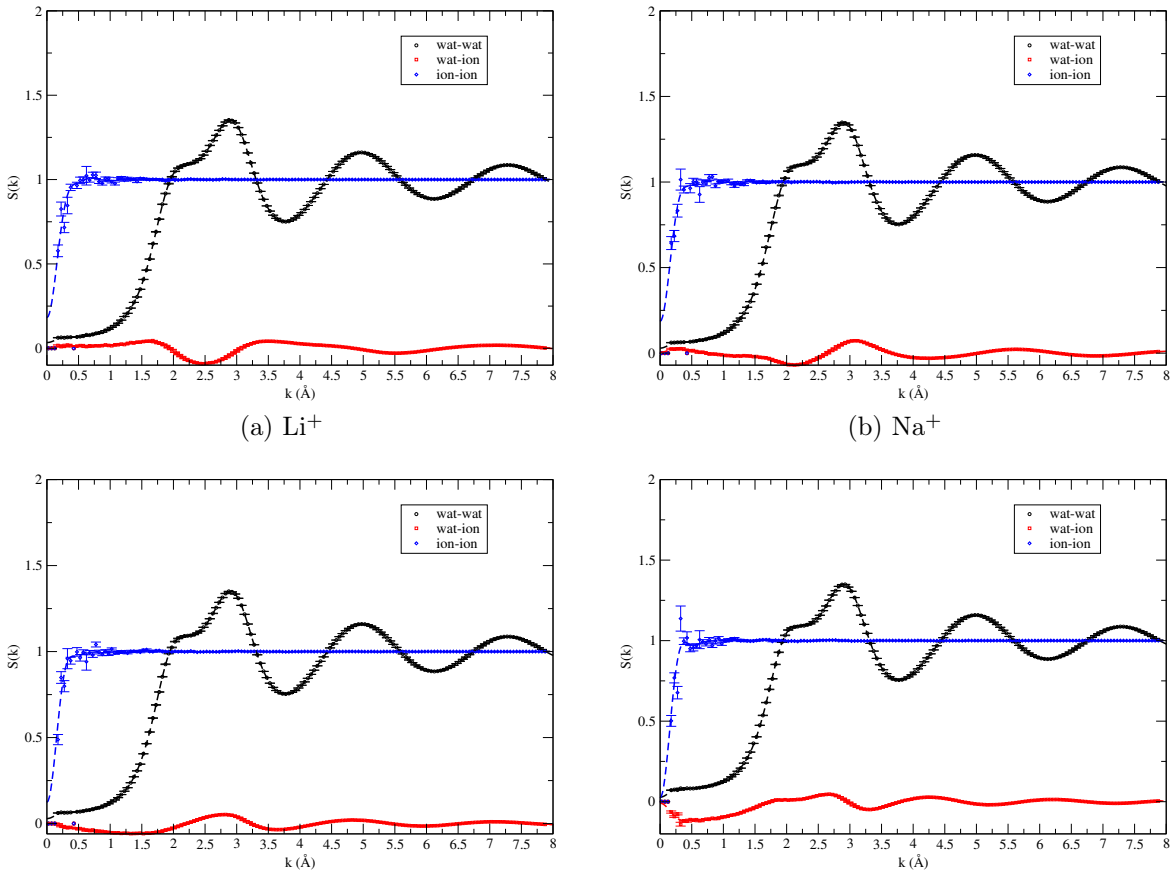

(a) Li^+ (b) Na^+

(c) K^+ (d) Cl^-

Figure 8.4: Structure factors obtained from single ion NVT simulations at $c \simeq 0.32$ M (2036 water molecules + 12 ions). (symbol) direct computation and (dashed lines) Fourier transform data.

The water-water structure factors[7] obtained from the two finite concentration (single-ion) simulations are used to estimate the concentration derivative δS_{00} (Eq. (8.29)). Let $\Delta_\pm S_{00}$ be the difference in structure factors obtained from concentrations at $c_\pm$ and $c_\pm + \Delta c_\pm$

$$\Delta_\pm S_{00} = S_{00}(c_\pm + \delta c_\pm) - S_{00}(c_\pm) \tag{8.42}$$

We approximate δS_{00} as

$$\delta S_{00} \approx \frac{\Delta_+ S_{00}}{\Delta c_+} + \frac{\Delta_- S_{00}}{\Delta c_-} \tag{8.43}$$

[7]In practice, these are taken to be the oxygen-oxygen structure factors.

The values obtained for $c_\pm = 0$ and 0.32 M , with $\Delta_\pm c \simeq 0.32$ M in both cases, show no significant variation. The results obtained for the latter, which are the ones we have used in the calculations, are presented in Figs. (8.5) and(8.6), for $\Delta_\pm S_{00}(k)$ and $\delta S_{00}(k)$, respectively.

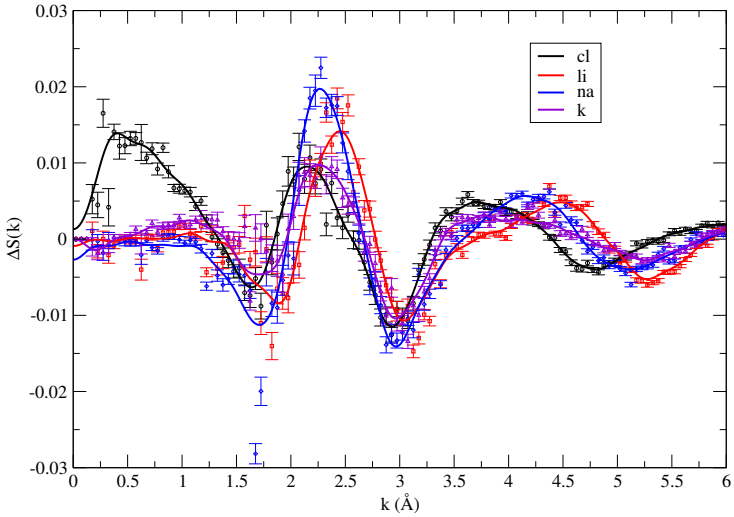

Figure 8.5: Difference between the water-water structure factors ΔS_{00} obtained at $c = 0.65$ and $c = 0.32$. (symbol) direct calculation and (dashed-line) Fourier transform data.

For $\Delta_\pm S_{00}(k)$, we have presented the values obtained from a direct calculation of $S_{00}(k)$ and from a Fourier transform of $h_{00}(r)$. Although the measured difference is seen to be very small ($\simeq 0.01$), the values (and the oscillations) of $\Delta S_{00}(k)$ are nonetheless larger than the statistical errors. The final values of $\delta S_{00}(k)$, for the three salts we have considered, present the same global trend: the location and amplitude of the peaks show only a very weak salt specificity. As mentioned before, the important range of q vectors lies around the first peak of $S_{00}(k)$, at $q \simeq 2$ Å^{-1}. For smaller values of q, the q^2 factor appearing in Eq. (8.30) will result in a vanishing contribution, while at larger values, the fluctuations will decay very rapidly ($\sim \exp(-D_0 q^2 t)$).

8.5.2 Mode-Coupling Calculations

Using the values previously calculated, we have computed the viscosity of three model electrolytes (Li^+-Cl^-, Na^+-Cl^-, and K^+-Cl^-). The binary Enskog contribution is computed from Eq. (8.20), for a three-component hard-sphere system with diameters taken from the radial distribution functions measured in MD simulations. The ion-ion mode-coupling term is computed from Eq. (8.32), for an implicit solvent (two-component) model, with the same ion diameters used for the binary term. Finally, we use water-water structure factors to compute the infinite dilution mode-coupling term. The only *external* parameters that are required are the infinite dilution self-diffusion coefficients (for the water and the ions), and the characteristic time τ used in the integration for the water-water term (Eq. (8.16))[8]. We have taken the experimental values for the diffusion

[8]For the ion-ion terms, whose dominant contributions come from the small q-values, with a characteristic decay time of the order of ~ 1 ns, we can take $\tau = 0$ (i.e. the binary term, due to collisions

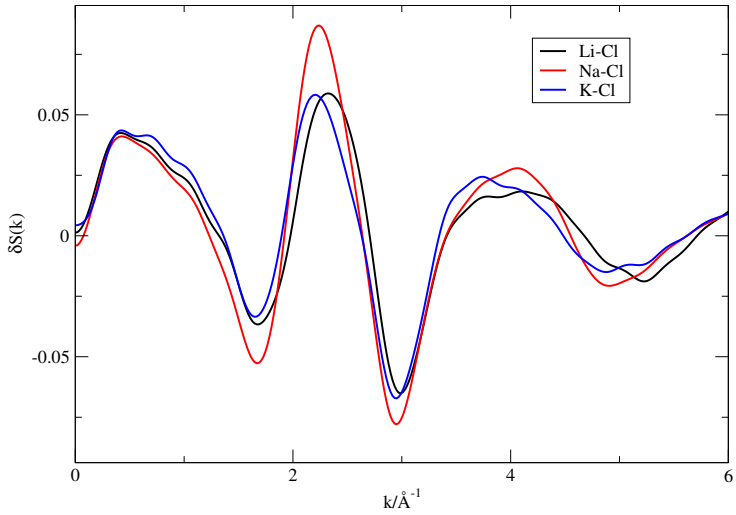

Figure 8.6: Derivative of the water-water structure factor, with respect to the salt concentration, obtained from a finite difference calculation.

coefficients: $D = 1.02, 1.33, 1.95,$ and 2.03 for Li^+, Na^+, K^+, and Cl^-, respectively, and $D = 2.4$ for water (in $10^{-9}\,m^2/s$) [42]. We have considered several values of τ in the range $0.1 < \tau/ps < 2$. The numerical integrations were performed using a simple trapezoidal rule [103], with the number of points consecutively increased until a fractional accuracy of 10^{-6} was achieved. The detailed results for the excess contributions to the viscosity are given in Figure 8.7, for $\tau = 0.24$ ps. In all cases, we observe the same global behaviour: (1) the binary contribution is positive and increases linearly with the concentration, (2) the water-water contribution is negative (this is true for all values of τ), and (3) the ion-ion contribution is positive, and also increases linearly with the concentration (except at low concentrations). A comparison between the fractional change in the viscosity, as a function of the concentration, for the three salts we have studied is presented in Figure 8.8. This precise value of τ was chosen because it gives the limit at which the Jones-Dole B coefficient becomes positive for Na^+-Cl^- and K^+-Cl^-. For lower values, the linear variation in the viscosity will be negative.

Unfortunately, these results predict that the viscosity of the Li^+ salt is to be less than that of Na^+ or K^+ (at all concentration); something which is in clear disagreement with the experimental data (see Figure 8.8b). We believe that this is due to the fact that we have not taken into account the strongly bound hydration sphere of Li^+. Not only should we consider an effective diameter given by the size of the hydrated ion, but we should also remove the water molecules within this hydration sphere from the calculation of $S_{00}(k)$. These modifications will result in a significant increase for the Enskog and the water-water (MCT) contribution to the viscosity. Finally, it should be possible to develop a consistent theory, by choosing the free parameters (D and τ) in such a way that the viscosity of bulk water is recovered. Our results are promising, since we have shown that the linear (salt) concentration dependence of the viscosity (arising from the long-time water-water fluctuations) may be negative. If this term is dominant, with respect to the short-time collision contribution and the long time ion-ion contribution, then we obtain a negative Jones-Dole B coefficient. However, further work is still necessary to improve the agreement with respect to experiments, particularly for small ions.

between ions, is negligible)

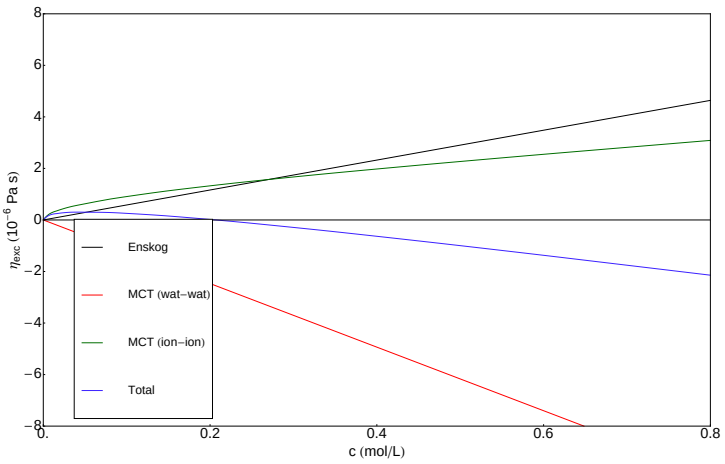

(a) Li^+-Cl^-

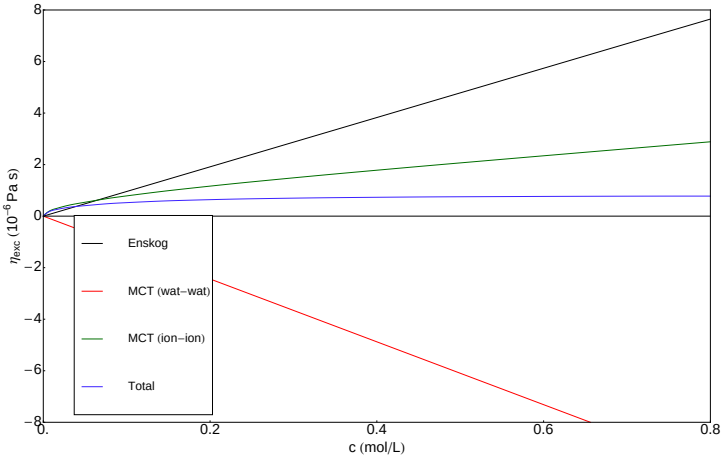

(b) Na^+-Cl^-

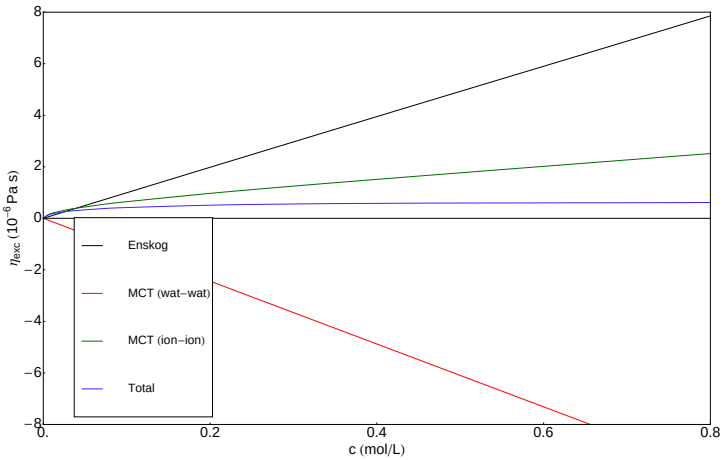

(c) K^+-Cl^-

Figure 8.7: Excess binary and long-time (MCT) contributions to the viscosity of simple electrolytes. The water-water term was computed using $\tau = 0.24$ ps.

8.6 Conclusions

In this chapter, we have considered a Mode-Coupling theory for the viscosity of electrolyte solutions which attempts to go beyond the work of Chandra and Bagchi [10], by

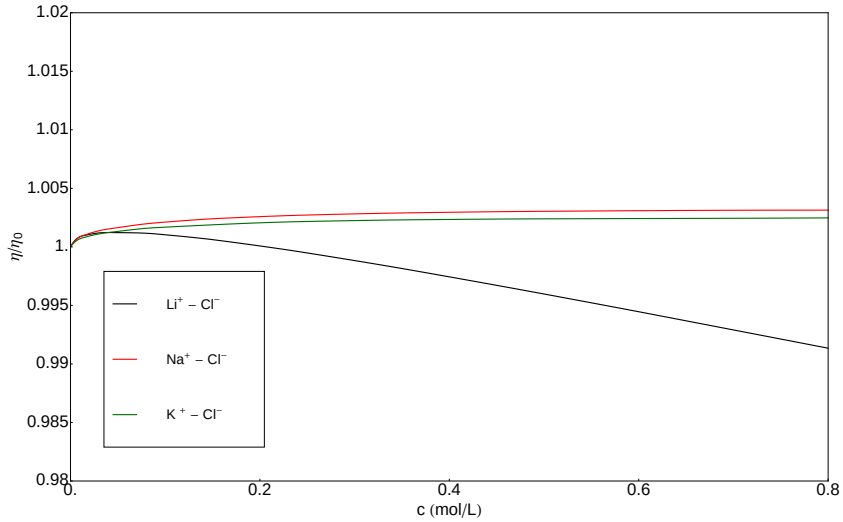

(a) MCT

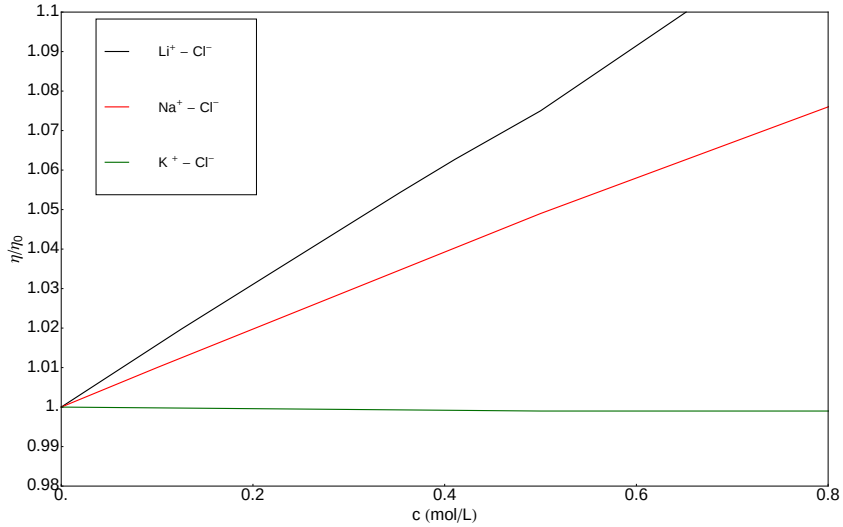

(b) Experiments

Figure 8.8: Fractional change in the viscosity, as a function of the concentration, obtained from (a) MCT calculations and (b) experiments [201]. The water-water term is computed using a characteristic time of $\tau = 0.24$ ps.

taking into account the effects of the salt on the water structure. As a first approximation, the viscosity of the solution is said to arise from two terms: a short-time (binary) contribution, due to the collisions between particles, and a long-time contribution, due to the collective (hydrodynamic) motion of the fluid. The first term is computed using the Enskog theory, by considering the system as being composed of hard spheres; while the second term, which is separated into ion-ion and water-water contributions, is computed using a mode-coupling calculation. The work of Chandra and Bagchi has shown the validity of using a Mode-Coupling approach, as they have been able to recover the exact limiting law for the excess ionic contribution to the viscosity (the Onsager-Falkenhagen law) using an implicit solvent model. We use a similar representation to compute the ion-ion terms; for the water-water calculations we use results obtained from MD simulations. We find that, to first order in the salt concentration, this (MCT) water-water term always gives a negative contribution to the viscosity. This provides us

with a glimpse into the seemingly anomalous behaviour of the Jones-Dole coefficient: it will be negative if the disruption to the water structure (due to the presence of the salt) is strong enough to overcome the effect of the collisions and the long-time ion-ion density correlations (which tend to increase the viscosity). The interpretation of the viscosity paradox mentioned before is the following. Small ions (Li^+ and Na^+) have a negative partial volume because of the strong polarization of the water molecules of their inner solvation shells. Nevertheless, this does not imply that the Jones-Dole coefficient B is negative, because the solvation sphere is rigidly bound to the ions, resulting in a larger effective solute particle, with a positive hydrodynamic volume. For the bigger ions (K^+), although the polarization of the inner-sphere is weaker, they modify the structure of the solvent, and this breaking structure effect is responsible for the negative value of the B coefficient (the positive binary term is not enough to overcome this hindering of the viscosity).

To end, we acknowledge that our theory is not yet self-consistent. We need to develop a method for unambiguously separating the relevant short- and long-time interactions. We must also determine whether the water molecules in the hydration sphere of the ions should be considered as individual particles, contributing the collision terms and the water-water density fluctuations, or if their effects should be taken into account through a large effective ion.

Chapter 9

General Conclusions

Throughout this work, we have developed a multi-scale description of ionic solutions. We have started by using *ab-initio* calculations to determine ion-specific properties such as the ionic polarizabilites in liquid water (which cannot be measured experimentally). Our results are in very good agreement with the (fitted) values of common classical potentials. Using a simple force-matching protocol, we have been able to parametrize a set of force-fields for monovalent ions in solution, which show relatively good agreement with the experimental results for various thermodynamic, structural, and dynamic properties. A description of electrolyte solutions using such a classical atomistic description allows us to easily measure the ion-water properties. However, the ion-ion properties require very expensive simulations, encouraging the development of simpler models.

By using the McMillan-Mayer theory, which is in principle exact, we have derived effective ion-ion potentials for an implicit solvent model. With this description, in which the solvent degrees of freedom have been averaged out, the calculation of ion-ion properties becomes practical (the calculation times are reduced, roughly, by an order of magnitude). However, this type of modelling is still unsuitable for some tasks, such as the study of complex systems typically encountered in engineering applications. Simple phenomenological models, which can be adjusted to reproduce the experimental data, are favored over the more *fundamental* descriptions in these cases. With this in mind, we have developed a coarse-graining procedure that allows us to derive a primitive model description[1] of electrolyte solutions. To derive these models we have used the standard perturbation theory of liquids, which provides a rigorous method for relating the properties of the system of interest (which are determined, in our case, by the complex McMillan-Mayer effective potentials) to those of a *simpler* system (for which we use a primitive model).

The advantage of representing electrolyte solutions as charged hard-spheres in a dielectric continuum, is the fact that several integral equations exist which provide accurate descriptions for the thermodynamic and structural properties. Among them, the most popular is probably the Mean Spherical Approximation (MSA), since it can be solved analytically. In particular, we have explicit expressions for the free energy and the radial distribution functions, which are the two quantities required for a first-order perturbation calculation. For a simple $1-1$ electrolyte, one would think that a

[1] We use the term primitive model in the broad sense, of an implicit solvent description in terms of hard-sphere (which may eventually be associated).

two-component hard-sphere system would provide a suitable representation[2]; however, within a first-order perturbation theory, the structure of the two systems (the system we want to study and the system we use as a reference) is assumed to be equal, and this imposes certain restrictions on the reference systems which can be used. In particular, for electrolyte systems, this is incompatible with a two-component *additive* representation. The reason for this is simple: ion sizes are strongly non-additive.

While the (static) picture of ions as hydrated charged spheres is suitable for isolated ions, or when describing the interaction between ions of equal sign charges, it breaks down when trying to describe the strongly attractive cation-anion interactions. In this case, it is possible for the ions to penetrate each others hydration spheres, giving rise to a *contact ion pair* (CIP). It is the relative stability of this pair with respect to the *solvent separated ion pair* (SSIP), which describes the interaction between hydrated cations and anions, that is difficult to represent using a simple two-component model. Regardless of the stability of the contact pair, or the fraction of pairs present in the solution at any given moment, it is necessary to take this interaction into account to obtain a suitable thermodynamic description. In fact, when we fitted the exact free energies of our systems (obtained from Monte-Carlo simulations) to a two-component MSA system, we observed that the cation-anion contact diameter could correspond to either the CIP or the SSIP, depending on the strength of the association (as characterized, for example, by the Bjerrum model). For the weakly associated Li^+ and Na^+ salts, the contact distance corresponds to the second peak in the radial distribution function (the SSIP), while for the more associated K^+ salts, the distance corresponds to the first peak (the CIP). By construction, a fit to the free energy (or the osmotic coefficients) will give very good agreement for the thermodynamics, but the accuracy with which it represent the structure of the fluid can vary significantly from one system to another.

In contrast, a (first-order) perturbation theory requires that the structure of the reference system be as close as possible to that of the *real* system. In order to achieve this, using an additive hard-sphere model, we are forced to adopt a three-component representation, in which the CIP is considered as a distinct chemical species. We have derived relations between the free energy and the pair interaction potentials of the two- and three-component systems in order to perform the perturbation calculations, as well as a relationship between the corresponding radial distribution functions. The results obtained using this type of reference system are in very good agreement with the *exact* results, and they show only a relatively small dependence on the representation used for the CIP. Furthermore, we also obtained an improved agreement for the structure of the fluid: we represent both the CIP and the SSIP, and we recover the correct contact distances for the cation-cation and anion-anion interactions. In general, our model remains valid up to molar concentrations, after which many of the assumptions we have made are no longer valid.

Several extensions to the theory we have presented are conceivable. The most obvious, is to consider a non-additive hard-sphere model. This would allow us to use a two-component reference system in our PFT calculations. Work in this direction is in progress. Furthermore, we must also investigate the development of similar models for the dynamics of electrolytes. We have started to study the viscosity of electrolytes

[2]This is the obvious choice, and the one that is used when *fitting* the MSA parameters to recover the experimental osmotic coefficients.

in an attempt to explain the ion-specificity of the Jones-Dole B coefficient. Using a Mode-Coupling calculation we show that the water-water density fluctuations can give a negative contribution to the viscosity. Finally, we end our work by noting that it is very unlikely that we should be able to develop a microscopic theory which shows better agreement with experiments than the fitted phenomenological models used by engineers. However, by using the result obtained from microscopic simulations, we can develop simple models which accurately represent the underling physics of our system. For complex systems, for which experimental data is scarce, this approach helps us to provide a realistic model, by defining the relevant parameters.

Publications Issued from this work

- J. J. Molina, J.-F. Dufrêche, M. Salanne, O. Bernard, M. Jardat, and P. Turq. "Models of electrolyte solutions from molecular descriptions: the example of NaCl", *Phys. Rev. E* **80**, 065103 (2009).
- J. J. Molina, M. Duvail, Ph. Guilbaud, and J.-F. Dufrêche. "Coarse-grained Lanthanoid chloride aqueous solutions", *J. Mol. Liq.* **153**, 107-111 (2010).
- J. J. Molina, S. Lectez, S. Tazi, M. Salanne, J.-F. Dufrêche, J. Roques, E. Simoni, P.A. Madden, and P. Turq. "Ions in solution: Determining their polarizabilities from first-principles", *J. Chem. Phys* **134**, 014511 (2011).
- J. J. Molina, M. Duvail, J.-F. Dufrêche, Ph. Guilbaud. "Atomistic descriptions of binary lanthanoid salt solutions: A coarse-grained approach", *J. Phys. Chem. B* **115**, 4329-4340 (2011).
- J. J. Molina, J.-F. Dufrêche, M. Salanne, O. Bernard, and P. Turq. " Primitive models of ions in solution from molecular descriptions: a perturbation approach", submitted to *The Journal of Chemical Physics*.
- S. Tazi, J. J. Molina, M. Salanne, B. Rotenberg, J.-F. Dufrêche, and P. Turq. "Classical force-fields of ions in solution derived from ab-initio calculations", in preparation.

Other Publications:

- J. J. Molina, C. Pierleoni, B. Capone, J.-P. Hansen, and I. S. Santos de Oliveira. "Crystal stability of diblock copolymer micelles in solution", *Mol. Phys* **107**, 535-548 (2009).

Appendix A

Principles of Monte Carlo Simulations

Monte-Carlo simulations provide a convenient simulation technique to measure ensemble averages of the type

$$\langle \mathcal{A} \rangle = \frac{\int \cdots \int \mathrm{d}\boldsymbol{r}^N \mathcal{A}(\{\boldsymbol{r}_i\}) e^{-\beta V_N}}{\int \cdots \int \mathrm{d}\boldsymbol{r}^N \, e^{-\beta V_N}} \tag{A.1}$$

even though we are unable to compute the integrals in the numerator, or the denominator, we can measure the ratio of the two. The trick is to perform a weighted random walk through configuration space Γ, such that the relative probability for visiting any two points A and B is equal to the ratio of their ensemble probabilities. The average of $\mathcal{A}$ along this stochastic trajectory will correspond to the ensemble average $\langle \mathcal{A} \rangle$. The master equation for the Markov Chain which describes this random walk, assuming discrete time steps, is given by

$$P(A, t + \Delta t) - P(A, t) = \sum_B \left[P(B, t) W_{B \longrightarrow A} - P(A, t) W_{A \longrightarrow B} \right] \tag{A.2}$$

where $P(A, t)$ is the probability of being in the state A at time t and $W_{a \longrightarrow B}$ gives the transition probability for going from state A to state B. For stationary systems, the left hand side of this equation gives zero (as the probabilities are time independent $P(A, t) = P_A$) and the following balance condition must be satisfied

$$\sum_B P_B W_{B \longrightarrow A} = \sum_B P_A W_{A \longrightarrow B} \tag{A.3}$$

which states that the average number of moves arriving at state A should be equal to the average number of moves leaving state A. There are many possible choices for $W_{A \longrightarrow B}$ which satisfy this equation, but it is convenient to enforce an even stronger *detailed balance* condition, such that

$$P(A) W_{A \longrightarrow B} = P(B) W_{B \longrightarrow A} \tag{A.4}$$

in which case the transition probabilities satisfy the following relation

$$\frac{W_{A \longrightarrow B}}{W_{B \longrightarrow A}} = \frac{P(B)}{P(A)} = e^{-\beta (V_B - V_A)} \tag{A.5}$$

Again, there is no unique way of choosing the transition probabilities to satisfy this equation, the only restriction that is imposed is that they must be ergodic: it should be possible, within a finite number of steps, to reach every point in the configuration space (regardless of the initial configuration) [20]. We use the scheme proposed by Metropolis [202]

$$W_{A\longrightarrow B} = \begin{cases} e^{-\beta(V_B - V_A)} & V_B \geq V_A \\ 1 & V_B < V_A \end{cases} \tag{A.6}$$

In practice, a Monte-Carlo simulation using the Metropolis algorithm would be implemented as follows

1. Choose a valid initial configuration A ($V_A < \infty$).
2. Generate a new configuration B.
3. Use the Metropolis scheme to accept/reject this new configuration. In both cases the final state is counted for the calculation of the average.
   - If $V_B < V_A$ always accept the move.
   - If $V_B > V_A$ generate a random number ϵ from a uniform distribution $\epsilon \in [0, 1]$. Accept the move if $\epsilon < \exp[-\beta(V_B - V_A)]$, reject it otherwise.
4. Set $A = B$ and return to step 2.

Although the metropolis rule gives a clear recipe for computing the acceptance (transition) probabilities, it says nothing about how to generate the new configurations. For simple systems, at moderate densities, it is usually sufficient to consider random displacements in the configurations, but for more complex systems (such as polymers or dense media) this approach is bound to fail, since the transition probabilities towards the new states are bound to be very low[1]. In these cases, it is usual to bias the generation of the new configurations, so that there is a high-probability of them being accepted. This results in much improved statistics, as the relevant (interesting) regions of phase-space are sampled more often, but the averages need to be corrected at the end, in order to remove the original bias [20]. Fortunately, for the solute gases studied here, the simple scheme of generating random displacements can be applied.

[1] This leads to a poor sampling of the phase space, and thus, to very poor statistics

Appendix B

Averages and Error Calculations

Summary

The properties measured during a molecular dynamics or Monte-Carlo simulation correspond to averages of microscopic, fluctuating quantities. In the limit of an infinitely long simulation run, the values obtained would be the exact values. However, as we are limited to finite simulations (in both time and size) it becomes necessary to provide an estimate of the error. One of most popular ways of achieving this, is to use the block-averaging technique. In what follows, we review the basic concepts of this blocking procedure, before showing how it can be implemented during a simulation.

B.1 Block-Averages

During a simulation, the microscopic properties of the system are periodically measured $\mathcal{A}(\{\boldsymbol{q}_i;\boldsymbol{p}_i\})$, and the average $\langle\mathcal{A}\rangle$ obtained at the end is used as an estimate of the corresponding macroscopic observable $\mathcal{A}$. This microscopic variable is assumed to be a random variable with a Gaussian distribution. The average and variance are then given by

$$\langle A\rangle_{\text{simulation}} = \frac{1}{N}\sum_{i=1}^{N} A_i \tag{B.1a}$$

$$\sigma^2(A) = \frac{1}{N}\sum_{i=1}^{N}(A_i - \langle A\rangle)^2 \tag{B.1b}$$

where N is the number of data points gathered during the simulation. For a sufficiently large number of measurements, the central limit theorem tells us that $\langle\mathcal{A}\rangle$ is in itself a random (Gaussian) variable, with average $\langle\mathcal{A}\rangle$ and variance

$$\sigma^2(\langle A\rangle) = \frac{\sigma^2(A)}{N} \tag{B.1c}$$

Aside from giving an estimate of the error, the variance is an intrinsic property of the system (for the given ensemble), which can be used to directly obtain such information as the isothermal compressibility (fluctuation in the number of particles) or the specific heat (energy fluctuations). Special care should be taken when applying Eq. (B.1b) to data obtained during a simulation, since it has been implicitly assumed that the A_i are mutually uncorrelated measurements (statistically independent). However, this will depend on the manner in which the measurements are collected. If the sampling is performed too frequently, consecutive measurements will fail to provide any new information, and thus lead to a high correlation among adjacent measurements. Additionally, we do not know the actual value of $\langle \mathcal{A} \rangle$, we only have the estimate provided by the simulation. Since there are only $N-1$ independent measurements[1] of A_i, $\sigma^2(\langle \mathcal{A} \rangle)$ (Eq. B.1b) should be replaced by the *unbiased* estimate of the variance $\sigma_s^2(\langle \mathcal{A} \rangle)$

$$\sigma_s^2(A) = \frac{1}{N-1} \sum_{i=1}^{N} (\mathcal{A}_i - \langle \mathcal{A} \rangle_{\text{simulation}})^2 \tag{B.2}$$

The optimal sampling frequency for obtaining uncorrelated measurements will obviously depend on the system, and the property being studied, but this can only be known after the simulation has been performed. Flyvbjerg and Petersen [20, 203, 204] have proposed a simple, but clever method of "block-averages" that provides a reliable estimate of the variance, from a given series of simulation data $\mathcal{A}_i$. Their idea is to successively group the data into blocks, producing a new data set $\mathcal{A}_i^{(M)}$, in which the $\mathcal{A}_i^{(M)}$ correspond to the averages of the i-th block of the previous iteration $(M-1)$. At any given level, the error of the average, and its own error estimate, is given by

$$\sigma(\langle A \rangle) \approx \frac{\sigma(A^{(M)})}{\sqrt{N_M - 1}} \left(1 \pm \frac{1}{\sqrt{2(N_M - 1)}} \right) \tag{B.3}$$

where N_M is the number of data points at level M. Initially, this value will increase as the number of blocking operations increases (in turn reducing the number of redundant, correlated, measurements), until a plateau is reached. This constant value is taken to be the error of the average.

The simplest blocking procedure is to divide the data in half at every iteration, by forming blocks of length two among consecutive data points $A_1^{(M)} = \frac{1}{2}(A_1^{(M-1)} + A_2^{(M-1)})$, ... An example of the results obtained from this blocking operation is given in Figure B.1 for the calculation of the mean-squared displacement $\langle \Delta x^2(t) \rangle$ of a single Na^+ ion in water, for several values of t. For this particular case, we see that the optimal number of block operations is $M = 8$; this means that we should group our data into blocks of length $2^8 = 256$ in order to obtain uncorrelated measurements. It is not convenient, or even necessary, to perform this block analysis every time, for every property, but it should be done at least once for a representative system, in order to obtain the optimal block size.

[1] The N-th data point $\mathcal{A}_N$ can be trivially obtained from knowledge of the other $N-1$ points and the estimated average.

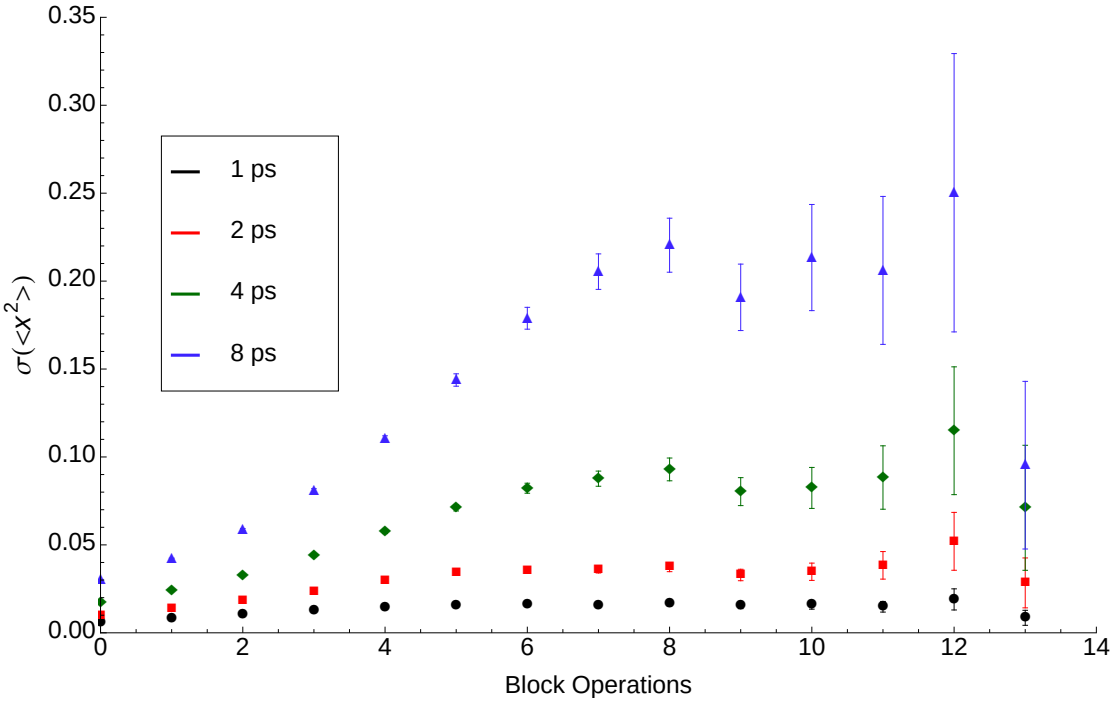

Figure B.1: Error of the mean as a function of the number of blocking operations, for the calculation of the mean-squared displacement at four distinct times.

B.2 Real-time Updating During a Simulation

In what follows we show how the variance of a given property can be updated in real-time during a simulation, as the estimate of the average is also updated. We assume that the x_i represent uncorrelated measurements (i.e. they have been obtained by a suitable block-average). At a given step N during the simulation, the running average $\langle x \rangle_N$ is trivially obtained from the same average at the previous step and the new value x_N

$$\begin{aligned} \langle x \rangle_N &= \frac{1}{N} \sum_{i=1}^{N} x_i \qquad \text{(B.4)} \\ &= \frac{1}{N} \left(\sum_{i=1}^{N-1} x_i + x_N \right) \\ &= \left(\frac{N-1}{N} \right) \left(\frac{1}{N-1} \sum_{i=1}^{N-1} x_i \right) + \frac{x_N}{N} \\ &= \frac{1}{N} \left((N-1) \langle x \rangle_{N-1} + x_N \right) \qquad \text{(B.5)} \end{aligned}$$

In the same manner, the variance at step N can be obtained from the variance and the average at step $N-1$, as well as ${x_N}^2$

$$\begin{aligned}
\sigma_N^2 &= \frac{1}{N}\sum_{i=1}^{N}\left(x_i - \langle x\rangle_N\right)^2 \qquad \text{(B.6)}\\
&= \left\langle x^2\right\rangle_N - \langle x\rangle_N^2\\
&= \frac{1}{N}\left(\sum_{i=1}^{N-1} x_i^2 + x_N^2\right) - \frac{1}{N^2}\left((N-1)\langle x\rangle_{N-1} + x_N\right)^2\\
&= \frac{N-1}{N}\left(\frac{1}{N-1}\sum_{i=1}^{N-1} x_i^2\right) - \frac{(N-1)^2\langle x\rangle_{N-1}^2}{N^2} + \frac{1}{N}x_N^2\\
&\quad - \frac{2(N-1)x_N\langle x\rangle_{N-1}}{N^2} - \frac{1}{N^2}x_N^2\\
&= \frac{N-1}{N}\left(\left\langle x^2\right\rangle_{N-1} - \frac{N-1}{N}\langle x\rangle_{N-1}^2\right) + \frac{N-1}{N^2}\left(x_N^2 - 2x_N\langle x\rangle_{N-1}\right)\\
&= \frac{N-1}{N}\left(\left\langle x^2\right\rangle_{N-1} - \langle x\rangle_{N-1}^2\right) + \frac{N-1}{N^2}\left(\langle x\rangle_{N-1}^2 - 2x_N\langle x\rangle_{N-1} + x_N^2\right)\\
&= \frac{N-1}{N}\left[\sigma_{N-1}^2 + \frac{1}{N}\left(\langle x\rangle_{N-1} - x_N\right)^2\right] \qquad \text{(B.7)}
\end{aligned}$$

Again, one should not use this value to compute the error of the mean, but instead use σ_s^2 (i.e. the final value should be multiplied by $N/(N-1)$).

[2]The alert reader will notice that this is not the simplest way of obtaining σ_N^2 from σ_{N-1}^2. This particular expression is advantageous, since it will not suffer from truncation errors (it is the sum of two non-negative values) which *can* appear and *do* lead to negative values for the variance. We can easily ignore these artifacts, but most computers are simply unwilling to compute the square-root of -0.0. The author learned this the hard way, which is why it merits a footnote!

Appendix C

Numerical Integration

Summary

C.1 Gaussian Quadratures

Numerical quadratures, which replace an integral by a weighted sum of the integrand at a finite number of points (within the integration interval), provide a fast and accurate method for approximating one-dimensional integrals. The simplest procedure is to divide the integration range into a grid of equally spaced points; the integration over each of these intervals can then be approximated by the area of the corresponding trapezoid. This leads to the Newton-Cotes family of quadrature rules [205, 103], which only vary in the weights used to perform the sum. In order for these methods to work, the grid spacing needs to be small enough to provide an adequate sampling of the function. Unfortunately, we do not always know what our function looks like before performing the integration, making it difficult to determine the "optimal" grid spacing. For these cases, the Gaussian quadratures present a very convenient alternative.

$W(x)$	(a,b)	polynomial	P_n
1	$(-1,1)$	Legendre	$P_n(x)$
$\frac{1}{\sqrt{1-x^2}}$	$(-1,1)$	Chebyshev	$T_n(x)$
$x^\alpha e^{-x}$	$(0,\infty)$	Laguerre	$L_n^{(\alpha)}(x)$
e^{-x^2}	$(-\infty,\infty)$	Hermite	$H_n(x)$
$(1-x)^\alpha(1+x)^\beta$	$(-1,1)$	Jacobi	$P_n^{(\alpha,\beta)}(x)$

Table C.1: Weight functions $W(x)$ and orthogonal polynomials P_n for the most common Gaussian quadratures.

The main idea behind the Gaussian quadrature method is to treat both the weights and the position of the abscissas as free parameters. If the integrand can be expressed

as $W(x)f(x)$, where $W(x)$ is a known weighting function, the general approximation is given by [206, 205]

$$\int_a^b \mathrm{d}x\, W(x)f(x) \approx \sum_{i=1}^{N} w_i f(x_i) \tag{C.1}$$

where the "optimal" weights w_i and abscissas x_i will depend on the specific weighting function $W(x)$. It turns out that if $f(x)$ is a polynomial of degree $M < 2N-1$, this approximation can be made exact using only N points x_i. This is accomplished by choosing the points to be the roots of the N-th order polynomial P_N of a particular class of polynomials: those which are orthogonal with respect to the same weighting function $W(x)$, and over the same interval (a, b), such that

$$\langle P_N | P_M \rangle \equiv \int_a^b W(x) P_N(x) P_M(x) \tag{C.2}$$

is exactly zero if $N \neq M$. The required weights are given by

$$w_i = \frac{A_N}{A_{N-1}} \frac{\langle P_N | P_N \rangle}{P_N(x_j) P'_{N+1}(x_j)} \tag{C.3}$$

where A_N is the coefficient of the leading term (x^N) in $P_N(x)$, and the prime denotes a derivative. The most common weight functions, along with the corresponding family of orthogonal polynomials, are given in Table C.1.

C.2 Gauss-Legendre Quadrature

For $W(x) = 1$, we obtain the Gauss-Legendre quadrature, which is the only quadrature used in this work. In order to evaluate integrals over an arbitrary interval (a, b), and not necessarily $(-1, 1)$, we must perform a change of variables, such that the quadrature is now given by [205]

$$\int_a^b \mathrm{d}y\, f(y) = \frac{a-b}{2} \sum_{i=1}^{N} w_i f(y_i) \tag{C.4}$$

where the abscissas y_i are defined in terms of the roots x_i of the N-th Legendre polynomial $P_N(x)$ as

$$y_i = \left(\frac{b-a}{2}\right) x_i + \left(\frac{b+a}{2}\right) \tag{C.5}$$

Finally, the weights are computed according to

$$w_i = \frac{2}{(1-x_i^2)\left[P'_N(x_i)\right]^2} \tag{C.6}$$

The values of y_i and w_i for the case of a 6- and 8-point Gauss-Legendre quadrature, over the interval $(0, 1)$, are given in Tables C.2 and C.3, respectively. These are the quadratures we have used to compute the hydration free energies from the λ-integration scheme.

i	y_i	w_i
1	0.03376524289842399	0.08566224618958517
2	0.1693953067668677	0.1803807865240693
3	0.3806904069584015	0.2339569672863455
4	0.6193095930415985	0.2339569672863455
5	0.8306046932331323	0.1803807865240693
6	0.9662347571015760	0.08566224618958517

Table C.2: Abscissas (y_i) and weights (w_i) required for a 6-point Gauss-Legendre quadrature over the interval $(0, 1)$.

i	y_i	w_i
1	0.01985507175123188	0.05061426814518813
2	0.10166676129318663	0.11119051722668724
3	0.2372337950418355	0.1568533229389436
4	0.4082826787521751	0.1813418916891810
5	0.5917173212478249	0.1813418916891810
6	0.7627662049581645	0.1568533229389436
7	0.8983332387068134	0.11119051722668724
8	0.9801449282487681	0.05061426814518813

Table C.3: Abscissas (y_i) and weights (w_i) required for a 8-point Gauss-Legendre quadrature over the interval $(0, 1)$.

Appendix D

Numerical Laplace Inversion

Summary

D.1 Introduction

The Laplace transform is very popular in science and engineering, particularly when dealing with differential equations, since they can usually be expressed as "simple" algebraic equations within the Laplace space (s). The problem, however, is that the conversion back to real-space is not always easy to perform. If $f(t)$ is a function within the (real) time domain, and $\widehat{f}(s)$ its Laplace transform in the s-domain, we have the following transform pair [207]

$$\widehat{f}(s) = \int_0^\infty \mathrm{d}t\, e^{-st} f(t), \qquad \Re(s) > \alpha \tag{D.1a}$$

$$f(t) = \frac{1}{2\pi i} \lim_{R\to\infty} \int_{\gamma-iR}^{\gamma+iR} e^{st} \widehat{f}(s), \qquad \gamma > \alpha \tag{D.1b}$$

where α is the abscissa of convergence of $\widehat{f}(s)$ and γ defines the vertical *Bromwich* contour along which the line integral is performed. Several numerical methods exists for performing the Laplace inversion which manage to avoid the use of complex analysis. We use two such methods in this work. The first is based on a Fourier representation of the inversion integral, while the second uses linear combinations of the so-called Gaver functionals to estimate $f(t)$.

D.2 The Fourier Expansion

The inversion integral (D.1b) is easily expressed as a Fourier transform for $s = \gamma + i\omega$ [207]

$$f(t) = \frac{e^{\gamma t}}{2\pi} \int_{-\infty}^{\infty} \mathrm{d}\omega \, \widehat{f}(\gamma + i\omega) e^{i\omega t} \tag{D.2}$$

and if $f(t)$ is a real function, this can be simplified to give

$$f(t) = -\frac{2e^{\gamma t}}{\pi} \int_{0}^{\infty} \mathrm{d}\omega \, \Im\Big(\widehat{f}(\gamma + i\omega)\Big) \sin \omega t \tag{D.3}$$

This last integral is easily evaluated using the Fast Fourier Transform routines (FFT) [103], which is what we have done to obtain the radial distribution functions given by the MSA solution to the primitive model. However, this method is only useful if $\widehat{f}(s)$ is easy to evaluate, since we generally require a large number of points ($N = 2^{12\sim17}$) to setup the grids required by the FFT.

D.3 The Gaver Functional Expansion

The Gaver approach to the Laplace inversion problem is based on the family of functionals $f_k(t)$ introduced by Gaver in the 1960s [207]

$$f_k(t) = k\tau \binom{2k}{k} \sum_{j=0}^{k} (-1)^j \binom{k}{j} \widehat{f}\left((k+j)\tau\right) \tag{D.4}$$

where $\tau = \ln 2/t$. If $f(t)$ possesses a Taylor expansion for all $t > 0$, then the Gaver functionals possess the following asymptotic expansion [208]

$$f_k(t) \underset{k\to\infty}{\sim} f(t) + \frac{c_1(t)}{k} + \frac{c_2(t)}{k^2} + \cdots \tag{D.5}$$

where the coefficients $c_i(t)$ are independent of k (i.e. they are the same for all the $f_k(t)$). This expansion shows precisely why the Gaver Functionals are useful: the first order term is the Laplace inverse we are looking for. Unfortunately, the series is very slow to converge, which is why several sequence accelerators have been developed [208]. The idea is simple, since all the $f_k(t)$ have the same expansion, "clever" combinations of these functionals can be used to eliminate the error terms $c_i(t)$.

Gaver-Stehfast

The Gaver-Stehfast (GS) method uses a linear combination of the first M Gaver Functionals $f_k(t)$ to construct an estimate for $f(t)$

$$f(t, M) = \sum_{k=1}^{M} W_k^{(M)} f_k(t) \tag{D.6}$$

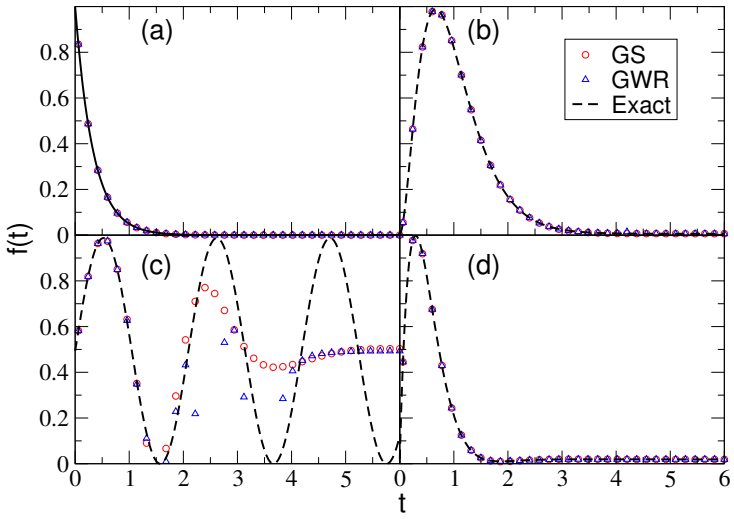

Figure D.1: Inverse Laplace transforms of four test functions using the Gaver-Stehfast (GS) and Gaver-Wynn-Rho (GWR) methods, the exact results for $f(t)$ are also shown. (a) $f(t) = \exp(-3t)$, (b) $f(t) = \exp(-3t)x^2/2$, (c) $f(t) = \sin(3t)$ and (d) $f(t) = \exp(-3t)\sin(2t)$. For convenience, all the results have been scaled and shifted so that $f(t) \in (0, 1)$.

where M is an even integer and the weights are given by

$$W_k^{(M)} = (-1)^{k+M} \frac{k^M}{M!} \binom{M}{k} \tag{D.7}$$

Gaver-Wynn-Rho

An alternative sequence accelerator is the Wynn-Rho (GWR) algorithm, which is expressed recursively as [208, 209]

$$\begin{aligned} \rho_{-1}^{(n)} &= 0, \qquad \rho_0^{(n)} = f_n(t), && n \geq 0 \\ \rho_k^{(n)} &= \rho_{k-2}^{(n+1)} + \frac{k}{\rho_{k-1}^{(n+1)} - \rho_{k-1}^{(n)}}, && k \geq 1 \end{aligned} \tag{D.8}$$

In this case, the estimate to $f(t)$ is given by

$$f(t, 2M) = \rho_{2M}^{(0)} \tag{D.9}$$

where M (which must again be even) is the largest index in the Gaver Functionals used to construct the approximation.

Performance

In theory, the estimate for $f(t)$ can always be improved upon by increasing the number of Gaver functionals M; however, when using fixed precision arithmetic, round-off errors will cause the accuracy to rapidly decrease after a certain optimal value. On a standard computer, with 8 byte real numbers (roughly 16 decimal digit precision), a value of $M = 16$ and $M = 8$ should be used for the GS and GWR methods, respectively [208, 210]. A comparison between the two methods is shown in Figure D.1, for four different test functions. It is clear that these methods do not provide "the" solution to the inverse Laplace problem: when they work, they work very well, but when they fail, they do it

miserably. In general, strongly oscillating functions should be avoided. While there is no appreciable difference in the GS and GWR results presented in the Figure, the latter is the preferred method, as it (consistently) provides a higher degree of accuracy [208]. This is the method we have used when computing the inverse Laplace transforms of the intermediate scattering functions $F(q, s)$.

Appendix E

Monte Carlo Results

Summary

E.1 Implict vs Explicit Solvent (MC vs MD)

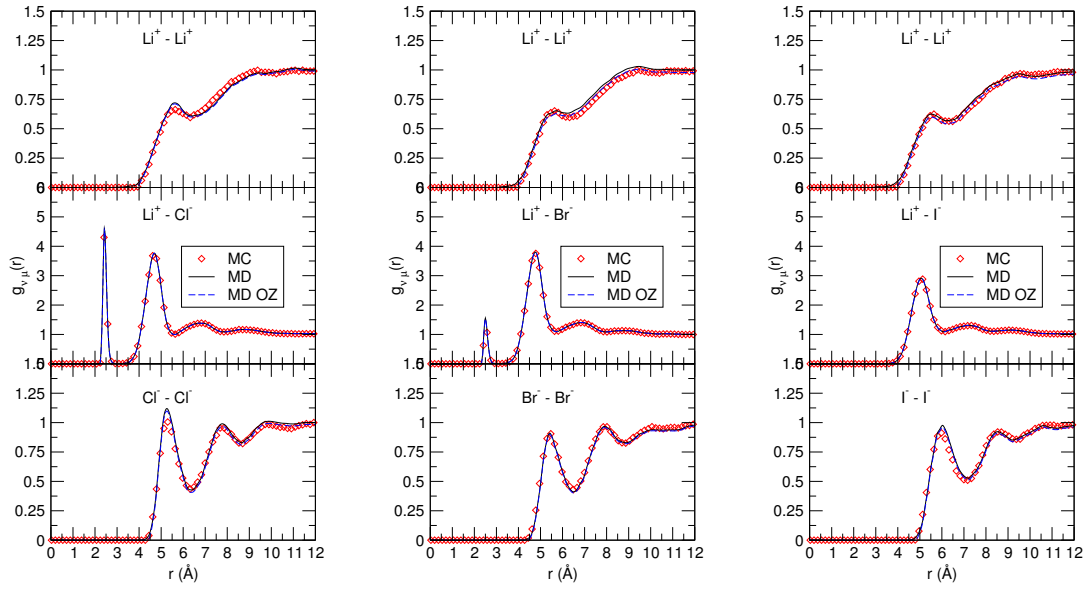

Figure E.1: Comparison between MD and MC radial distribution functions for Li^+ salts at $c = 0.64$ M.

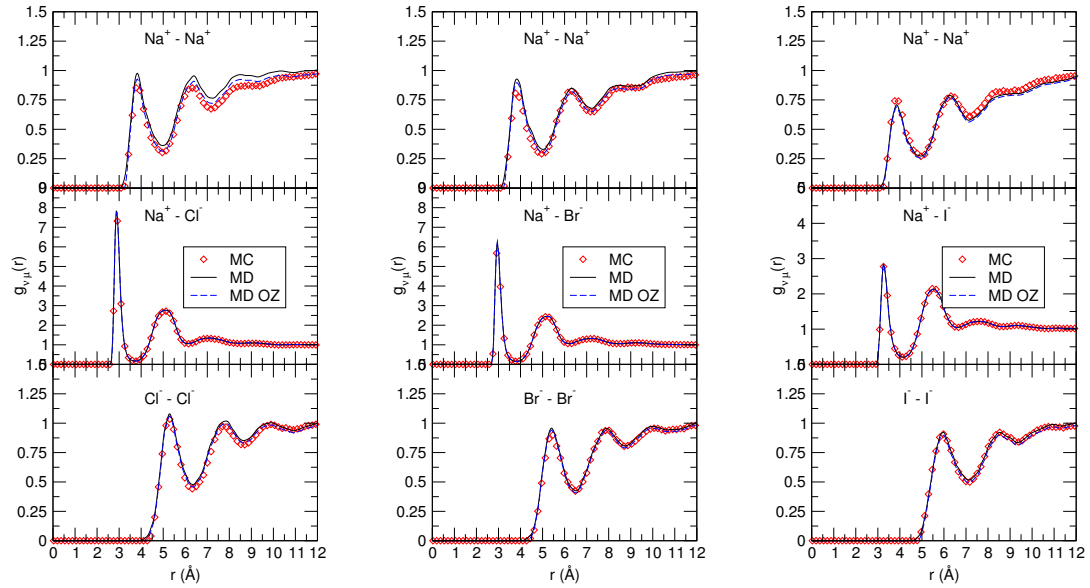

Figure E.2: Comparison between MD and MC radial distribution functions for Na^+ salts at $c = 0.64$ M.

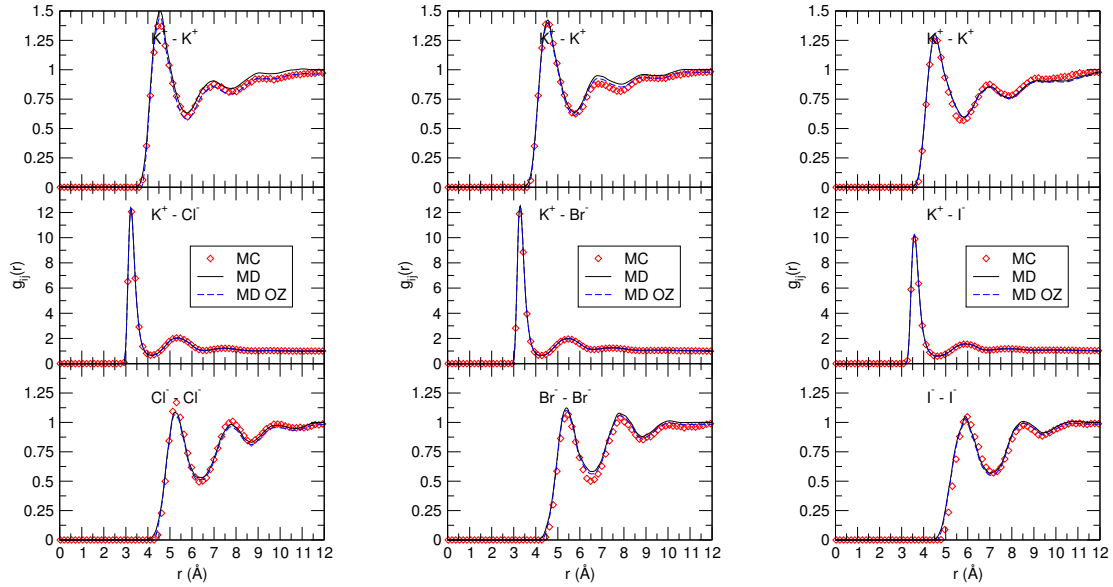

Figure E.3: Comparison between MD and MC radial distribution functions for K^+ salts at $c = 0.64$ M.

E.2 McMillan-Mayer Energy and Pressure

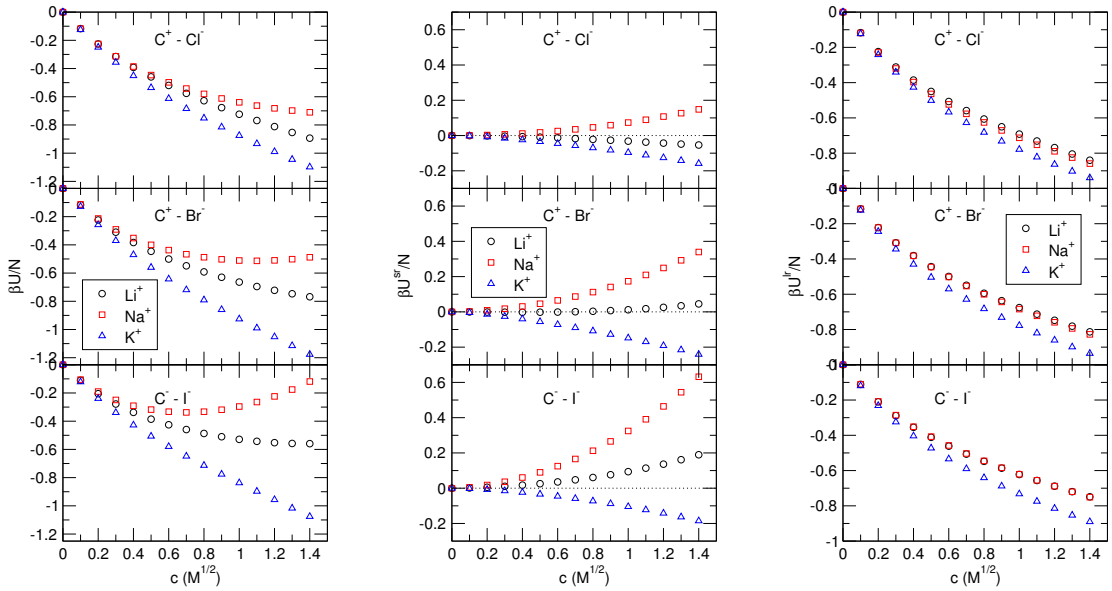

Figure E.4: Total (left), short (center), and long range (right) internal energy per particle obtained from MC simulations, as a function of the cation C^+.

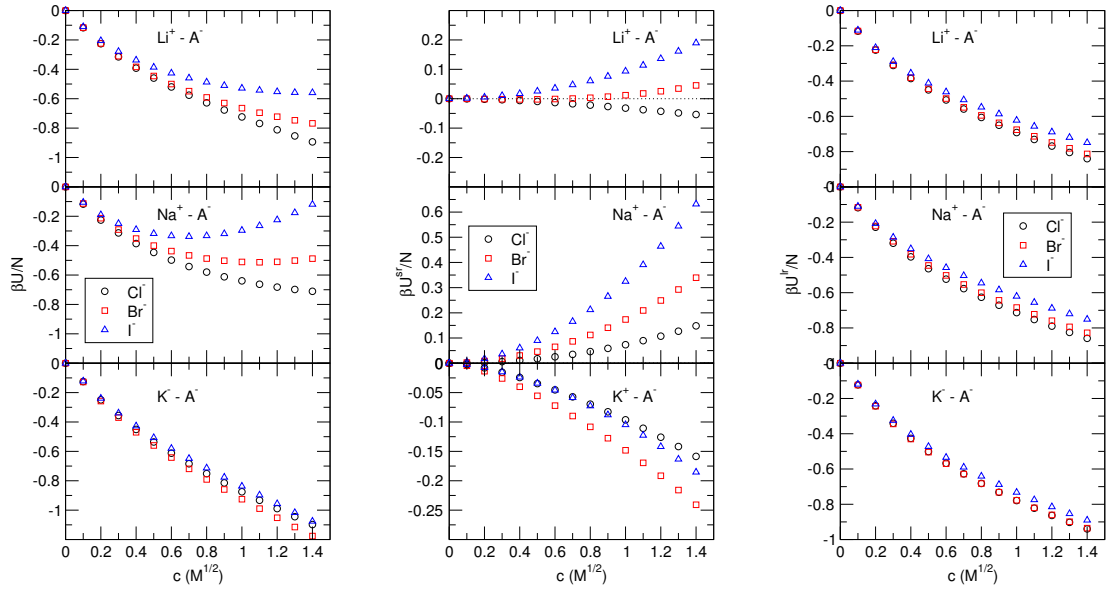

Figure E.5: Total (left), short (center) and long range (right) internal energy per particle obtained from MC simulations, as a function of the anion A^-.

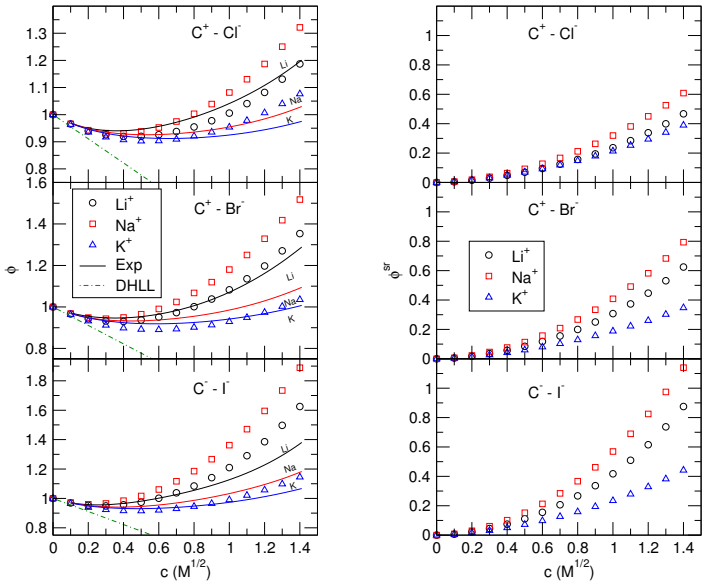

Figure E.6: Total (left) and short range (right) contributions to the osmotic coefficient obtained from MC simulations, as a function of the cation C^+. The experimental values for the osmotic coefficient ϕ are also given, along with the Debye-Hückel limiting law (DHLL).

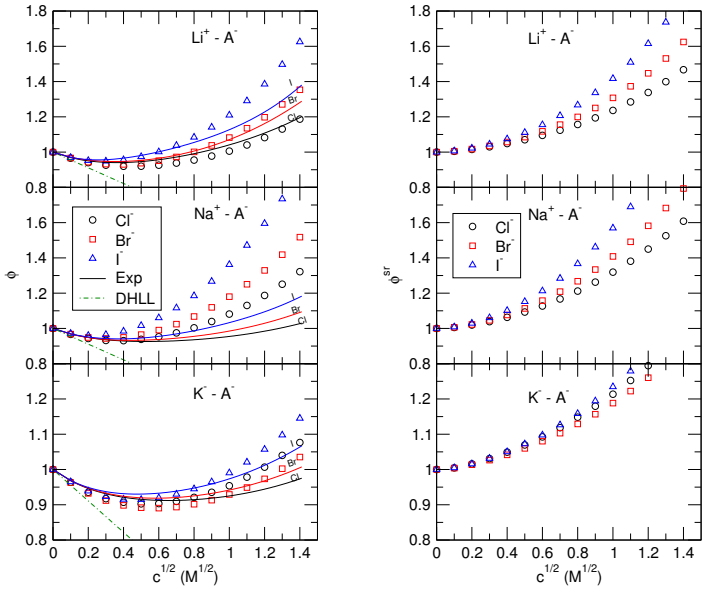

Figure E.7: Total (left) and short range (right) contributions to the osmotic coefficient obtained from MC simulations, as a function of the anion A^-. The experimental values for the osmotic coefficients ϕ are also given, along with the Debye-Hückel limiting law (DHLL).

E.3 Structure of the Solute Gas

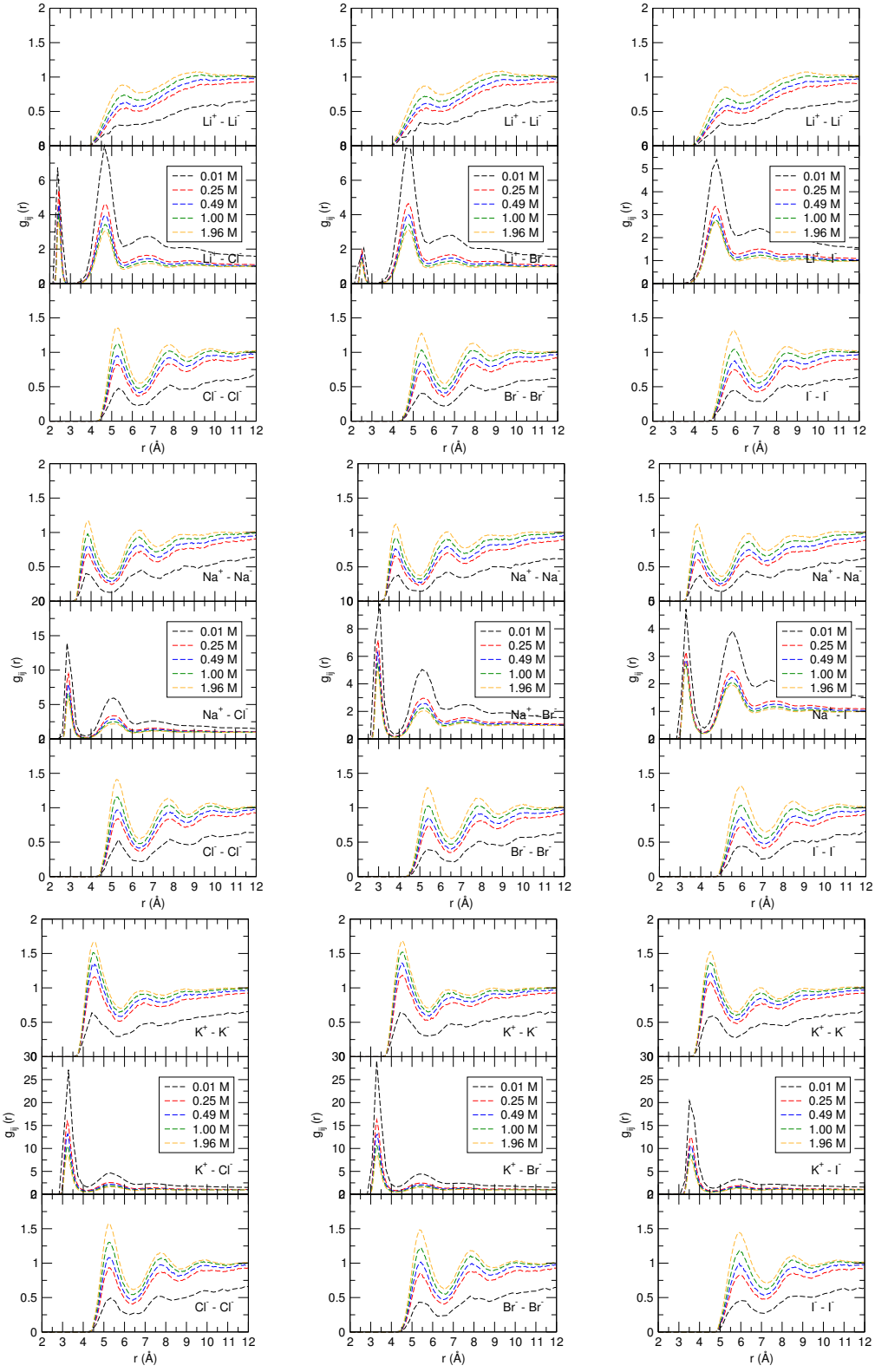

Figure E.8: Concentration variation of the radial distribution functions obtained from MC simulations for the nine different salts. From left to right, $A^- = Cl^-$, Br^-, I^-, and from top to bottom, $C^+ = Li^+$, Na^+, K^+.

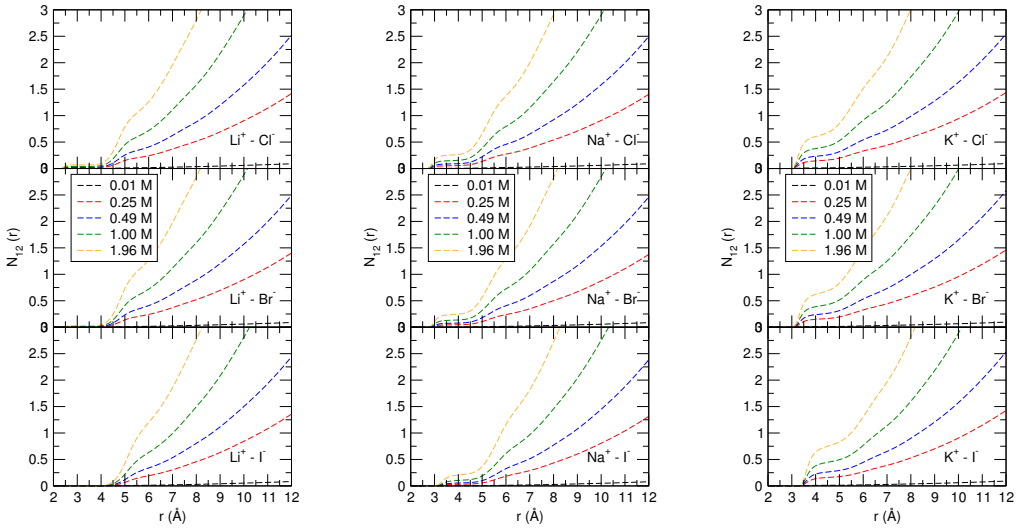

Figure E.9: Concentration variation of the average cation-anion C^+-A^- coordination number, obtained by integration of the MC generated radial distribution functions.

E.4 Minimum Distance Distributions

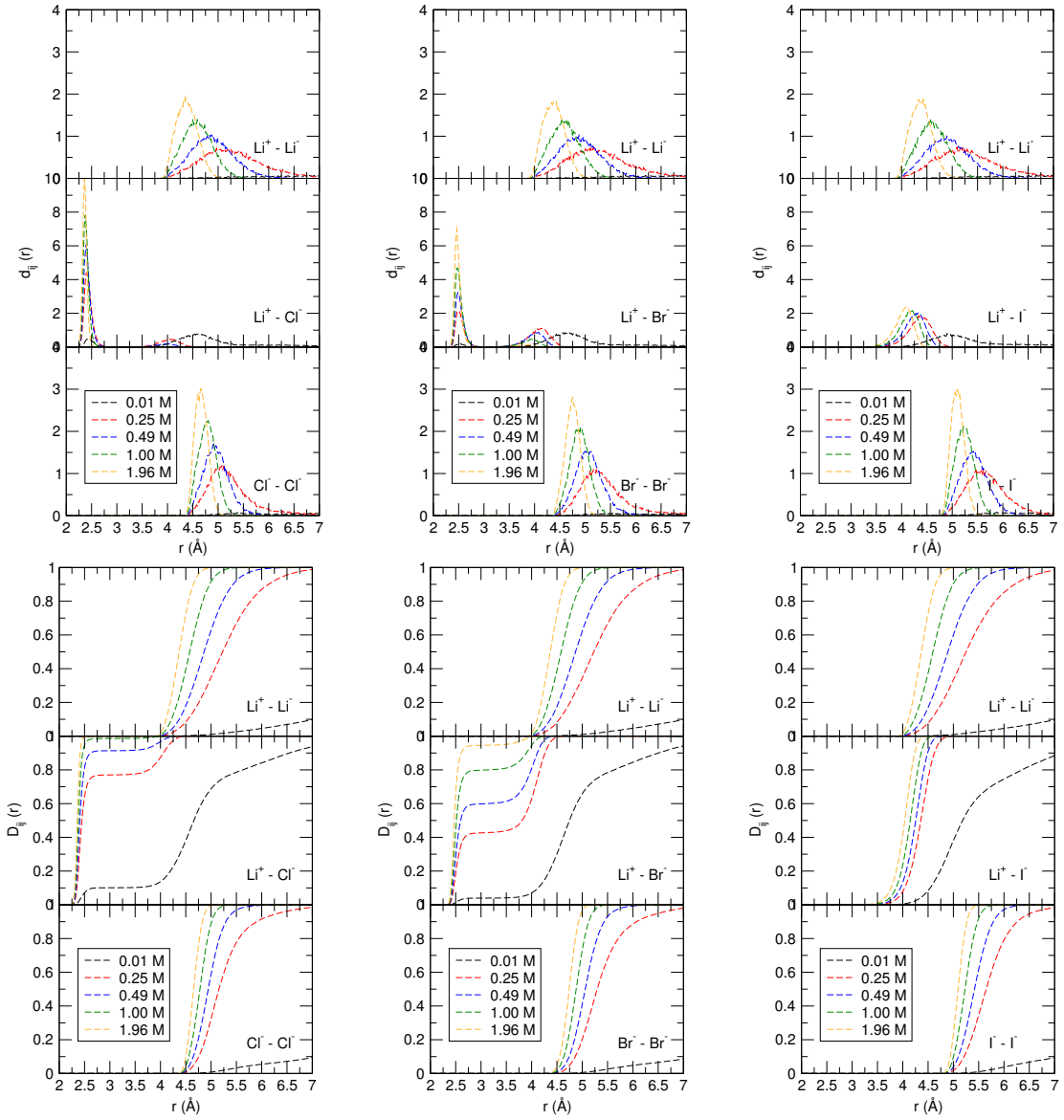

Figure E.10: Overlap distribution functions $d_{ij}(r)$ (top)and $D_{ij}(r)$ (bottom) calculated from MC simulations for Li^+ salts at various concentrations.

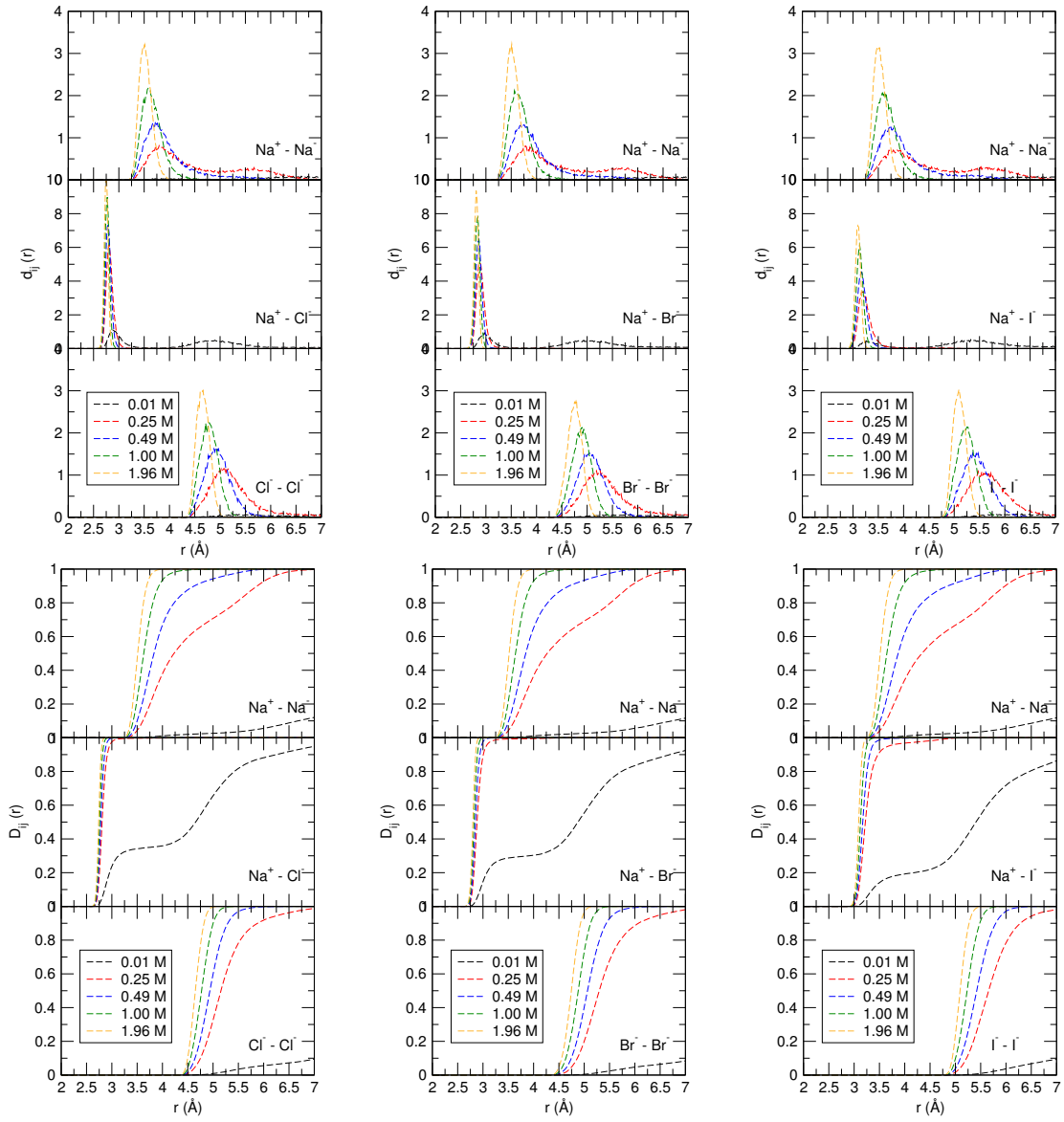

Figure E.11: Overlap distribution functions $d_{ij}(r)$ (top)and $D_{ij}(r)$ (bottom) calculated from MC simulations for Li^+ salts at various concentrations.

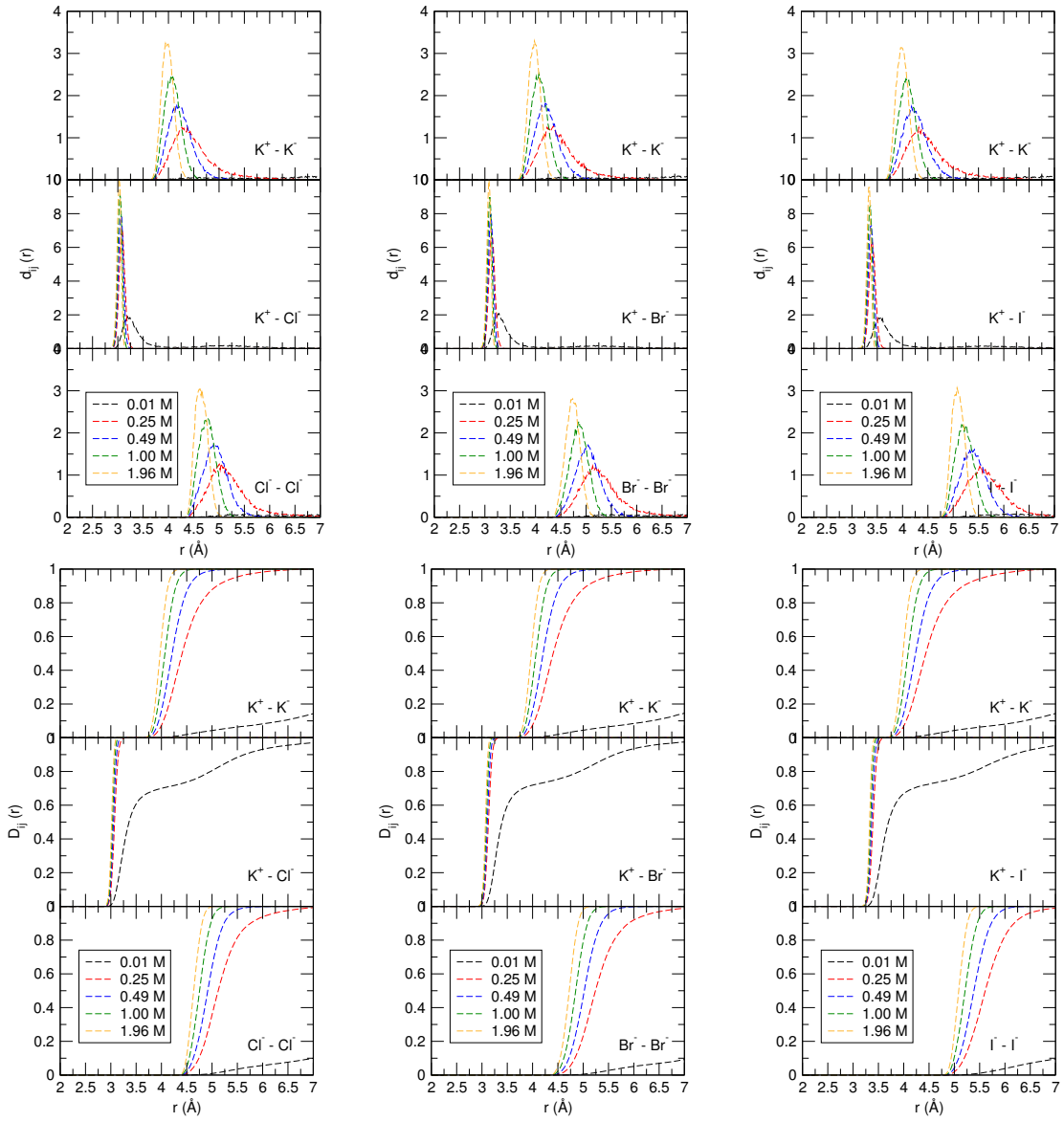

Figure E.12: Overlap distribution functions $d_{ij}(r)$ (top)and $D_{ij}(r)$ (bottom) calculated from MC simulations for Li^+ salts at various concentrations.

Appendix F

PFT Results

Summary

F.1 Free Energy

- $\beta f^{\text{ex}} = \beta F^{\text{ex}}/V$

  Excess free energy density obtained through PFT calculations using various reference systems, "exact" MC results are also shown.

- $\phi = \beta PV/N$

  Osmotic coefficients obtained through PFT calculations using various reference systems, "exact" MC results are also shown.

- $\beta f_0^{\text{ex}} = \beta(f^{\text{ex}} - \Delta f^{\text{ex}})$

  Reference excess free energy, defined as the difference between the total excess free energy and the free energy perturbation. Note that in the case of a three component reference, this term is not given just by the excess free energy of the reference, there is an extra contribution due to the difference in the ideal free energy between the two and three component systems.

- $\Delta\beta f^{\text{ex}}$

  Perturbation free energy

- ρ_p/ρ_0

  Fraction of pairs obtained from the PFT calculations in the case of a three-component reference system.

- Error$\beta f^{\text{ex}} = \frac{f^{\text{ex}} - f^{\text{ex}}_{\text{MC}}}{f^{\text{ex}}_{\text{MC}}}$

Relative error of the excess free energy given by the PFT calculations with respect to the "exact" MC results.

- $\Delta f^{\mathrm{ex}}/f_0^{\mathrm{ex}}$

  Relative magnitude of the perturbation free energy to the corresponding reference free energy obtained from PFT calculations.

- $\Delta f^{\mathrm{ex}}/f^{\mathrm{ex}}$

  Relative magnitude of the perturbation free energy to the corresponding total free energy obtained from PFT calculations.

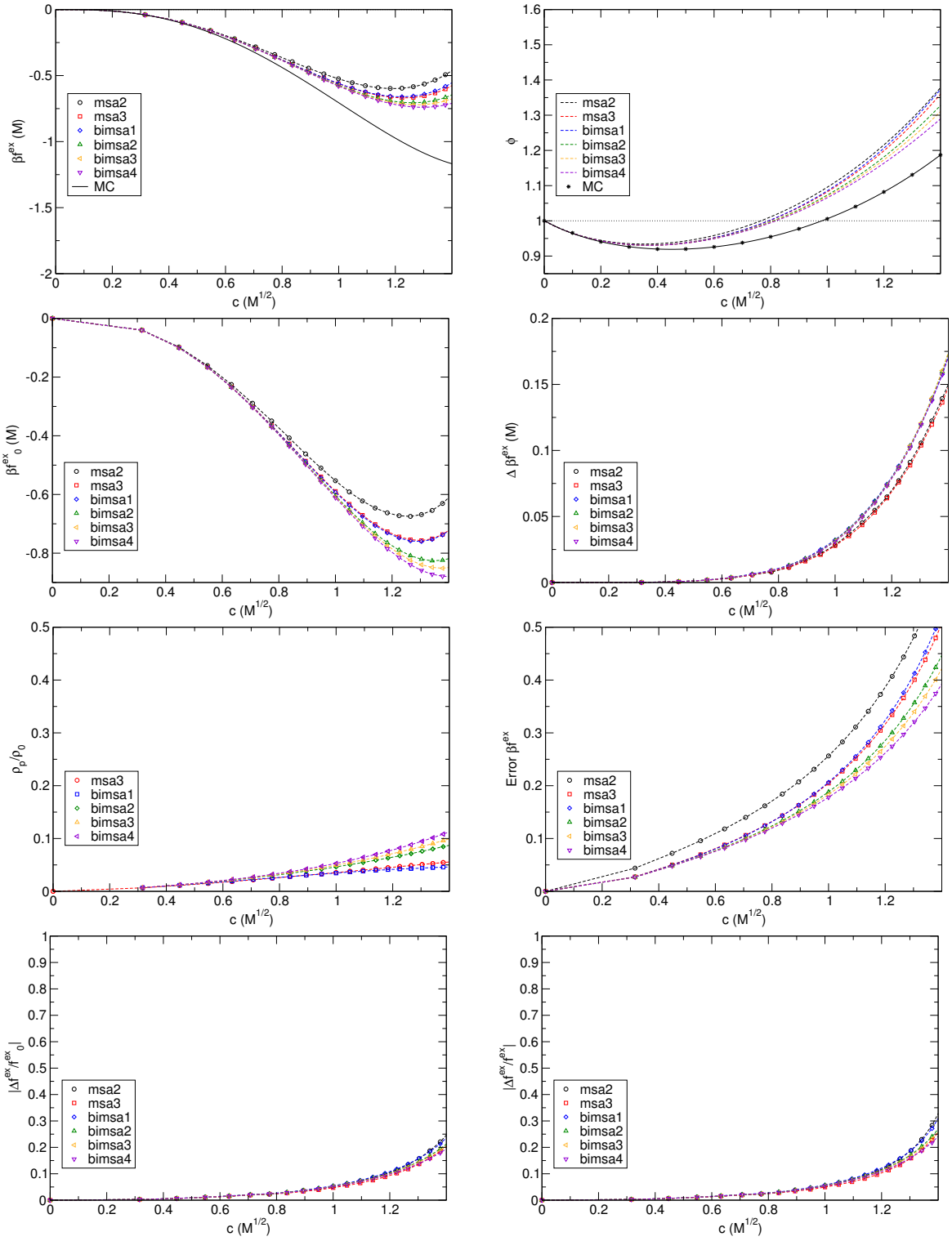

Figure F.1: LiCl PFT results

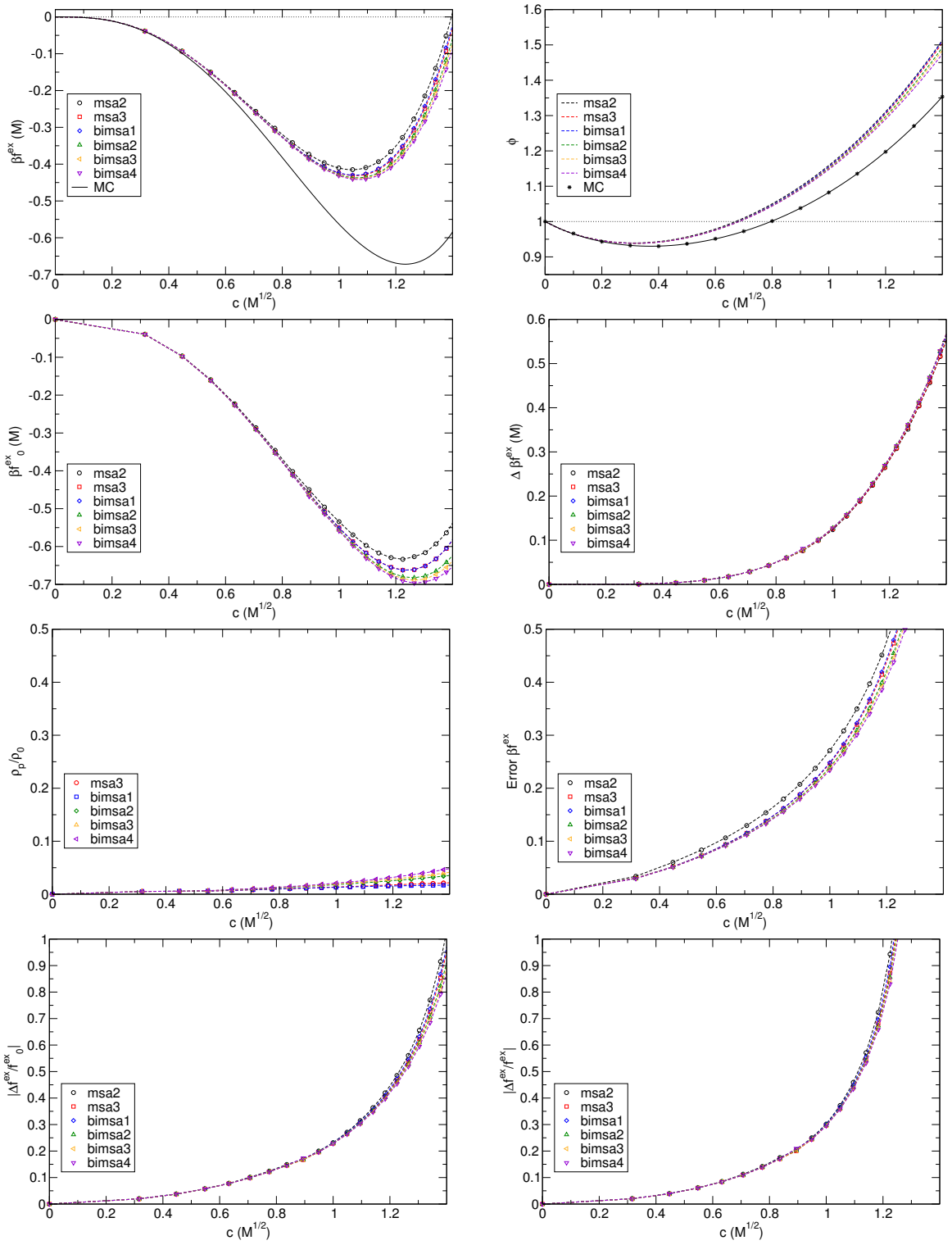

Figure F.2: LiBr PFT results

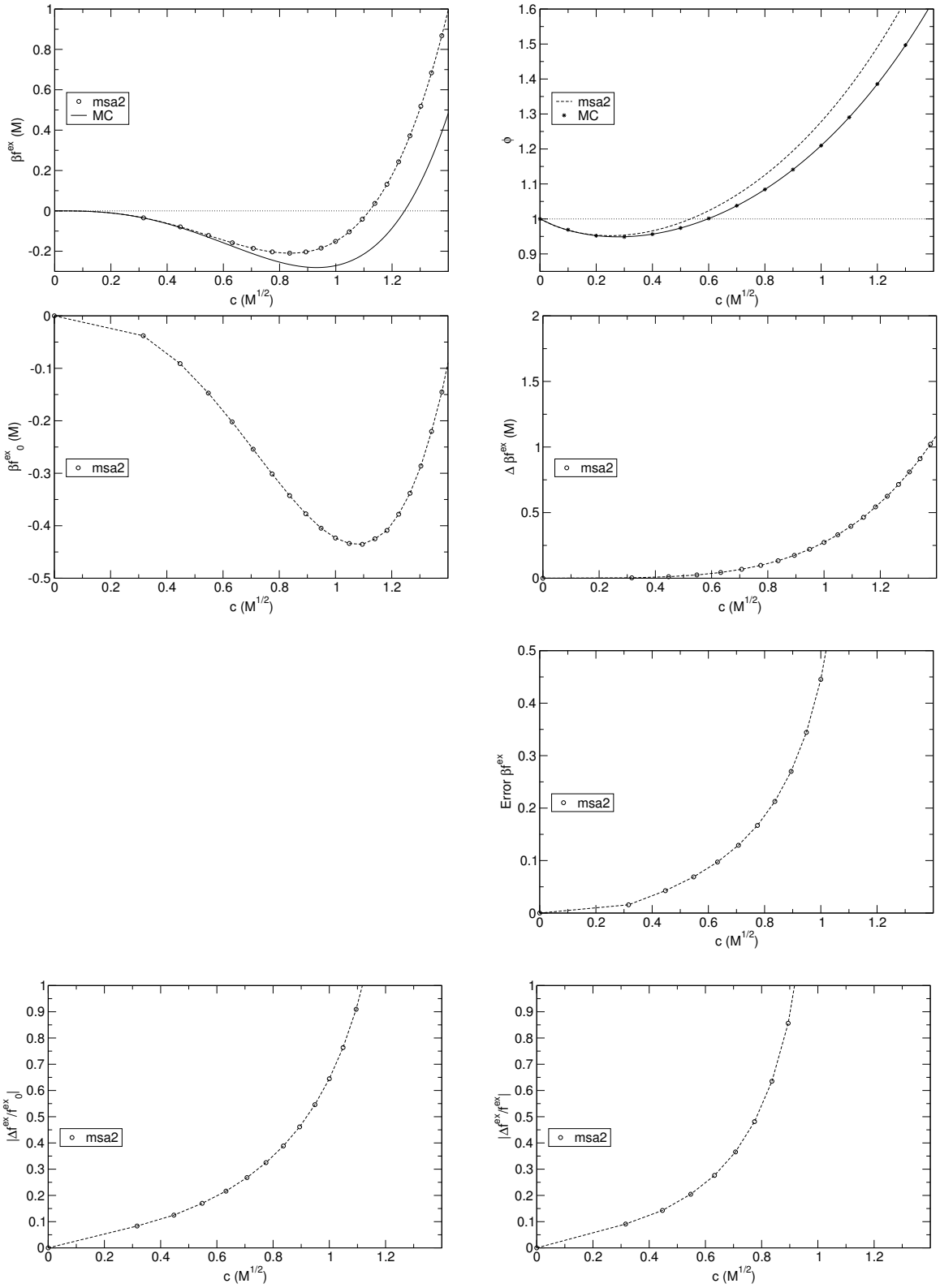

Figure F.3: LiI PFT results

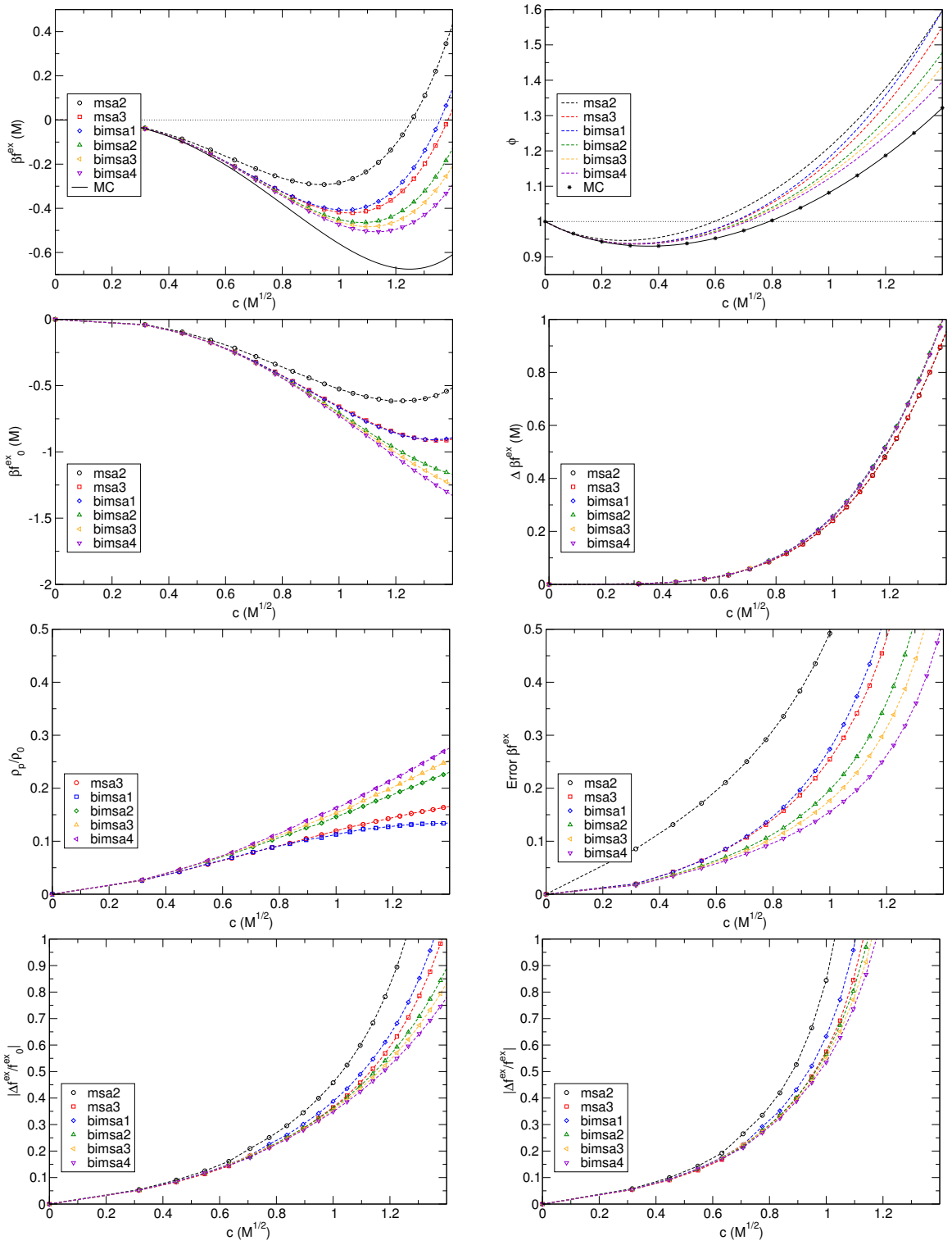

Figure F.4: NaCl PFT results

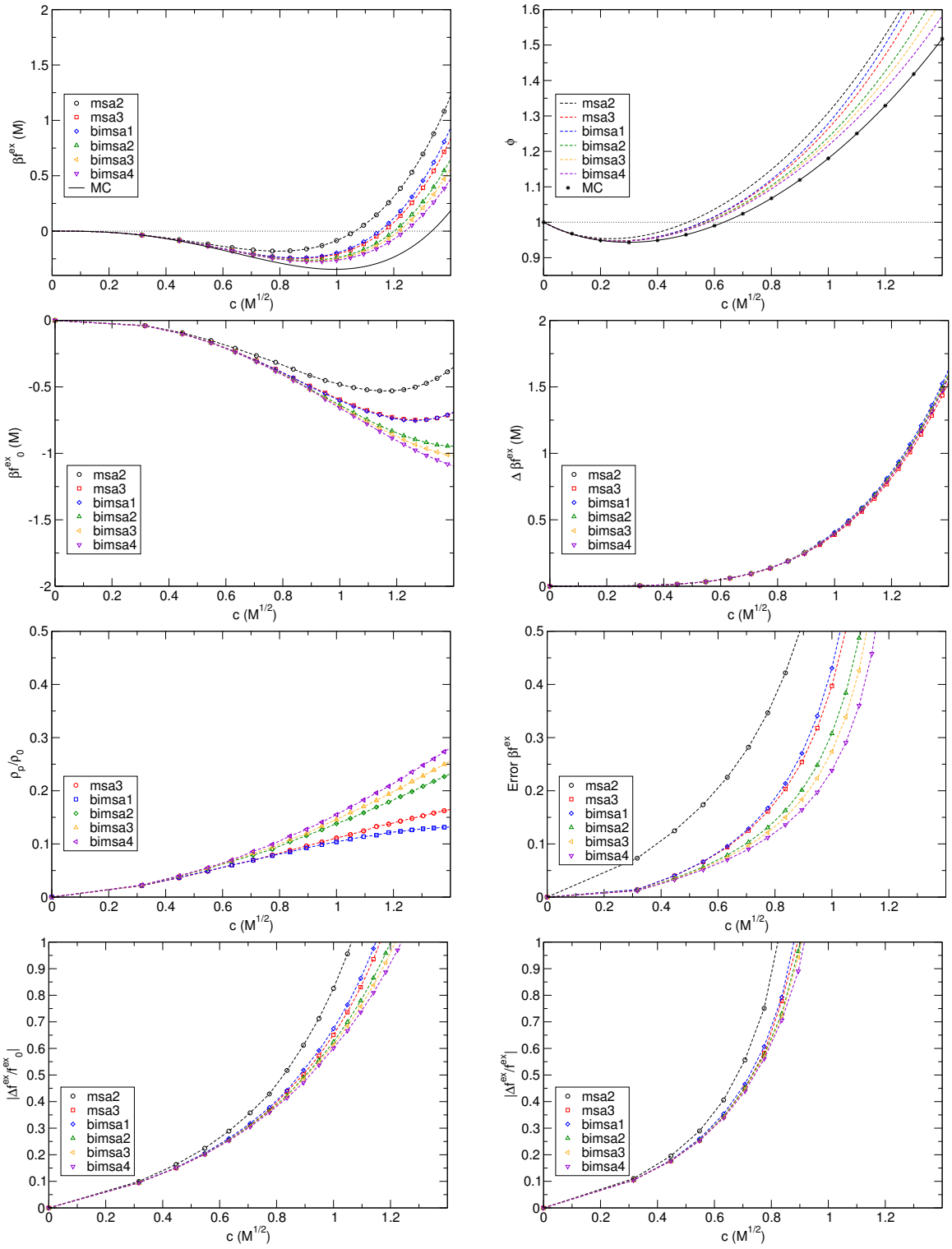

Figure F.5: NaBr PFT results

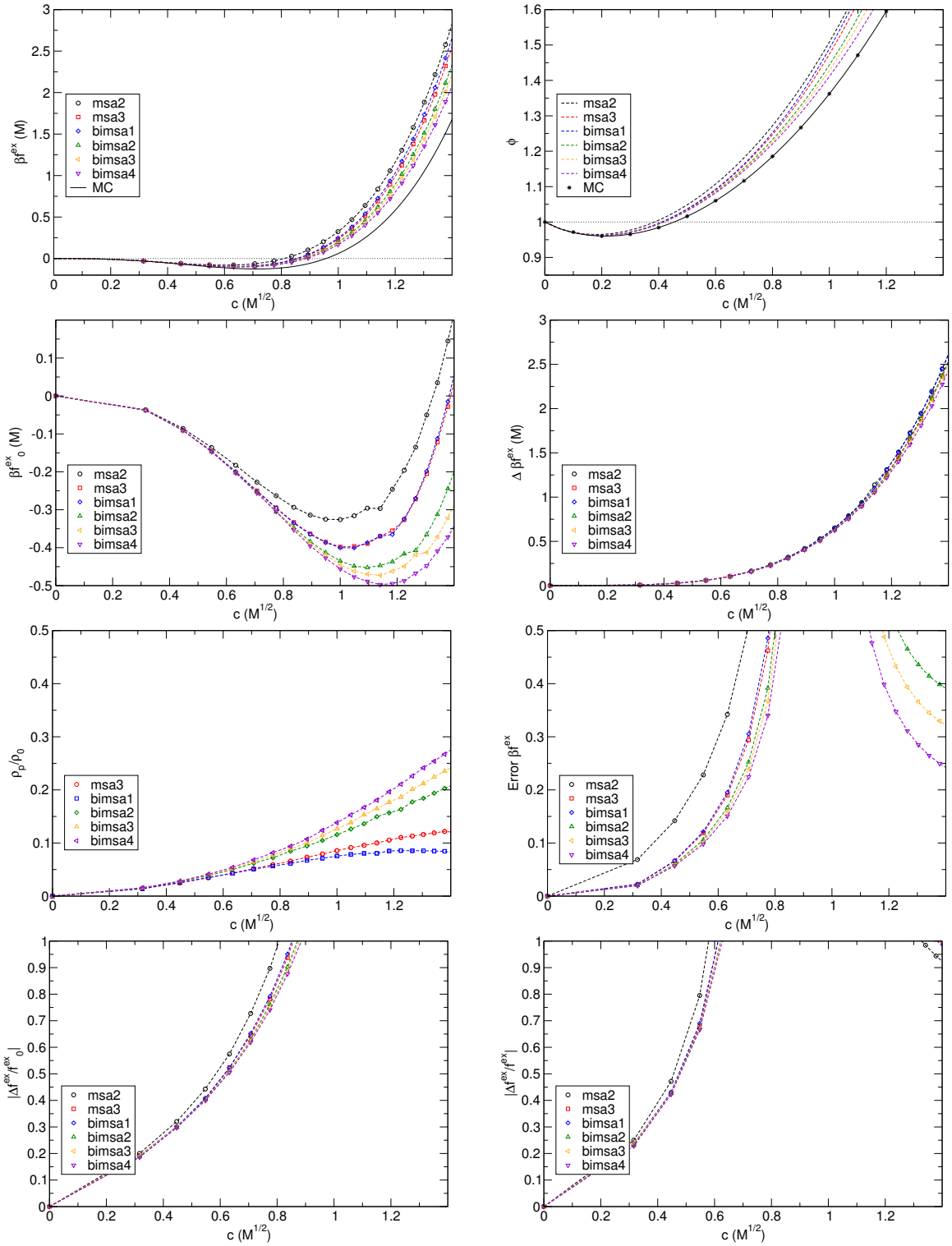

Figure F.6: NaI PFT results

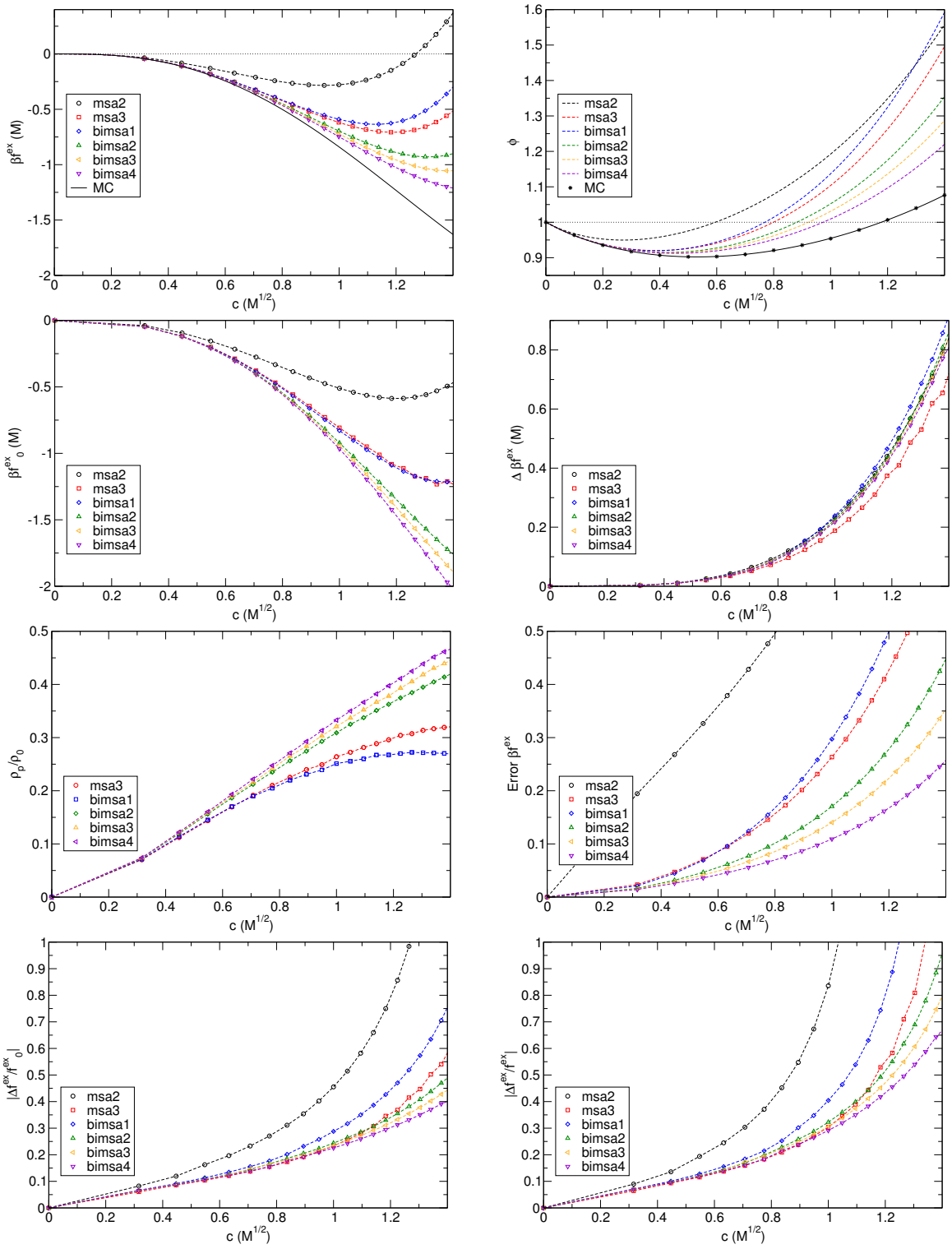

Figure F.7: KCl PFT results

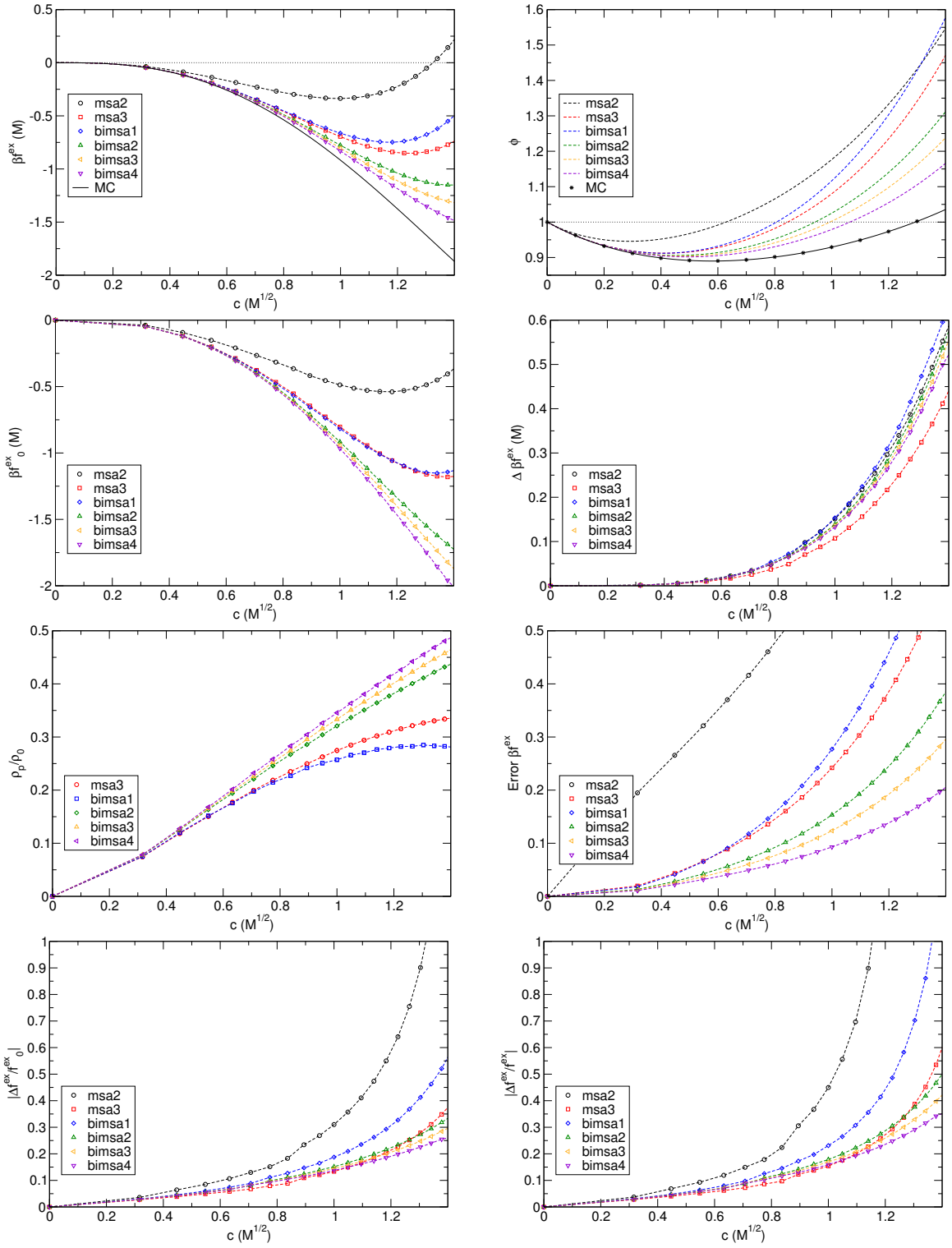

Figure F.8: KBr PFT results

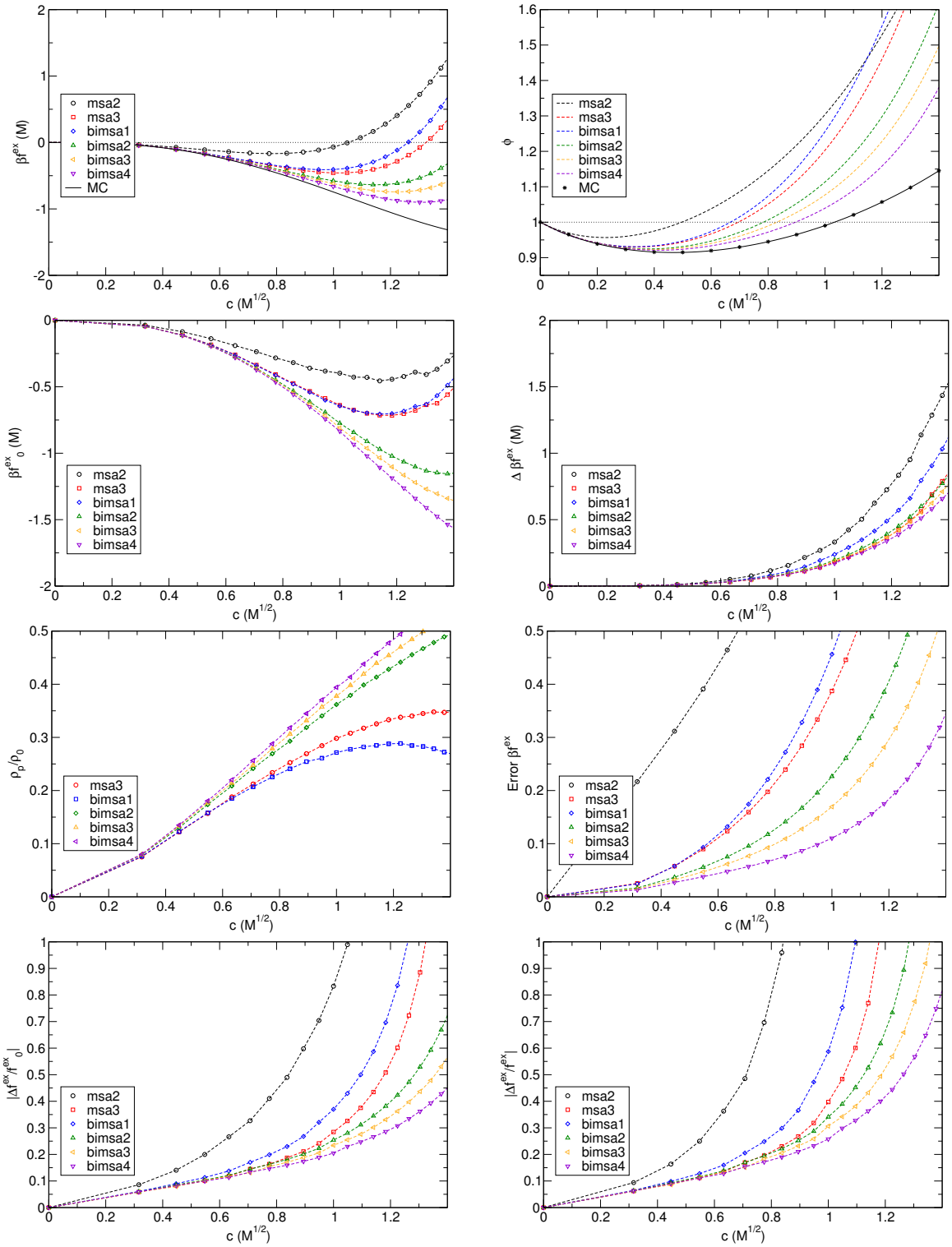

Figure F.9: KI PFT results

F.2 Minimization Diameters

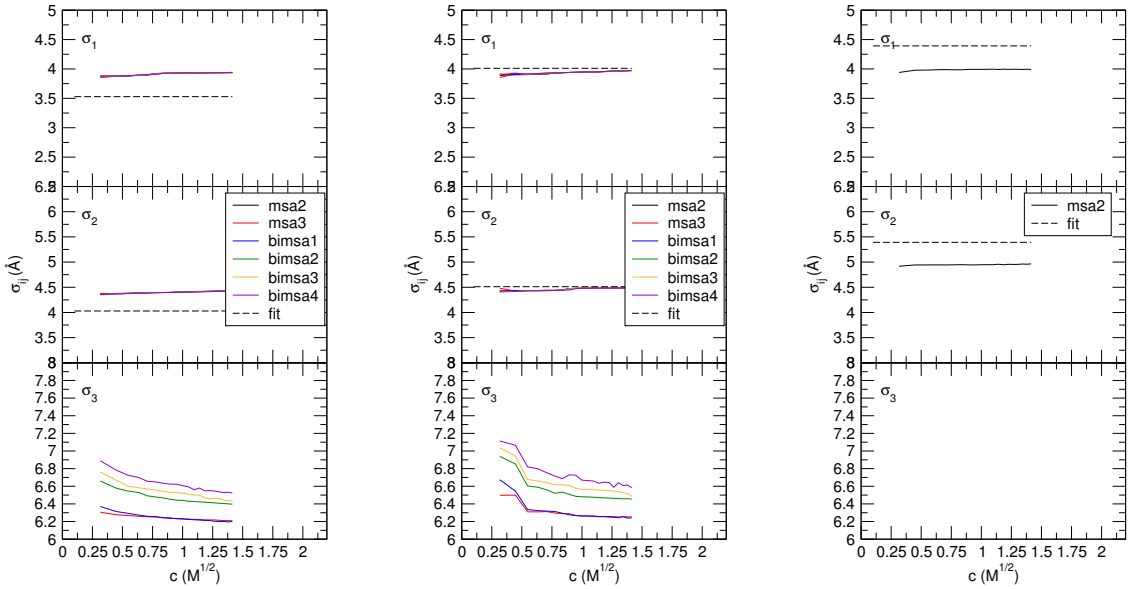

(a) LiCl (b) LiBr (c) LiI

Figure F.10: Minimization diameters for Li^+ salts

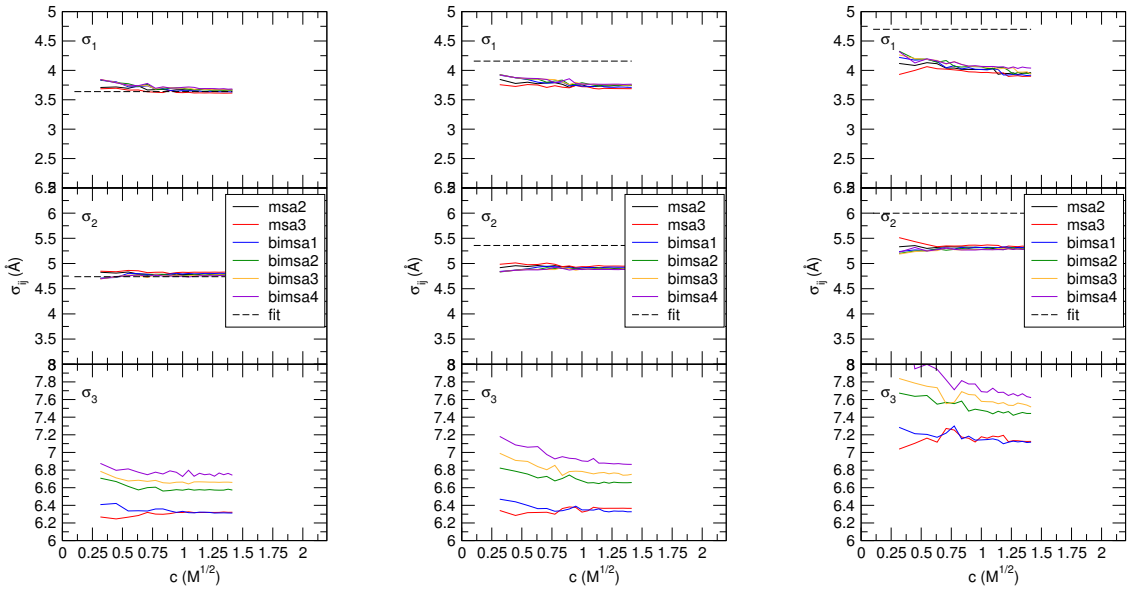

(a) NaCl (b) NaBr (c) NaI

Figure F.11: Minimization diameters for Na^+ salts

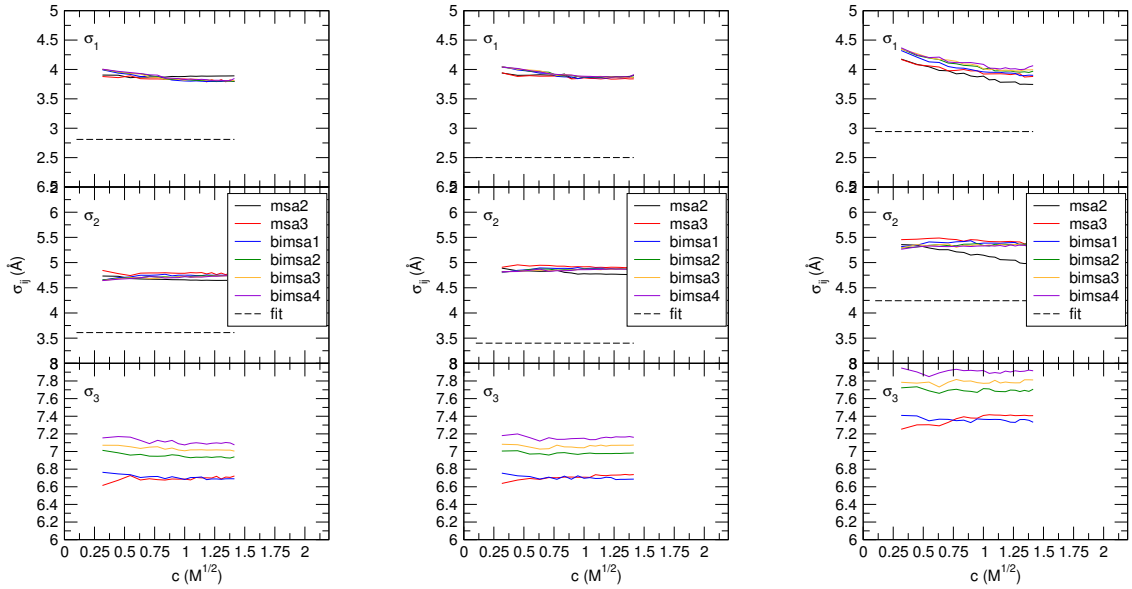

(a) KCl (b) KBr (c) KI

Figure F.12: Minimization diameters for K^+ salts

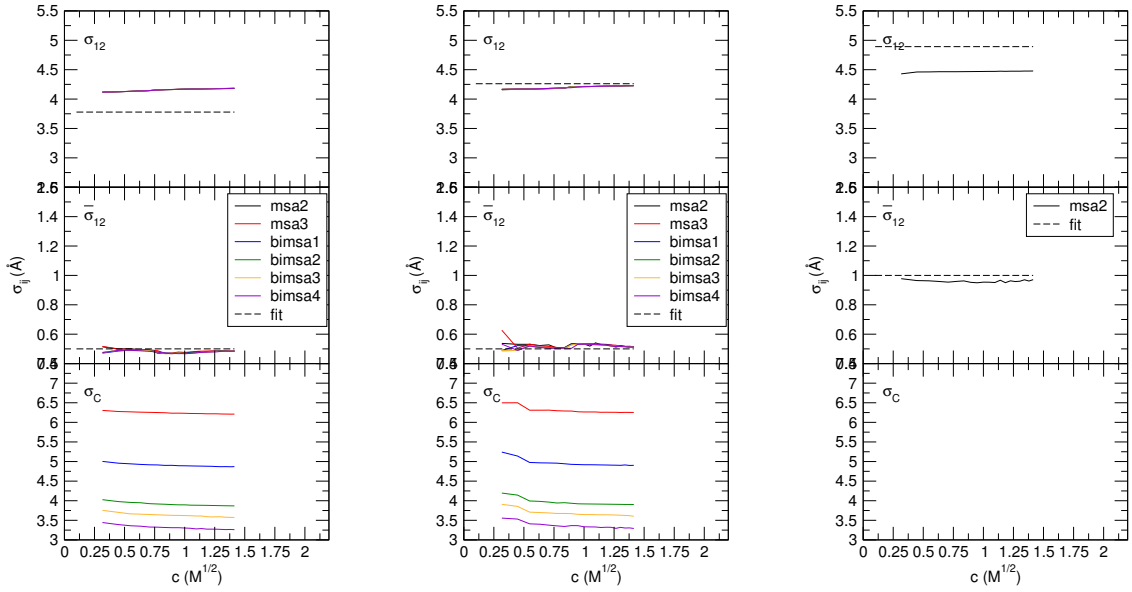

(a) LiCl (b) LiBr (c) LiI

Figure F.13: Minimization diameters for Li^+ salts (average and difference).

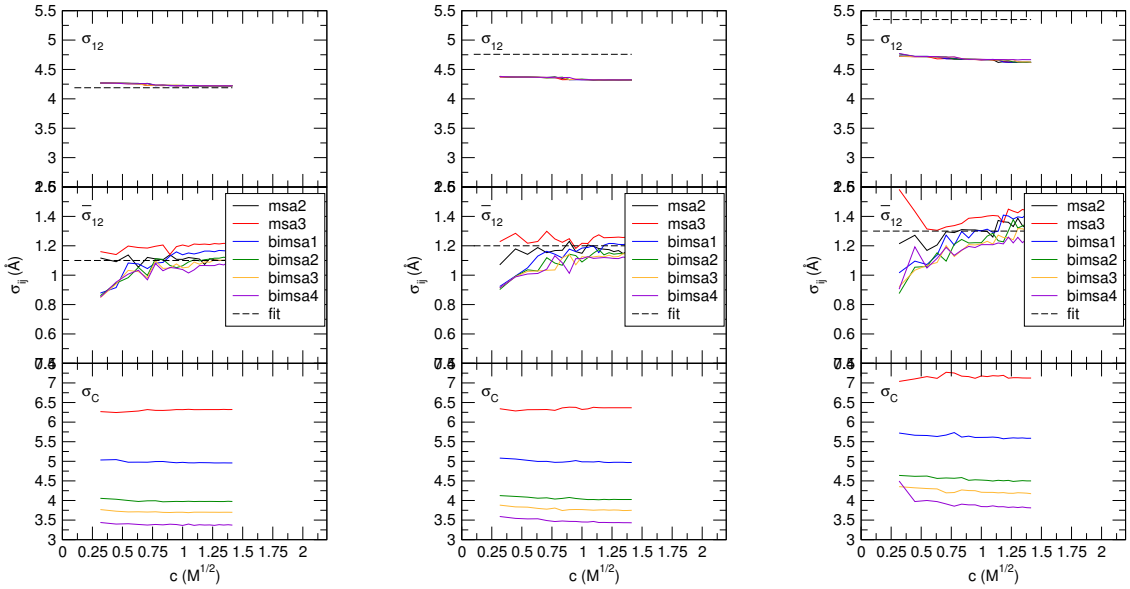

(a) NaCl (b) NaBr (c) NaI

Figure F.14: Minimization diameters for Li^+ salts (average and difference).

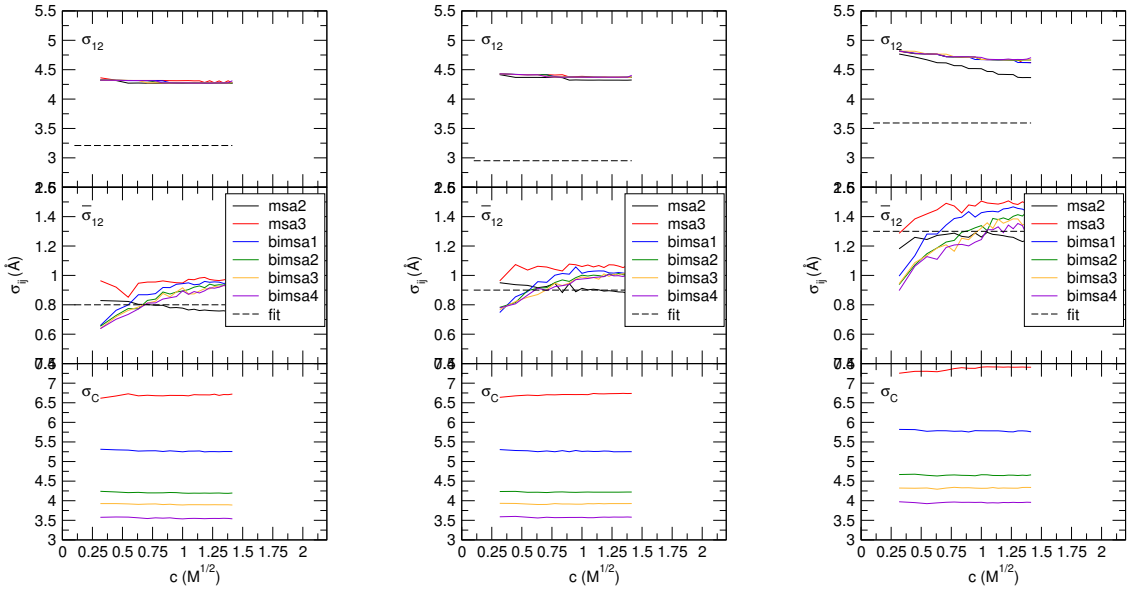

(a) KCl (b) KBr (c) KI

Figure F.15: Minimization diameters for K^+ salts (average and difference).

F.3 Radial Distribution Functions

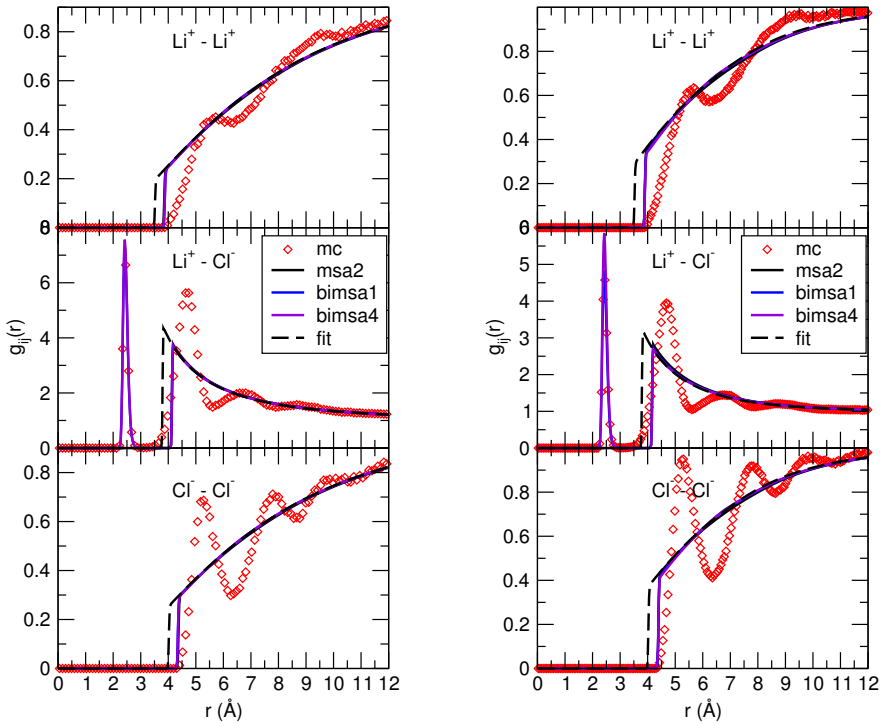

(a) c=0.1 M

(b) c=0.5 M

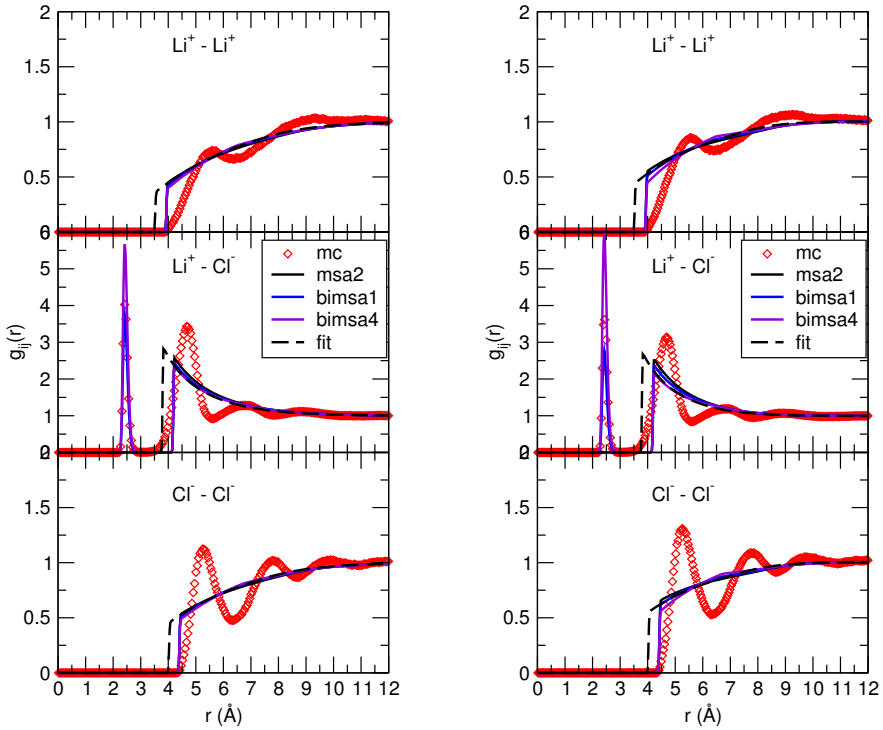

(c) c=1.0 M

(d) c=1.7 M

Figure F.16: Comparison between RDFs obtained from MC and PFT calculations for LiCl at several concentrations. The results obtained from fitting the exact free energy (MC) to a concentration independent two-component model, as given by the MSA solution, are also shown.

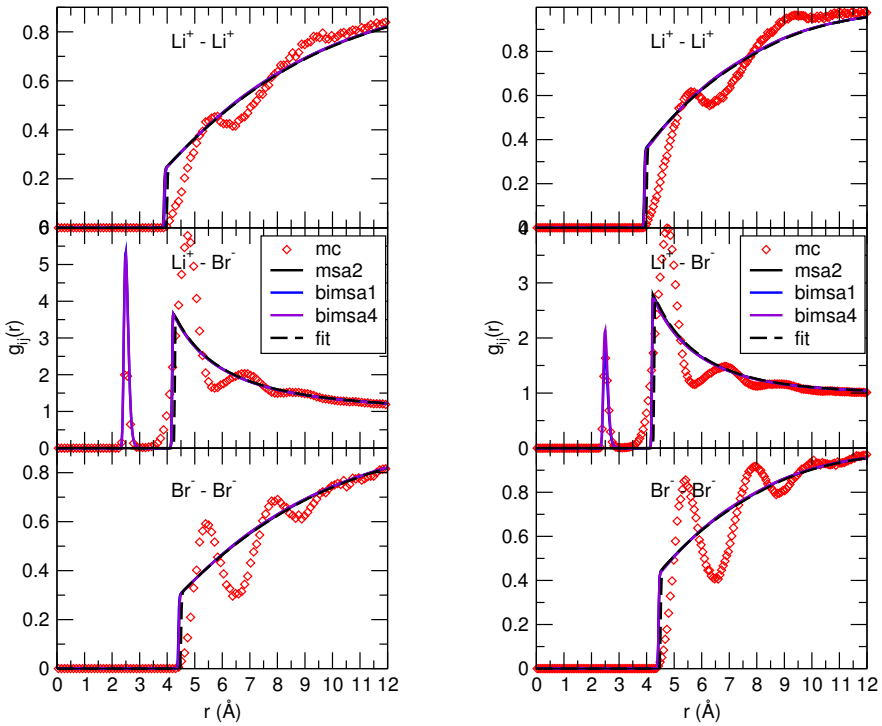

(a) c=0.1 M

(b) c=0.5 M

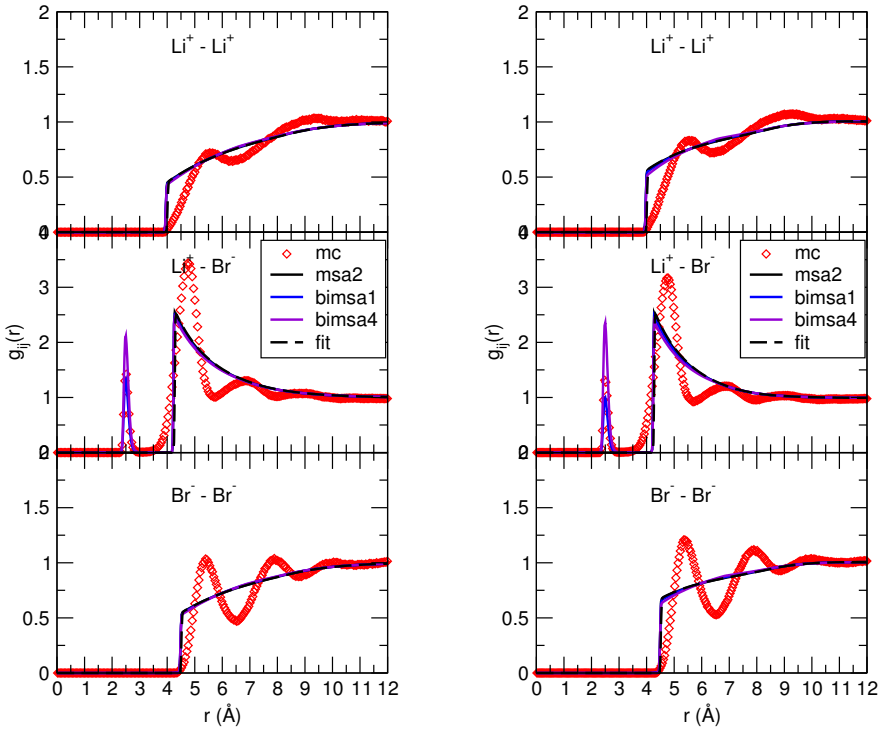

(c) c=1.0 M

(d) c=1.7 M

Figure F.17: Comparison between RDFs obtained from MC and PFT calculations for LiBr at several concentrations. The results obtained from fitting the exact free energy (MC) to a concentration independent two-component model, as given by the MSA solution, are also shown.

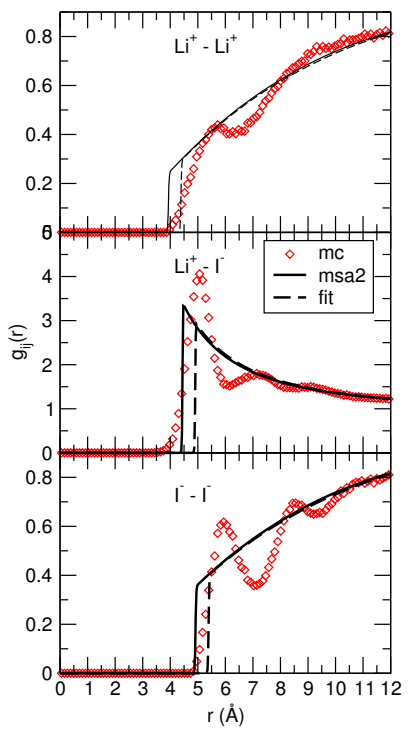

(a) c=0.1 M

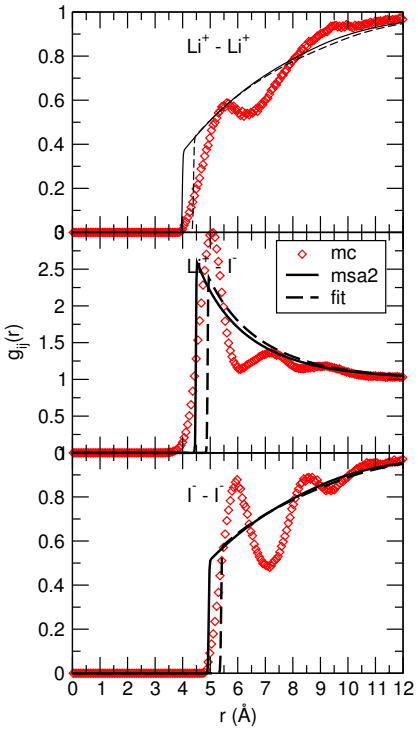

(b) c=0.5 M

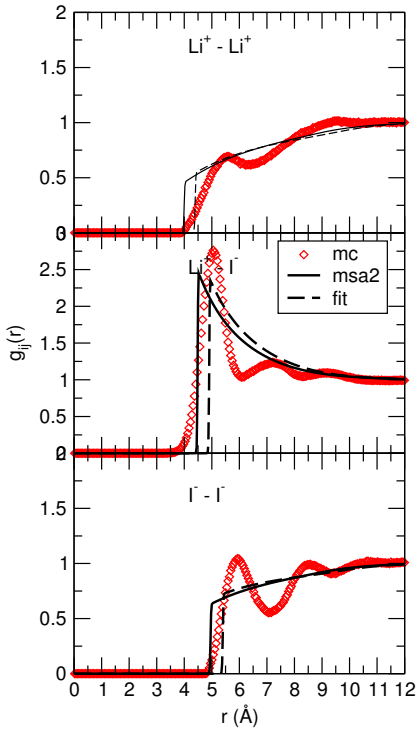

(c) c=1.0 M

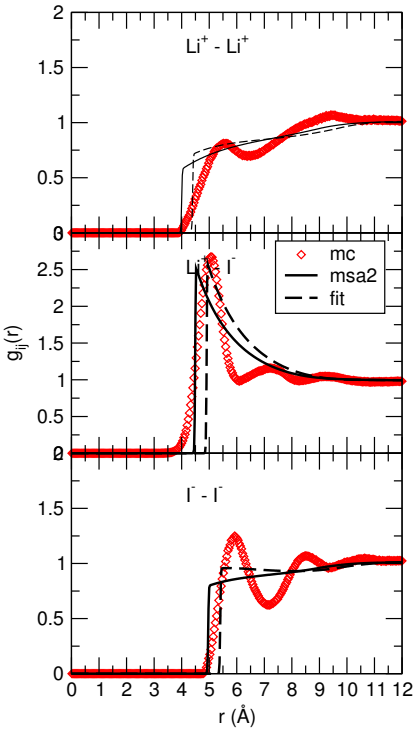

(d) c=1.7 M

Figure F.18: Comparison between RDFs obtained from MC and PFT calculations for LiI at several concentrations. The results obtained from fitting the exact free energy (MC) to a concentration independent two-component model, as given by the MSA solution, are also shown.

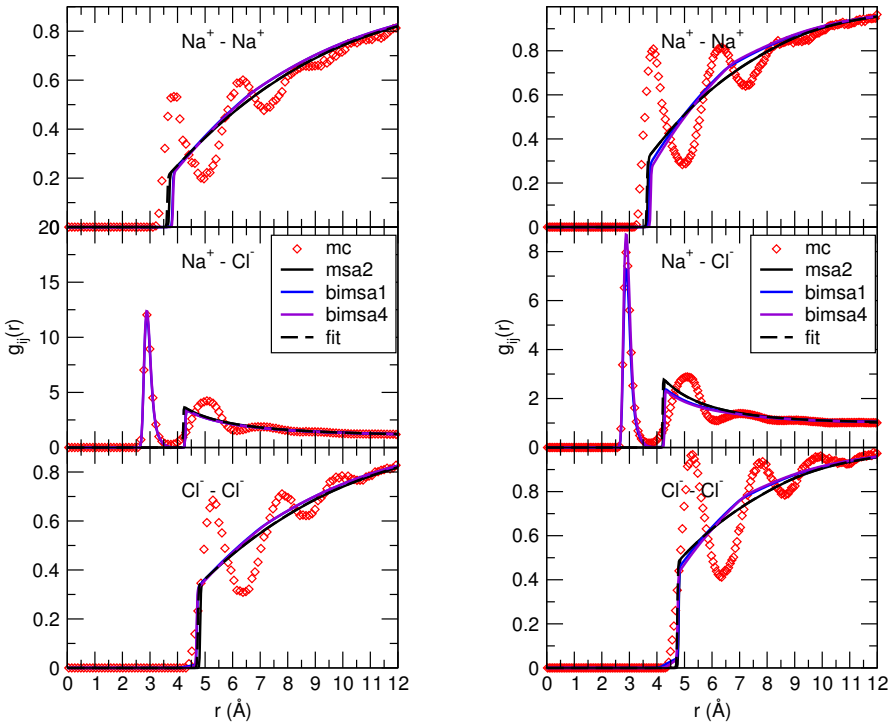

(a) c=0.1 M (b) c=0.5 M

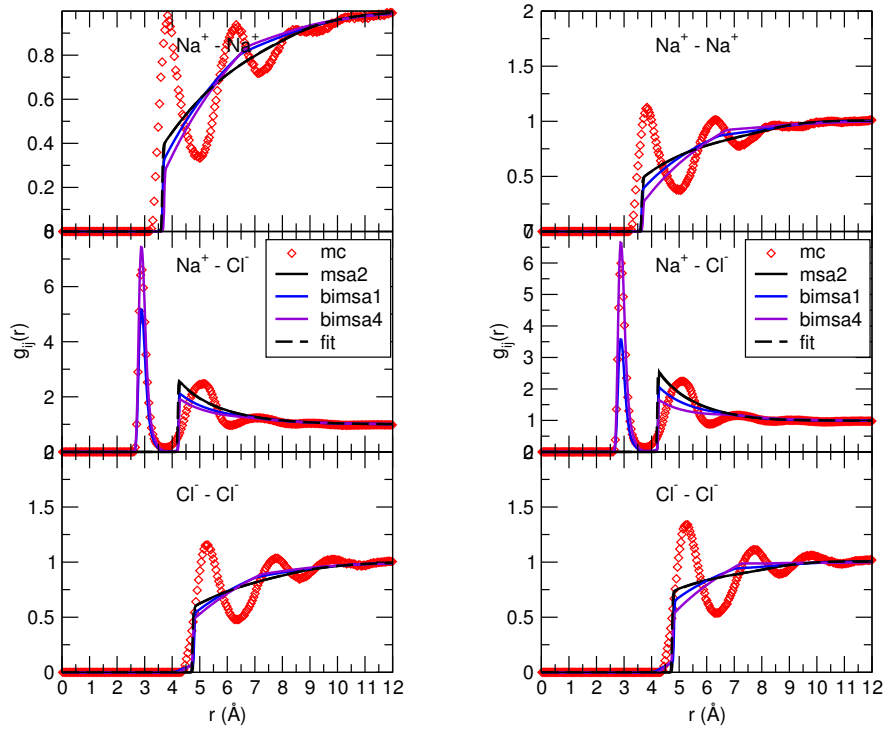

(c) c=1.0 M (d) c=1.7 M

Figure F.19: Comparison between RDFs obtained from MC and PFT calculations for NaCl at several concentrations. The results obtained from fitting the exact free energy (MC) to a concentration independent two-component model, as given by the MSA solution, are also shown

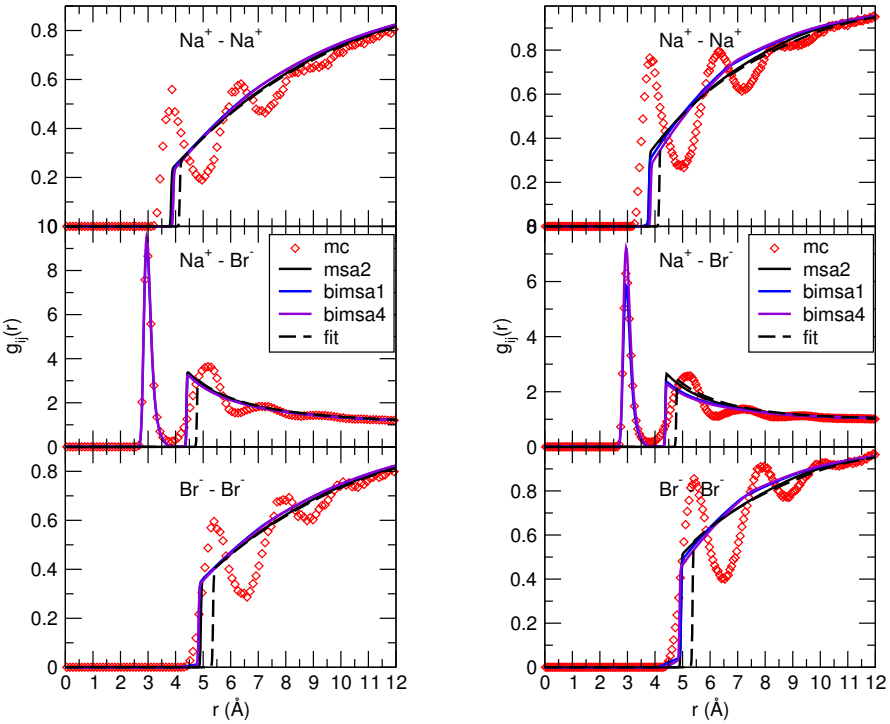

(a) c=0.1 M

(b) c=0.5 M

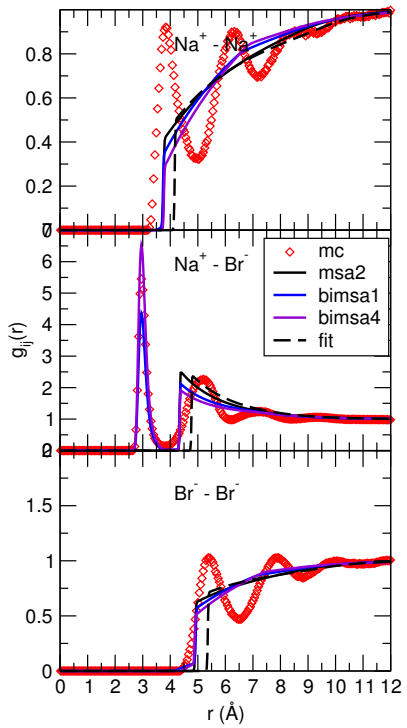

(c) c=1.0 M

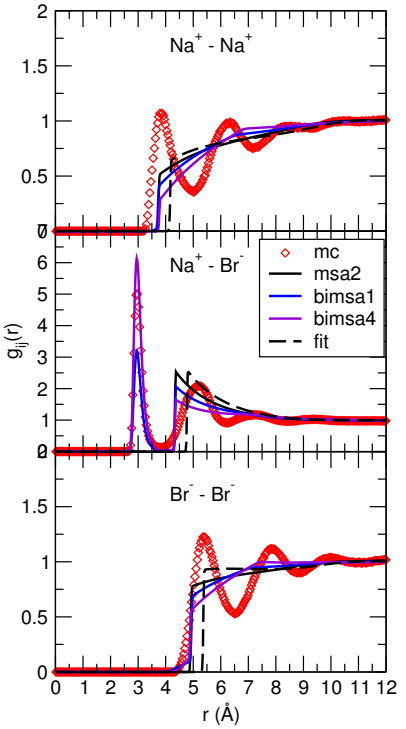

(d) c=1.7 M

Figure F.20: Comparison between RDFs obtained from MC and PFT calculations for NaBr at several concentrations. The results obtained from fitting the exact free energy (MC) to a concentration independent two-component model, as given by the MSA solution, are also shown

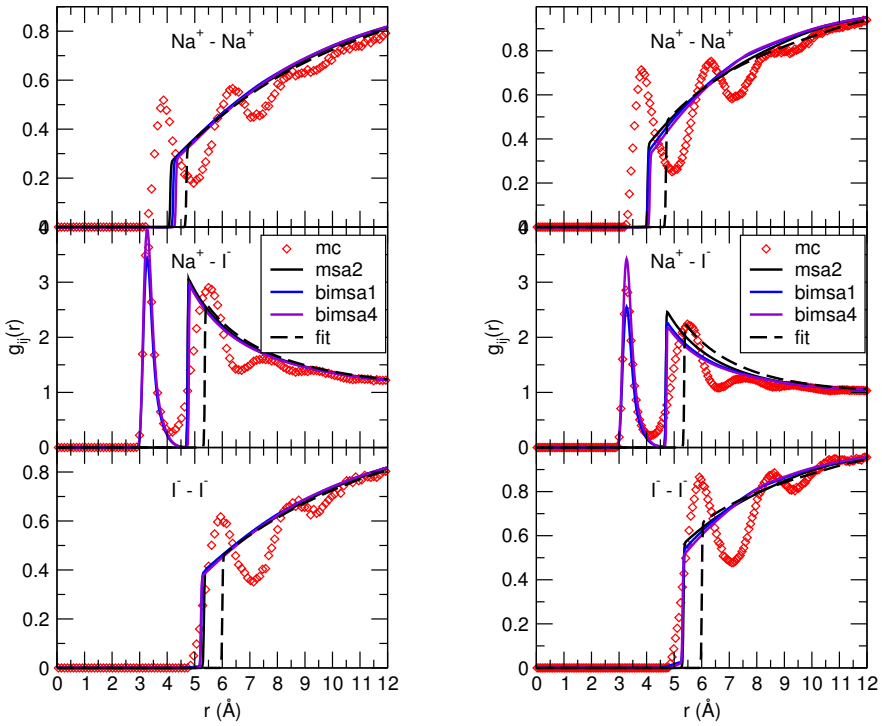

(a) c=0.1 M

(b) c=0.5 M

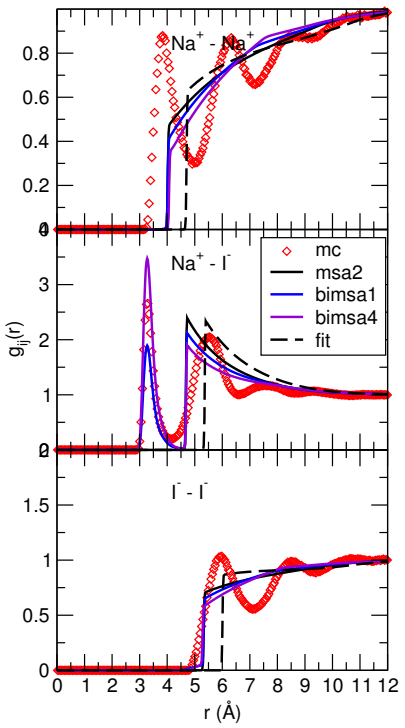

(c) c=1.0 M

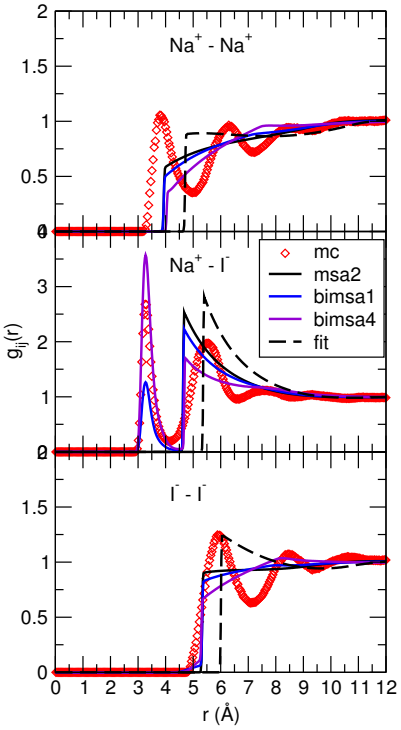

(d) c=1.7 M

Figure F.21: Comparison between RDFs obtained from MC and PFT calculations for NaBr at several concentrations. The results obtained from fitting the exact free energy (MC) to a concentration independent two-component model, as given by the MSA solution, are also shown.

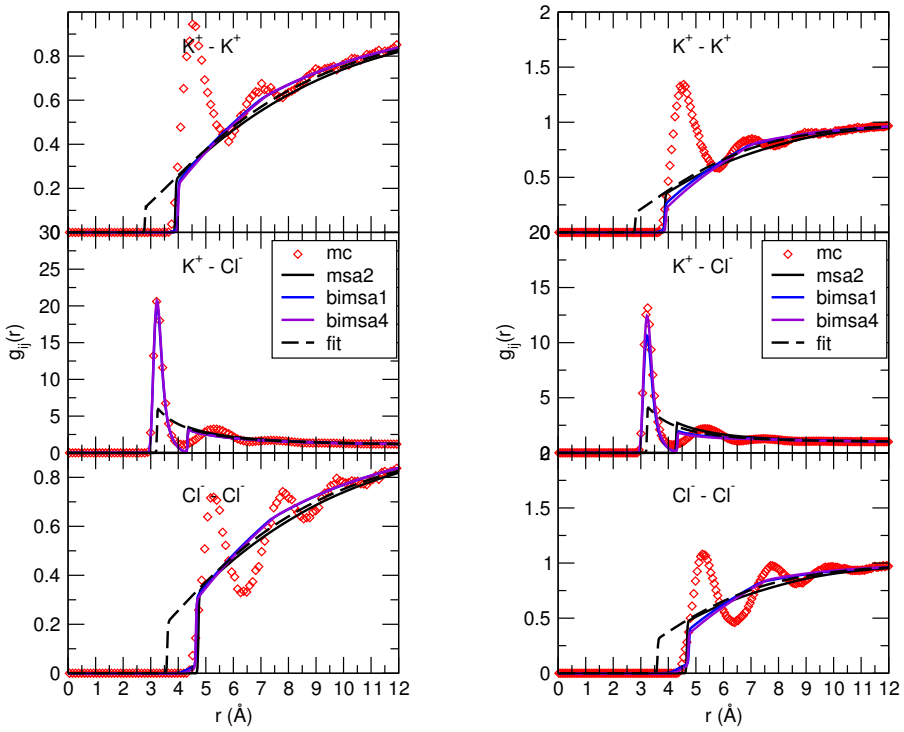

(a) c=0.1 M

(b) c=0.5 M

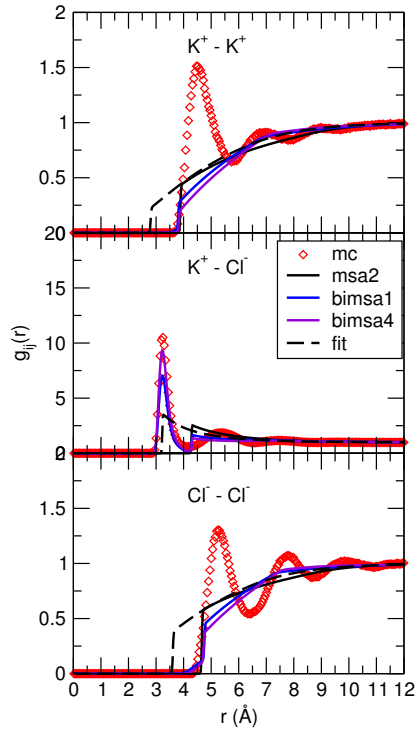

(c) c=1.0 M

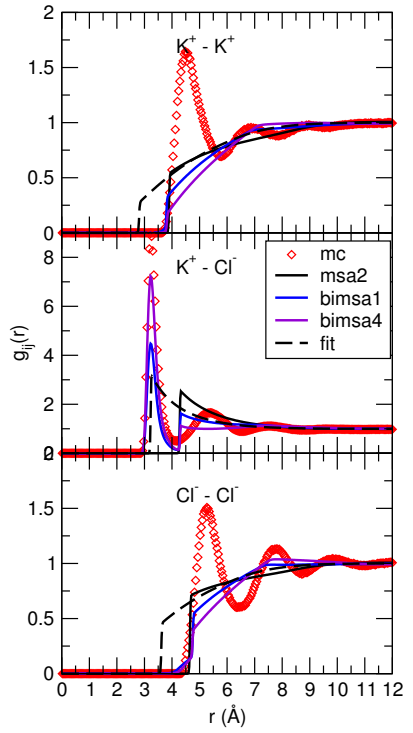

(d) c=1.7 M

Figure F.22: Comparison between RDFs obtained from MC and PFT calculations for KCl at several concentrations. The results obtained from fitting the exact free energy (MC) to a concentration independent two-component model, as given by the MSA solution, are also shown.

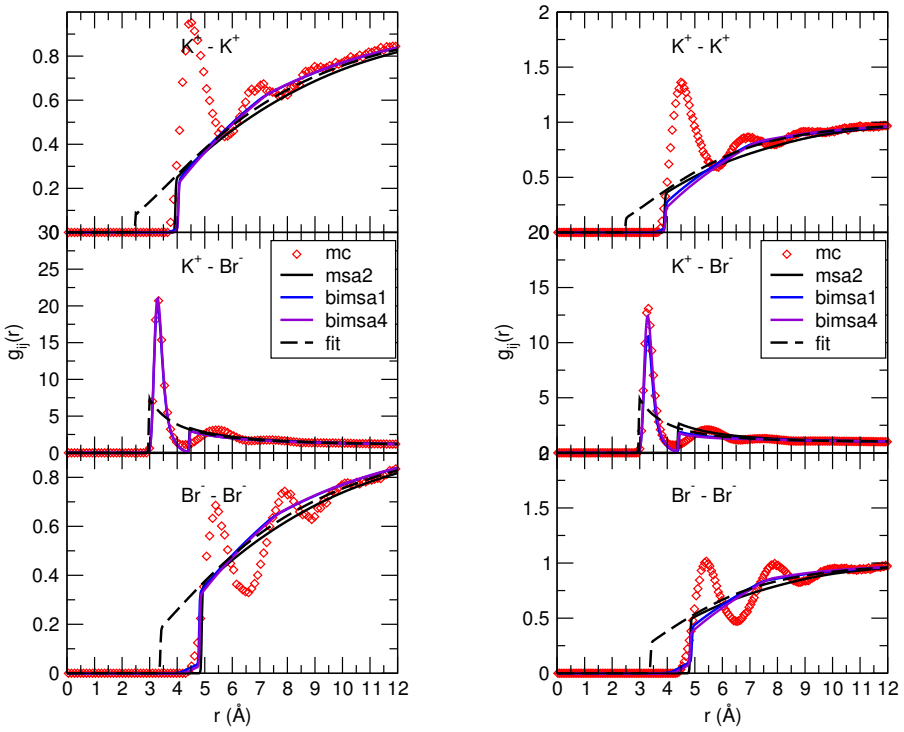

(a) c=0.1 M

(b) c=0.5 M

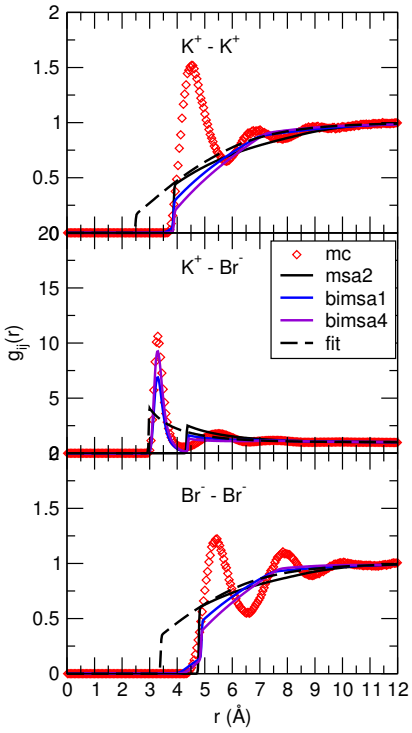

(c) c=1.0 M

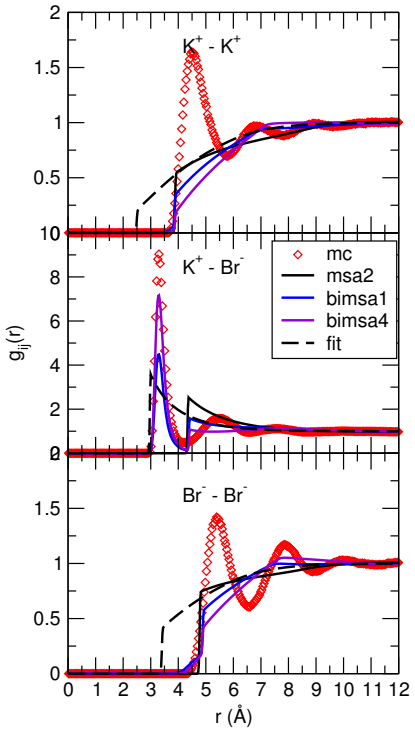

(d) c=1.7 M

Figure F.23: Comparison between RDFs obtained from MC and PFT calculations for KBr at several concentrations. The results obtained from fitting the exact free energy (MC) to a concentration independent two-component model, as given by the MSA solution, are also shown.

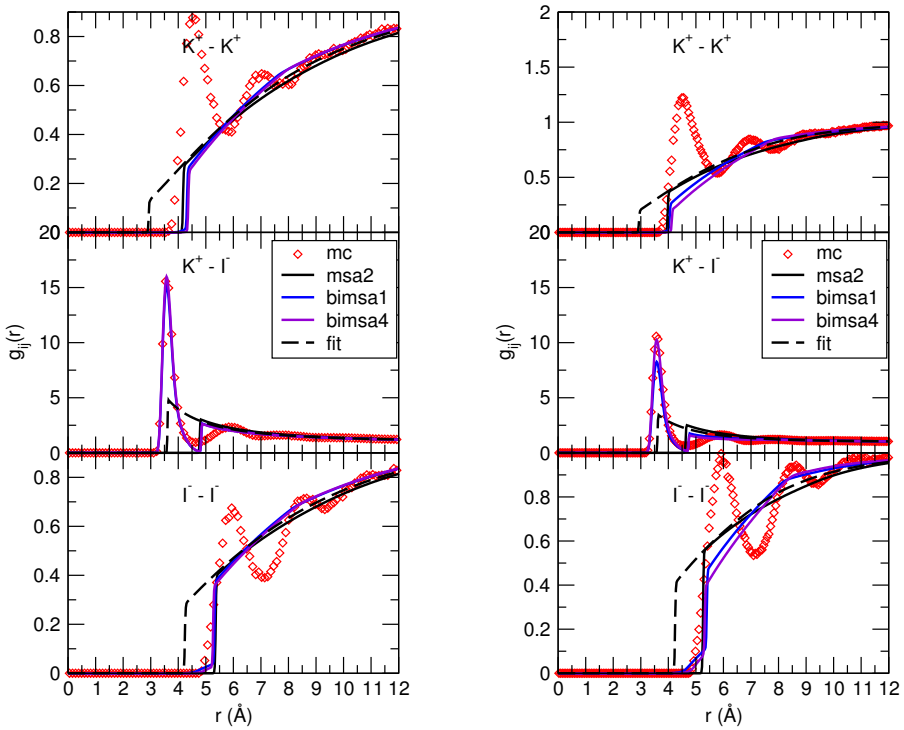

(a) c=0.1 M

(b) c=0.5 M

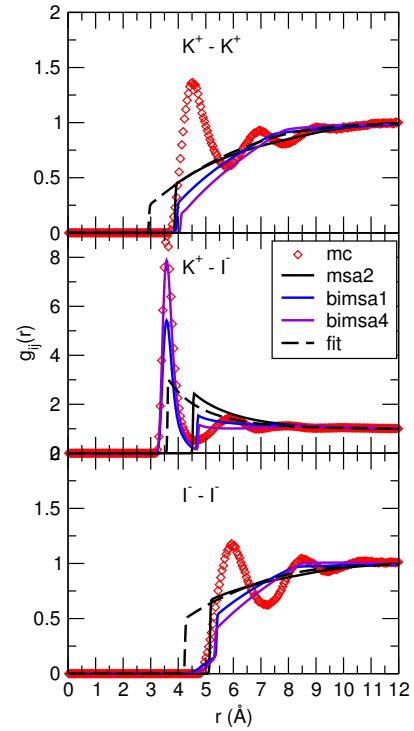

(c) c=1.0 M

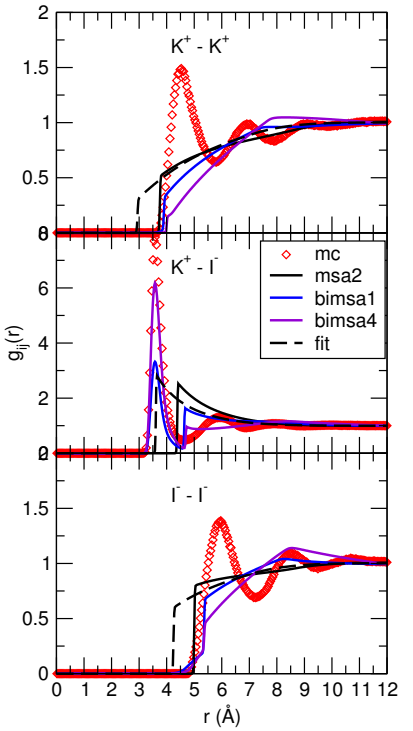

(d) c=1.7 M

Figure F.24: Comparison between RDFs obtained from MC and PFT calculations for KI at several concentrations. The results obtained from fitting the exact free energy (MC) to a concentration independent two-component model, as given by the MSA solution, are also shown.

Bibliography

[1] Y. Marcus, *Ion solvation*. John Wiley & Sons, 1985.

[2] V. Dahirel, F. Paillusson, M. Jardat, M. Barbi, and J.-M. Victor, "Nonspecific DNA-Protein Interaction: Why Proteins Can Diffuse along DNA," *Physical Review Letters*, vol. 102, no. 22, p. 228101, 2009.

[3] S. W. Hunt, M. Roeselová, W. Wang, L. M. Wingen, E. M. Knipping, D. J. Tobias, D. Dabdub, and B. J. Finlayson-Pitts, "Formation of Molecular Bromine from the Reaction of Ozone with Deliquesced NaBr Aerosol: Evidence for Interface Chemistry," *Journal of Physical Chemistry A*, vol. 108, no. 52, pp. 11559–11572, 2004.

[4] B. Bonin, *Le traitement - recyclage du combustible nucléaire usé*. La séparation des actinides - Applications à la gestion des déchets, Paris: Le Moniter Editions, 2008.

[5] A. Aguado, L. Bernasconi, S. Jahn, and P. A. Madden, "Multipoles and interaction potentials in ionic materials from planewave-DFT calculations," *Faraday Discussions*, vol. 124, pp. 171–184, 2003.

[6] A. Ruas, P. Moisy, J.-P. Simonin, O. Bernard, J.-F. Dufreche, and P. Turq, "Lanthanide salts solutions: Representation of osmotic coefficients within the binding mean spherical approximation," *Journal of Physical Chemistry B*, vol. 109, no. 11, pp. 5243–5248, 2005.

[7] P. Sillren and J.-P. Hansen, "Pertubation theory for systems with strong short-ranged interactions," *Molecular Physics*, vol. 105, pp. 1803–1811, 2007.

[8] P. Sillren and J.-P. Hansen, "On the critical non-additivity driving segregation of asymmetric binary hard sphere fluids," *Molecular Physics*, vol. 108, no. 1, pp. 97–104, 2010.

[9] L. Onsager and R. M. Fuoss, "Irreversible Processes in Electrolytes. Diffusion, Conductance, and Viscous Flow in Arbitrary Mixtures of Strong Electrolytes," *The Journal of Physical Chemistry*, vol. 36, no. 11, pp. 2689–2778, 1932.

[10] A. Chandra and B. Bagchi, "Ionic contribution to the viscosity of dilute electrolyte solutions: Towards a microscopic theory," *The Journal of Chemical Physics*, vol. 113, no. 8, p. 3226, 2000.

[11] R. K. Pathria and P. D. Beale, *Statistical Mechanics*. Butterworth-Heinemann, 2nd ed., 1996.

[12] K. Huang, *Statistical Mechanics*. New York: John Wiley and Sons, 2nd ed., 1987.

[13] H. L. Friedman, *A Course in Statistical Mechanics*. Prentice Hall College Div, 1985.

[14] D. A. McQuarrie, *Statistical Mechanics*. New York: HarperCollins, 1976.

[15] L. D. Landau and E. M. Lifshitz, *Statistical Physics, Part 1 (Course of Theoretical Physics)*, vol. 5. Butterworth-Heinemann, 3rd ed., 1980.

[16] L. P. Pitaevskii and E. M. Lifshitz, *Statistical Physics, Part 2 (Course of Theoretical Physics)*, vol. 9. New York: Butterworth-Heinemann, 3rd ed., 1980.

[17] J.-P. Hansen and I. R. McDonald, *Theory of Simple Liquids*. New York: Academic Press, 3rd ed., 2008.

[18] A. Ben-Naim, *Molecular Theory of Solutions*. New York: Oxford University Press, 2006.

[19] J. W. Gibbs, *Elementary Principles in Statistical Mechanics*. Developed with Especial Reference to the Rational Foundation of Thermodynamics, Cambridge Univ Pr, 2010.

[20] D. Frenkel and B. Smit, *Understanding Molecular Simulation*. San Diego: Academic Press, 2002.

[21] S. Velasco, "The Ornstein-Zernike equation in the canonical ensemble," *Europhysics Letters*, vol. 54, no. 5, pp. 475–481, 2001.

[22] T. Morita and K. Hiroike, "A New Approach to the Theory of Classical Fluids. III," *Progress of Theoretical Physics*, vol. 25, no. 4, pp. 537–578, 1961.

[23] J. Percus and G. J. Yevick, "Analysis of classical statistical mechanics by means of collective coordinates," *Physical Review*, vol. 110, no. 1, pp. 1–13, 1958.

[24] R. J. Baxter, "Percus - Yevick equation of hard spheres with sufrace adhesion," *The Journal of Chemical Physics*, vol. 49, no. 6, pp. 2770–2774, 1968.

[25] M. Wertheim, "Exact solution of the Percus-Yevick integral equation for hard spheres," *Physical Review Letters*, vol. 10, no. 8, pp. 321–323, 1963.

[26] J. Lebowitz, "Exact solution of generalized Percus-Yevick equation for a mixture of hard spheres," *Physical Review*, vol. 133, no. 4A, pp. A895–A899, 1964.

[27] L. Blum, "Mean spherical model for asymmetric electrolytes," *Molecular Physics*, vol. 30, no. 5, pp. 1529–1535, 1975.

[28] L. Blum and J. Høye, "Mean spherical model for asymmetric electrolytes. 2. Thermodynamic properties and the pair correlation function," *The Journal of Physical Chemistry*, vol. 81, no. 13, pp. 1311–1316, 1977.

[29] L. Blum, *Theoretical Chemistry: Advances and Perspectives*, vol. 5. New York: Academic Press, 1980.

[30] T. Morita, "Theory of Classical Fluids: Hyper-Netted Chain Approximation. III—A New Integral Equation for the Pair Distribution Function—," *Progress of Theoretical Physics*, vol. 23, no. 5, pp. 829–845, 1960.

[31] M. Jardat, O. Bernard, P. Turq, and G. R. Kneller, "Transport coefficients of electrolyte solutions from Smart Brownian dynamics simulations," *The Journal of Chemical Physics*, vol. 110, no. 16, pp. 7993–7999, 1999.

[32] L. Belloni, "Inability of the hypernetted chain integral equation to exhibit a spinodal line," *The Journal of Chemical Physics*, vol. 98, no. 10, pp. 8080–8095, 1993.

[33] J. Caillol, D. Levesque, and J. Weis, "Critical Behavior of the Restricted Primitive Model," *Physical Review Letters*, vol. 77, no. 19, pp. 4039–4042, 1996.

[34] P. J. Camp and G. N. Patey, "Ion association and condensation in primitive models of electrolyte solutions," *The Journal of Chemical Physics*, vol. 111, no. 19, pp. 9000–9007, 1999.

[35] J. G. Kirkwood, "Statistical Mechanics of Fluid Mixtures," *The Journal of Chemical Physics*, vol. 3, no. 5, pp. 300–313, 1935.

[36] J. Barker and D. Henderson, "What is" liquid"? Understanding the states of matter," *Reviews Of Modern Physics*, vol. 48, no. 4, pp. 587–671, 1976.

[37] R. Zwanzig, "High - Temperature Equation of State by a Perturbation Method. I. Nonpolar Gases," *The Journal of Chemical Physics*, vol. 22, no. 8, pp. 1420–1426, 1954.

[38] J. Weeks, D. Chandler, and H. Andersen, "Perturbation theory of the thermodynamic properties of simple liquids," *The Journal of Chemical Physics*, vol. 55, pp. 5422–5423, 1971.

[39] J. Barker and D. Henderson, "Perturbation Theory and Equation of State for Fluids: The Square - Well Potential," *The Journal of Chemical Physics*, vol. 47, pp. 2856–2861, 1967.

[40] S. Viscardy, J. Servantie, and P. Gaspard, "Transport and Helfand moments in the Lennard-Jones fluid. I. Shear viscosity," *The Journal of Chemical Physics*, vol. 126, no. 18, p. 184512, 2007.

[41] S. Viscardy, J. Servantie, and P. Gaspard, "Transport and Helfand moments in the Lennard-Jones fluid. II. Thermal conductivity," *The Journal of Chemical Physics*, vol. 126, no. 18, p. 184513, 2007.

[42] R. A. Robinson and R. H. Stokes, *Electrolyte Solutions*. New York: Dover, 2002.

[43] H. B. Callen, *Thermodynamics and an Introduction to Thermostatistics*. New York: Wiley, 2nd ed., 1985.

[44] J.-P. Simonin, "Study of experimental-to-McMillan-Mayer conversion of thermodynamic excess functions," *Journal of The Chemical Society-Faraday Transactions*, vol. 92, no. 19, pp. 3519–3523, 1996.

[45] L. Blum and O. Bernard, "The general solution of the binding mean spherical approximation for pairing ions," *Journal of Statistical Physics*, vol. 79, pp. 569–583, 1995.

[46] O. Bernard and L. Blum, "Binding mean spherical approximation for pairing ions: An exponential approximation and thermodynamics," *The Journal of Chemical Physics*, vol. 104, no. 12, pp. 4746–4754, 1996.

[47] T. Boublík, "Hard-sphere equation of state," *The Journal of Chemical Physics*, vol. 53, pp. 471–472, 1970.

[48] G. Mansoori, N. Carnahan, K. Starling, and T. Leland Jr, "Equilibrium thermodynamic properties of the mixture of hard spheres," *The Journal of Chemical Physics*, vol. 54, pp. 1523–1525, 1971.

[49] J. Salacuse and G. Stell, "Polydisperse systems: Statistical thermodynamics, with applications to several models including hard and permeable spheres," *The Journal of Chemical Physics*, vol. 77, no. 7, pp. 3714–3725, 1982.

[50] T. Vilarino, O. Bernard, and J.-P. Simonin, "Ionic solutions in the binding mean spherical approximation. Thermodynamics of associating electrolytes up to very high concentrations," *Journal of Physical Chemistry B*, vol. 108, pp. 5763–5770, 2004.

[51] W. G. McMillan and J. E. Mayer, "The statistical thermodynamics of multicomponent systems," *The Journal of Chemical Physics*, vol. 13, no. 7, pp. 276–305, 1945.

[52] J. G. Kirkwood and F. P. Buff, "The statistical mechanical theory of solutions. I," *The Journal of Chemical Physics*, vol. 19, no. 6, pp. 774–777, 1951.

[53] P. G. Kusalik and G. Patey, "The thermodynamic properties of electrolyte solutions: Some formal results," *The Journal of Chemical Physics*, vol. 86, no. 9, pp. 5110–5116, 1987.

[54] L. L. Lee, "Thermodynamic consistency and reference scale conversion in multisolvent electrolyte solutions," *Journal of Molecular Liquids*, vol. 87, no. 2-3, pp. 129–147, 2000.

[55] F. H. Spedding, H. O. Weber, V. Saeger, H. Petheram, J. Rard, and A. Habenschuss, "Isopiestic determination of the activity coefficients of some aqueous rare earth electrolyte solutions at 25 degrees. 1. The rare earth chlorides," *Journal Of Chemical And Engineering Data*, vol. 21, no. 3, pp. 341–360, 1976.

[56] P. Novotny and O. Sohnel, "Densities of binary aqueous solutions of 306 inorganic substances," *Journal Of Chemical And Engineering Data*, vol. 33, no. 1, pp. 49–55, 1988.

[57] F. H. Spedding, V. Saeger, K. Gray, P. K. Boneau, M. Brown, C. de Kock, J. Baker, L. E. Shiers, H. O. Weber, and A. Habenschuss, "Densities and apparent molal volumes of some aqueous rare earth solutions at 25 degrees. 1. Rare earth chlorides," *Journal Of Chemical And Engineering Data*, vol. 20, no. 1, pp. 72–81, 1975.

[58] J. Heyda and T. Hrobárik, "Ion-Specific Interactions between Halides and Basic Amino Acids in Water," *Journal of Physical Chemistry A*, vol. 113, pp. 1969–1975, 2008.

[59] B. Rotenberg, V. Marry, N. Malikova, and P. Turq, "Molecular simulation of aqueous solutions at clay surfaces," *Journal of Physics: Condensed Matter*, vol. 22, p. 284114, 2010.

[60] M. Head-Gordon, "Quantum Chemistry and Molecular Processes," *The Journal of Physical Chemistry*, vol. 100, no. 31, pp. 13213–13225, 1996.

[61] C. Danilo, V. Vallet, J.-P. Flament, and U. Wahlgren, "Effects of the first hydration sphere and the bulk solvent on the spectra of the f2 isoelectronic actinide compounds: U4+, NpO2+, and PuO22+," *Physical Chemistry Chemical Physics*, vol. 12, no. 5, pp. 1116–1130, 2010.

[62] R. G. Parr and W. Yang, *Density Functional Theory of Atoms and Molecules*. The International Series of Monographs on Chemistry, New York: Oxford University Press, 1989.

[63] R. Vuilleumier, *Density Functional Theory based Ab Initio Molecular Dynamics Using the Car-Parrinello Approach*. Berling Heidelberg: Springer-Verlag, 2006.

[64] C. Fiolhais, F. Nogueira, and M. A. L. Marques, eds., *A Primer in Density Functional Theory*, vol. 620 of *Lecture Notes in Physics*. Berlin: Springer, 2003.

[65] W. Kohn and L. J. Sham, "Self-Consistent Equations Including Exchange and Correlation Effects," *Physical Review*, vol. 140, no. 4A, pp. A1133–A1138, 1965.

[66] C. Cohen-Tannoudji, B. Diu, and F. Laloë, *Mechanique Quantique*, vol. 1-2. Paris: Hermann, 1977.

[67] D. M. Ceperley and B. J. Alder, "Ground State of the Electron Gas by a Stochastic Method," *Physical Review Letters*, vol. 45, no. 7, pp. 566–569, 1980.

[68] A. D. Becke, "Density-functional exchange-energy approximation with correct asymptotic behavior," *Physical Review A*, vol. 38, no. 6, pp. 3098–3100, 1988.

[69] C. Lee, W. Yang, and R. G. Parr, "Development of the Colle-Salvetti correlation-energy formula into a functional of the electron density," *Physical Review B*, vol. 37, no. 2, pp. 785–789, 1988.

[70] J. P. Perdew, K. Burke, and M. Ernzerhof, "Generalized Gradient Approximation Made Simple," *Physical Review Letters*, vol. 77, no. 18, pp. 3865–3868, 1996.

[71] N. Troullier and J. L. Martins, "Efficient pseudopotentials for plane-wave calculations," *Physical Review B*, vol. 43, no. 3, pp. 1993–2006, 1991.

[72] S. Goedecker, M. Teter, and J. Hutter, "Separable dual-space Gaussian pseudopotentials," *Physical Review B*, vol. 54, no. 3, pp. 1703–1710, 1996.

[73] C. Hartwigsen, S. Goedecker, and J. Hutter, "Relativistic separable dual-space Gaussian pseudopotentials from H to Rn," *Physical Review B*, vol. 58, no. 7, pp. 3641–3662, 1998.

[74] M. Krack, "Pseudopotentials for H to Kr optimized for gradient-corrected exchange-correlation functionals," *Theoretical Chemistry Accounts: Theory, Computation, and Modeling (Theoretica Chimica Acta)*, vol. 114, no. 1-3, pp. 145–152, 2005.

[75] N. Marzari and D. Vanderbilt, "Maximally localized generalized Wannier functions for composite energy bands," *Physical Review B*, vol. 56, no. 20, pp. 12847–12865, 1997.

[76] P. L. Silvestrelli, "Maximally localized Wannier functions for simulations with supercells of general symmetry," *Physical Review B*, vol. 59, no. 15, pp. 9703–9706, 1999.

[77] G. Berghold, C. Mundy, A. Romero, J. Hutter, and M. Parrinello, "General and efficient algorithms for obtaining maximally localized Wannier functions," *Physical Review B*, vol. 61, no. 15, pp. 10040–10048, 2000.

[78] P. L. Silvestrelli and M. Parrinello, "Water molecule dipole in the gas and in the liquid phase," *Physical Review Letters*, vol. 82, no. 16, pp. 3308–3311, 1999.

[79] L. Bernasconi, M. Wilson, and P. Madden, "Cation polarizability from first-principles: Sn2+," *Computational Materials Science*, vol. 22, pp. 94–98, 2001.

[80] L. Bernasconi, P. Madden, and M. Wilson, "Ionic to molecular transition in AlCl3: an examination of the electronic structure," *Physchemcomm*, vol. 5, no. 1, pp. 1–11, 2002.

[81] R. Kingsmith and D. Vanderbilt, "Theory of polarization of crystalline solids," *Physical Review B*, vol. 47, no. 3, pp. 1651–1654, 1993.

[82] D. Vanderbilt and R. Kingsmith, "Electric polarization as a bulk quantity and its relation to surface - charge," *Physical Review B*, vol. 48, no. 7, pp. 4442–4455, 1993.

[83] I. Souza, T. Wilkens, and R. Martin, "Polarization and localization in insulators: Generating function approach," *Physical Review B*, vol. 62, no. 3, pp. 1666–1683, 2000.

[84] P. A. Madden, "Ewald summation of electrostatic multipole interactions up to the quadrupolar level," *The Journal of Chemical Physics*, vol. 119, no. 14, pp. 7471–7483, 2003.

[85] T. Laino and J. Hutter, "Notes on "Ewald summation of electrostatic multipole interactions up to quadrupolar level" [J. Chem. Phys. 119, 7471 (2003)]," *The Journal of Chemical Physics*, vol. 129, no. 7, p. 074102, 2008.

[86] P. Umari and A. Pasquarello, "Ab initio Molecular Dynamics in a Finite Homogeneous Electric Field," *Physical Review Letters*, vol. 89, no. 15, 2002.

[87] P. Umari and A. Pasquarello, "Density functional theory with finite electric field," *International Journal of Quantum Chemistry*, vol. 101, no. 6, pp. 666–670, 2005.

[88] R. Resta, "Quantum-Mechanical Position Operator in Extended Systems," *Physical Review Letters*, vol. 80, no. 9, pp. 1800–1803, 1998.

[89] J. Schmidt, J. VandeVondele, I. F. W. Kuo, D. Sebastiani, J. I. Siepmann, J. Hutter, and C. J. Mundy, "Isobaric - Isothermal Molecular Dynamics Simulations Utilizing Density Functional Theory: An Assessment of the Structure and Density of Water at Near - Ambient Conditions," *Journal of Physical Chemistry B*, vol. 113, no. 35, pp. 11959–11964, 2009.

[90] P. L. Silvestrelli, "Van der Waals interactions in DFT made easy by Wannier functions," *Physical Review Letters*, vol. 100, no. 5, p. 053002, 2008.

[91] B. Rotenberg, M. Salanne, C. Simon, and R. Vuilleumier, "From Localized Orbitals to Material Properties: Building Classical Force Fields for Nonmetallic Condensed Matter Systems," *Physical Review Letters*, vol. 104, no. 13, p. 138301, 2010.

[92] Y. Andersson, D. Langreth, and B. Lundqvist, "van der Waals Interactions in Density-Functional Theory," *Physical Review Letters*, vol. 76, no. 1, pp. 102–105, 1996.

[93] R. Car and M. Parrinello, "Unified approach for molecular-dynamics and density-functional theory," *Physical Review Letters*, vol. 55, no. 22, pp. 2471–2474, 1985.

[94] G. Ciccotti, M. Ferrario, and J. Ryckaert, "Molecular dynamics of rigid systems in cartesian coordinates A general formulation," *Molecular Physics*, vol. 47, no. 6, pp. 1253–1264, 1982.

[95] H. Andersen, "Rattle - A velocity version of the shake algorithm for molecular dynamics calculations," *Journal of Computational Physics*, vol. 52, no. 1, pp. 24–34, 1983.

[96] W. Hoover, "Canonical dynamics: Equilibrium phase-space distributions," *Physical Review A*, vol. 31, no. 3, pp. 1695–1697, 1985.

[97] S. Nosé, "A molecular dynamics method for simulations in the canonical ensemble," *Molecular Physics*, vol. 52, no. 2, pp. 255–268, 1984.

[98] S. Nosé, "A unified formulation of the constant temperature molecular dynamics methods," *The Journal of Chemical Physics*, vol. 81, no. 1, p. 511, 1984.

[99] G. Martyna and D. Tobias, "Constant pressure molecular dynamics algorithms," *Constant pressure molecular dynamics algorithms*, vol. 101, no. 5, 1994.

[100] H. C. Andersen, "Molecular dynamics simulations at constant pressure and/or temperature," *The Journal of Chemical Physics*, vol. 72, no. 4, pp. 2384–2393, 1980.

[101] H. J. C. Berendsen, J. P. M. Postma, W. F. van Gunsteren, A. DiNola, and J. R. Haak, "Molecular dynamics with coupling to an external bath," *The Journal of Chemical Physics*, vol. 81, no. 8, pp. 3684–3690, 1984.

[102] J. Stenhammar, M. Trulsson, and P. Linse, "Some comments and corrections regarding the calculation of electrostatic potential derivatives using the Ewald summation technique," *The Journal of Chemical Physics*, vol. 134, no. 22, p. 224104, 2011.

[103] W. H. Press, B. P. Flannery, S. A. Teukolsky, and W. T. Vetterling, *Numerical Recipes in Fortran: The Art of Scientific Computing*. Cambridge University Press, 2nd ed., 1992.

[104] L. X. Dang and T.-M. Chang, "Molecular dynamics study of water clusters, liquid, and liquid-vapor interface of water with many-body potentials," *The Journal of Chemical Physics*, vol. 106, no. 19, pp. 8149–8159, 1997.

[105] CPMD, "CPMD Simulation Code," Copyright IBM Corp 1990-2008, Copyright MPI für Festkörperforchung Stuttgart 1997-2001. www.cpmd.org/.

[106] J. R. Hammond, N. Govind, K. Kowalski, J. Autschbach, and S. S. Xantheas, "Accurate dipole polarizabilities for water clusters n=2–12 at the coupled-cluster level of theory and benchmarking of various density functionals," *The Journal of Chemical Physics*, vol. 131, no. 21, p. 214103, 2009.

[107] J. W. Ponder, "TINKER Molecular Modeling Package ," http://dasher.wustl.edu/tinker.

[108] L. X. Dang, "Development of nonadditive intermolecular potentials using molecular dynamics: Solvation fo Li+ and F- ions in polarizable water," *The Journal of Chemical Physics*, vol. 96, no. 9, pp. 6970–6977, 1992.

[109] L. X. Dang and B. C. Garrett, "Photoelectron spectra of the hydrated iodine anion from molecular dynamics simulations," *The Journal of Chemical Physics*, vol. 99, no. 4, pp. 2972–2977, 1993.

[110] L. X. Dang and P. A. Kollman, "Free energy of association of the K+:18-Crown-6 complex in water: A new molecular dynamics study," *The Journal of Physical Chemistry*, vol. 99, no. 1, pp. 55–58, 1995.

[111] H. J. C. Berendsen, J. Grigera, and T. P. Straatsma, "The missing term in effective pair potentials," *The Journal of Physical Chemistry*, vol. 91, no. 24, pp. 6269–6271, 1987.

[112] G. Lamoureux and B. Roux, "Absolute Hydration Free Energy Scale for Alkali and Halide Ions Established from Simulations with a Polarizable Force Field," *Journal of Physical Chemistry B*, vol. 110, pp. 3308–3322, 2006.

[113] P. Ren and J. W. Ponder, "Polarizable Atomic Multipole Water Model for Molecular Mechanics Simulation," *Journal of Physical Chemistry B*, vol. 107, pp. 5933–5947, 2003.

[114] A. Grossfield, P. Ren, and J. W. Ponder, "Ion Solvation Thermodynamics from Simulation with a Polarizable Force Field," *Journal of the American Chemical Society*, vol. 125, no. 50, pp. 15671–15682, 2003.

[115] D. Jiao, C. King, A. Grossfield, T. A. Darden, and P. Ren, "Simulation of Ca 2+and Mg 2+Solvation Using Polarizable Atomic Multipole Potential," *Journal of Physical Chemistry B*, vol. 110, no. 37, pp. 18553–18559, 2006.

[116] J.-P. Piquemal, L. Perera, G. A. Cisneros, P. Ren, L. G. Pedersen, and T. A. Darden, "Towards accurate solvation dynamics of divalent cations in water using the polarizable amoeba force field: From energetics to structure," *The Journal of Chemical Physics*, vol. 125, no. 5, p. 054511, 2006.

[117] P. Salvador, J. E. Curtis, D. J. Tobias, and P. Jungwirth, "Polarizability of the nitrate anion and its solvation at the air/water interface," *Physical Chemistry Chemical Physics*, vol. 5, no. 17, pp. 3752–3757, 2003.

[118] P. Jungwirth, J. E. Curtis, and J. D. Tobias, "Polarizability and aqueous solvation of the sulfate dianion," *Chemical Physics Letters*, vol. 367, pp. 704–710, 2003.

[119] P. Jungwirth and D. J. Tobias, "Ions at the Air/Water Interface," *Journal of Physical Chemistry B*, vol. 106, no. 25, pp. 6361–6373, 2002.

[120] P. L. Silvestrelli and M. Parrinello, "Structural, electronic, and bonding properties of liquid water from first principles," *The Journal of Chemical Physics*, vol. 111, no. 8, pp. 3572–3580, 1999.

[121] C. Sagui, P. Pomorski, T. A. Darden, and C. Roland, "Ab initio calculation of electrostatic multipoles with Wannier functions for large-scale biomolecular simulations," *The Journal of Chemical Physics*, vol. 120, no. 9, p. 4530, 2004.

[122] G. Mahan, "Modified Sternheimer equation for polarizability," *Physical Review A*, vol. 22, no. 5, pp. 1780–1785, 1980.

[123] C. Hättig and B. A. Hess, "TDMP2 calculation of dynamic multipole polarizabilities and dispersion coefficients for the halogen anions F, Cl, Br and I," *The Journal of Chemical Physics*, vol. 108, no. 10, pp. 3863–3870, 1998.

[124] H. Yu, T. W. Whitfield, E. Harder, G. Lamoureux, I. Vorobyov, V. M. Anisimov, A. D. Mackerell, and B. Roux, "Simulating Monovalent and Divalent Ions in Aqueous Solution Using a Drude Polarizable Force Field," *Journal of Chemical Theory And Computation*, vol. 6, no. 3, pp. 774–786, 2010.

[125] L. X. Dang, J. E. Rice, J. Caldwell, and P. A. Kollman, "Ion solvation in polarizable water: molecular dynamics simulations," *Journal of the American Chemical Society*, vol. 113, no. 7, pp. 2481–2486, 1991.

[126] T.-M. Chang and L. X. Dang, "Recent Advances in Molecular Simulations of Ion Solvation at Liquid Interfaces," *Chemical Reviews*, vol. 106, no. 4, pp. 1305–1322, 2006.

[127] T.-M. Chang and L. X. Dang, "Computational Studies of Structures and Dynamics of 1,3 - Dimethylimidazolim Salt Liquids and their Interfaces Using Polarizable Potential Models," *Journal of Physical Chemistry A*, vol. 113, no. 10, pp. 2127–2135, 2009.

[128] J. J. Molina, S. Lectez, S. Tazi, M. Salanne, J.-F. Dufreche, J. Roques, E. Simoni, P. A. Madden, and P. Turq, "Ions in solutions: Determining their polarizabilities from first-principles," *The Journal of Chemical Physics*, vol. 134, no. 1, p. 014511, 2011.

[129] J. N. Wilson and R. M. Curtis, "Dipole polarizabilities of ions in alkali halide crystals," *The Journal of Physical Chemistry*, vol. 74, no. 1, pp. 187–196, 1970.

[130] M. Wilson, P. A. Madden, P. Jemmer, P. W. Fowler, A. Batana, J. Bruno, R. W. Munn, and M. C. Monard, "Models of environmental effects on anion polarizability," *Molecular Physics*, vol. 96, no. 10, pp. 1457–1467, 1999.

[131] Jemmer, P. Fowler, and M. Wilson, "Environmental Effects on Anion Polarizability: Variation with Lattice Parameter and Coordination Number," *Journal of Physical Chemistry A*, vol. 102, no. 43, pp. 8377–8385, 1998.

[132] B. Bauer, T. Lucas, A. Krishtal, and C. Van, "Variation of Ion Polarizability from Vacuum to Hydration: Insights from Hirshfeld Partitioning," *Journal of Physical Chemistry A*, vol. 114, no. 34, pp. 8984–8992, 2010.

[133] P. Bultinck, C. van Alsenoy, P. W. Ayers, and R. Carbo-Dorca, "Critical analysis and extension of the Hirshfeld atoms in molecules," *The Journal of Chemical Physics*, vol. 126, no. 14, p. 144111, 2007.

[134] L. X. Dang, "Computational Study of Ion Binding to the Liquid Interface of Water," *Journal of Physical Chemistry B*, vol. 106, pp. 10388–10394, 2002.

[135] T. M. Chang and L. X. Dang, "Ion solvation in polarizable chloroform: A molecular dynamics study," *Journal of Physical Chemistry B*, vol. 101, no. 49, pp. 10518–10526, 1997.

[136] F. James and M. Roos, "Minuit - a system for function minimization and analysis of the parameter errors and correlations," *Computer Physics Communications*, vol. 10, pp. 343–367, 1975.

[137] CP2K developers group, "CP2K Simulation Code," http://cp2k.berlios.de.

[138] I. Yeh and G. Hummer, "System-size dependence of diffusion coefficients and viscosities from molecular dynamics simulations with periodic boundary conditions," *Journal of Physical Chemistry B*, vol. 108, no. 40, pp. 15873–15879, 2004.

[139] I. Yeh and G. Hummer, "Diffusion and electrophoretic mobility of single-stranded RNA from molecular dynamics simulations," *Biophysical Journal*, vol. 86, no. 2, pp. 681–689, 2004.

[140] M. Kastenholz and P. Hunenberger, "Computation of methodology-independent ionic solvation free energies from molecular simulations. I. The electrostatic potential in molecular liquids," *The Journal of Chemical Physics*, vol. 124, no. 12, p. 124106, 2006.

[141] M. A. Kastenholz and P. Hunenberger, "Computation of methodology-independent ionic solvation free energies from molecular simulations. II. The hydration free energy of the sodium cation," *The Journal of Chemical Physics*, vol. 124, no. 22, p. 224501, 2006.

[142] I. Kalcher and J. Dzubiella, "Structure-thermodynamics relation of electrolyte solutions," *The Journal of Chemical Physics*, vol. 130, no. 13, p. 134507, 2009.

[143] J. T. Chayes and L. Chayes, "On the validity of the inverse conjecture in classical density functional theory," *Journal of Statistical Physics*, vol. 36, no. 3-4, pp. 471–488, 1984.

[144] J. T. Chayes, L. Chayes, and E. H. Lieb, "The inverse problem in classical statistical - mechanics," *Communications In Mathematical Physics*, vol. 93, no. 1, pp. 57–121, 1984.

[145] A. Lyubartsev and S. Marčelja, "Evaluation of effective ion-ion potentials in aqueous electrolytes," *Physical Review E*, vol. 65, p. 041202, 2002.

[146] G. Zerah and J.-P. Hansen, "Self - consistent integral equations for fluid pair distribution functions: Another attempt," *The Journal of Chemical Physics*, vol. 84, no. 4, pp. 2336–2343, 1986.

[147] A. Lyubartsev and A. Laaksonen, "Calculation of effective interaction potentials from radial distribution functions: A reverse Monte Carlo approach," *Physical Review E*, vol. 52, no. 4, pp. 3730–3737, 1995.

[148] M. D'Alessandro and F. Cilloco, "Information-theory-based solution of the inverse problem in classical statistical mechanics," *Physical Review E*, vol. 82, no. 2, p. 021128, 2010.

[149] D. J. Mitchell, D. A. McQuarrie, A. Szabo, and J. Groeneveld, "On the Second-Moment Condition of Stillinger and Lovett," *Journal of Statistical Physics*, vol. 17, no. 1, pp. 15–20, 1977.

[150] J. J. Molina, C. Pierleoni, B. Capone, J.-P. Hansen, and I. S. S. de Oliveira, "Crystal stability of diblock copolymer micelles in solution," *Molecular Physics*, vol. 107, no. 4-6, pp. 535–548, 2009.

[151] A. B. Bhatia and D. E. Thornton, "Structural Aspects of the Electrical Resistivity of Binary Alloys," *Physical Review B*, vol. 2, no. 8, pp. 3004–3012, 1970.

[152] J. J. Molina, M. Duvail, J.-F. Dufreche, and P. Guilbaud, "Atomistic Description of Binary Lanthanoid Salt Solutions: A Coarse-Graining Approach," *Journal of Physical Chemistry B*, vol. 115, no. 15, pp. 4329–4340, 2011.

[153] G. Hummer, N. Gronbech-Jensen, and M. Neumann, "Pressure calculation in polar and charged systems using Ewald summation: Results for the extended simple point charge model of water," *The Journal of Chemical Physics*, vol. 109, no. 7, pp. 2791–2797, 1998.

[154] Y. Marcus and G. Hefter, "Ion pairing," *Chemical Reviews*, vol. 106, no. 11, pp. 4585–4621, 2006.

[155] U. Essmann, L. Perera, M. L. Berkowitz, T. Darden, H. Lee, and L. G. Pedersen, "A smooth particle mesh Ewald method," *The Journal of Chemical Physics*, vol. 103, no. 19, pp. 8577–8593, 1995.

[156] L. X. Dang and D. E. Smith, "Mean force potential for the calcium-chloride pair in water - Comment," *The Journal of Chemical Physics*, vol. 102, no. 8, pp. 3483–3484, 1995.

[157] L. X. Dang, "Mechanism and thermodynamics of ion selectivity in aqueous solutions of 18-Crown-6 ether: A molecular dynamics study," *Journal of the American Chemical Society*, vol. 117, no. 26, pp. 6954–6960, 1995.

[158] S. Koneshan, J. C. Rasaiah, R. M. Lynden-Bell, and S. H. Lee, "Solvent structure, dynamics, and ion mobility in aqueous solutions at 25 degrees C," *Journal of Physical Chemistry B*, vol. 102, no. 21, pp. 4193–4204, 1998.

[159] J. C. Rasaiah and R. M. Lynden-Bell, "Computer simulation studies of the structure and dynamics of ions and non-polar solutes in water," *Philosophical Transactions Of The Royal Society Of London Series A-Mathematical Physical And Engineering Sciences*, vol. 359, no. 1785, pp. 1545–1574, 2001.

[160] L. Vrbka, M. Lund, I. Kalcher, J. Dzubiella, R. R. Netz, and W. Kunz, "Ion-specific thermodynamics of multicomponent electrolytes: A hybrid HNC/MD approach," *The Journal of Chemical Physics*, vol. 131, no. 15, p. 154109, 2009.

[161] P. G. Kusalik and I. M. Svishchev, "The Spatial Structure in Liquid Water," *Science*, vol. 265, no. 5176, pp. 1219–1221, 1994.

[162] C. J. Fennell, A. Bizjak, V. Vlachy, and K. A. Dill, "Ion Pairing in Molecular Simulations of Aqueous Alkali Halide Solutions," *Journal of Physical Chemistry B*, vol. 113, no. 19, pp. 6782–6791, 2009.

[163] J. J. Molina, J.-F. Dufreche, M. Salanne, O. Bernard, M. Jardat, and P. Turq, "Models of electrolyte solutions from molecular descriptions: The example of NaCl solutions," *Physical Review E*, vol. 80, no. 6, p. 065103, 2009.

[164] M. Patra and M. Karttunen, "Systematic comparison of force fields for microscopic simulations of NaCl in aqueous solutions: Diffusion, free energy of hydration, and structural properties," *Journal of Computational Chemistry*, vol. 25, no. 5, pp. 678–689, 2004.

[165] M. Fyta, I. Kalcher, J. Dzubiella, L. Vrbka, and R. R. Netz, "Ionic force field optimization based on single-ion and ion-pair solvation properties," *The Journal of Chemical Physics*, vol. 132, no. 2, p. 024911, 2010.

[166] B. Hess, C. Holm, and N. F. A. van der Vegt, "Osmotic coefficients of atomistic NaCl (aq) force fields," *The Journal of Chemical Physics*, vol. 124, p. 164509, 2006.

[167] B. Hess, C. Holm, and N. van der Vegt, "Modeling Multibody Effects in Ionic Solutions with a Concentration Dependent Dielectric Permittivity," *Physical Review Letters*, vol. 96, no. 14, p. 147801, 2006.

[168] D. A. Case, T. A. Darden, T. E. Cheatham, C. L. Simmerling, J. Wang, R. E. Duke, R. Luo, M. Crowley, R. C. Walker, W. Zhang, K. M. Merz, B. Wang, S. Hayik, A. Roitberg, G. Seabra, I. Kilossvary, K. F. Wong, F. Paesani, J. Vanicek,

X. Wu, S. R. Brozell, T. Steinbrecher, H. Gohlke, L. Yang, C. Tan, J. Mongan, V. Hornak, G. Cui, D. H. Mathews, M. G. Seetin, C. Sagui, V. Babin, and P. A. Kollman, "AMBER 10," 2008.

[169] T. Darden, D. York, and L. Pedersen, "Particle mesh Ewald: An N log(N) method for Ewald sums in large systems," *The Journal of Chemical Physics*, vol. 98, no. 12, p. 10089, 1993.

[170] J. W. Caldwell and P. A. Kollman, "Structure and Properties of Neat Liquids Using Nonadditive Molecular Dynamics: Water, Methanol, and N-Methylacetamide," *The Journal of Physical Chemistry*, vol. 99, no. 16, pp. 6208–6219, 1995.

[171] E. C. Meng and P. A. Kollman, "Molecular Dynamics Studies of the Properties of Water around Simple Organic Solutes - The Journal of Physical Chemistry (ACS Publications)," *The Journal of Chemical Physics*, vol. 100, no. 27, pp. 11460–11470, 1996.

[172] D. E. Smith and L. X. Dang, "Computer simulations of NaCl association in polarizable water," *The Journal of Chemical Physics*, vol. 100, no. 5, pp. 3757–3766, 1994.

[173] M. Duvail, A. Ruas, L. Venault, P. Moisy, and P. Guilbaud, "Molecular Dynamics Studies of Concentrated Binary Aqueous Solutions of Lanthanide Salts: Structures and Exchange Dynamics," *Inorganic Chemistry*, vol. 49, no. 2, pp. 519–530, 2010.

[174] J. J. Molina, M. Duvail, P. Guilbaud, and J.-F. Dufreche, "Coarse-grained lanthanoid chloride aqueous solutions," *Journal of Molecular Liquids*, vol. 153, no. 2-3, pp. 107–111, 2010.

[175] K. K. Mon, "Hard sphere perturbation theory of dense fluids with singular perturbation," *The Journal of Chemical Physics*, vol. 112, no. 7, pp. 3245–3247, 2000.

[176] K. K. Mon, "Application of hard sphere perturbation theory for thermodynamics of model liquid metals," *Physical Review E*, vol. 63, no. 6, p. 061203, 2001.

[177] K. K. Mon, "Hard sphere perturbation theory for thermodynamics of soft-sphere model liquid," *The Journal of Chemical Physics*, vol. 115, no. 10, pp. 4766–4769, 2001.

[178] G. Ciccotti, P. Turq, and F. Lantelme, "Cluster Approach to Ion Association in Electrolyte Solutions," *Chemical Physics*, vol. 88, no. 2, pp. 333–338, 1984.

[179] J.-F. Dufreche, T. O. White, and J.-P. Hansen, "Charged-stabilized colloidal suspensions: counterion condensation and phase diagrams," *Molecular Physics*, vol. 101, no. 11, pp. 1741–1759, 2003.

[180] J. D. Jackson, *Classical Electrodynamics Third Edition.* Hoboken: Wiley, 3rd ed., 1998.

[181] H. Eyring, D. Henderson, and W. Jost, *Physical Chemistry: An Advanced Treatise*, vol. VIIIA. New York: Academic Press, 1971.

[182] P. Attard, "Spherically inhomogeneous fluids. II. Hard-sphere solute in a hard-sphere solvent," *The Journal of Chemical Physics*, vol. 91, p. 3083, 1989.

[183] P. Attard, "Spherically inhomogeneous fluids. I. Percus-Yevick hard spheres: Osmotic coefficients and triplet correlations," *The Journal of Chemical Physics*, vol. 91, p. 3072, 1989.

[184] P. Attard and G. Patey, "Hypernetted-chain closure with bridge diagrams. Asymmetric hard sphere mixtures," *The Journal of Chemical Physics*, vol. 92, p. 4970, 1990.

[185] R. M. Fuoss and L. Onsager, "Conductance of unassociated electrolytes," *The Journal of Physical Chemistry*, vol. 61, no. 5, pp. 668–682, 1957.

[186] P. Turq, "Higher terms in the concentration dependence of self-diffusion coefficients in electrolytes," *Chemical Physics Letters*, vol. 15, no. 4, pp. 579–583, 1972.

[187] C. Micheletti and P. Turq, "Ionic transport in unsymmetrical electrolytes," *Journal of the Chemical Society, Faraday Transactions 2*, vol. 73, no. 6, pp. 743–754, 1977.

[188] J.-F. Dufreche, O. Bernard, S. Durand-Vidal, and P. Turq, "Analytical Theories of Transport in Concentrated Electrolyte Solutions from the MSA," *Journal of Physical Chemistry B*, vol. 109, no. 20, pp. 9873–9884, 2005.

[189] G. Jones and M. Dole, "The viscosity of aqueous solutions of strong electrolytes with special reference to barium chloride," *Journal of the American Chemical Society*, 1929.

[190] Y. Marcus, "Effect of Ions on the Structure of Water: Structure Making and Breaking," *Chemical Reviews*, vol. 109, no. 3, pp. 1346–1370, 2009.

[191] A. Einstein, "Eine neue Bestimmung der Moleküldimensionen," *Annalen der Physik*, vol. 324, no. 2, pp. 289–306, 1906.

[192] A. Einstein, "Berichtigung zu meiner Arbeit: "Eine neue Bestimmung der Moleküldimensionen"," *Annalen der Physik*, vol. 339, no. 3, pp. 591–592, 1911.

[193] U. Balucani and M. Zoppi, *Dynamics of the Liquid State*. Oxford: Oxford University Press, 2003.

[194] H. Mori, "Transport, Collective Motion, and Brownian Motion," *Progress of Theoretical Physics*, vol. 33, no. 3, pp. 423–455, 1965.

[195] H. Mori, "A Continued-Fraction Representation of the Time-Correlation Functions," *Progress of Theoretical Physics*, vol. 34, no. 3, pp. 399–416, 1965.

[196] J. P. Boon and S. Yip, *Molecular Hydrodynamics*. Dover Publications, 1992.

[197] T. Geszti, "Pre-vitrification by viscosity feedback," *Journal of Physics C: Solid State Physics*, 1983.

[198] B. Bagchi and S. Bhattacharayya, *Mode Coupling Approach to the Liquid-State Dynamics*, vol. 116 of *Advances in Chemical Physics*. Advances in Chemical Physics, john wiley & sons ed., 2001.

[199] S. Chapman, T. G. Cowling, and C. Cercignani, *The Mathematical Theory of Non-uniform Gases: An Account of the Kinetic Theory of Viscosity, Thermal Conduction and Diffusion in Gases* . Cambridge: Cambridge University Press, 3rd ed., 1991.

[200] M. K. Tham and K. E. Gubbins, "Kinetic theory of multicomponent dense fluid mixtures of rigid spheres," *The Journal of Chemical Physics*, vol. 55, no. 1, pp. 268–279, 1971.

[201] V. M. M. Lobo, *Electrolyte Solutions: Literature Data on Thermodynamic and Transport Properties*, vol. I and II. Lisbon, Portugal: Coimbra Editora, 1984.

[202] N. Metropolis, A. W. Rosenbluth, M. N. Rosenbluth, and A. H. Teller, "Equation of state calculations by fast computing machines," *The Journal of Chemical Physics*, vol. 21, no. 6, pp. 1087–1092, 1953.

[203] H. Flyvbjerg, *Advances in Computer Simulation*, vol. 501 of *Lecture Notes in Physics*. Springer Berlin Heidelberg, 1998.

[204] H. Flyvbjerg and H. G. Petersen, "Error estimates on averages of correlated data," *The Journal of Chemical Physics*, vol. 91, no. 1, p. 461, 1989.

[205] M. Abramowitz and I. A. Stegun, eds., *Handbook of Mathematical Functions: with Formulas, Graphs, and Mathematical Tables*. New York: Dover Publications, 1965.

[206] F. B. Hildebrand, *Introduction to Numerical Analysis: Second Edition (Dover Books on Advanced Mathematics)*. Dover Publications, 2nd ed., 1987.

[207] B. Davies, *Integral Transforms and Their Applications* . Texts in Applied Mathematics, Springer, 3rd ed., 2010.

[208] P. Valko and J. Abate, "Comparison of sequence accelerators for the Gaver method of numerical Laplace transform inversion," *Computers & Mathematics With Applications*, vol. 48, no. 3-4, pp. 629–636, 2004.

[209] J. Abate and P. Valko, "Multi-precision laplace transform inversion," *International Journal For Numerical Methods In Engineering*, vol. 60, no. 5, pp. 979–993, 2004.

[210] P. Valko and J. Abate, "Numerical Laplace inversion in rheological characterization," *Journal Of Non-Newtonian Fluid Mechanics*, vol. 116, no. 2-3, pp. 395–406, 2004.